

Process Optimisation and Numerical Modelling of Powder Metallurgical Aluminium Matrix Composites

by

Gareth O'Donnell, B.Sc. (Eng.)

A thesis submitted in part fulfilment of the requirement for the degree of

Doctor of Philosophy

Supervisor:

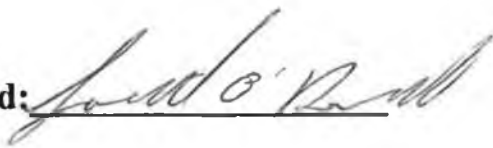
Dr. L. Looney

Dublin City University
School of Mechanical and Manufacturing Engineering
May 1999

DECLARATION

I hereby certify that this material, which I now submit for assessment on the programme of study leading to the award of Doctor of Philosophy is entirely my own work and has not been taken from the work of others save and to the extent that such work has been cited and acknowledged within the text of my work.

Signed:

A handwritten signature in dark ink, appearing to read 'Gareth O'Donnell', written over a horizontal line.

ID No.: 95971271

Gareth O'Donnell

Date: May 1999

ACKNOWLEDGEMENTS

Many individuals have come to my assistance during the present work. I offer many thanks to all, and in particular I would like to acknowledge the contributions of:

Dr. Lisa Looney of Dublin City University (DCU) for her guidance, limitless energy, encouragement and equanimity, and Professor Saleem Hashmi of DCU for useful discussion regarding material modelling.

Stephan Sternowsky of Universität Bremen, for his invaluable discussion and input at the early stages of this work, and his continued support, communication and friendship.

Dr. Peter McHugh of NUI Galway, Ireland for his time, energy and enthusiastic encouragement.

All my fellow students within Dublin City University and elsewhere, for their assistance, support and friendship. Special thanks to Brian Cahill, Niall Moran, JC Tan, Giovanni Pepe, Yusof Ismail, Shaestagir Chowdhury, Joseph Stokes, Helen Murphy, Dave Read, Khalid Bakkar, Mohammad Iqbal, Declan Brazil, Bjarne Bergquist and Frank Müller.

Liam Domican, Martin Johnson, Ian Hooper, Veronica Dobbyn, Michelle Considine, David O'Callaghan, Denis McKeon and all the technical staff involved in this work, for helpful discussion and for providing me with all I requested and more.

Both the Irish American Partnership and the School of Mechanical and Manufacturing Engineering DCU, without whose funding this project would not have been possible.

My parents and siblings for their encouragement and up-lifting confidence in my ability.

My family, Zillah and Autumn Louise, to whom the present work is dedicated, for providing me with a platform for success and so much more. Thanks.

Table of Contents

	Page
Title Page	i
Declaration	ii
Acknowledgements	iii
Table of Contents	iv
Abstract	xii
<u>CHAPTER 1</u> INTRODUCTION	1
1.1 NEW MATERIALS	1
1.2 METAL MATRIX COMPOSITE MATERIALS	3
1.2.1 Historical Developments	3
1.2.2 Recent Developments	4
1.2.3 Current Developments	7
1.2.4 Aluminium Matrix Composites	8
1.3 MMC PROCESSING	10
1.4 MMC MODELLING	12
1.5 PRESENT RESEARCH	13
1.5.1 PRAMC Processing	13
1.5.2 PRAMC Modelling	13
1.6 OVERVIEW OF RESEARCH REPORT	14

<u>CHAPTER 2</u> LITERATURE SURVEY	15
2.1 COMPOSITE MATERIALS	15
2.1.1 Composite History	15
2.1.2 Engineering Composites	17
2.1.3 Polymeric Matrix Composites	20
2.1.4 Ceramic Matrix Composites	22
2.2 METAL MATRIX COMPOSITES	24
2.2.1 Matrix Materials	26
2.2.2 Reinforcement	27
2.2.3 Effects of Combination	31
2.3 MMC PROCESSING	33
2.3.1 Casting	34
2.3.2 Infiltration	36
2.3.3 Physical Vapour Deposition	38
2.3.4 Spray Deposition	39
2.3.5 In-Situ (reaction) Processing	40
2.3.6 Diffusion Bonding	41
2.4 POWDER METALLURGICAL PROCESSING	42
2.4.1 Metal Powder Atomisation	45
2.4.2 Reinforcement Particle Production	47
2.4.3 Mixing	48
2.4.4 Powder Conditioning	50
2.4.5 Compaction	53
2.4.6 Sintering	56
2.4.7 Heat Treatment	60

2.5 PARTICLE REINFORCED ALUMINIUM MATRIX COMPOSITES	62
2.5.1 Strengthening Mechanisms	64
2.6 COMPOSITE MODELLING	67
2.6.1 Subcontinuum Models	70
2.6.2 Continuum Crystallographic Models	75
2.6.3 Continuum Solid Models	79
 <u>CHAPTER 3</u> EXPERIMENTAL WORK	 87
3.1 MATERIAL SELECTION	96
3.1.1 Matrix Material	96
3.1.2 Reinforcement	98
3.1.3 Lubricant	99
3.2 PROCESSING EQUIPMENT AND PROCEDURES	100
3.2.1 Powder Mixing	100
3.2.2 Powder Conditioning	103
3.2.3 Powder Pouring	106
3.2.4 Powder Compaction	109
3.2.5 Ejection	114
3.2.6 Compact Annealing	116
3.2.7 Sintering	118
3.2.8 Repressing	122
3.2.9 Precipitation Heat Treatment	123

3.3 ANALYSIS EQUIPMENT AND PROCEDURES	124
3.3.1 Powder Shape	124
3.3.2 Powder Size	124
3.3.3 Mixed Powder Homogeneity	124
3.3.4 H ₂ O Content	125
3.3.5 Powder Compressibility	125
3.3.6 Die Wall Frictional Stress	126
3.3.7 Green Strength (Green compacts)	126
3.3.8 Microstructural (Green compacts)	127
3.3.9 Diametrical Compressive Strength (Sintered material)	128
3.3.10 Hardness	128
3.3.11 Compressive Strength	129
3.3.12 Tensile Response	130
3.3.13 Microstructural (Sintered material)	130

CHAPTER 4 EXPERIMENTAL RESULTS AND OBSERVATIONS

4.1 POWDER ANALYSES	133
4.1.1 Powder Shape	133
4.1.2 Powder Size	133
4.1.3 Mixed Powder Homogeneity	134
4.1.4 H ₂ O Content	134

4.2 COMPRESSIBILITY TESTING	136
4.2.1 SiC Content	136
4.2.2 Aluminium Powder and SiC Particle Size	138
4.2.3 Aluminium Powder to SiC Particle Size Ratio	140
4.2.4 Powder Heat Treatment Temperature/Time	143
4.2.5 Powder Heat Treatment Atmosphere	144
4.2.6 Lubricant Type and Quantity	145
4.2.7 Aluminium Alloy Type	145
4.2.8 Compaction Rate	146
4.3 EJECTION STRESS ANALYSIS	147
4.3.1 Lubricant Type and Quantity	147
4.3.2 Powder Heat Treatment Atmosphere	148
4.3.3 Compaction Rate	148
4.4 GREEN STRENGTH ANALYSIS	149
4.4.1 Powder Heat Treatment	149
4.4.2 Heat Treatment Atmosphere and Lubricant Type	150
4.5 GREEN COMPACT MICROSTRUCTURAL ANALYSIS	151
4.6 SINTERED DENSITY ANALYSIS	153
4.6.1 Sintering Temperature	153
4.6.2 Sintering Time	154
4.6.3 Sintering Atmosphere	155
4.6.4 Powder Heat Treatment	156
4.7 DIAMETRICAL COMPRESSIVE STRENGTH ANALYSIS	157

4.8 HARDNESS TESTING	158
4.8.1 Hardness Test Methods	158
4.8.2 SiC Content	158
4.8.3 Powder Heat Treatment	159
4.8.4 Sintering Temperature	159
4.8.5 Sintering Time	160
4.9 AXIAL COMPRESSIVE STRENGTH TESTING	162
4.9.1 SiC Content	162
4.9.2 Powder Heat Treatment	163
4.10 FRACTURE SURFACE DEFECTS AND TENSILE RESPONSE	164
4.10.1 Fracture Surface Defects	164
4.10.2 Tensile Response	167
4.11 SINTERED SAMPLE MICROSTRUCTURAL ANALYSIS	170
4.11.1 Sintering Atmosphere	170
4.11.2 Powder Size	172
4.11.3 SiC Content	174
4.11.4 Hardness Testing	174
4.11.5 Sintering Time	175
4.11.6 Interfacial Bonding	176
4.11.7 Cracked Particle Infiltration	177
4.11.8 Fracture Surface Analyses	179
4.12 SUMMARY	181

<u>CHAPTER 5 MODELLING WORK</u>	182
5.1 MODEL DESIGN CONSIDERATIONS	182
5.2 GEOMETRIC MODEL	185
5.3 MODELLING ANALYSIS INPUT	188
5.4 NUMERICAL RESULTS	196
<u>CHAPTER 6 DISCUSSION</u>	208
6.1 PROCESS OPTIMISATION	209
6.1.1 Material Selection	210
6.1.2 Powder and Particle Size Selection	215
6.1.3 Mixing Method	222
6.1.4 Powder Heat Treatment	223
6.1.5 Lubrication	227
6.1.6 Powder Pouring	228
6.1.7 Compaction	228
6.1.8 Ejection	230
6.1.9 Green Compact Handling	231
6.1.10 Sintering	231
6.1.11 Repressing	233
6.1.12 Composite Material Heat Treatment	233
6.1.13 Outline of the Process Optimisation Work Findings	234
6.2 NUMERICAL MODELLING	235
6.2.1 Model Design Considerations	236
6.2.2 Modelling Analyses	242
6.2.3 Outline of the Numerical Modelling Work Findings	253
6.3 MATERIALS DEVELOPMENT	254

<u>CHAPTER 7</u> CONCLUSIONS, CONTRIBUTIONS AND PROPOSED FURTHER RESEARCH	256
7.1 CONCLUSIONS	256
7.2 CONTRIBUTIONS	257
7.3 PROPOSED FURTHER RESEARCH	257
REFERENCES	260
APPENDIX A (Tensile Test Sample Dimensions)	A1
APPENDIX B (Kiln PLC Programming and Module Run Procedure)	B1
APPENDIX C (Results Data Information)	C1
APPENDIX D (Individual Sample Data)	D1
APPENDIX E (Publications Arising From The Present Work)	E1

ABSTRACT

Process Optimisation and Numerical Modelling of Powder Metallurgical Aluminium Matrix Composites

Gareth O'Donnell, B.Sc. (Eng.)

The present research focuses on optimisation of a novel application of the cold uni-axial pressing and liquid phase sintering powder metallurgical method to the processing of ceramic particulate reinforced aluminium matrix composites and the numerical modelling of these advanced materials. The investigated process areas include material selection, powder mixing and powder heat treatment, lubrication type, quantity and method, compaction and ejection, green sample conditioning, sintering time, temperature and atmosphere, and sintered compact heat treatment. The methods of analysis used include particle size, shape and H₂O content analysis, powder compressibility testing, ejection stress analysis, green strength testing, green compact and sintered material density measurement, macrohardness, compression and tensile testing, and both optical and scanning electron microscopy. The present numerical modelling work involves the development and use of a new geometrically versatile continuum mechanics based finite element analysis model capable of allowing the isolation of particulate volume fraction, size, and distribution variations and simulating the constitutive response of a specific composite material.

The process investigations have elucidated many of the factors affecting the mechanical properties of the final material and have found that small to medium sized net shape and near net shape aluminium matrix composite components may be produced by this conventional powder metallurgical processing method. It has been identified that the success of this process is strongly dependent on factors including aluminium powder and reinforcement particle size, powder heat treatment and component sintering conditions. Also, the present numerical model provides a method of predicting the response of these composite materials to thermal and mechanical loading, and allows for independent adjustment of the constitutive material properties and geometric model form to aid in the design of these versatile composites. The modelling investigations carried out indicate that internal stress development within a discontinuously reinforced metal matrix composite depends primarily on the proximity of particles, the relative orientation of particles in close proximity and the directionality of loading.

CHAPTER 1 INTRODUCTION

1.1 NEW MATERIALS

For many years traditional engineering materials, such as metallic alloys, polymers and ceramics, have been successfully developed by means of conventional materials science technology and elementary process design to meet the needs of industry. However, over the past four decades many specialised applications have required materials which can withstand combinations of stimuli including high multi-directional stress, thermal shock, thermal extremes, and also exhibit such characteristics as low density, high specific strength, high specific stiffness and high fracture toughness. These demanding requirements cannot be accommodated by the development of traditional materials. Consequently, a number of alternative materials have been developed. These advanced materials include solid thin films, functionally gradient materials, structural ceramics, and polymeric, ceramic and metal matrix composites [1-4]. Many variations of these new materials have been, and are presently being developed to both accommodate the further evolution of existing industries, and meet with the stringent demands of new technologies. In parallel and as a consequence of these developments many new processing technologies and advanced material design techniques, such as numerical modelling, have also emerged over the last four decades.

All areas of industry have been involved to some degree in the development of new materials to facilitate their needs. Many aerospace, military and scientific projects over the last three decades were made possible only by the project driven development of advanced materials. The US space shuttle, the Hubble space telescope and the US air force Stealth bomber are prime examples of the successful use of many materials

which were not available 30 years ago. Due to these developments a large number of new materials are now utilised in commercial aircraft, road vehicles and sports goods [4-9]. The present research detailed in this report focuses on the processing and computer aided numerical modelling of the advanced materials group referred to as metal matrix composites (MMCs).

1.2 METAL MATRIX COMPOSITE MATERIALS

1.2.1 Historical Developments

MMCs can be defined as materials consisting of a metal, or more normally a metallic alloy, as a primary or matrix material, which is combined with one or more dissimilar phases to produce a material with a range of properties superior to those of the individual constituent materials for a given application. The dissimilar phase or phases may be metallic alloys, intermetallic systems or ceramics [9-12]. Of these, the most common phase types used in MMCs at present are ceramic. In tracing the origins of this family of advanced materials, patented processing research carried out by Schmid in the mid-nineteen twenties on the consolidation of aluminium powder with fine alumina particulate can be seen as the first step in their development [13,14]. Materials of this type are referred to as dispersion strengthened metal systems, whereby strengthening of the matrix material occurs due to the dispersed fine non-metallic particles. In the particular case where the non-metallic particles are oxides, these materials are referred to as oxide dispersion strengthened (ODS) systems [15]. The main strengthening mechanism associated with these materials is the impedance of dislocation motion by the dispersoids within the matrix, which is described as the Orowan mechanism [14,16,17]. This mechanism can be described mathematically based on the circumvention of a moving dislocation around a dispersoid. The strengthening due to the dispersoids can be formulated from this mathematical description, leading to a mathematical model of the material strength. Very little load transfer, if any, takes place from the matrix to the minute non-metallic phase in dispersion strengthened systems, and therefore load bearing is carried out by the matrix material only. The size of the strengthening phase normally ranges from 10nm to 70nm for these materials.

In parallel with the development of dispersion strengthened systems came interest and research into precipitation strengthening in metallic alloys. The precipitation strengthening mechanism is also believed to be based on the impedance of dislocation motion and no load is carried by the strengthening precipitates. In this case however,

the impedance mechanism is mainly based on the shearing of precipitates by dislocation movement. As with the dispersion strengthened systems the degree of strengthening due to the precipitates may be described mathematically. The size of precipitates within these systems is normally well below that of the strengthening elements within dispersion strengthened systems. Precipitate sizes normally range from 1nm to 10nm. A distinct difference also exists between the origin of the reinforcement elements in each system. In dispersion strengthened systems the reinforcement is mixed with the matrix material and does not alter in chemical composition or form throughout processing. Conversely, in the case of precipitation strengthened systems the elemental materials that make up the precipitates are mixed with the matrix material and these elemental materials chemically combine during heat treatment to form precipitates throughout the matrix. The dispersion and precipitation strengthened systems have been extensively researched and developed over the past five decades resulting in many commonly available materials [18]. Both of these systems may be referred to as MMCs. However, the vast majority of recent MMC research and development has focused on systems more similar to that of the former, in that strengthening phase material is combined with the matrix and remains distinct.

1.2.2 Recent Developments

The experimental research carried out over the last 35 years in the field of MMCs has extended from the sub-micron systems of dispersion and precipitation strengthened materials. Interest in metallic materials reinforced with relatively large diameter continuous ceramic fibres grew rapidly in the nineteen sixties [14,19]. These continuous fibres typically range in diameter from 5 μm to 150 μm . The strengthening mechanism involved with these continuous fibre reinforced MMCs (CFMMCs) is based on the transfer of load from the matrix to the high strength fibres. Where the continuous fibre reinforcement is aligned in one direction only, many material properties can be modelled with reasonable accuracy [18] on the basis of the traditional rule of mixtures approach. The matrix simply provides a medium through which load is transferred. Therefore, the majority of the load is carried by the fibres.

However, although CFMMCs were found to exhibit excellent material properties, the material costs, production costs, primary and secondary processing technology and the problems of machinability made these materials unsuitable for many potential applications [19,20].

Due to these overwhelming economic and technical factors, interest in the research of CFMMCs declined dramatically during the nineteen seventies. Most further research and development of these composite systems has been carried out in connection with highly specialised military and aero-space applications [4,9,19,20]. In these applications the cost of the advanced composite material can be justified by the need to attain critical material properties. This trend of specialised application based research dominates the majority of present CFMMC related investigations [21-23]. The most well known continuous fibre MMC application at present is the fuselage support structure struts of the previously mentioned US space shuttle [2,3,19,24]. Continuous boron fibre reinforced aluminium alloy tubular struts are employed in the support structure due to the high specific strength (strength/density), high specific stiffness (elastic modulus/density), low coefficient of thermal expansion and the high temperature strength exhibited by the composite [3,19,20,24].

The decline of CFMMCs research activities during the nineteen seventies marked an increased interest in the development of discontinuously reinforced MMCs (DRMMCs) [14,19,25]. In the case of DRMMCs the strengthening inclusions may be in the form of whiskers, platelets, short fibres or particulate. The strengthening mechanisms associated with DRMMCs include load transfer from the matrix to the reinforcement, matrix microstructural refinement and dislocation density related strengthening. The increased interest in DRMMCs can be attributed to many factors. The reduction in raw material costs and composite production costs are substantial when changing from continuous to discontinuous reinforcement inclusions. Also, the production methods which can be applied to the primary and secondary processing of DRMMCs are far more wide ranging compared to the non-conventional production routes required for the production of continuous reinforcement systems [3,9,10]. The conventional, and near conventional production processes applicable to DRMMCs

include casting, powder metallurgy (PM), spray forming, and secondary processes such as extrusion, forging and rolling. Another intrinsic advantage of DRMMCs is the ease with which material properties can be altered to suit a specific application by the control of parameters such as reinforcement volume fraction, processing method and initial raw material selection [2,9,26-29]. This tailorability, in addition to the material cost and processing factors, has been of fundamental importance to the industrial interest in DRMMCs.

Due to the extreme strength of ceramic single crystal whiskers, these minute fibres became the prime alternative to continuous fibres in the mid-nineteen seventies. Research emphasis was placed on MMCs reinforced with Silicon Carbide (SiC) whiskers. The cost of SiC whiskers hindered their widespread use until 1973, when a production method was developed which allowed for the inexpensive production of β -SiC whiskers through the pyrolyzing of rice hulls [30,31]. This breakthrough led to the extensive development of composite materials containing whisker reinforcement [32]. The diameter of these whiskers typically range from 0.1 μm to 1 μm , and they may be between 1 μm and one hundred microns in length. These whisker reinforced composites were found to exhibit increased strength of up to 100 per cent compared to their unreinforced matrix materials. Unfortunately, all development related to ceramic whiskers decelerated rapidly in the mid-nineteen eighties when it was realised that SiC whiskers were both carcinogenic and toxic after inhalation [14,17]. The costs associated with adequate safe handling of these fibres became prohibitive.

Compared to whisker, short fibre and particulate reinforced composites, little research has been carried out on platelet composites. The cost of this form of reinforcement has not yet been sufficiently reduced to allow extensive development. However, some researchers have reported excellent material properties for these composites and it is believed that platelet reinforced MMCs may be found to be one of the successful composite systems of the future [9,14,17,33,34]. As a consequence of the safety hazards associated with whiskers and the elevated cost of platelets, strong emphasis is currently placed on the use of the less hazardous and relatively inexpensive forms of reinforcement which include short fibres and particulate.

1.2.3 Current Developments

Over the last decade the majority of MMC processing research has focused on particulate reinforced composites containing particles ranging in size from 1 μm to 150 μm . This interest in particulate reinforced MMCs (PRMMCs) is due to many cost related and technical factors. Due to their common use in polishing, grinding and cutting technologies, many particulate materials which are suitable for use as reinforcement are readily available and inexpensive [35,36]. This factor, coupled with the relative ease with which the particles can be combined with matrix materials through conventional, or near conventional processing, has made possible the availability of affordable MMCs.

Until recently DRMMC research mainly concentrated on the potential use of these materials in aerospace applications. This focus was due to the high specific strength and specific stiffness exhibited by these composites. Density related properties are of great importance in the selection of materials to be employed in aircraft design due to the direct relationship between fuel consumption and aircraft mass. However, the well documented low ductility of DRMMCs [9,24,35,37-45] has played a major role in preventing their widespread use in the commercial aircraft industry. Due to this factor the general application areas for DRMMCs have changed from aerospace to automotive and rail vehicle components, and sporting equipment [3,5-9,24]. The density related strength and stiffness characteristics are still of great importance for these applications. In the case of dynamic components such as brake discs, the reduced inertial forces achieved are very attractive [7]. However, also of major importance are the properties of high wear resistance, attractive high temperature strength, low coefficient of thermal expansion and high thermal conductivity [6,19]. Although it has been found that the magnitude of strengthening and increases in stiffness associated with particulate reinforcement is normally less than that of whisker and short fibre MMCs [37,38], in many cases the required properties for a particular application can be obtained by the use of a suitable volume fraction of particulate reinforcement. The combination of these application based, cost related and technical factors has had the effect of greatly increasing the development and use of PRMMCs.

1.2.4 Aluminium Matrix Composites

Various metallic alloys have been used as matrix materials for MMCs through both research and industry. These matrix materials include magnesium, beryllium, zinc, copper, iron, titanium and aluminium alloys [11,18,35,46-48]. However, other than aluminium, very few of these systems have been successfully applied commercially due to factors such as high manufacturing costs and lack of reliable materials data. The vast majority of MMC research has been based on aluminium composites. Table 1.1 lists examples of MMC systems which are presently produced commercially and their applications, showing the dominance of aluminium.

Table 1.1. Commercial MMC materials and applications.

MMC system [†]	Application	Company	Ref.
Al/B _{cf}	Space shuttle struts	Textron	[3,19]
Al/5% Al ₂ O _{3sf}	Piston insert	Art Metal Co. for Toyota	[3,24]
Al/20% Al ₂ O _{3p}	Drive shaft	Duralcan	[2]
Al/25% SiC _p	Aircraft rack	DWA Composite Spec.	[14,24]
Al-Si/20% SiC _p	Brake disc	Duralcan	[14,24]
Al-Si/12%Al ₂ O _{3sf} +C _{sf}	Cylinder block	Honda	[2]
Al-Mg-Si/10%Al ₂ O _{3p}	Bicycle frames	Duralcan	[14]
Al-Cu/20%SiC _p	Bicycle frames	BP Metals Composites	[24]
Ti-Al-V/15%TiC _p	Ballistic plates	Dynamet	[4,49]
Be/20-60%BeO _p	Electronic packaging	Brush Wellman	[11]

One of the primary factors which led to the initial focus on aluminium alloy matrix systems is the relative low density of aluminium alloys compared to ferrous alloys. With the change of emphasis from aircraft to ground based applications the specific strength and stiffness characteristics have become less critical and other material properties are recognised as having a strong influence on the selection of suitable matrix material. However, aluminium matrix composites (AMCs) are still by far the

[†] Subscripts cf, sf and p refer to continuous fibre, short fibre and particulate respectively and Al refers to aluminium alloys in all cases.

most widely researched and most highly developed systems within the family of MMCs [35]. This continued interest in AMCs can be attributed to many factors. Aluminium alloys have the advantages of exhibiting relatively high strength, being of low density, and being readily available. Also, many aluminium alloys exhibit attractive age hardening characteristics, good corrosion resistance properties, high formability and useful thermal and electrical properties. It has been found that many common ceramic reinforcement materials such as SiC and Al₂O₃ particulate are compatible with a variety of aluminium alloys [19,37,41,50,51] and can be used for the manufacture of particle reinforced aluminium matrix composites (PRAMCs). Based on these factors, the experimental materials investigated in the present work consist solely of aluminium composites.

1.3 MMC PROCESSING

Since the synthesis of the first MMCs in the mid-nineteen twenties [13] one of the most significant pitfalls encountered by researchers has been the lack of suitable processing technology. It was soon discovered that MMC production was complex, and that process design considerations would have to be altered from those required for conventional material manufacture. In the case of CFMMCs it was found that all conventional processes had degrading effects on the continuous fibres.

The novel process of diffusion bonding, which involves the hot pressing of continuous fibre preforms, or the pressing of alternate layers of matrix foils and fibre tows, was found to be the only process which could be utilised effectively for the production of CFMMCs [9]. More recently CFMMC production methods involving melt infiltration and modified casting processing have been developed [24]. Each of these methods involve specialised machinery, costly material preparation and novel process technology [9,10,52].

When considering the processing of DRMMCs many possibilities exist. The discontinuous reinforcement phase can be mixed into a melt and cast, blended with a matrix powder, pressed and sintered, or co-sprayed with metallic droplets. Alternative processes have also been developed which include perform infiltration or squeeze casting and XDTM (exothermic dispersion) processing. Both of these non-conventional processes have been developed in recent years in an attempt to increase the volume fraction of reinforcement which can be included in the composites, and also to overcome the problem encountered with the more conventional casting, PM and spray processes.

Due to the hard particle inclusions within these materials machining difficulties exist. However, research carried out in the areas of PRMMC machining optimisation, cutting mechanism modelling, novel machining methods and tool material improvement have led to cost effective machining practices [8,29,53-55]. In the case of conventional single point turning of PRMMCs many varieties of diamond coated

tools are now commercially available, which avoid the excessive rates of tool wear observed with the use of more conventional tooling [53].

In the past decade most successful MMC research, both industrial and academic, has been application driven resulting in a number of products being produced on a large scale, such as MMC engine blocks, diesel engine piston crowns, auto-engine connecting rods and light weight bicycle frames [2-8,19,37,56,57]. A number of other recent processing related developments which have indicated and encouraged industrial confidence in MMCs include the AlcanTM casting production facility development, mass production of cast MMCs by the LanxideTM corporation and the PM processed composites being produced by Aerospace Metal Composites Ltd. The advanced development of the OspreyTM, XDTM synthesis, CeraconTM, direct metal oxidation and preform infiltration processes also indicate the commercial viability of MMCs manufacture at a mass production level [2]. However, although MMC processing technology has reached both material characteristic requirements and economic success through these large scale applications, many researchers have stressed the extreme importance of the further refinement of existing routes and the development of alternative methods with the aim of increasing the applicability of these new materials, by reducing the cost of processing.

1.4 MMC MODELLING

Due to the current improvements in PRMMC processing technology these advanced materials are being used in, and targeted for, an expanding range of applications. Consequently, considerable research emphasis has been placed on the development of models capable of both predicting composite material properties and investigating the individual parameters which affect these properties. Due to many factors, modelling these inherently inhomogeneous materials has proved difficult. However, a comprehensive understanding of the mechanisms involved in composite deformation has grown through experimental research over the past decade, which has led to the development of a number of promising composite modelling methods.

The vast majority of PRMMC models are continuum mechanics based and the inclusion of subcontinuum parameters such as dislocation movement and matrix plasticity, are normally dealt with using phenomenological description [58]. The crystal plasticity based models consider crystallographic slip in a continuum mechanics framework, therefore avoiding complex dislocation motion based descriptions of deformation [58-60]. Analytical continuum models, such as those based on the Eshelby equivalent ellipsoidal inclusion method, have indicated relationships between PRMMC properties and the reinforcement shape, volume fraction and alignment [61,62]. The use of an aligned ellipsoidal inclusion in the Eshelby method allows for mathematically rigorous solutions to be obtained within a linear constitutive property range. However, the geometric and constitutive approximations assumed in Eshelby type models fail to accurately describe the largely irregular geometry of reinforcement commonly found in PRMMCs and impose difficulties in describing matrix plasticity [14]. Consequently, the majority of composite modelling research in recent years has focused on continuum based numerical methods, such as the finite element method (FEM). The FEM provides a powerful and flexible method of composite analysis capable of accommodating geometric complexity and constitutive non-linearities [63]. The present PRMMC modelling investigation utilises the power and flexibility of the FEM within a continuum mechanics based framework.

1.5 PRESENT RESEARCH

1.5.1 PRAMC Processing

In light of the need to further advance PRMMC processing, the present research focuses on the optimisation of the powder metallurgical (PM) cold pressing and sintering processing route applied to these new engineering materials. The composite systems investigated in the experimental analyses for this research consist of silicon carbide (SiC) particle reinforced aluminium alloys (AA6061, AA2124). The aim of this work is to contribute to the advancement of MMC processing technologies, thus enhancing the reliability, consistency and competitiveness of MMCs in the industrial market. The primary considerations regarding the accomplishment of these goals are founded upon low cost processing, consistent high quality material production and the material characteristics demanded by engineering industry.

1.5.2 PRAMC Modelling

As industrial interest in PRAMCs continues to grow, both a greater understanding of the micromechanics governing the composite material properties and modelling methods capable of predicting composite behaviour are required in order to further expand the application range of these attractive materials. Many existing modelling approaches simplify the description of PRAMCs by assuming that the composite can be represented by a regular array of reinforcement particles distributed evenly throughout a matrix material. However, real PRAMCs do not consist of regular arrays of aligned reinforcement particles. The new geometric composite model developed and used in the present work is based on a three-dimensional random array of short hexagonal prisms contained within a matrix material. This finite element method (FEM) micromechanical continuum based model is designed to analyse the effect of various parameters on the response of PRAMCs to applied loading. The loading and model parameters investigated in the present work include thermal strain, uniaxial tensile stress and both reinforcement volume fraction (5%, 10%, 15%, 20%)

and reinforcement size (20 μ m, 10 μ m). The material properties applied to the constituent elements of the model are those of the aluminium alloy AA6061 (T6) produced by powder metallurgy as the matrix, and SiC for the reinforcing particles.

1.6 OVERVIEW OF THESIS

Following from this introduction, chapter 2 summaries the literature survey carried out for this research and includes the topics of MMC processing, composite material characteristics, PM processing and existing composite mechanics theory and modelling methods. Since the primary matrix materials used throughout this research are aluminium alloys, the processing based sections of the literature survey focus mainly on aluminium based composite systems. Also, due to the continuum mechanics based nature of the present computational modelling investigations, the theoretical and modelling literature surveyed focuses primarily on continuum mechanics theory, applications and FEM investigations. Chapter 3 describes the experimental investigations carried out, including descriptions of the materials, processing equipment used and the test procedures carried out. The results obtained from the experimental work described in chapter 3 are presented in chapter 4. The composite modelling investigations carried out in the present work are detailed in chapter 5. This chapter includes detailed descriptions of the fundamental geometric model developed, the continuum mechanics considerations related to the present model, the numerical methods employed for model computation and the results obtained from this work. Discussion based on the experimental and modelling work is presented in chapter 6. Finally, chapter 7 draws conclusions from the present research, highlights the contributions arising from this research and pin-points areas of research which may further contribute to this field of study.

CHAPTER 2 LITERATURE SURVEY

2.1 COMPOSITE MATERIALS

2.1.1 Composite History

Many examples of composites can be found in history, where man realised that by combining materials with differing properties a new composite material could be produced which would exhibit a combination of these properties suitable for a particular application. Table 2.1 lists examples of these composites and their applications.

Table 2.1. Examples of historical and recent composite materials.

Year	Composite material	Application	Reference
8000 BC	Clay mixed with sand and mica	Ancient Japanese Jamon Pottery	[64]
800 BC	Straw reinforced concrete	Structural Building Material	[9]
1867	Iron mesh reinforced concrete	Tubes, Plant Pots	[65]
1950	Fibre glass reinforced polymers	Filament-Wound Rocket Motor	[3]
1975	Boron fibre reinforced aluminium	US Space Shuttle	[2,3,19,24]
1989	SiC fibre reinforced SiC	SNECMA M53 Engine	[57]

Modern engineering composites have had a major impact on the materials market over the last 50 years. These composites can be seen in many everyday applications. Table 2.2 lists some common composite materials and their application areas. The development and application of engineering composites has grown in line with the growing demands of both advanced and conventional engineering technologies. At present many monolithic materials are being replaced by superior advanced engineering composites.

Table 2.2. Common engineering composite materials and their applications.

Composite Type	Application
Fibre glass reinforced polymers	Sail boats, Sports equipment, Baths, Shower basins, Industrial piping, Pump housings, Static and dynamic aircraft components, Motor car body parts
Metal wire reinforced rubber	Car tyres
Laminated glass	Impact resistant windscreens
Reinforced aluminium	Advanced bicycle frames, Honda Prelude™ engine blocks, Motor car driveshafts
Metal wire reinforced ceramics	Prosthetic implants
TiC cermet	Cutting tools

2.1.2 Engineering Composites

An engineering composite can be defined as a material comprised of two or more macroscopically distinct materials which exhibit interfacial bonds and are physically distinguishable. The three engineering composite groups of greatest importance to materials science researchers and design engineers are the polymer, ceramic and metal matrix composites, referred to as PMCs, CMCs and MMCs respectively. The material combinations for each of these groups are described in figure 2.1.

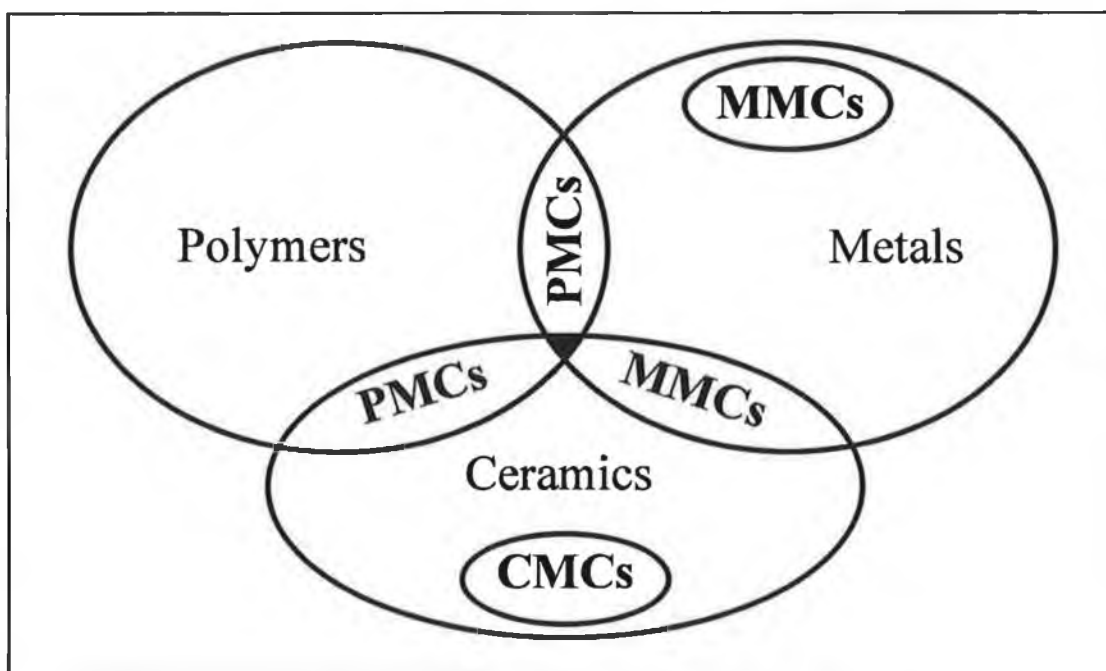


Figure 2.1. Monolithic material groups and the material combinations used to create engineering composites. PMCs, CMCs and MMCs refer to polymer, ceramic and metal matrix composites respectively.

The aim of these composites is to achieve a combination of material properties superior to those of any of the individual constituent materials, for a given engineering application [9]. A comparative schematic representation of the developmental and applications history of each group can be seen in figure 2.2.

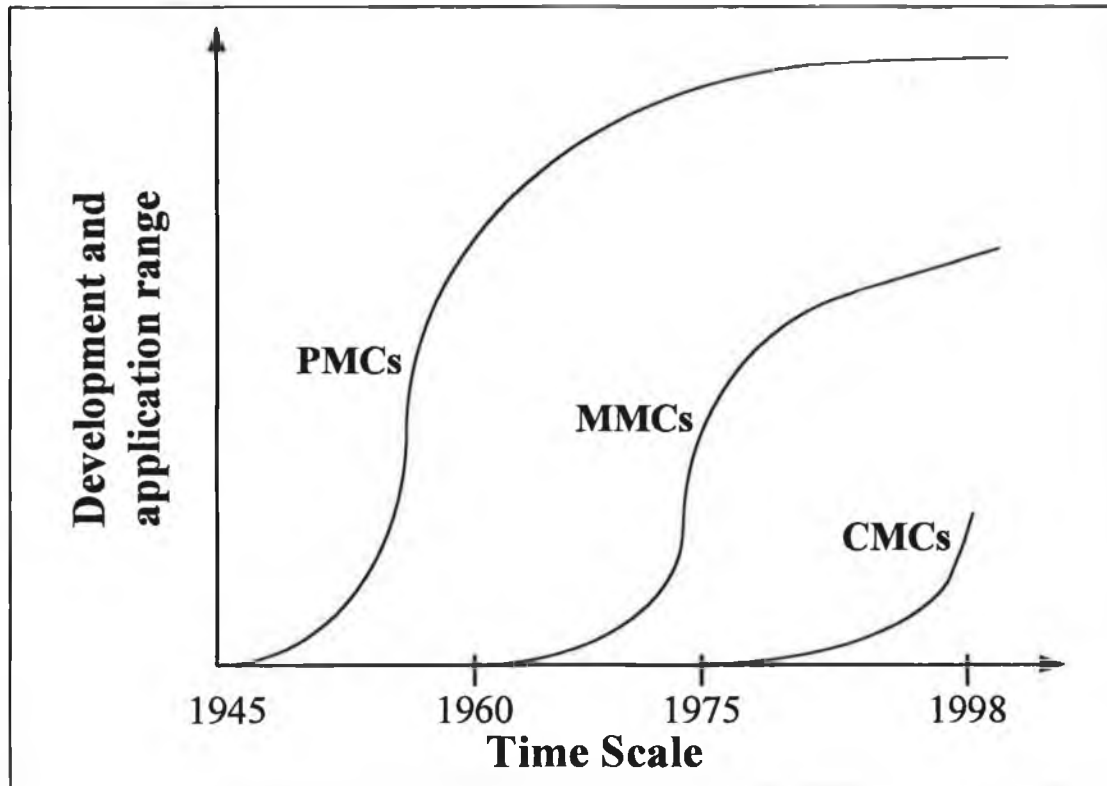


Figure 2.2. Schematic representation of the developmental and application history of the three engineering composite groups.

The convention normally used to describe a composite material is based on both the composite group to which the material belongs, and the geometry of the reinforcing phase used. Figure 2.3 describes the various reinforcement geometries commonly employed in engineering composites. Continuous fibre reinforced composites include one, two and three dimensional reinforcement systems. The dimensional based description of these materials is due to the anisotropic strengthening which is observed in composites containing parallel fibres only. Therefore, the dimensional based description primarily relates to the directionality of the strengthening caused by the fibre reinforcement type used. Discontinuously reinforced composites are normally described by the geometry of the reinforcing phase which include short fibre, whisker and particulate. Anisotropic properties can also be observed in the case of these composites. However, the extent of this anisotropy is negligible compared to that of continuous fibre reinforced systems, and is therefore not included in their description.

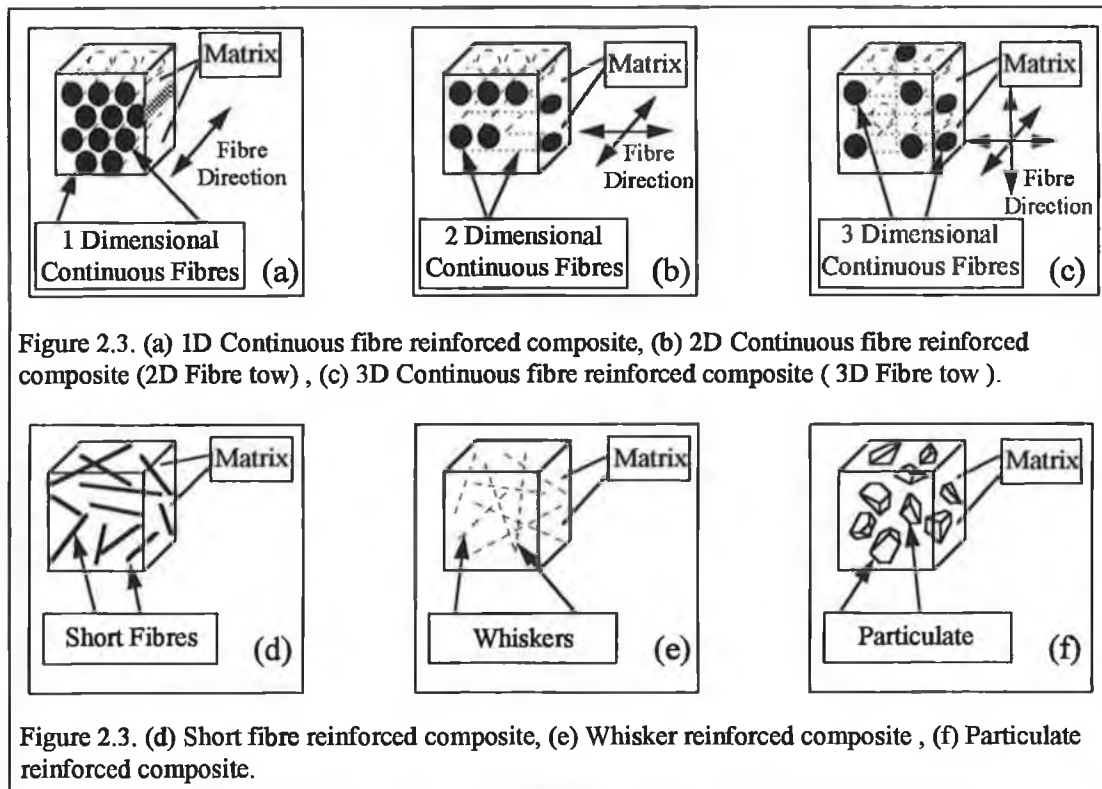


Figure 2.3. Composite systems description based on the form of reinforcement.

Composite systems other than those described in figure 2.3 have also been developed. Such systems include laminated composites, platelet reinforced composites and hybrid composites containing more than one reinforcement type [3-5,66,67].

2.1.3 Polymeric Matrix Composites

In the nineteen forties, during World War II, it was realised that although aluminium alloys could provide the high specific strength (strength/density) and high specific stiffness (elastic modulus/density) required in aircraft structures, problems relating to corrosion and fatigue of these materials needed to be addressed [3]. Due to this situation researchers began to concentrate on improving the mechanical properties of polymer based composites to replace the aluminium alloys. By the end of the war in 1945 glass fibre reinforced polymers had been successfully used in various applications [3]. Consequently the composite group known as PMCs grew rapidly.

PMCs can be described as a polymer, or combination of polymers (matrix material), combined with a non-polymeric reinforcement which enhances the overall properties of the final material compared to the matrix material alone. Table 2.3 lists some of the polymers and reinforcement types which are used to manufacture PMCs.

Table 2.3. Common PMC matrix materials and reinforcing fibres [3].

Polymers
Polyester, Vinyl ester resins, Epoxy resins, Bismaleimide resins, Polyimide resins, Polyether etherketone (PEEK), Polyphenylene sulfide (PPS)
Fibre reinforcement types
Aluminium Oxide, E-Glass, S-Glass, Carbon (Pitch & Pan based Graphite), Aramid (Kevlar TM 49), Boron, Silicon Carbide

PMCs have found a large number of applications in a wide variety of areas such as sports equipment (tennis rackets, canoes and golf club shafts), household goods (electrical appliances, bath tubs and shower basins), aircraft parts (rudders, flaps and rotor blades) and industry components (chemical resistant piping and motor drive

shafts) [3,57]. Near net shape PMC component production is often possible through the use of the most frequently employed method of PMC processing referred to as lay-up [3]. The lay-up procedure involves the manual or automated layering of previously prepared polymer composite sheet. These sheets are referred to as prepregs due to the resin impregnation process used in their manufacture. The prepregs contain a combination of either the reinforcement and final matrix polymer, or the reinforcement and a polymeric precursor resin depending on the thermoset or thermoplastic nature of the polymer matrix.

Due to the complexities of these non-conventional processes the material costs are normally considerably higher than those of monolithic polymers or metals for a given application [3]. However, the attractive density related properties of many polymer based composite systems have justified their use in many specific strength and specific stiffness sensitive applications. The polymeric properties combined with the properties of the high strength reinforcement have placed PMCs at the forefront of low temperature engineering applications technology [57]. At present PMCs are by far the most extensively used engineering composite group.

2.1.4 Ceramic Matrix Composites

Monolithic engineering ceramic materials are known for their high compressive strength, hardness, low density and resistance to chemical attack, wear and high temperature environments. However, ceramics are inherently brittle and exhibit inadequate thermal shock resistance for many potential applications [68,69]. In order to utilise the advantageous properties and overcome the inadequacies of monolithic ceramics researchers are presently developing many ceramic matrix composites [70].

CMCs can be described as materials consisting of a ceramic matrix and a reinforcing phase. This group of composites is one of the most recent additions to the field of materials science. The vast majority of CMC research and development has taken place over the last 25 years [64], and has been aimed at highly specialised application areas.

Table 2.4. CMC matrix and reinforcement materials [3,68].

Matrix
Carbon (C), Alumina (Al_2O_3), Mullite ($3\text{Al}_2\text{O}_3 \cdot 2\text{SiO}_2$), Silicon Carbide (SiC), Silicon Nitride (Si_3N_4), Boron Nitride (BN), Sialons ($(\text{Si},\text{Al})(\text{O},\text{N})_4$) based ceramics
Reinforcement
Silicon Carbide based fibres (SiC + various ceramics), Alumina, Carbon fibres (C), Boron fibres (B), Silica and Metallic glass fibres, Boron Nitride/Carbide fibres (BN)/(B ₄ C), Metallic fibres, Boron Carbide (B ₄ C), Alumina based fibres (Al_2O_3 + various oxides), Silicon Carbide

Table 2.4 lists some matrix materials and reinforcement materials which have been used in the manufacture of these composites. As can be seen from table 2.4, CMCs are generally made up of a ceramic matrix combined with a ceramic reinforcing phase. Some examples of CMC systems which have been produced include carbon fibre

reinforced carbonaceous matrix materials, silicon carbide whisker reinforced alumina and continuous carbon or silicon carbide fibre reinforced silicon carbide or silicon nitride [3,68,70].

The main advantages of CMCs include high temperature strength, thermal shock resistance, corrosion resistance, microstructural stability under thermal cycling and thermal deformation resistance. Due to these characteristics CMCs have been used as after burners components in high performance jet engines, and for other extreme temperature applications where material density is also a major consideration [68,70].

Many CMC processing methods have been investigated [3,71,72]. These processes include hot pressing, chemical vapour infiltration, reaction synthesis, chemical vapour deposition and cold pressing and sintering [3]. In addition, a number of novel processes have recently been successfully developed. These include the directed metal oxidation process (DIMOXTM), the polymer infiltration and pyrolysis process (PIP) using the pre-ceramic polymer CERASETTM [71], and reaction based powder metallurgical technique for the processing of alumina-aluminide composites. Although these advanced processes have been used to produce CMCs which exhibit suitable properties for many advanced thermal applications, the raw material and processing costs prohibit the use of these materials. Due to the processing complexities and the costly raw materials required for the production of CMCs manufacture has become highly specialised over the last decade. Currently CMC applications are almost exclusively within the advanced aerospace, aircraft and military areas where the high costs can be justified by specific material requirements. One example of the successful application of CMC material is the silicon carbide coated carbon reinforced carbonaceous matrix materials used as a thermal protection material in the US space shuttle [57]. Considerable raw material cost reduction, processing refinement and improvement in both material predictability and reliability are required before the true potential of these materials may begin to be exploited.

2.2 METAL MATRIX COMPOSITES

MMCs can be described as materials consisting of a metal or metallic alloy (matrix material) reinforced with a non-metallic or distinctly different metallic phase. These composites have historical origins dating as far back as 7000 BC in Turkey, where copper awls produced by repeated folding and hammering have been found to contain non-metallic inclusions which strengthened the copper matrix [14]. However, as described in section 1.2.1, it was not until the mid-nineteen twenties that any significant metallic composite processing research began [13]. At this time composites in the form of dispersion hardened metal systems became recognised as engineering materials which could improve on the mechanical properties of alloyed systems. Over the following three decades both precipitation and dispersion hardened materials were researched extensively, and are now well established in the materials market [18]. In more recent years the developmental direction of metallic based engineering composites has shifted from these minute reinforcement systems to composites reinforced with relatively large continuous and discontinuous phases.

In the nineteen sixties substantial interest in continuous fibre reinforced metal matrix composites (CFMMCs) grew in parallel with the availability of this form of reinforcement [9,24]. This interest declined rapidly at the end of the decade due to both the high cost of the fibres, and the difficulties involved in material processing [9,14,35]. Discontinuously reinforced metal matrix composites (DRMMCs) became attractive alternatives.

MMCs exhibit high specific strength and stiffness, good creep resistance and low density. These properties are of paramount importance in applications such as aircraft and spacecraft structural materials, automotive and aero-engine components, and applications where low inertial momentum is desirable [8,9,29]. Other attractive attributes associated with MMCs are high wear resistance, low coefficients of thermal expansion, high temperature strength and good corrosion resistance. In addition to these material attributes, MMCs can be specifically tailored to suit a particular

application [2,26-29]. This material property tailoring is normally achieved by varying such parameters as the volume fraction of reinforcement, the reinforcement size or the reinforcement form.

Unfortunately, these versatile materials are difficult to process and generally exhibit low ductility and low fracture toughness compared to their matrix materials. The inferior tolerance to fracture compared to existing materials has prevented the widespread application of MMCs in the aircraft industry, where major cost saving would be made due to the density related properties of these composites. However, recent processing developments and successful MMC applications indicate that the future of these materials is promising [5-8]. Table 2.5 lists matrix materials, reinforcement materials and reinforcement types which have been used as the constituent materials for MMCs.

Table 2.5. Matrix and reinforcement materials used in MMCs [9,11,18,35,38,46-49].

Matrix alloys systems
Aluminium, Titanium, Magnesium, Copper, Iron, Beryllium, Zinc, Bronze, Nickel, Lead, Silver, Superalloys (Nickel and Iron based)
Reinforcement
Silicon carbide (SiC) [continuous, short fibre, whiskers, particulate, platelets] Alumina (Al ₂ O ₃) [continuous, short fibre, whiskers, particulate, platelets] Titanium carbide (TiC) [continuous, particulate] Carbon (C) [continuous, short fibre] Boron (B) [continuous], Boron Carbide (B ₄ C) [particulate] Silicon Nitride (Si ₃ N ₄) [particulate, whiskers] Titanium Diboride (TiB ₂) [continuous] Stainless Steel [continuous filament]

2.2.1 Matrix Materials

MMC matrix material is either a pure metal or, more commonly, a metallic alloy. The metal alloys most frequently employed at present include aluminium, titanium, magnesium and copper alloys. Of these aluminium matrix composites (AMCs) are by far the most common MMCs [35]. They are employed in, and targeted for, applications where low density, high strength, high stiffness and corrosion resistance are of critical importance. Some aluminium matrix alloys which have been investigated are listed in table 2.6. The most frequently researched aluminium alloys include AA6061[†], AA2014, AA2124 and A356.

Table 2.6. Various aluminium alloy groups used as matrix materials [20,26,73].

Alloy Group	Designation
Al-Mg	A356 Duralcan TM , AA5082
Al-Cu	AA2219
Al-Cu-Mg-Si	AA2009, X2080 Innometal TM , AA2014, AA2048, AA2124,
Al-Mg-Si-Cu	AA6061, AA6090, AA6013
Al-Zn-Mg-Cu	AA7064, AA7075, AA7475, AA7090, AA7091
Al-Li-Cu-Mg-Zr	AA8090
Al-Fe-V-Si	FVS0812
Al-Si-Mg	A359 Duralcan TM

Titanium alloys such as Ti-6Al-4V have been combined with SiC for use in high temperature applications ($< 650^{\circ}\text{C}$) [49]. However, titanium matrix composites are still very expensive to manufacture and have only been tested for use in a number of specialised dynamic aero-engine applications [2,3,10,11,14,24,57,74,75]. Interest in magnesium matrix composites has grown over the last 5 years mainly due to the greater property improvements possible compared to AMCs [35]. Relatively little research has been carried out on other metallic based composites.

[†] AA refers to the Aluminium Association

2.2.2 Reinforcement

As can be seen in table 2.5 a large number of reinforcement types exist in various geometric forms. In the case of MMCs the vast majority of reinforcement is ceramic. Reinforcement materials can be divided into two main categories, continuous (figures 2.3 a, b and c,) and discontinuous (figures 2.3 d, e and f).

Continuous Reinforcement

Continuous fibres can be supplied as mono-filaments (single fibres) or multi-filament tows (woven/braided fibres). Due to the technology required to produce continuous fibres this form of reinforcement is very expensive compared to discontinuous reinforcement. Commonly available fibres include Boron, Borsic, Carbon, NicalonTM (SiC based fibres) and Saffil[®] (Al₂O₃ based fibres).

The mechanical properties recorded for continuous fibre reinforced MMCs (CFMMCs) show that these materials offer great potential [10]. However, due to the high cost of the reinforcement, relatively few applications have been found for these MMCs. One application is in turbine engine components, making use of CFMMC's high strength and resistance to thermal expansion [2].

Discontinuous Reinforcement

The three main geometric forms of discontinuous reinforcement employed in the processing of MMCs are whiskers, short fibres, and particulate. Discontinuous ceramic whiskers have been employed as reinforcement for many MMCs. They generally have an aspect ratio (length/diameter) of between 10 and several hundred, and are normally prismatic or acicular in shape. Whiskers are mono-crystalline (single crystals) and have extremely high tensile strength due to their defect free nature. The diameters of these single crystals typically ranges from 0.1µm to 1µm and whiskers can have lengths of up to one hundred microns. MMCs produced using this form of reinforcement have generally exhibited enhanced mechanical properties over comparable particle reinforced composites [37]. However, it has been found that

whisker agglomeration is common and that this agglomeration can have adverse effects on the final material strength [38].

It has also been reported that due to the size and shape of these minute single crystals they can easily become airborne and subsequently inhaled or ingested [17]. Whiskers, when touched, inhaled or ingested, perforate the skin, lungs or digestive tracts causing extreme irritation. It is also believed that SiC whiskers, which have been the most commonly used single crystals, have carcinogenic effects [17]. These health factors were recognised in the early nineteen eighties giving rise to a substantial decline in the production and use of whiskers in MMC research. However, in the last nine years there has been a noticeable increase in whisker related research [66,67,76-81]. The results of these recent investigations have again highlighted the improvements to thermo/mechanical and mechanical properties achievable with the use of this form of reinforcement [80,81].

Short fibres are polycrystalline fibres which are normally available in larger diameters but smaller aspect ratios compared to whiskers. The tensile properties of these fibres are not as attractive as whiskers [14]. Also, when combined with a matrix material, holding volume fraction constant, the spatial distance between fibres increases compared to whiskers, which directly effects material properties. However, health and safety risks are greatly reduced with handling short fibres compared to whiskers and they are therefore an acceptable alternative reinforcement. Alignment of these fibres can be desirable and may be achieved by processing such as extrusion and rolling. Unfortunately, both whiskers and short fibres have the disadvantage of undergoing breakage during deformation processing which leads to a reduced reinforcement aspect ratio, creates possible points of crack initiation and may also aid in crack propagation. Although both short fibre and whisker reinforced MMCs have been found to exhibit attractive material properties, the high cost and processing difficulties associated with these composites have restricted their development and application. The most commonly available whisker and short fibre materials are SiC and Al_2O_3 .

Particulate reinforcement is the least expensive and the most readily available form of reinforcement due to the use of particulate ceramics in the abrasives, grinding and cutting tool industries. Considerations involved when choosing from the wide range of particulate available include particle size, shape and morphology, chemical purity, cost, mechanical properties and matrix to reinforcement compatibility. Particle diameter generally ranges from $1\mu\text{m}$ to $150\mu\text{m}$.

Particulate reinforcement has the major advantage over other forms of reinforcement of being reasonably compatible with most conventional processing routes such as casting, spray deposition, and being particularly compatible to the powder metallurgy processing route. Although less than that of continuous fibre, short fibre or whisker reinforcement, substantial improvements in material properties can be achieved by incorporating this particulate type reinforcement within a matrix compared to unreinforced matrix material [19,35-38,82]. Also, an advantage of particulate reinforced MMCs (PRMMCs) over the other forms of MMCs is isotropy of their material property.

Compared to handling difficulties and safety hazards associated with whiskers, particulate reinforcement can be handled easily and safely without the need for specialised equipment. Prolonged exposure to particulate materials can cause serious irritation of the skin and respiratory system [17,83]. However, to avoid these problems simple preventative and precautionary measures such as the use of suitable respiratory and skin protection are adequate.

Due mainly to the property improvements achievable, the low cost and availability of particulate materials, and the processing compatibility of particulate reinforced materials to conventional technology, PRMMCs are presently the most extensively researched and most widely applied MMC type. The most regularly used particulate reinforcing materials are SiC, Al_2O_3 , Si_3N_4 , TiC and B_4C . Due mainly to the reported compatibility between many aluminium alloys and SiC particulate [37], aluminium matrix composites (AMCs) reinforced with SiC particulate are presently the most commonly researched and applied MMC systems.

Figure 2.4 shows the range of ultimate tensile strengths measured for AMCs reinforced with various forms of reinforcement compared to that of common monolithic aluminium alloys [2,4,14,83]. It can be seen that the strength improvement provided by the continuous fibres is far greater than either the whisker or particulate. However, in comparison to continuous reinforcement, the advantages of employing discontinuous forms of reinforcement are the reduced material cost factors, the ability to produce DRMMCs by near conventional processing methods and the significant improvements in material strength achieved compared to the monolithic matrix material.

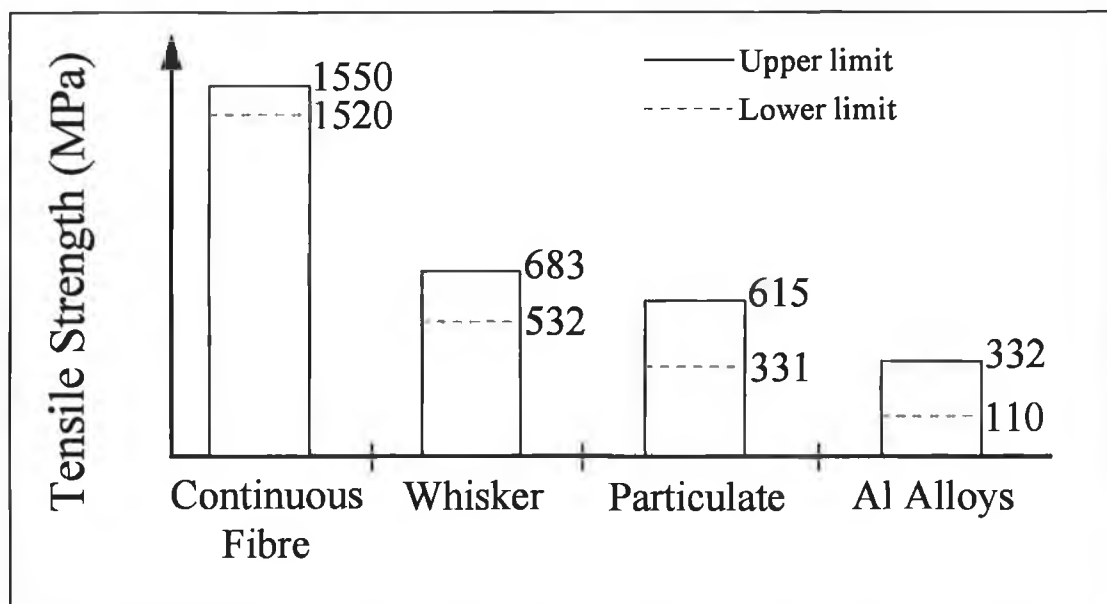


Figure 2.4. Reinforcement form effect on AMCs / Al alloys ultimate tensile strength [2,4,14,83].

2.2.3 Effects of Combination

The primary objective of combining high strength reinforcement with a comparatively weak metallic material is to improve on the material properties of the metallic material. In the case of CFMMCs the composite material exhibits far greater strength and stiffness compared to the unreinforced material. These improvements are attributable primarily to the load transfer from the metallic matrix to the reinforcement [21]. The extent to which the strength and stiffness of the composite material exceeds that of the unreinforced metallic material is dependent on the properties of the reinforcement and matrix materials, the fibre content and the both the extent and strength of the bonding between the materials. The interfacial bond between the reinforcement and the matrix is created during the processing of the composite. The extent and strength of the interfacial bonding depends on the chemical compatibility between the reinforcement and the matrix, the processing method and the processing parameters applied [21].

In addition to the load transfer mechanism, the inclusion of continuous fibre reinforcement has the affect on altering the material properties of the metallic material to which it is combined [25]. Both the strength and stiffness exhibited by the matrix material within the composite are greater than that of the unreinforced material. This effect can be explained by the stress fields created within the matrix material during cooling from the processing temperature. The strain due to the stress fields caused by the difference between the coefficient of thermal expansion of the matrix and that of the fibre (thermal strain), can have a decisive effect on the properties of the matrix material [2,10]. Therefore, the two main strengthening mechanisms associated with CFMMCs are load transfer and thermal strain induced matrix strengthening.

In the case of DRMMCs the load transfer from the matrix to the reinforcement and the thermal strain induced matrix strengthening are also important strengthening mechanisms. However, in addition to these mechanisms many other mechanisms significantly affect the overall properties of the composite. These additional mechanisms include constrained plastic flow, internal localised stress concentration,

refined precipitation strengthening and matrix grain refinement [63]. Therefore, the overall properties of a DRMMC depend on the factors affecting all of these contributing mechanisms. These factors include the constitutive properties of the devisable phases, the reinforcement quantity, size and size distribution, the reinforcement shape, surface morphology and distribution throughout the matrix, and also the chemical compatibility between the reinforcement and the matrix material. The processing methods and processing parameters used during production also have a very strong influence on these factors [38].

Unfortunately, the strengthening effect of combining discontinuous reinforcement with a metallic material is normally accompanied by a drop in ductility. The reduced ductility can be attributed to a number of factors such as poor interfacial bonding during processing, fracture of large reinforcement particles, inclusion of undesirable brittle reaction products formed during processing, reinforcement clustering and thermal stress induced ductility reduction of the metallic material [35]. It has been suggested that, in order to maximise the ductility of a composite containing a particular volume fraction of reinforcement the reinforcement must be homogeneously distributed and small in size ($<10\mu\text{m}$) [35]. Also, the processing of the composite must result in the formation of strong interfacial bonds devoid of undesirable reaction products.

2.3 MMC PROCESSING

The objective of MMC primary processing is to form a fully consolidated or partially consolidated combination of the matrix and reinforcement materials. Over the past decade MMC research has concentrated primarily on the refinement of existing processing methods and the development of new processes with the aim of reducing the cost of manufacture and improving both material ductility and process repeatability. Due to the relationship between reinforcement clustering and both low ductility and material consistency [84], one of the main processing challenges involved with DRMMC production is to achieve a homogenous distribution of reinforcement throughout the matrix material.

The primary MMC production methods include casting, infiltration, physical vapour deposition, spray deposition, in-situ (reactive) processing, diffusion bonding and powder metallurgy. In the following sub-sections the salient attributes of each processing area are outlined in order to provide an overview of the material and processing constraints involved in the production of MMCs. Due to the use of the powder metallurgical (PM) processing route in the present experimental research, PM processing is described separately in detail in section 2.4. Also, due to the discontinuous form of reinforcement investigated in this research, an emphasis is placed on the processing of DRMMCs.

2.3.1 Casting

Casting is one of the oldest and in many cases most cost effective forms of primary metal processing. When this economically attractive route was first applied to the production of MMCs it was found that many problems arose due to the inclusion of reinforcement [2,14,35,38,84,85]. These problems include the settling of the reinforcement, the reduction of melt fluidity at conventional melt temperatures, undesirable interfacial reactions at high casting temperatures, residual porosity, particle agglomeration and particle segregation. In spite of these initial observations interest in the area of MMC casting continued due to the low cost potential of the casting process [2,14]. MMC casting research has led to the development of casting methods which involved melt stirring and pressure assisted casting and rapid solidification [19,35,86]. These alternative processes overcome many of the problems related to the conventional casting of MMCs. However, interfacial reactions and segregation during solidification can still be observed. The extent of the interfacial reaction is primarily related to the melt temperature and the chemical composition of both the matrix and reinforcement material.

The segregation of reinforcement which can occur during casting solidification is dependent on the rate of solidification. Rapid cooling has the effect of reducing segregation. Reinforcement inhomogeneity can also be minimised by secondary processing such as extrusion or rolling [35]. These material and process alterations add to the processing cost and therefore, make the casting route less attractive.

Alcan Aluminium Ltd, San Diego, U.S.A., successfully produce cast aluminium alloys reinforced with SiC and Al₂O₃ on a commercial scale by the DuralcanTM proprietary compocasting method [86]. The process is primarily designed for the production of aluminium matrix composites containing particulate reinforcement. In this process interfacial reactions are minimised by reinforcement coating and the addition of large quantities of silicon to the aluminium alloy [35,86-89].

Compocasting, also referred to as either slurry casting or stir casting, has been developed from the basic principles of rheocasting. Rheocasting involves the continuous agitation of a solidifying liquid metal slurry. The effect of this agitation in rheocasting is to break up dendritic structures as they form, therefore creating spherical particles and maintaining sufficient fluidity of the slurry for adequate flow and mould infiltration. Compocasting also employs this principle of maintaining low viscosity by agitation but not by the breaking up of dendrites as in rheocasting [14,20]. Instead, this agitation encourages wetting, breaks up agglomerates of the reinforcing phase and aims to minimise sedimentation, all of which will reduce the melt viscosity [85,86]. Following the mixing process the composite melt is cast. Rapid solidification die casting has been employed for the production of MMCs in order to minimise segregation.

Die cast MMCs have shown positive results regarding segregation, however this form of casting is costly and requires high fluidity which can increase the possibility of interfacial reaction due to the high temperatures involved [14,35]. In the case of AMCs melt temperatures no more than 150°C above the liquidus temperature of the matrix can be used. Above this temperature undesirable chemical reactions will occur between the molten matrix and the reinforcement. These reactions can produce water soluble Al_4C_3 and adversely affect the matrix alloy composition [88,90]. Although conventional casting is a relatively inexpensive processing route compared to powder metallurgy or spray deposition, the specialised equipment and the processing conditions required for the casting of net shape or near net shape MMCs substantially affect the final processing cost.

2.3.2 Infiltration

Infiltration of a reinforcement preform has been found to be a very useful method of MMC production. Three infiltration routes have been investigated which include pressure driven, pressureless and vacuum driven infiltration. Other novel processes such as low pressure vibration assisted processing, electromagnetic infiltration and centrifugal force driven infiltration have also been investigated [2]. The basic principle of the infiltration process is to infiltrate a porous preform of reinforcement material with a molten matrix material and, in so doing, produce a composite material. In the case of both the pressure driven and vacuum driven processes the need for an applied pressure to aid infiltration is mainly due to the lack of spontaneous wetting of the reinforcement by the liquid metal. Also, other factors such as viscous and capillary forces influence the process [91,92].

Pressure Driven Infiltration

Also referred to as squeeze casting and squeeze infiltration this process has found a number of practical applications and has become an economically viable MMC production process. Pressure is applied to the molten matrix material which is in turn forced to infiltrate a reinforcement preform. This applied force overcomes viscous friction, capillary effects and can also influence processing speed, chemical reactions, matrix microstructure and can minimise deformation due to shrinkage during solidification.

Both mechanical and gas-driven systems have been utilised [2]. Mechanical systems generally operate at pressures of between 10 MPa and 100 MPa. Gas systems are restricted by safety factors which limit the maximum pressure to approximately 17 MPa. This process produces virtually pore free composites. However due to the application of pressure, preform deformation and fracture may occur. Al_2O_3 reinforced Al alloy engine piston inserts produced by this process have been manufactured by Toyota Motor Co. and Art. Metal Manufacturing Co., and used to replace Ni cast iron inserts [2,20,24].

Vacuum Driven Infiltration

The localised vacuum, on which this process depends, is created within the reinforcement preform due to chemical reactions which take place during infiltration. This process has been applied to the production of composites which combine alumina fibres (Du Pont FP fibres) with Al-Li alloys [2]. In the case of these Al-Li composites the vacuum is created due to the reduction of alumina by lithium. Excessive reduction of the alumina can degrade these fibres. Therefore the control of the lithium content is hugely important. Another process makes use of the oxidation of Mg as it infiltrates either Al_2O_3 or SiC preforms. This creation of MgO produces a vacuum ahead of the infiltrating molten Mg which promotes further infiltration. Both of these processes are dependent on the matrix and reinforcement phase chemical characteristics and are therefore limited to these materials [2,20].

Pressureless Infiltration

Spontaneous wetting has been found to occur in certain situations which can eliminate the need for an external force. The advantage of pressureless processing is that since no force is applied, there is little chance of preform deformation or reinforcement fracture. Systems such as titanium-carbide reinforced steel and also some nickel based alloys exhibit good wetting characteristics and have been produced by pressureless means. A number of methods have been developed so as to encourage spontaneous wetting. Fibres have been coated with Ti and B prior to infiltration by aluminium [2] and the LanxideTM Corporation have developed a process where by Al-Mg alloys can infiltrate ceramic preforms in a nitrogen rich atmosphere at a temperature between 750°C and 1050°C without external pressure [20,35]. These processes are quite slow and require a very high degree of process parameter control, and are therefore very expensive [2,10,20,71].

2.3.3 Physical Vapour Deposition

Physical vapour deposition (PVD) in the context of MMC processing involves the vaporising and subsequent condensation of metal onto continuous fibres. This process is then followed by either a hot isostatic pressing (HIP'ing) or a diffusion bonding operation. Reinforcement volume fractions of up to 80% with very uniform distribution have been obtained [14]. Three main processing methods exist which include evaporation, ion beam plating and sputtering [10]. Evaporation PVD is the most common deposition method due to the relatively fast deposition rate achievable. It involves the application of an electrical voltage between a molten metal and the reinforcement fibre bundle. Metallic vapour is deposited from the melt to the fibres. This process takes place in a high vacuum chamber. Ion beam plating relies on the bombardment of the reinforcement material by ions of both the coating metal and the atmospheric gas (normally argon) and generates a very dense deposition. Sputtering, which is the slowest of the three methods, occurs in a similar way to ion plating but has the advantage of being applicable to a wide range of materials.

Overall, the PVD process has many advantages related to material properties and highly specialised composite materials have been produced on an industrial scale by Sumitomo Electric for thermal shock applications [2]. There are little or no chemical reactions between the matrix metal and the reinforcement material. Also, the high percentage of reinforcement and the uniformity of its distribution delivers composite materials with excellent mechanical properties. However, due to the use of expensive continuous fibres, non-conventional processing equipment and very slow production rates this process has little potential other than as a fibre coating method.

2.3.4 Spray Deposition

A number of spray deposition processes have been developed [14]. In the majority of these processes molten metal and solid discontinuous reinforcement are sprayed simultaneously onto a substrate where solidification occurs. The alternative method of incorporating the reinforcement phase is for reinforcement to be placed on the substrate prior to molten metal spraying. There are many difficulties involved with spray deposition which include the avoidance of high levels of porosity, inhomogeneous distribution and the control of volume fractions of the reinforcement phase. Other processing difficulties include the management of the large amounts of waste composite powder created, high costs of gas atmospheres required and the necessity of subsequent processing such as machining. However, advantages such as low levels of segregation, minimisation of interfacial chemical reactions, refined grain structure and the effect of high rates of solidification, have sustained interest and further development in this processing area [10,20,35,93].

Melt Atomisation

Melt atomisation, also referred to as codeposition, involves the incorporation of reinforcement particles into the molten metal during atomisation. The reinforcement phase is introduced into the flow of the atomising gas which subsequently impinges upon the molten metal flow and in doing so combines each phase. One such process, the OspreyTM process (proprietary process of Osprey Ltd. UK), is primarily used for monolithic materials due to the advantages of high solidification rates and refined grain structure achieved by spray deposition [20]. In the 1980s it was realised that composites could be produce in this way. Since then commercial MMCs have been manufactured using the OspreyTM process as a primary consolidation step.

Thermal Spraying

High velocity Oxy-fuel (HVOF) and plasma spraying technique can be employed to produce composite materials. HVOF is mainly used to produce wear resistant coatings on substrate components. Plasma spraying can be used to provide a coating on reinforcement materials prior to a primary MMC production process. Neither of

these methods have being developed to process large quantities of composite material [10,14,94].

2.3.5 In-Situ (Reaction) Processing

In-situ processing of MMCs generally involves the chemical reaction of gases, molten metals and/or solid metal systems within a controlled environment. The end product contains reinforcement material compounds which have been synthesised during processing. The Martin Marietta Corp. (XDTM) and the Lanxide Corp. (DIMOXTM) have developed in-situ processes which have produced highly specialised materials [2,14,35].

XDTM (exothermic dispersion) processing relies on the chemical reactions of the primary materials in order to produce a composite system. The reactions which take place are self-propagating and produce thermodynamically stable composite material. These reactions generally take place between liquid metal and either solid ceramic or solid metal. DIMOXTM (direct metal oxidation) processing is similar to the XDTM. The process relies on the reaction of the primary materials with a controlled gas atmosphere. This method can also produce thermodynamically stable MMCs materials. Very little information is available relating to either of these process. However, it is believed the processing rates involved are very low in both cases and that morphological instabilities can occur within these materials at a microstructural level [14,71].

2.3.6 Diffusion Bonding

Diffusion bonding of composite layers, composite foils or the metal coated fibres referred to in section 2.3.3 can be used to produce MMC material [14,19]. The process simply involves the hot pressing of pre-determined quantities of composite layers or bundles. This process is normally applied to the production of continuous fibre composite materials. Titanium matrix composites have been found to be particularly suited to the diffusion bonding process due to the ease with which the surface oxide layer on titanium can be broken down at relatively low temperatures. Temperatures of 900°C and times of several hours are normally required for the diffusion bonding process.

2.4 POWDER METALLURGICAL PROCESSING

In order to minimise or eliminate the occurrence of undesirable chemical reactions between the matrix material and the reinforcement which occurs during casting (section 2.3.1), improve reinforcement distribution and also increase the reinforcement volume fractions beyond that possible with either spray deposition or casting of MMCs many researches have focused on powder metallurgical (PM) processing routes for the production of DRMMCs [14,19,20,26,35,41,43,49,73,89, 95-105]. PM processing routes can also allow for net shape and near net shape production of component parts and can permit material usage efficiency of up to 95 per cent [106].

The PM processing of DRMMCs involves the blending of atomised elemental or prealloyed metal powder with discontinuous reinforcement, followed by the consolidation of the resulting powder blend. The objective of the blending procedure is to produce a powder blend which exhibits a uniform distribution of reinforcement throughout. The consolidation step is generally made up of a number of stages. A container filled with the composite powder blend is normally isostatically pressed at room temperature resulting in a partially consolidated powder compact referred to as a green compact. The pressing operation is followed by the removal of undesirable gases from within the compact (degassing) and the subsequent sealing of the container (canning). The green compact must be sufficiently consolidated to ensure that no fracture or degradation of the compact occurs during these degassing and canning stages. This resistance to damage is dictated by the strength of the green compact, normally referred to as green strength. However, although the green strength must be sufficient to avoid compact damage the compact must also exhibit a level of interstitial porosity which will allow adequate degassing. Therefore, a balance between green strength and porosity must be achieved during the cold pressing consolidation stage.

Following the degassing and canning procedures the green compact may be further consolidated by heating to an elevated temperature below the liquidus temperature of the metal matrix materials (sintering). This sintering procedure is normally

simultaneously accompanied by a deformation process such as isostatic pressing, extrusion or rolling. These elevated temperature deformation processes are referred to as hot isostatic pressing, hot extrusion and hot rolling respectively. After the deformation procedure the container encapsulating the material is removed and the material may be heat treated if required. Figure 2.5 outlines both the main processing routes used for the PM production of DRMMCs.

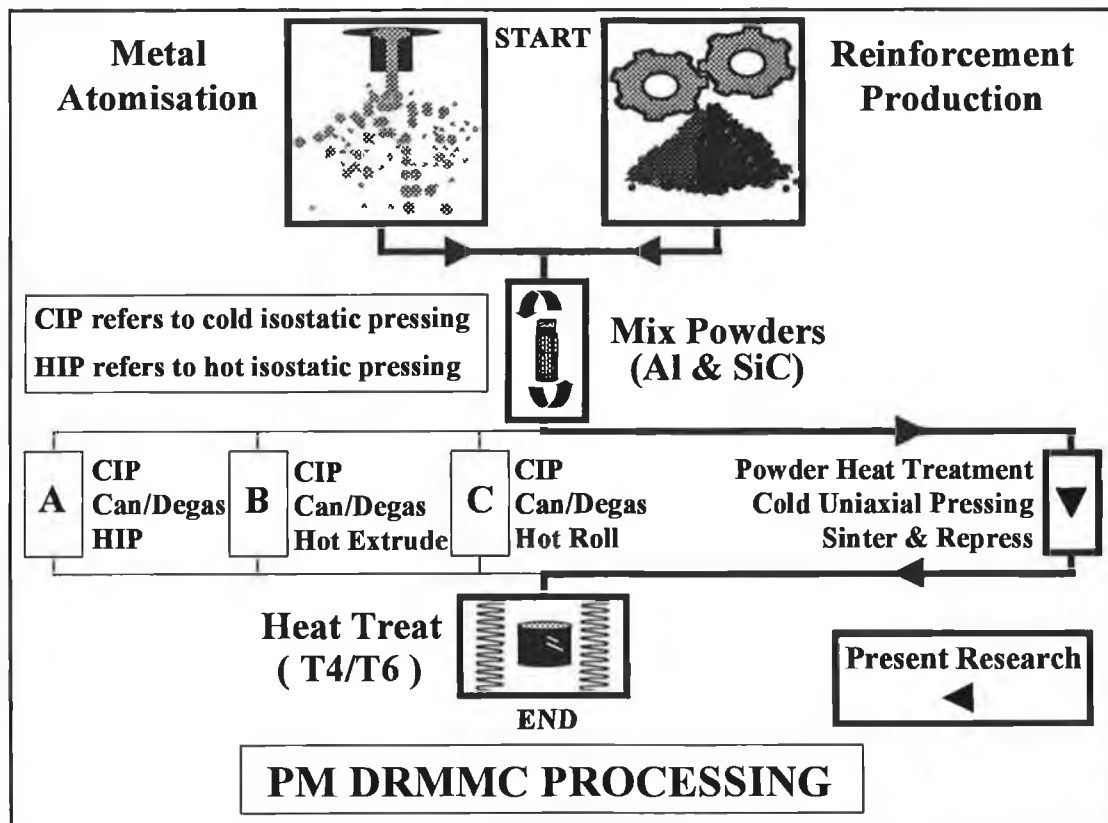


Figure 2.5. Common PM DRMMC processing routes and the processing route employed for the present research.

Although the maximum temperatures reached during processing are normally below the liquidus temperature of the matrix material, fully dense composites can be produced by the PM processing methods. This relatively low temperature processing removes, or at least minimises, the possibility of undesirable chemical reaction between the matrix and reinforcement which can easily occur during higher

temperature processing such as casting. Also, due to the fine powder form of the raw material, composites containing exact quantities of reinforcement can be produced. Therefore, material compositional consistency is more easily achieved by PM than by the casting or spray deposition routes.

The following sections describe the various possible stages which can be included in a given PM route. An emphasis is place on the processing of aluminium alloys and SiC particulate. However, the following descriptions apply to PM processing in general. The main factors restricting the widespread development of PM processed DRMMCs are the manufacturing costs arising from the specialised powder canning, isostatic pressing and degassing equipment required. The present experimental research focuses on the development of PM processing of DRMMCs which does not include the use of this equipment. This alternative PM route is outlined in figure 2.5.

2.4.1 Metal Powder Atomisation

The production of aluminium powder for use in PM is normally carried out by an atomising process. Molten aluminium or aluminium alloy is allowed to flow from a heated crucible through an orifice, creating a narrow stream of molten metal. The stream of aluminium is then disintegrated into droplets by blasting the molten stream with air, inert gas, water or ultrasound [17,83,106]. The droplets are normally allowed to rapidly solidify and are then either continuously removed from a collection area or are removed on completion of the atomisation run. After removal from the atomisation unit the atomised powder is sieved and separated into batches of various size ranges. Atomised powders are referred to as either elemental powders if they are produced from a non-alloyed melt or prealloyed powders if produced from an alloyed melt. Care must be taken whilst handling all powders. However, safety is of paramount importance when handling fine aluminium powders due to their explosive characteristics [83].

Due to the strong affinity between aluminium and oxygen a thin layer (2-40nm) of Al_2O_3 develops on the surface of the powders during atomisation. Although the oxide layer is very thin it can greatly affect the powder compressibility, sintering response and the material strength. This layer contains physically and chemically absorbed H_2O [83]. During high temperature processing the H_2O breaks up as follows:



This reaction begins to occur at approximately 70°C with the break up of the physically absorbed H_2O and is followed by the break up of the chemically absorbed H_2O which continues up to 450°C [107].

The evolved O_2 combines with any available reactive metals to create metal oxides such as Al_2O_3 or MgO . This oxidation can affect the alloy content by effectively reducing the available alloying elements and therefore altering the matrix composition. The evolved H_2 will not react in the same manner. However, this gas can cause

internal porosity, delamination or blistering in the final material. The canning and degassing step employed as part of most PM processing is used to minimise these reactions by both reducing the H₂O level within the surface layer of the powders and evacuating any air and other gases from the powders [73].

The nominal size and size distribution of any batch of powder depends on both the atomisation process and the powder sieving carried out after collection. It is difficult to produce atomised powder which exhibits a very close size distribution ($\pm 3\mu\text{m}$) without some form of size separation such as sieving. Therefore, if a specific size or close size distribution is required this must be achieved by the extraction of the suitably sized powders from an atomised batch containing a wide distribution of sizes. This procedure will greatly increase the cost of the powders and should be avoided if possible. However, the aluminium powder size and size distribution can greatly affect the processing parameters and the final material characteristics of AMC's [35] and should therefore always be carefully considered. The nominal aluminium powder sizes which are readily available range from $5\mu\text{m}$ to $150\mu\text{m}$ [109]. The shape and the surface morphology of the powder varies with atomisation method. In the case of argon atomised aluminium powders used in the present work the shape and morphology can be described as irregular, as shown in figure 2.6.

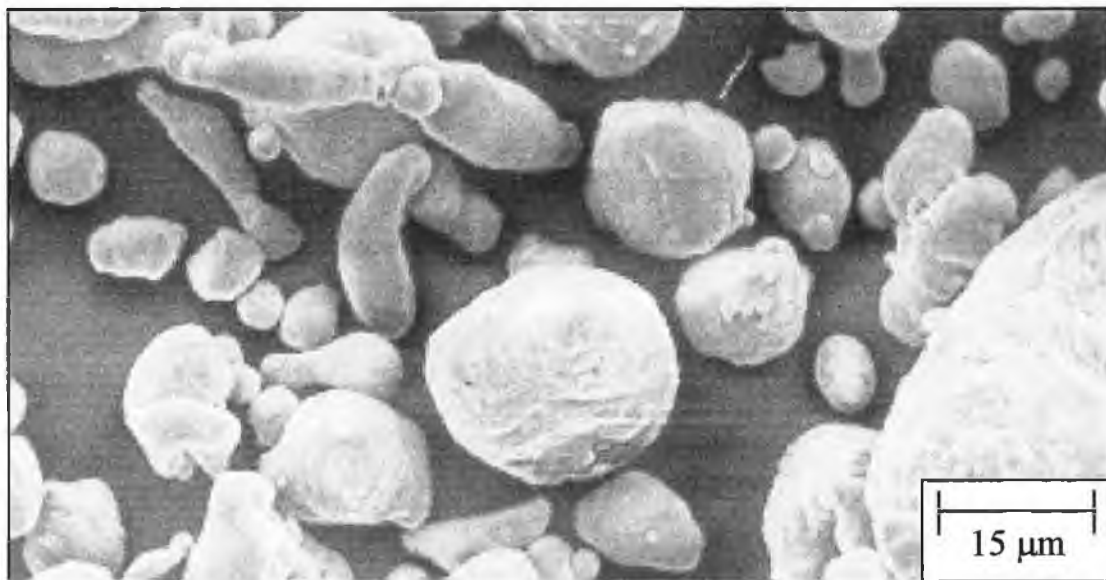


Figure 2.6. Argon atomised aluminium alloy AA6061 (irregular), SEM micrograph.

2.4.2 Reinforcement Particle Production

The most commonly employed particle reinforcement material used in the production of AMCs is SiC particulate. This is mainly due to the reported compatibility between SiC and aluminium [37] and the low cost, high strength and availability of these material [14]. These particles are produced on a large scale for use in the abrasives and machining industries. The particles are produced by the reaction of silica and carbon at a temperature of 2400°C [68]. The polycrystalline granules produced by this reaction are then pulverised and sieved into size range groupings. SiC particles are typically angular in shape, as shown in figure 2.7. The SiC particulate used in the present work is of this type.

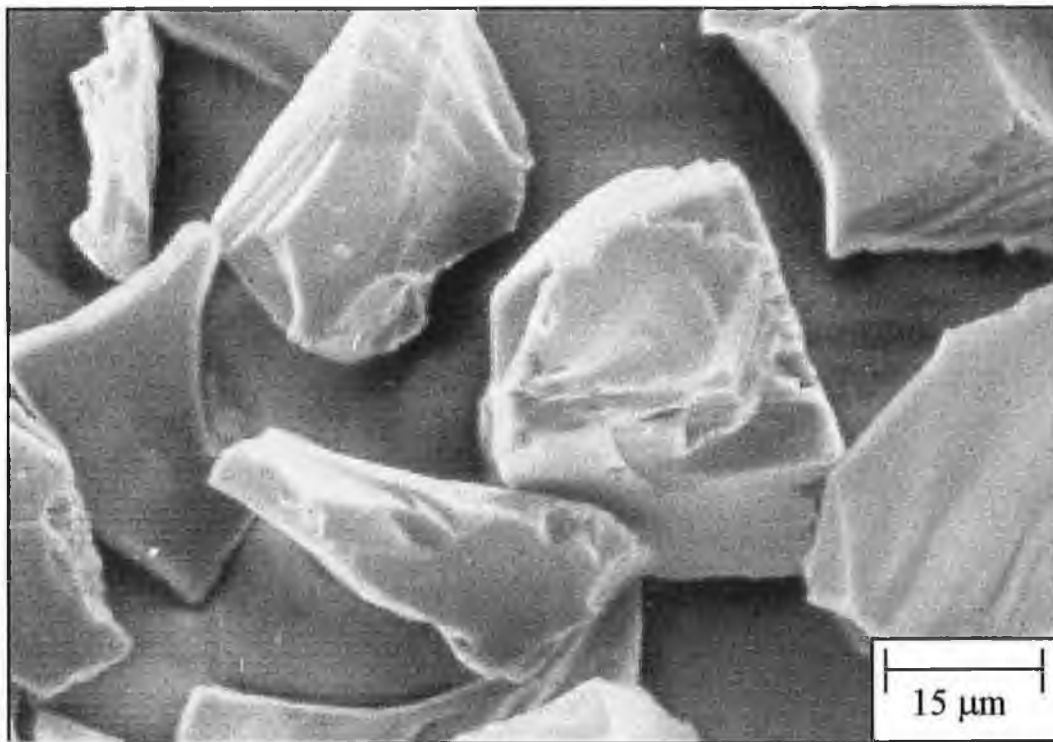


Figure 2.7. Abrasive grade SiC powder (angular), SEM micrograph.

2.4.3 Mixing

The aim of the mixing process is to create a homogenous mixture of the reinforcement and matrix powders required for the production of the composite material. Due to the direct relationship between the distribution of the reinforcement material in the powder mixture and the distribution of the reinforcement in the fully processed composite, the effectiveness of the mixing process is of prime importance.

A powder mixture is normally comprised of either prealloyed matrix powders or a blend of elemental powders blended with reinforcing particles. In the case of cold uni-axial processing a lubricant powder is also normally included in the mix. This powder lubricant is added to reduce die wall friction during both compaction and ejection and is not required in the case of isostatic pressing or powder mixture which will undergo hot deformation processing such as hot extrusion..

Mixing is normally carried out by the mechanical rotation of a suitably shaped sealed vessel containing a charge of powder made up of the matrix powders, a predetermined quantity of reinforcement and powder lubricant if required. This method of mechanical mixing is referred to as dry blending and is regularly carried out using a Turbula™ mixing unit or a V-shaped mixer [43,96,110-112]. Alternative mixing methods which have been used include the ultrasonic stirring of a powder combination within an alcoholic based solvent followed by drying [113] and also the agitation of a powder combination within a high energy grinding mill (attritor) [114,115]. The mechanisms involved in the mixing process are complex and can be influenced by many factors [83,116-121]. The final homogeneity of the mix depends on matrix powder to reinforcement size ratio, absolute powder size, powder density, charge volume to mixing container volume ratio, speed, direction and duration of mixing and container shape. Due mainly to the complexity of the mixing processes, mixing process parameters are normally founded on the results of statistically based empirical models [116].

The distribution analysis of powder blends is carried out by statistical means. Samples of powder can be extracted from a batch, chemically or physically analysed, and compared to a theoretical standard distribution. The distribution of reinforcement particles in the final composite material is directly dependent on the effectiveness of the mixing process. Image analysis of micrographs have been used to quantify and compare the homogeneity of fully processed composites [25,40,61,98,116,122-124]. However this form of analysis could be misleading since the micrographs are only two dimensional images of a three dimensional material. No standard method of distribution investigation has been devised for these materials.

In the case of mixing fine aluminium powders ($< 5\mu\text{m}$) consideration must be given to the explosive nature of the material. Electro-static charges can build up during mixing which can initiate ignition and explosion. Skin, eye and respiratory protection must be used during the handling of these powder to prevent over exposure in the event of an accidental spillage during mixing [83].

2.4.4 Powder Conditioning

Following the mixing of composite powders the materials may be in an unsuitable condition for further processing. Some powder conditioning may be required before these powders can be further processed. The form of conditioning depends on the material characteristics of the powder and the consolidation method being applied.

Lubrication

Lubrication is not required for isostatic powder pressing due to the flexible die involved in this pressing mechanism. However, in the case of cold uni-axial pressing the composite powder normally requires lubrication. The quantity of lubricant used can range from approximately 0.2 per cent to 3 per cent by weight. However, it has been suggested that lubricant quantities above 1 per cent should not be used to avoid degradation of the material [106]. Common powder lubricants used in PM processing include zinc stearate, lithium stearate, calcium stearate and both synthetic and organic waxes [83,125,126]. These lubricant powders which are introduced to the powder during the mixing stage, or either sprayed or brushed on the die walls are subsequently burnt off from the composite material after ejection from the die. This burn off step is normally incorporated in the sintering stage. The addition of lubricant affects a number of mechanisms. During uni-axial compaction of the powders, die wall friction acts in opposition to the applied force. This resistance has the effect of limiting the compressibility of the powder. By lubricating, the powder blend compressibility can be increased by reducing this die wall frictional resistance. Also, during both compaction and ejection the metal powder can physically adhere to the die wall surface (galling) [83]. This galling can damage both the compacted material and the tooling. The use of lubrication can avoid or at least reduce this damage.

The compact ejection force is directly related to the material properties of the composite powder, the compaction force applied, the condition of the die wall, the surface area in contact with the die and the type and quantity of lubricant employed. If an insufficient quantity or an unsuitable lubricant type is used, damage of both the compact and the die may occur. Conversely, care must be taken not to include an

excessive quantity of lubricant. Excess lubricant can reduce the green strength of the compact, reduce the compressibility, hinder powder cold welding and can cause contamination of the final material due to incomplete burn off during sintering [17,83,125,127]. In order to minimise these undesirable effects powder lubricant quantities should be kept to a minimum, and if possible lubricant should be avoided. Die wall lubrication, applied by either spraying or brushing may be used to eliminate the need for mixed in lubrication and therefore, eliminate the possibility of burn off residue contamination or chemical reaction within the sintered compact. The use of split dies and multi-section dies can also reduce the need for mixed in lubricant. In this case the die may be withdrawn from the pressed compact before ejection. However, uniform die wall lubrication is technically difficult to achieve and the use of sectional die mechanisms can reduce the processing rate and increase the machinery costs. In the case of mixed in lubrication, if the lubrication and ejection conditions are correctly selected, the ejected green compact should exhibit a consistent burnished surface and the die should exhibit no residual galling.

Powder Heat Treatment / Degassing

During atomisation metal droplets are subjected to extremely high rates of solidification. This rapid solidification has the effect of inducing a refined microstructure due to restricted dendritic growth. Consequently, the strength of these rapidly solidified powders is high compared to an equivalent wrought or cast alloy [15]. This is regarded as an advantageous attribute. However, the increase in material strength also has the effect of greatly reducing the compressibility of the metal powder. Annealing or normalising heat treatment can be used to soften the powders and therefore increase their compressibility [83]. The powder heat treatment may be carried out within a controlled gaseous environment in order to promote surface oxidation, surface reduction or oxide layer dehydration [15].

SiC particles have a tendency to react with Al at temperatures above 660°C producing the water soluble compound Al_4C_3 [35,88,90,128-130]. SiC particulate can be treated at high temperature in an oxygen rich atmosphere to create a surface layer of SiO_2 on the SiC particles. This in turn reduces the possibility of the formation of Al_4C_3

[90,130]. Metal powders normally exhibit an oxide layer on their surface which can reduce compressibility, reduce cold welding and in some cases cause contamination of the final material. Reduction of this oxide layer can be carried out for some metal powders [17,83]. However, atmospheric reduction of the oxide layer on the surface of aluminium powder is extremely difficult.

A number of consolidation processes involve sealing the composite powders within a container before the application of pressure. The volume of the container may be in the order of the volume of powder required to produce a single component (cylindrical sample: diameter 35mm, height 52mm [108]), or as large as that required to produce a billet for forging, extrusion or rolling [43,105]. If the powder is sealed and compacted the gases within the pores of the original charge of powder will have no way of escaping from the sealed container and will degrade the material properties [96,102-104]. As a consequence, the powder charge within the sealed container must be degassed. Also atomised aluminium powders have a naturally formed oxide layer which can range from 2nm to 40nm in thickness [83,107,129]. This layer of Al_2O_3 contains chemically and physically absorbed H_2O . Sealed aluminium powders which have not been degassed produce H_2 gas on heating which evolves from the H_2O . This evolved H_2 can cause a reduction in final material strength and can also pose safety concerns relating to explosion [108].

The degassing procedure is carried out at elevated temperatures and can involve many cycles. Each cycle may include the application of a high vacuum followed by a charge of inert gas. Once this procedure is complete the container must be sealed. The container must remain situated in a vacuum environment during the sealing operation. This is normally carried out using laser welding or similar techniques. The degassing step can also be incorporated in the pressing step by applying a vacuum to the charge during the application of pressure [19,43,108].

2.4.5 Compaction

The compaction stage of PM MMC production can take many forms, as shown in figure 2.5. Hot isostatic pressing (HIP'ing) and hot extrusion have been found to produce composite material which exhibit excellent material characteristics. However, these processes involve canning, degassing, specialised consolidation equipment and can involve long processing times. These costly production routes are used extensively and a number of companies have developed mass production facilities based on HIP'ing and hot extrusion [2,20,105].

The HIP'ing procedure involves the positioning of a degassed container of composite powder in the centre of a cavity within the HIP'ing unit. The heating element within the cavity surrounds the container. Heat and isostatic pressure are applied to the container simultaneously. The pressure is produced by pumping either argon or nitrogen gas into the cavity surrounding the container. The temperature, pressure and duration of the cycle is dependent on the materials being processed [131]. After the hot pressing cycle is complete the pressure is released and the container is removed from the cavity. The composite billet is then extracted from the original container by stripping the container walls. HIP'ing can produce near net shape components which only require minimal machining.

Cold uni-axial pressing and cold isostatic pressing (CIP'ing) are normally used to provide manageable green billets of partially consolidated powder before degassing, sintering and/or hot working is applied [43]. The CIP'ing process utilises a fluid medium to apply pressure in all directions and therefore produces a uniformly compacted green billet. Cold uni-axial pressing does not provide the same uniformity of pressure distribution throughout the green compact [17,83,126]. The density distribution of the green material will vary with distance from the planes of pressure application. In the case of double action and floating die uni-axial pressing the axially central volume of the powder compact will exhibit a low density compared to the areas closer to the punch contact areas. The density variation is due mainly to the friction between the powders and the die wall. If excessive, this density variation in

the green compact can cause geometric and possibly microstructural inconsistencies of the composite material after hot processing [17,83]. A major European powder compaction modelling research program, PM Modnet (EPMA), is currently being undertaken which aims to elucidate the factors which affect the pressed density distribution of powder compacts through computational modelling. However, at present no quantitative description of the mechanisms relating to compact density distribution can be found in the available literature. The extent of the density variation may be minimised by powder or die wall lubrication and also by keeping the height of the powder compact to a minimum [126]. The successful mass production of many axially pressed components to high geometric accuracy indicates that the level of density variation exhibited by these compacts does not prevent the use of this conventional pressing method.

A number of mechanisms contribute to the strength of the cold compacted metal powder billets (green strength) [83,121,126,132-136]. During initial pressing the powder density is primarily increased by the movement of the powders into a close packed arrangement. As the possibilities for powder rearrangement diminish, each pair of metal powder particles which are in contact with each other begin to flatten in the contact area. In the non-contact areas localised extrusion can also occur. During pressing the particles may become work hardened and therefore more brittle. Fracture of these hardened particles may occur in the final stages of compaction due to the increased pressing stress. The pressed billet of powder is held together by cold welding and interlocking of the particles. The green strength of the compact is vitally important since these billets must be handled during further processing. The mechanisms involved in compaction depend on the powder material properties and therefore can vary greatly. Although a number of researchers have investigated the mechanisms involved in the compaction of metal and ceramic powders [121,132-136], no literature relating to the mechanisms involved in the cold compaction of a mixture of both metallic and ceramic powders has been found.

Many factors can affect the cold compaction process. Powder hardness and applied pressure greatly affect the compressibility. Particle shape, particle size distribution, die

and particle surface conditions, absolute size of powders and, in the case of powder blends particle size ratio can all play a role in determining both the compressibility and the green strength. Also, other contributing parameters which will affect the pressing mechanism including compaction rate and hardness ratio in the case of bi-model systems such as composites.

Other advanced forms of PM consolidation include the CeraconTM process, Rapid Omni-directional Compaction (ROC), STAMPTM and CAP processes [83,137-139]. The CeraconTM process involves the hot consolidation of a powder preform by transferring axially applied pressure through a ceramic powder which completely surrounds the powder preform. The complete pressing container is then ejected from the main die and the ceramic powder medium is poured out and reused leaving behind a near net shape consolidated component. The ROC process is similar to the CeraconTM process. However, the ROC utilises a molten metal fluid to transmit pressure to a powder preform. The STAMPTM process incorporates the atomisation of the powder so that powder atomisation is not a separate process. Consolidation by atmospheric pressure (CAP) involves the vacuum sealing of powder in a glass container which is subsequently heated. On the heating of the glass container the atmospheric pressure consolidates the enclosed powder due to the vacuum. These advanced processes have been developed in order to reduce the processing costs involved in PM manufacture.

2.4.6 Sintering

Metal powder compacts produced through cold compaction primarily depend on particle interlocking and interparticle cold welding for strength (green strength) [83,126]. This strength is normally well below that required for materials used in structural applications. Therefore, the interparticle bonds must be further strengthened before the material can be considered for use in such applications. In order to significantly strengthen the interparticle bonds it is necessary to form a substantial bridge of material between the individual particles. In many powder based material systems this is achieved by the solid or semi-solid thermal processing (sintering) of the powder compact material. Sintering of metal based compacts can be described as a thermally activated process which causes the transportation of material between powders in close proximity to each other, resulting in metallic lattice based interparticle bridging throughout the material. The main thermally activated transport mechanisms which may occur during sintering are listed in table 2.7.

Table 2.7. Transport mechanisms which can occur during sintering [17]

Diffusion of Atoms and/or Ions	Particle Surface Diffusion
	Volume Diffusion Via Vacancies
	Volume Diffusion Via Interstitials
	Grain Boundary Diffusion
	Vaporisation and Re-Condensation
Bulk Movement	Plastic Flow
	Localised Infiltration
	Viscous Flow
	Grain Boundary Sliding
	Particle Rearrangement

The sintering process varies considerably depending on the compact materials and the final material required. However, in all cases the sintering of a metallic compact involves heating the compact within a controlled atmosphere to a temperature, above which atomic diffusion will take place between the particles in the compact, and

below which the compact will contain such a quantity of liquid as for it to significantly geometrically deform or collapse. The powder compact is held at this sintering temperature for a predetermined period of time to allow the compact to strengthen to the required extent. The sintering temperature, atmosphere and time strongly depend on the constituent materials involved, the size of the particles and the level of densification and strength required.

At temperatures below the solidus temperature (sub-solidus) of all of the constituents the dominant sintering mechanisms include atomic diffusion both between adjacent particles and within individual particles. These mechanisms result in the formation of a primary bridge (neck) [17,83] between adjacent particles. However, other than the interparticle necks the particles remain discrete and no significant densification of the compact occurs. During this form of sintering no liquid phase exists. This sub-solidus sintering is referred to as solid phase sintering. At temperatures above the solidus temperature (super-solidus) of at least one constituent material within the compact a liquid phase will exist. In this case, both diffusion and bulk transport mechanisms such as solid particle rearrangement and interparticle liquid infiltration may occur. These mechanisms cause the formation of continuum lattice structures between particles. As a result adjacent particles become integrated and are no longer discrete. The extent of this integration and the rate at which it occurs depends strongly on the quantity of liquid which is present during sintering. The liquid phase contributes greatly to the consolidation and strengthening of the compact material. Sintering of this type is referred to as liquid phase sintering. Compared to solid phase sintering, liquid phase sintering normally causes significant densification of the compact. In the case of both solid phase and liquid phase sintering the extent to which interparticle bonding takes place is directly dependent of the sintering time applied.

The atmospheric condition within which sintering takes place can encourage or prevent chemical reactions, prevent evaporation of alloying elements, remove unwanted atmospheric contaminants, aid heat transfer or provide hydrostatic pressure [17] during the sintering cycle. These atmospheres can be chemically neutral, oxidising, reducing, carburising, decarburising, nitriding or decomposing in nature.

Due to the high temperatures involved in sintering the moisture content and the oxygen content of the gaseous atmosphere used will affect the sintered material. The moisture and oxygen provide available oxygen atoms which will chemically react to produce metallic oxides. This oxidation may prevent complete sintering, slow down sintering or contaminate the final material [17,140].

Shrinkage of the powder compact normally occurs during liquid phase sintering. This shrinkage is due to the densification of the compact. In the case of compacts which have under gone non-isostatic processing this shrinkage can geometrically distort the compact due to the density gradient within the material [83]. The extent of this distortion is directly dependent of the density distribution, being largest in the areas of the compact exhibiting low compact density (green density). Repressing of the deformed sintered compact can be used to achieve the correct geometric form required.

Aluminium Sintering

Aluminium powder compact sintering is recognised as being difficult to achieve [17,83,107,108,140,141]. The surface oxide layer (Al_2O_3) which encapsulates atomised aluminium powder particles acts as a barrier to the diffusion mechanisms during solid sintering and obstructs mechanisms such as capillary infiltration and liquid phase diffusion during liquid phase sintering. This hindrance is difficult to overcome. Alloying additions can be used to break down the oxide layer in order to allow the diffusion of the aluminium [17,141-143]. Also, precompaction mechanical deformation of the powder material can fracture the surface oxide layer to expose non-oxidised aluminium which can readily sinter [17].

Sintering of aluminium based powder compacts has been carried out at temperatures ranging from 300°C to 630°C [17,83,135,140,144,145]. However, the reported material characteristics for the aluminium materials sintered at temperatures below approximately 580°C indicates that insufficient consolidation occurs below this temperature. A sintering atmosphere commonly used for the sintering of aluminium is nitrogen. The nitrogen gas atmosphere is non-reactive within the sintering

temperature of aluminium [146] and acts as an oxidation inhibitor. Sintering times of between ten minutes and 24 hours have been reported [83,144,145,147]. However, a combination of high temperature and short sintering time results in improved material properties compared to combinations of low temperature and long sintering times [140,144].

Besides the present work, very little research has been carried out on the application of the cold pressing and sintering route for the production of AMCs. However, a recent US patent [112] reports the use of this processing route combined with hot extrusion for the production of boron carbide particulate reinforced aluminium alloy AA6061. In the described process the V-blended, degassed composite powder is cold isostatically pressed at 65,000psi (448.2 MPa) followed by sintering at 625°C for 45 minutes within a vacuum furnace. The sintered material is then hot extruded and heat treated to the T6 condition (see section 2.4.7 for details on heat treatment). The resulting composite material exhibits ultimate tensile strengths ranging from 483 MPa to 717 MPa depending on the fraction of boron carbide used. A similar process was used for the production of SiC reinforced aluminium alloy AA6061 [43]. In this process Turbula™ blended, degassed composite powder was sintered at 630°C for one hour within a vacuum furnace. The resulting material was then hot rolled and heat treated to a nominal condition of T6. These heat treated materials exhibited ultimate tensile strengths ranging from 339 MPa up to 392 MPa.

2.4.7 Heat Treatment

Most aluminium alloys can be heat treated by various methods in order to achieve specific material properties. The material properties of a heat treatable aluminium alloy are strongly dependent on the form of heat treatment carried out. Therefore, the heat treatment condition of an alloy must be specified when describing that alloy. This is carried out with the attachment of a suitable heat treatment code. The most common codes include O, T4 and T6.

O (Annealed condition)

Annealing is carried out by heating the material to a temperature of between 400°C and 450°C, soaking at this temperature and slow cooling (30°C/hour) to 250°C. The cooling rate from 250°C to room temperature is unimportant in the annealing process [148].

T4 and T6 (Solution heat treated and naturally or artificially aged)

In order to precipitation heat treat aluminium alloys which are suited to this heat treatment the material must be solutionised by heating to a temperature above 500°C, soaked at this temperature followed by rapid quenching. If this solutionised material is allowed to remain at room temperature after quenching it will harden considerably over a four to ten day period. This hardening phenomena is referred to as natural ageing. Aluminium alloys which have been subjected to solution heat treatment followed by natural ageing are coded T4. If the quenched material is heated to between 160°C and 200°C the hardness will increase substantially over four to twenty four hours. This temperature assisted hardening is referred to as artificial ageing or precipitation heat treatment. Aluminium alloys which have been subjected to solution heat treatment followed by artificial ageing are coded T6. The mechanisms involved in these phenomena are based on the atomic diffusion of alloying elements which nucleate precipitates in vacancies and dislocations throughout the alloy. The precipitates act as strengthening features within the material [148,149].

This precipitation mechanism is of vital importance in aluminium based particulate reinforced MMC materials. It has been found by many researchers that accelerated aging occurs in the case of these MMC materials [41,42,50,77,80,95,98,101,103,

124,150-166], which is believed to be due to the increased dislocation density throughout the matrix material. This dislocation density increase is due to the stress field created around the hard particulate inclusions. The stress is attributed to the differences in the coefficient of thermal expansion between the matrix material and the reinforcement within these composite systems. The increased dislocation density increases both the rate of diffusion and the available nucleation points.

2.5 PARTICLE REINFORCED ALUMINIUM MATRIX COMPOSITES

Particle reinforced aluminium matrix composites (PRAMCs) are the most commonly researched, manufactured and applied MMC. These PRAMCs have been found to exhibit many superior properties compared to their unreinforced matrix material. This has been the main driving force behind the research and development of these lightweight materials. Many aluminium based composite systems have been investigated and a large number of both conventional and novel processing routes have been applied [35]. However, at present the majority of research is focused on casting, spray deposition, infiltration and powder metallurgical processing of Al-Mg-Si, Al-Cu and Al-Si aluminium alloys.

The focus on these alloys is due mainly to the material cost and availability, alloy to reinforcement compatibility and technical processing considerations. The Al-Mg-Si alloy AA6061 has been used extensively as a matrix material. AA6061 is a medium strength alloy which derives its strength from the precipitation of Mg_2Si . The ratio of magnesium to silicon included in the alloy is such that the weight fraction of each element relates to the atomic mass ratios of the Mg_2Si compound [148]. The quantity of each element is dictated by their solubility within the solid aluminium during the heat treatment procedure [148]. AA6061 contains approximately 1.1%Mg, 0.7%Si and 0.35%Cu and 0.32%Fe (nominal percentage by weight).

The AA2xxx series of aluminium alloys are Al-Cu alloys which form the precipitate Al_2Cu and are of higher strength than the AA6xxx series. The Al-Si alloys, such as A356, are employed when liquid processing of SiC reinforced aluminium is employed. The high temperature processing involved in casting normally promotes the formation of Al_4C_3 which is water soluble and therefore undesirable [88,90]. The addition of Si in the alloy minimises the possibility of the formation of this compound.

The most frequently used reinforcement materials used are abrasive grade SiC particulate and Al₂O₃ particulate. Table 2.8. lists some common PRAMCs, the processing routes employed and the ultimate tensile strength recorded for each composite.

Table 2.8. Common particle reinforced AMCs (PRAMCs).

Al Alloy	Reinforcement	UTS (MPa)	Processing Route	Reference
AA6061	30%SiC _p (wt.)	416 (T6)	PM/HIP	[167]
AA6061	30%SiC _p (wt.)	328 (T6)	PM/CIP/Extruded	[167]
AA6061	25%SiC _p (vol.)	498 (T6)	PM/CIP/Extruded	[24]
AA6061	20%SiC _p (vol.)	498 (T6)	PM/CIP/Extruded	[99]
AA6061	15%SiC _p (vol.)	364 (T6)	Cosprayed	[35]
AA6061	15%SiC _p (vol.)	330 (T6)	Spray & Extruded	[164]
AA6061	15%SiC _p (vol.)	360 (T6)	Cast & Extruded	[61]
AA6061	10%SiC _p (vol.)	375 (T6)	Cast & Extruded	[168]
AA6061	17%SiC _p (vol.)	590 (T6)	Spray-Rolled	[87]
AA2124	15%SiC _p (vol.)	570 (T6)	PM/CIP/Extruded	[99]
AA2124	30%SiC _p (vol.)	584 (T6)	PM/CIP/Extruded	[99]
AA2014	5%Al ₂ O _{3p} (vol.)	280 (NA)	Slurry Cast	[87]
AA2014	20%Al ₂ O _{3p} (vol.)	252 (NA)	Slurry Cast	[87]
AA2124	10%SiC _p (vol.)	484(NA)	Spray-Rolled	[87]
A356	10%SiC _p (vol.)	303 (T6)	Cast (Duralcan)	[20]
A356	15%SiC _p (vol.)	331 (T6)	Cast (Duralcan)	[20]
A356	20%SiC _p (vol.)	352 (T6)	Cast (Duralcan)	[20]

Note: The code T6 refers to the reported heat treatment condition of the material. For a description of this heat treatment condition and others, refer to section 2.4.7. NA is used where the heat treatment condition is not reported in the reference.

2.5.1 Strengthening Mechanisms

Although the load transfer mechanism influences the strength of PRAMCs, a large number of other factors can also strongly affect the mechanical properties of these composites. These factors include the precipitation of alloying elements, alloy type, oxide dispersion strengthening, interfacial compounds and bonding, porosity, contamination, dislocation distribution and density, reinforcement volume fraction, distribution, type and particle size, heat treatment and deformation history and matrix grain structure. Any one of these factors can greatly affect the condition of the final material.

Table 2.9 The effect of parameter variation on the material properties of PRAMC
[14,19,84,169,170].

PARAMETER VARIATION	Parameter Limits	UTS	Ductility	Macro hardness	Fatigue Strength	Elastic Modulus
Particle Size Decrease	150 μm to 1 μm	↑	↑	↑	↑	↑
% Vol. Fraction Increase	0% to 45%	↑	↓	↑	↑	↑
Distribution Homogenisation	NA	↑	↑	NA	NA	NA
Porosity Decrease	10% to 0%	↑	↑	↑	NA	↑
Interfacial Bond Strength Increase	NA	↑	NA	↑	↑	↑
Matrix Strength Increase	170 MN/m^2 - 570 MN/m^2	↑	NA	↑	↑	↑

Note: ↑ indicates an increase, ↓ indicates a decrease, NA indicates information not available or not applicable.

Due to the difficulties involved in producing low porosity and uncontaminated composite material considerable variation can be observed in the material properties of composites with similar composition, as indicated by the tensile strength values listed in table 2.8. The main variables affecting the material properties and the tendency of their effects are detailed in table 2.9. As discussed in section 2.6, the modelling of these materials has proven difficult due to the complexity of the factors which influence the material properties. Consequently, many models utilise empirical descriptions of the constituent materials

Dislocation Density and Precipitation

The mechanism described as precipitation strengthening exhibited by many aluminium alloys has greatly influenced the development of aluminium as a light weight structural material. Precipitation occurs due to the thermal conditioning of the solid material and is dependent on the alloy type and the form of heat treatment used. Aluminium alloy AA6061 is one of the most commonly used alloys that exhibits the precipitation mechanisms. When this material is solutionised at 515°C the alloying elements are distributed throughout the composite. The material is then quenched from 515°C to room temperature or below. The alloying elements are held in a super-saturated solid solution (SSS) due to this quenching. If the material is allowed to remain at room temperature the hardness of the material will increase. This mechanism of hardening at room temperature is referred to as natural ageing. Hardening will also occur when the composite is heated to a temperature between 150°C and 220°C. This heat assisted hardening is referred to as artificial age hardening. The increase in hardness in both natural and artificial ageing is attributable to the formation of the Mg_2Si precipitates throughout the AA6061 alloy. The precipitates nucleate in vacancy rich zones, dislocations and grain boundaries. These zones are referred to as Guinier-Preston zones (GPZ). The development of the precipitate can go through three stages, as listed in order of development below [164].

1. Needle shaped, semicoherent phase (β'')
2. Rod shaped, transition phase (β')
3. Incoherent, equilibrium Mg_2Si phase (β)

In the case of AA6061 containing SiC it has been found that the rate at which the precipitates develop is noticeably faster than for the unreinforced alloy. The explanation of this phenomena is found in the dislocation rich areas that mainly surround the periphery of the inclusions [101,159,162,163]. The increased dislocation density is due to the differences in the coefficients of thermal expansion between the matrix and the reinforcement. When the material is at the solutionising temperature only minor stresses exist within the material. However, when the material is rapidly quenched the matrix and reinforcement contract by different amounts. Stresses due to this mismatch generate dislocations in the affected areas [162-164]. The accelerated precipitation is a well accepted phenomena. Unfortunately, the increase in precipitation rate is not always matched with an increase in microhardness of the matrix material which could further strengthen the composite.

Alloy development has been suggested by a number of commentators [14,26,37,105] with the objective of utilising the increased dislocation density by increasing the quantity of precipitate forming alloying constituents. This may have the affect of increasing the precipitate density and therefore the strength of the matrix material and also counterbalance the loss of alloying element to chemical reactions during processing. However, no literature has been found which deals with the investigation of the effects of alloy composition on the overall material properties.

2.6 COMPOSITE MODELLING

Due to the recent advances in DRMMC processing technology, considerable research emphasis has been placed on the development of models capable of both predicting composite material properties and investigating the individual parameters which affect these properties. In order to achieve a deeper understanding of the microstructural mechanisms involved in these advanced materials it is necessary to isolate the factors affecting the constitutive properties and, in doing so, quantify the effect of the individual factors. However, due to the processing and microstructural complexities associated with DRMMCs it is well recognised that this isolation is either impractical or impossible to achieve experimentally. As an example, it is not possible to increase the reinforcement volume fraction of a composite without directly affecting the dislocation density within the matrix and therefore affecting the constitutive properties of the metallic phase [171]. Fortunately material modelling can accommodate this parameter isolation. In order to ensure that the material model used is truly representative of the composite, an extensive understanding of the microstructural factors, deformation mechanisms and theoretical modelling approach involved is essential.

Unfortunately, the modelling of composite materials is far more complex than that of monolithic materials. The distribution of stress within a geometrically smooth homogeneous monolithic material can be described as approximately uniform throughout. Therefore, in order to predict the response to a load or system of loading only the material properties and the use of conventional continuum mechanics are required. Conversely, the stress distribution throughout a composite can be described as non-uniform due to the material property inhomogeneities within the material. Therefore, an approach based on conventional continuum mechanics alone is not suitable for predicting the response of these microstructurally complex materials. Due to this complexity the modelling of DRMMCs has proved difficult. However, despite these difficulties a number of composite models have been developed which closely simulate the response of these materials [101]. This recent progress has been made

possible by the knowledge gained from the experimental investigations of composite microstructure and DRMMC deformation mechanisms. In addition, the increasing computational power available at present allows for the incorporation of numerical complexities which were previously unmanageable.

Experimental DRMMC research has elucidated many of the mechanisms involved in the microstructural development and deformation of these materials, and has also indicated the material parameters which affect these mechanisms [45,50,80,101, 124,159,165,166,172-174]. The mechanisms which have been identified include matrix to reinforcement load transfer, thermal expansion and stiffness mismatch residual stress development, internal localised stress concentration, refined precipitation strengthening, matrix grain refinement, constrained plastic flow and both interfacial and reinforcement based crack initiation and propagation [63]. The factors which have been recognised as affecting these mechanisms, and therefore the overall properties of the composites, include the constitutive properties of the devisable phases, reinforcement quantity (volume fraction), size and size distribution, reinforcement shape and surface morphology, distribution throughout the matrix, and the compatibility between the reinforcement and the matrix material. The processing methods used at each stage of manufacture have a very strong influence on these factors.

Although a number of the factors mentioned above are directly related to crystallographic dislocation mechanisms, few MMC models directly incorporate subcontinuum crystal lattice micromechanics [14]. The majority of MMC modelling research has utilised the framework of advanced continuum mechanics alone. The various DRMMC modelling methods can be divided into three areas based on the mechanistic framework used to describe the response of the constituent materials to loading. These frameworks include subcontinuum, continuum crystallographic and continuum solid mechanics. Each modelling approach has provided both qualitative and quantitative insight into the mechanisms involved in the deformation mechanics of many composite systems. However, although considerable success has been achieved in the modelling of composites within the elastic range, the modelling of composite

plasticity, work hardening and rate dependent deformation remains underdeveloped. Also, the accuracy and validation of these plastic deformation models strongly depends on the accuracy to which the individual constitutive materials are described and the quality of the experimental material prepared for comparative validation.

The vast majority of DRMMC models are continuum mechanics based and the incorporation of subcontinuum parameters are normally dealt with empirically. Crystal plasticity based models consider crystallographic slip in a continuum mechanics framework, therefore avoiding complex dislocation motion based descriptions of matrix deformation. Analytical continuum models, such as those based on the Eshelby equivalent inclusion method, have indicated relationships between DRMMC properties and the reinforcement shape, volume fraction and alignment. The use of an aligned ellipsoidal inclusion in the Eshelby method allows for mathematically rigorous solutions to be obtained within a linear constitutive property range. However, the geometric and constitutive approximations assumed in Eshelby type models fail to accurately describe the geometry of the reinforcement types commonly found in DRMMCs and impose difficulties in describing composite plasticity. Consequently, the majority of composite modelling research in recent years has focused on continuum based numerical methods, such as the finite element method (FEM). This computational method provides a powerful and flexible method of composite analysis capable of accommodating geometric complexity and constitutive non-linearities with relative ease compared to purely analytical approaches.

2.6.1 Subcontinuum Models

Subcontinuum mechanics, often referred to as dislocation theory or micromechanics, has been considered as a modelling platform for composite materials [80,165,173,174]. In the case of metallurgy, this theory describes matter, not as a continuum, but as monocrystallographic or polycrystallographic structures. Therefore, the mechanisms of material deformation are at an atomic or dislocation level. The factors influencing the properties of a metallic material at this nanomechanics scale include dislocation density and point defect conditions, nano-scale coherent and incoherent particle inclusion, and both grain size and grain boundary orientation [16,165,175]. The ceramic reinforcement materials normally used in DRMMCs do not exhibit the same mechanisms of deformation, and are not influenced by the same crystallographic factors. These hard particles are normally described as either rigid or purely linearly elastic continuum solids, and their direct contribution to the overall properties of the composite are commonly described using continuum theory. Importantly, the inclusion of these ceramic particles within a metallic matrix influences the previously mentioned crystallographic characteristics of the matrix. These effects include dislocation density enhancement, particle strengthening and both grain size and sub-grain structure modification.

Dislocation Density

Investigations of the reaction of DRMMCs to solution, and subsequent precipitation heat treatment, have shown that these composites exhibit increased dislocation densities compared to similarly processed monolithic material after quenching from elevated temperatures [80,101,159,162,165,172,176]. The increased dislocation density is caused during thermal processing by the effect of the coefficient of thermal expansion mismatch which exists between the matrix material and the reinforcement, and is most noticeable within both the interfacial regions and the matrix material surrounding sharp edges of the reinforcement [101,162,163,176]. This increased dislocation density restricts the movement of dislocations within the matrix during loading, and also results in accelerated rates of strain hardening due to the resultant dislocation pile-ups [41,165]. This strengthening mechanism may be thought of as a

localised internal strain hardening effect. It has been proposed [165] that the dislocation density strengthening contribution (σ_d) can be defined theoretically as

$$\sigma_d = \alpha G b \sqrt{\rho} \quad (1)$$

where,

$$\rho = \frac{12(\delta C \delta T) F_v}{b L}, \quad [165] \quad (2a)$$

or

$$\rho = \frac{\delta C \delta T N A}{b}, \quad [194] \quad (2b)$$

and ρ is the average dislocation density, G is the shear modulus of the material, b is the Burgers vector, α is a material dependent constant, δC is the difference in the coefficients of thermal expansion, δT is the temperature drop, F_v is the reinforcement volume fraction, L is the equivalent length of a particle, N is the number of particles and A is the total surface area of each particle. It is suggested that the stress σ_d should simply be added to the yield strength of a similarly processed monolithic matrix material in order to obtain the current yield strength of the matrix material within the composite. However, the factors affecting the value of α are not clearly stated in the available literature. Arsenault [33] states that α will be approximately unity, while Humphreys [165] and Miller et al. [16] note that this value may vary from 0.5 to 1.0. It is intuitively clear that the observed increase in dislocation density will affect the constitutive properties of the matrix material and therefore affect the properties of the composite. Due to the low level of strengthening predicted using a combination of equations (1) and (2a), Humphreys [165] has noted that it may be necessary to include the effects of point defects in a similar manner to increase the accuracy of the prediction.

Particle Strengthening

Under the heading of subcontinuum mechanics, particle strengthening refers to the strengthening mechanisms involving dislocation motion resistance by precipitates and dispersoids ($\leq 1\mu\text{m}$) within metal lattice structures [16]. In the case of DRMMCs this is in contrast to the strengthening mechanisms of load bearing due to the larger reinforcement particles ($>1\mu\text{m}$) distributed throughout a matrix [14]. The deformation mechanisms which occur at this subcontinuum level involve either the shearing of particles by dislocation movement or the circumvention of the dislocations around the inclusions, the so-called Orowan strengthening mechanism [177]. These mechanisms may only occur if a metallic material contains particles such as precipitates and dispersoids.

Many DRMMCs are composed of precipitation hardening aluminium alloys, such as the AA6xxx and the AA2xxx series, combined with ceramic reinforcement. The reinforcement has the effect of increasing the overall dislocation density within the matrix material as discussed in the previous sub-section. Experimental investigations of the effects of this dislocation density increase on the response of the matrix to heat treatment has indicated an accelerated rate of precipitation formation, and, in a number of cases, a higher matrix peak microhardness has been observed, compared to that of the monolithic matrix material [149,150,153,156,166]. Also, in the case of powder metallurgical aluminium matrix composites the matrix will contain fine dispersoids of Al_2O_3 originating from the surface of the aluminium alloy powder [15,178]. The strengthening attributable to either, or both, precipitates and dispersoids (σ_p) strongly depends on the interparticle free matrix spacing (S) [165,16,177,179,180]. It has been proposed [165,177] that

$$\sigma_p = 2Gb/S \quad (3)$$

where

$$S = 0.6d \left(\frac{2\pi}{F_v} \right)^{1/2} \quad (4)$$

and d is the average particle size, assuming all particles to be equiaxed and G , b and F_v are as described in the previous sub-section. Using equations (3) and (4), it can be shown that σ_p is negligible for $d \geq 1\mu\text{m}$. Therefore, the reinforcement particles normally included in DRMMCs do not directly contribute to the material strength by this mechanism, rather the precipitates and dispersoids within the matrix.

Grain Size

Grain refinement and subgrain development are commonly observed in DRMMCs due to the effects of the included particles on the recrystallisation of the matrix material [181]. These effects include grain refinement caused by particle based grain nucleation during recrystallisation, and subgrain development due to relaxation of the thermally induced stresses caused by the coefficient of thermal expansion and stiffness mismatch between the matrix and the inclusions. The strength contributions of these microstructural adjustments (σ_g) can be modelled using a Hall-Petch type relationship [165,177],

$$\sigma_g = \frac{k_y}{\sqrt{D}} \quad (5)$$

and,

$$D = d^3 \sqrt{\frac{(1 - F_v)}{F_v}} \quad (6)$$

where k_y is typically $0.1 \text{ MNm}^{-3/2}$ in the case of grain refinement and $0.05 \text{ MNm}^{-3/2}$ in the case of subgrain strengthening, F_v is the reinforcement volume fraction, d is the average particle size and D is the average grain size or subgrain size.

Combined Effects

The above equations (1-6) show the generalised models describing the effects of the individual subcontinuum mechanisms on the strength of the matrix material. However, a quantitative model which takes account of the close interaction between these

various parameters has not yet been developed. Consequently, the majority of DRMMC modelling methods describe the subcontinuum criteria of the modelled composite empirically. It is recognised [33,165] that the combined contribution of these criteria (σ_{sc}) can account for a considerable portion of the composite strength compared to that of the load bearing effects of the reinforcement, and that σ_{sc} is a function (ϕ) of the above mentioned factors and a number of other minor contributions (σ_o), as shown in equation (7).

$$\sigma_{sc} = \phi(\sigma_d, \sigma_p, \sigma_g, \sigma_o) \quad (7)$$

Further experimental research is required in each of these areas in order to quantify both the effects of the individual mechanisms and the relationship between the various strengthening factors.

2.6.2 Continuum Crystallographic Models

Due to the important effects of subcontinuum factors on the constitutive properties of DRMMCs, considerable effort has been made to incorporate these various mechanisms in some tractable way. One of the most promising modelling approaches in this area is referred to as crystal plasticity [58]. This modelling approach, which has only recently been applied to DRMMCs, describes the plastic deformation of the matrix material as crystallographic movement along specified slip planes. In real metallic based composites these slip planes are a result of the motion of dislocations along lattice glide planes. However, the continuum mechanics based description of the dislocation motion avoids many of the complications involved with considerations involving multiple dislocation interaction. The theory of crystal plasticity applied to single crystals and polycrystalline materials is discussed in detail by Harren et al. [59] and is briefly explained in the following section. It should be noted that the use of a polycrystalline description of the matrix material, in conjunction with an elastic continuum description of the reinforcement, enables the simulation of the important non-uniform deformation of the matrix relative to the hard particles [60]. This is not possible in the case of purely analytical continuum solid modelling, as described in section 2.6.3.

Crystal Plasticity Theory

Due to the complexity involved in the mathematical description of the multi-dimensional conditions exhibited by metallic crystalline materials during deformation, the use of tensor analysis is employed in the investigation of such systems. The constitutive framework considered in the following section is a rate dependent plastic, finite strain, crystallographic slip theory, which excludes thermal loading. This theoretical approach, extended to include thermal loading is describe by McHugh et al. [58], and an equivalent rate independent approach is described by Needleman [182].

In order to describe the deformation of a single crystal it is necessary to accurately define the transition of an arbitrary point within the material from a datum condition

(reference configuration) to a deformed condition (current configuration). Each particle may be defined by its reference position vector, \mathbf{X} . The new position of this same particle in the current configuration can be defined by its current position vector, \mathbf{x} . The relationship between \mathbf{X} and \mathbf{x} is described by the deformation gradient \mathbf{F} , where

$$\mathbf{F} = \partial \mathbf{x} / \partial \mathbf{X} \quad (8)$$

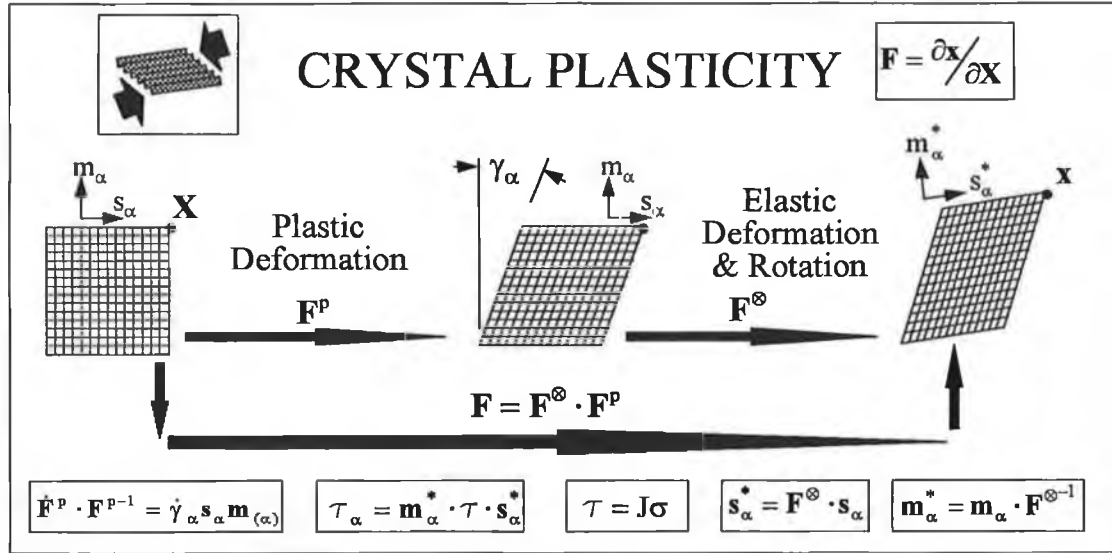


Figure 2.8. Schematic representation of the crystal plasticity description of single crystal kinematic deformation with respect to the α^{th} slip system.

The deformation gradient can be decomposed into two distinct sections, as shown in figure 2.8 and explained as follows,

$$\mathbf{F} = \mathbf{F}^\otimes \cdot \mathbf{F}^P \quad (9)$$

where, \mathbf{F}^P is the plastic deformation gradient, also referred to as the residual deformation gradient, and \mathbf{F}^\otimes is the elastic deformation gradient, which is made up of both elastic distortion and rigid body rotation. By using this decomposition it is

possible to isolate \mathbf{F}^p from \mathbf{F}^\otimes and therefore consider the plastic deformation mechanism alone. Since the plastic deformation is considered to occur along specific slip systems, the rate of change of \mathbf{F}^p ($\dot{\mathbf{F}}^p$) can be related to the rate of change of shear on the α^{th} slip system ($\dot{\gamma}_\alpha$) by

$$\dot{\mathbf{F}}^p \cdot \mathbf{F}^{p-1} = \dot{\gamma}_\alpha \mathbf{s}_\alpha \mathbf{m}_{(\alpha)} \quad (10)$$

where \mathbf{s}_α is the unit vector aligned with the direction of the α^{th} slip system and \mathbf{m}_α is the unit vector normal to the plane of that system, both in the reference configuration. The value of \mathbf{F}^p may now be obtained by path dependent integration of equation (10). In accordance with crystallographic theory, the slip occurring on the α^{th} slip system is dependent on the resolved shear stress (τ_α) acting on this system. This resolved shear stress is related to the Cauchy stress (true stress, σ) by the following equations,

$$\tau_\alpha = \mathbf{m}_\alpha^* \cdot \boldsymbol{\tau} \cdot \mathbf{s}_\alpha^* \quad (11)$$

$$\boldsymbol{\tau} = \mathbf{J}\boldsymbol{\sigma} \quad (12)$$

$$\mathbf{s}_\alpha^* = \mathbf{F}^\otimes \cdot \mathbf{s}_\alpha \quad (13)$$

$$\mathbf{m}_\alpha^* = \mathbf{m}_\alpha \cdot \mathbf{F}^{\otimes-1} \quad (14)$$

where the superscript * denotes description in relation to the current configuration (deformed), J is the Jacobian determinant of the deformation gradient \mathbf{F} , denoted by $\det(\mathbf{F})$, and $\boldsymbol{\tau}$ is referred to as the Kirchhoff stress.

In order to complete the plastic model of this single crystal system it is necessary to define the relationship between the resolved shear stress and the rate of shear on the slip system. This relationship is described by

$$\dot{\gamma}_{\alpha} = \dot{a}_{\alpha} \operatorname{sgn}\{\tau_{\alpha}\} \left(\tau_{\alpha} / g_{\alpha} \right)^{1/m} \quad (15)$$

where the constant \dot{a}_{α} is the reference shear rate on the α^{th} slip system, $\operatorname{sgn}\{\}$ denotes the sign of $\{\}$, the variable g_{α} is the slip system hardness and m is the rate sensitivity exponent. This crystallographic description of the plastic deformation, in conjunction with a similarly derived elastic constitutive law, may be used to describe the deformation of the matrix material within a DRMMC model. However, the material variables must be available and be reliable.

As in the case of subcontinuum modelling, the reinforcing particles are generally described as elastic isotropic materials and perfect interfacial bonding is assumed between the matrix and reinforcement [58]. The implementation of this model type is normally carried out using a two dimensional hexagonal grain/particle geometric model, within a FEM framework [58,60].

2.6.3 Continuum Solid Models

The classical rule of mixtures approach to continuum based composite mechanics can be applied successfully to continuous fibres MMC systems. However, in order to describe the complexities involved in DRMMCs more versatile approaches are required. The continuum solid modelling of DRMMCs can be sub-divided into two important areas based on the theoretical approach involved. These include the Eshelby [183] and the finite element methods [63]. Other approaches, such as the shear lag method, have also been investigated with limited success [14,184]. Although the rule of mixtures approach is unsuitable for use in the modelling of DRMMCs the concepts involved in the use of this approach are worth noting.

Rule of Mixtures

The rule of mixtures is a predictive method which is applicable to composite systems containing aligned continuous fibres within a homogeneous matrix, under a load which acts parallel to the axial direction of the fibres. The composite is considered as being a block or slab of matrix material perfectly bonded to a slab of the fibre material. This geometric model is referred to as the slab model [14]. It is assumed that the strain (ϵ_I) experienced by the inclusions (fibres) is equal to the matrix material strain (ϵ_M) and therefore, equal to the composite strain (ϵ_c).

$$\epsilon_c = \epsilon_I = \epsilon_M \quad (15)$$

From this assumption of equal strain (15) it can be found that

$$\epsilon_c = \frac{\sigma_I}{E_I} = \frac{\sigma_M}{E_M} \quad (16)$$

where σ_I and E_I represent the stress and the Young's modulus of the inclusion and, σ_M and E_M represent the stress and the Young's modulus of the matrix. In order to describe the stiffness of the composite the contribution of each phase must be

considered, based on the respective volume fractions. Therefore, the composite stress (σ_c) can be described as follows,

$$\sigma_c = (1 - f)\sigma_M + f\sigma_I \quad (17)$$

where f is the volume fraction of the inclusions. Combining equation (16) and (17) the Young's modulus of the composite (E_c) can be expressed as

$$E_c = \frac{\sigma_c}{\epsilon_c} = \frac{[(1 - f)\sigma_M + f\sigma_I]}{\sigma_I/E_I} \quad (18)$$

Therefore,

$$E_c = E_I \left[\frac{(1 - f)\sigma_M}{\sigma_I} + f \right] \quad (19)$$

Considering the relationship expressed in equation (16) it is found that,

$$\boxed{E_c = (1 - f)E_M + fE_I} \quad (20)$$

where

E_c = Young's modulus (E) of the composite (c) in the direction of the fibre axis.

E_M = Young's modulus (E) of the matrix (m).

E_I = Young's modulus (E) of the inclusions (i).

f = Volume fraction of fibres in the composite.

Equation 20 is known as the rule of mixtures. The validity of predictions based on this rule of mixtures is greatly dependent on the assumption of equal strain throughout the

composite. Therefore, the use of this predictive tool is only valid for long continuous fibre reinforced composites where equal strain is approached. In order to predict the behaviour of composite materials with more complex applied stresses and non-continuous forms of reinforcement more advanced models have been developed.

Eshelby Method

Analytical predictive techniques rely on the suitability of the geometric model to mathematical description. Due to this geometric dependency many composite models are unsuitable for analytical analysis. For example, if an inclusion within a composite is described as a parallelepiped and a material deformation occurs, the original inclusion may be transformed into a complex shape exhibiting non-uniform stress fields. This transformation may not be mathematically tractable [14]. However, the analytical composite analysis commonly known as the Eshelby method can be applied to a wide variety of composite systems and has been used to accurately predict many material properties [61,62]. J.D. Eshelby developed this method in the 1950s [183] based on a model where an inclusion is considered to be ellipsoidal in shape as shown in figure 2.9. The choice of an ellipsoidal geometric description is due to the tractability of the transformation kinematics involved in the regular deformation of this shape, and also the simplicity with which the uniform stress fields within any ellipsoid may be described.

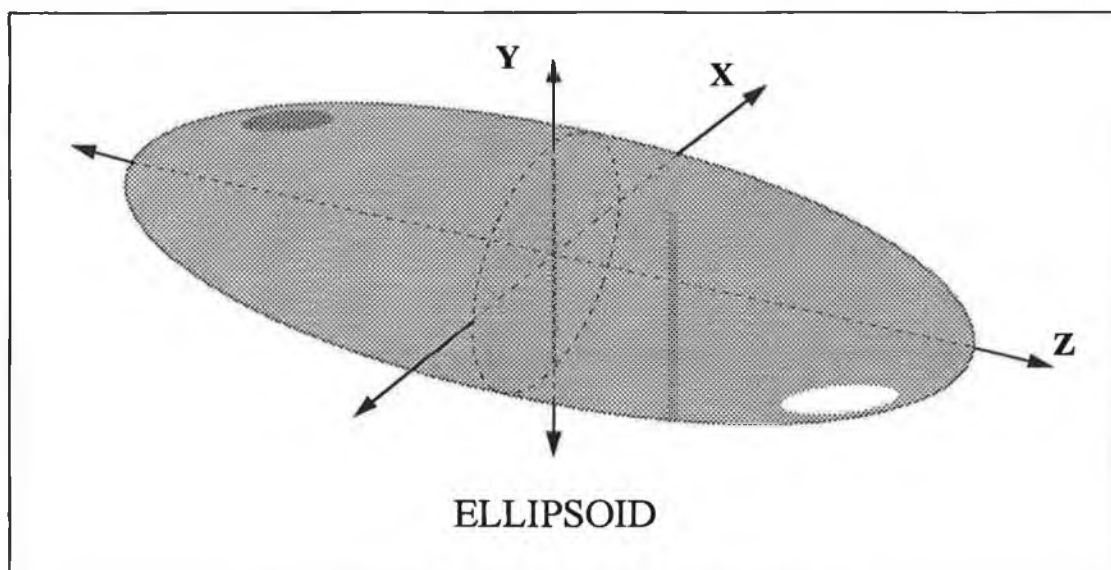


Figure 2.9. Three dimensional ellipsoid inclusion.

The fundamental concept involved in the Eshelby technique applied to MMCs is that for any inclusion within a homogeneous matrix there exists an equivalent matrix material inclusion, such that the replacement of the original inhomogeneity by this matrix equivalent maintains the same stress field in the matrix surrounding the inclusion. The use of an inclusion which exhibits the same stiffness as the original matrix avoids elastic inhomogeneity, and therefore simplifies the description of the stress fields within the matrix surrounding the inclusion. Figure 2.10 shows a step by step diagrammatic explanation of this concept based on an inclusion/matrix thermally induced misfit strain problem.

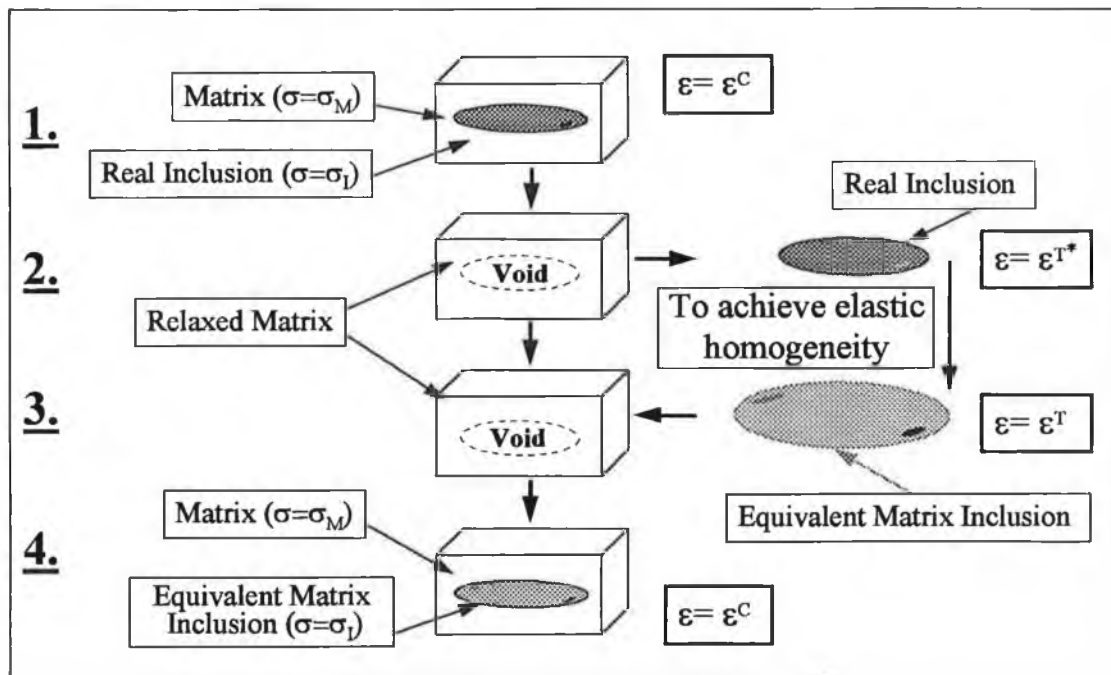


Figure 2.10. Equivalent matrix inclusion concept employed in the Eshelby technique.

Note: ϵ^{T*} refers to the transformation strain for the real inclusion and ϵ^T refers to the transformation strain of the equivalent matrix inclusion.

The inclusion is considered to be under uniform stress (σ_I), and the matrix is under non-uniform stress (σ_M). The strain experienced by this real inclusion whilst within the matrix material is referred to as the constrained strain (ϵ^C). By removing the real inclusion, a void is created and the matrix material recovers. The real inclusion will also deform once removed from the matrix. The unconstrained strain is referred to as

the transformation strain for the real inclusion (ϵ^{T*}). The relationship between σ_I , ϵ^C and ϵ^{T*} is dependent on the stiffness tensor for the inclusion material (C_I). By using Hooke's law,

$$\sigma_I = C_I (\epsilon^C - \epsilon^{T*}) \quad (21)$$

An ellipsoid of matrix material exists, such that, if the void is filled with this ellipsoid the original matrix will again experience the same stress and strain as with the real inclusion in place. This matrix material ellipsoid is referred to as the equivalent matrix inclusion. The unconstrained strain of this ellipsoid is referred to as the transformation strain of the equivalent matrix inclusion (ϵ^T). By inserting the equivalent inclusion within the void and fixing the relative positions of the ellipsoid surface to that of the void, the strain of this inclusion will become ϵ^C . Again, using Hooke's law, and the stiffness tensor for the matrix material (C_M),

$$\sigma_I = C_M (\epsilon^C - \epsilon^T) \quad (22)$$

Also, with the equivalent inclusion fixed in place, the stress within the original matrix material is again σ_M . Therefore, the stress field throughout the matrix material surrounding the inclusion will be identical for both the real inclusion and the equivalent matrix inclusion. Eshelby found that ϵ^C can be found from ϵ^T by a tensor operation.

$$\epsilon^C = S \epsilon^T \quad (23)$$

This Eshelby tensor (S) is dependent on the aspect ratio of the ellipsoid, and the Poisson's ratio of the matrix material. By combining equations (21) and (23) it is found that

$$\sigma_I = C_I (S \epsilon^T - \epsilon^{T*}) \quad (24)$$

Also, combining equations (22) and (23),

$$\sigma_I = C_M (S \epsilon^T - \epsilon^T) \quad (25)$$

From equations (24) and (25),

$$C_I(S\varepsilon^T - \varepsilon^{T*}) = C_M(S\varepsilon^T - \varepsilon^T) \quad (26)$$

Therefore,

$$\varepsilon^T = C_I \varepsilon^{T*} [S(C_I - C_M) + C_M]^{-1} \quad (27)$$

Combining equations(25) and (27),

$$\sigma_I = C_I \varepsilon^{T*} [S(C_I - C_M) + C_M]^{-1} (C_M(S - I)) \quad (28)$$

where I denotes the identity matrix.

Equation (28) can be used to calculate the stresses and strains within a single ellipsoidal inclusion due to a misfit strain and therefore can be used to describe the matrix stress field [14].

Also, in the case of an applied external load (σ^A) [14],

$$\sigma_I + \sigma^A = (C_I - C_M) \varepsilon^A [S(C_I - C_M) + C_M]^{-1} (C_M(S - I)) + C_M \varepsilon^A \quad (29)$$

The equations (21)-(29) are based on a single inclusion. However, it is possible to consider composites with more than one inclusion, varying ellipsoidal dimensions and various volume fractions [62,185-191]. This mean stress approach can be useful for the prediction of many composite material properties, with reasonable accuracy. Unfortunately, due to the approximations and assumptions made in Eshelby type models, failure to accurately describe both the geometry of the reinforcement types commonly found in DRMMCs and the matrix material non-linear properties limits its usefulness in the area of composite plasticity [14].

Finite Element Method

The majority of composite modelling research in recent years has focused on continuum based numerical modelling methods, such as the FEM, which employ isotropic phenomenological descriptions of both the matrix material and the reinforcement [45,192-194]. The FEM provides a powerful and flexible method of composite analysis capable of accommodating geometric complexity and constitutive non-linearities, and is ideally suited to composite plasticity and internal stress investigations. A number of geometric modelling approaches have been investigated. One common approach to the geometric description of the composite is to consider it as a homogeneous matrix material containing a periodic array of uniformly shaped reinforcement particles [76,166,193-202]. The purpose of this description is to allow for unit cell isolation and axisymmetric approximation of the total composite. Figure 2.11 shows the steps involved in this geometric simplification.

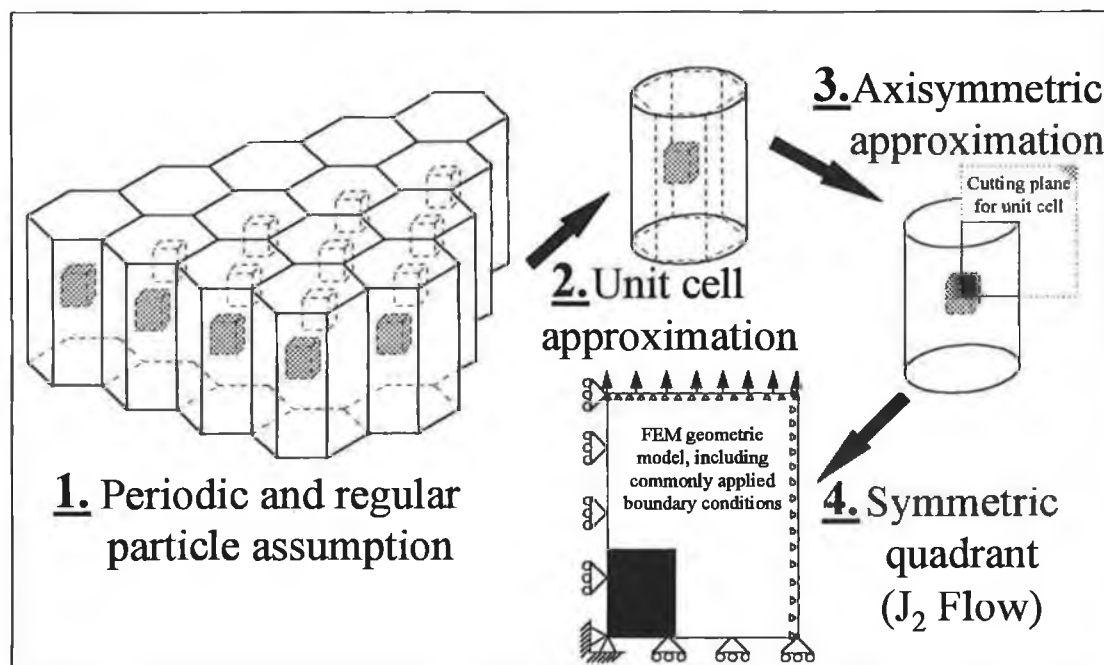


Figure 2.11. Frequently used method of geometric simplification in finite element modelling of DRMMCs

The repeat unit geometry may be hexagonally cylindrical, as in figure 2.11, or parallelepiped [198]. Common particle shapes include spherical [193], ellipsoidal [202], hexagonal cylindrical [192,201] and circular cylindrical [198]. Analysis of three dimensional unit cell models are uncommon due to their computational complexity.

Normally the three dimensional unit cell is simplified by using an axisymmetry, plane stress or plane strain approximation. A number of alternative approaches have been investigated which attempt to take account of such factors as the random distribution of particles [203-206] and particle clustering [63,207,208] found in real DRMMCs. Although the FEM shows great potential as a composite modelling tool, quantitative errors can easily occur due to inaccurate phenomenological descriptions of the constituent materials. These errors will become less likely as the understanding of composite micromechanics develops further and as more accurate material property descriptors become available.

CHAPTER 3 EXPERIMENTAL WORK

The present experimental research focuses on the optimisation of the powder metallurgical (PM) powder pressing and sintering production of particle reinforced aluminium matrix composite (PRAMC) material. Aluminium alloys AA6061 and AA2124 were selected as matrix materials and silicon carbide (SiC) particulate was selected as reinforcement. The basis of selection for both the matrix and reinforcement materials chosen for this work is discussed in section 3.1. Both aluminium alloys were supplied in prealloyed powder form and these powders were produced by argon atomisation. The SiC particulate used was industrial abrasive grade SiC which was supplied in an unconditioned form (mechanically pulverised only). The nominal size and size distribution of the aluminium powders and the SiC particles used are discussed in sections 3.1.1, 3.1.2 and 4.2.2.

Figure 3.1 outlines the fundamental steps involved in the processing route which was investigated in the present experimental research. These fundamental steps include the mixing of the matrix and reinforcement powders, the uniaxial pressing of the resulting composite powder into either cylindrical or tensile test sample shaped green compacts and the liquid phase sintering of these green compacts.

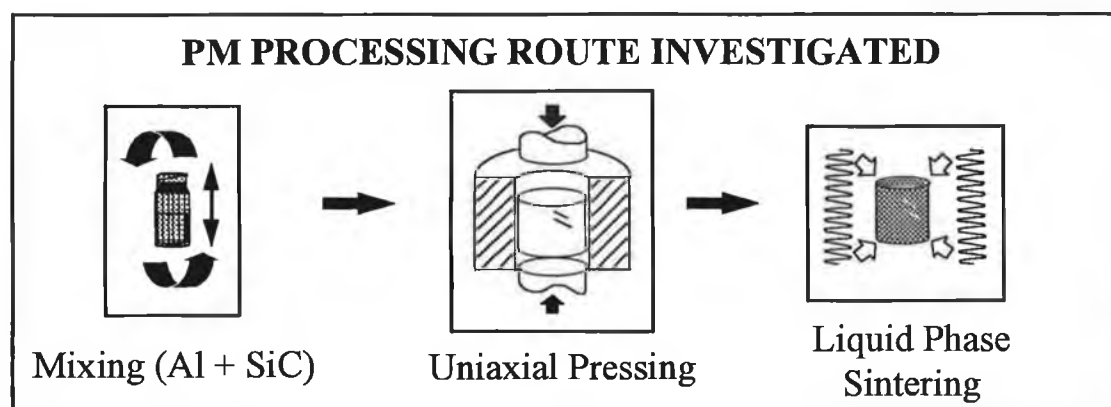


Figure 3.1. The fundamental steps involved in the processing route investigated in the present experimental research.

Many additional stages were incorporated in this basic PM process in order to improve the condition of the final composite material. These additions include precompaction powder heat treatment (annealing/normalising), mixed-in powder lubrication or die wall lubrication, sintered billet repressing and sintered billet heat treatment. Unlike the majority of processing methods used for the production of PRAMCs, the process investigated did not involve composite powder canning, degassing or isostatic pressing stages.

The systematic experimental work carried out consists of four sequential test matrices, each of which concentrates on a number of individual processing parameters. The first three test matrices carried out deal with the processing of cylindrical samples (17mm diameter), whereas the final test matrix is specific to the processing of tensile test samples. Figures 3.2, 3.3, 3.4 and 3.5 describe each test matrix by indicating the materials used, the parameters varied within each stage and the analyses carried out. As described below, the design of each test matrix was founded on the results of prior matrices resulting in sequentially improving final composite material.

Sequential Experimental Work Overview

The processing method and parameter values used, and also the materials selected in the first test matrix (test matrix no. 1, figure 3.2) were chosen primarily on the basis of the results obtained and observations made in previous related experimental work [210]. The analyses carried out in this test matrix highlighted the importance of aluminium powder size and reinforcement size selection, and also strongly indicated the need for a carefully controlled sintering atmosphere. In addition, it was observed that clusters of both the SiC particulate and the solid lubricant used were not adequately deagglomerated during the powder mixing process.

On the basis of the results and observations from test matrix no. 1 alterations were made to the process. A heat treatment unit with a nitrogen gas supply system was designed and constructed to allow atmospheric control during sintering for test matrix

no. 2 (figure 3.3). Also, based on the microstructural observations made in test matrix no. 1, the aluminium powder size and the SiC particle size selected for test matrix no. 2 were chosen so as to minimise the possibility of SiC clustering due to aluminium powder/SiC particle size mismatch. In order to investigate the possibility of improved mixing, test matrix no. 2 incorporated a qualitative mixing analysis to compare the mixing process used in test matrix no. 1 with that of manual rapid reciprocation mixing.

Incorporating process improvements in test matrix no. 2 facilitated an investigation designed to compare the processing characteristics of precompaction heat treated composite powders with those of composite powders in the as-supplied form. This analysis was considered on the basis of the proposition that by softening the high strength rapidly solidified atomised aluminium powder it should be possible to increase the compressibility of the composite powder.

The processing method used in test matrix no. 3 (figure 3.4) was selected on the basis of the results and observations from test matrix no. 2. Test matrix no. 3 focused on the effects of processing parameter and material type variation on composite quality. The variables investigated include aluminium alloy type, lubricant type, lubricant quantity, precompaction powder heat treatment atmospheric condition, powder compaction rate, sintering temperature and time and sintered material heat treatment condition. The results and observations from test matrix no. 3 were used to design the process for the production of tensile test samples in test matrix no. 4.

The main objective of test matrix no. 4 (figure 3.5) was to investigate the technical feasibility of the PM powder pressing and sintering process for the production of a relatively geometrically complex PRAMC component. In addition to this overall objective a number of materials selection and processing based variables were incorporated in the test matrix in order to further elucidate the effects of these parameters. The material based variables considered include aluminium powder size, SiC particle size, SiC volume fraction and lubrication method. Also, analyses were carried out to investigate the microstructure of the green compacts. These analyses

explored the possibility of a relationship between the green compact microstructure and the good sintering response of these aluminium powder based compacts. The primary processing factors investigated and the main findings of these investigations are as follows,

Test Matrix No. 1 (96 cylindrical samples)

Experimental work

- Effect of powder size investigated.
- Processing parameters based on previous work [210] and reviewed literature.

Findings

- Correct selection of powder size combinations can improve the final material.
- Sintering atmosphere must be closely controlled.
- Rotary mixing produces poor mixtures.

Test Matrix No. 2 (88 cylindrical samples)

Experimental work

- Powder heat treatment investigated. (new concept)
- Processing parameters and powder size selection based on test matrix no. 1 and reviewed literature.
- Sintering atmosphere controlled.
- Reciprocation mixing compared to rotary mixing.

Findings

- Powder heat treatment can greatly improve the final material.
- Controlled sintering atmosphere can greatly improve final material.
- Process can produce well consolidated composite material.
- Primary processing parameters identified.
- Reciprocation mixing is superior to rotary mixing.

Test Matrix No. 3 (71 cylindrical samples)

Experimental work

- Variation of sintering conditions.
- Solid lubricant variables.
- Powder heat treatment atmosphere.

Findings

- Both sintering time and sintering temperature affect consolidation.
- Solid lubricant quantity should be minimised.
- Nitrogen powder heat treatment better than heat treatment in air.

Test Matrix No. 4 (46 tensile test samples)

Experimental work

- Complex net shape component production.
- Tensile properties of the material.
- Effect of powder size investigated.

Findings

- Complex net shape components can be produced by this process.
- Acceptable tensile properties.
- Small size aluminium powders led to improved material.

The analysis techniques employed in the present experimental work include visual, optical and scanning electron microscopy (SEM) powder inspection, laser diffraction powder size analysis, powder compressibility testing, ejection force analysis, diametrical green strength testing, SEM analysis of the green powder compacts, sintered material density analysis, hardness compression and tensile testing, optical microstructural investigation of the sintered composite and SEM fracture surface analysis of the tensile test samples. These analysis techniques and the analysis procedures followed are described in section 3.3.

TEST MATRIX No. 1 (CYLINDRICAL COMPONENTS)

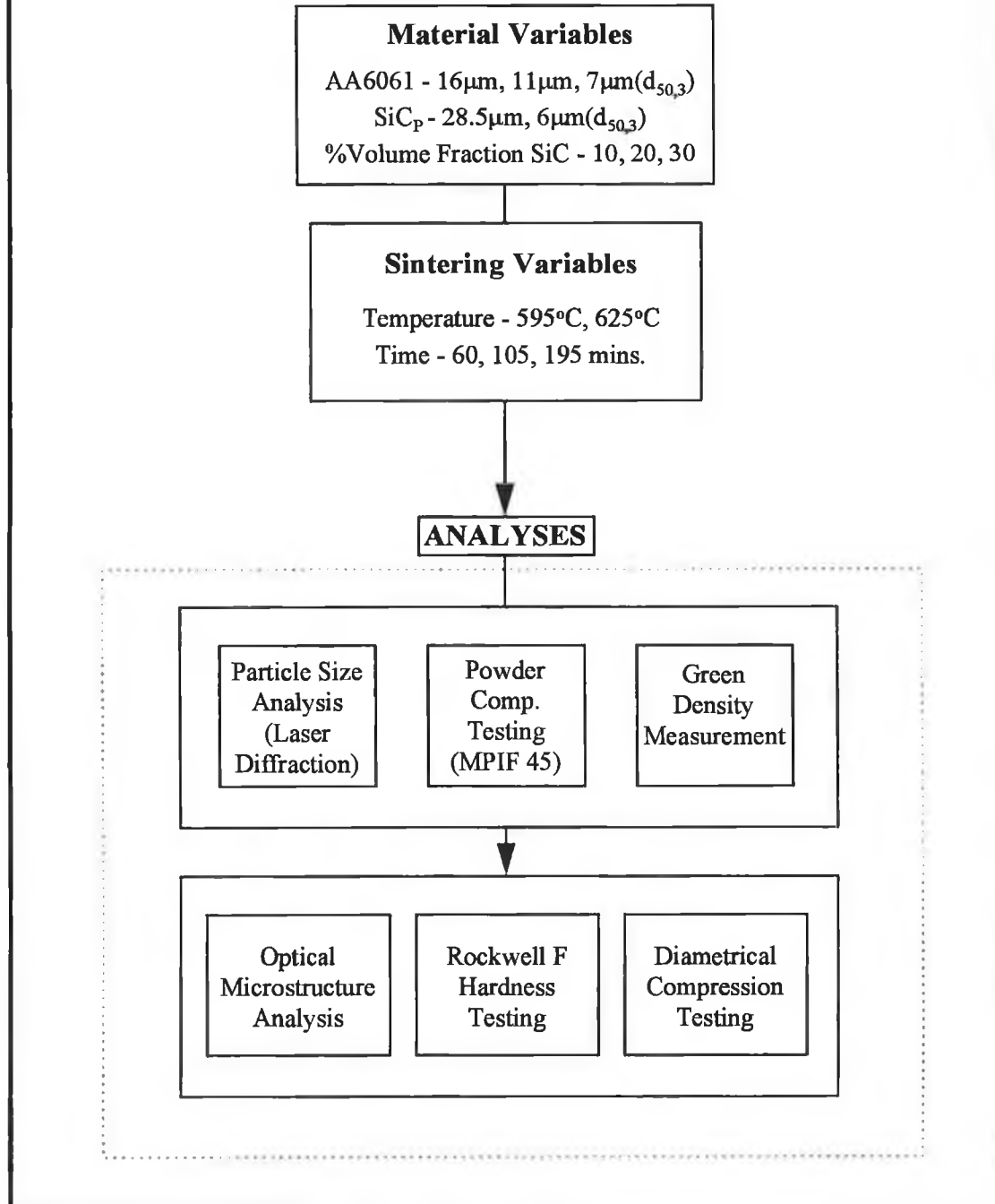


Figure 3.2. Test matrix number 1 flow chart.

TEST MATRIX No. 2 (CYLINDRICAL COMPONENTS)

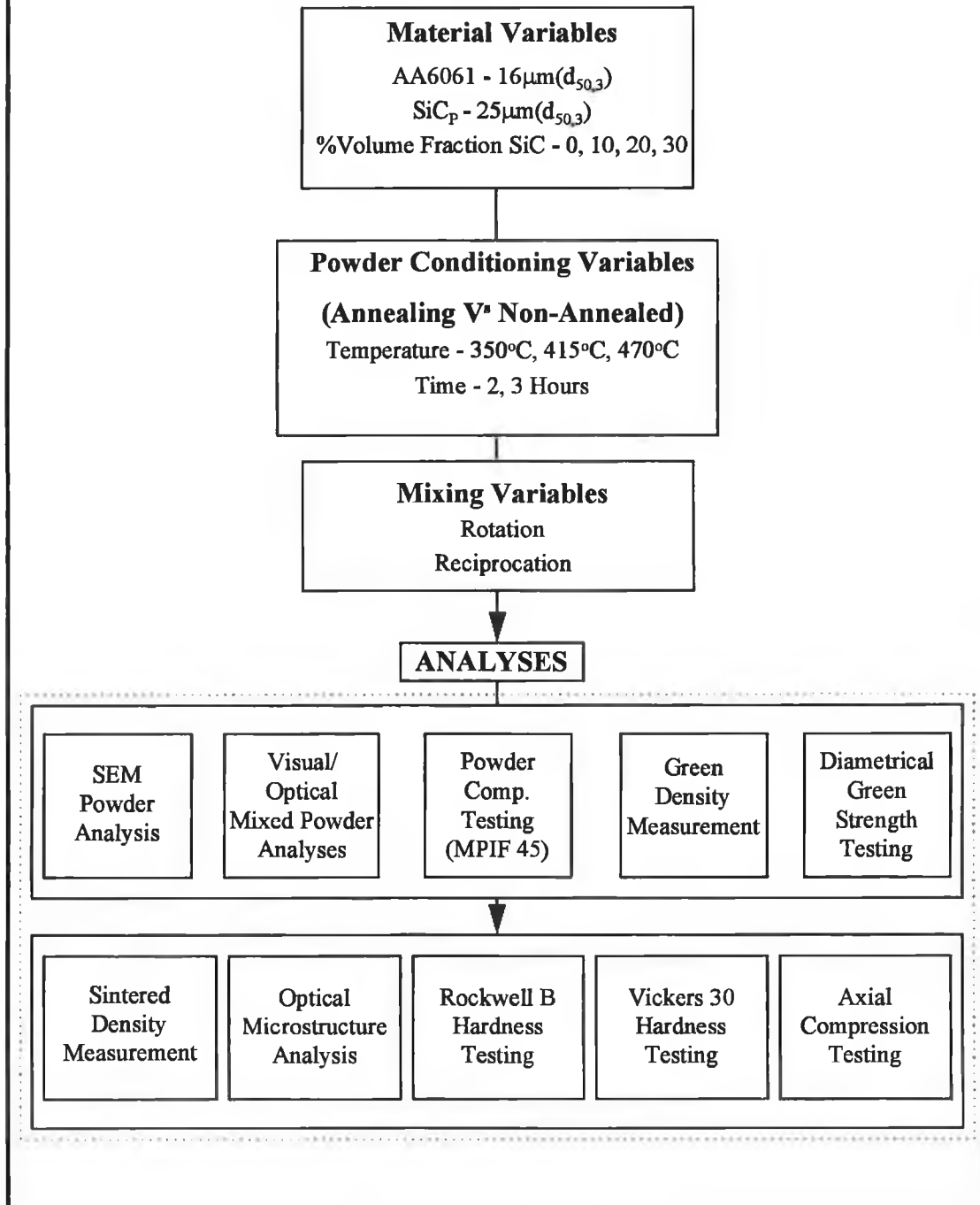


Figure 3.3. Test matrix number 2 flow chart.

TEST MATRIX No. 3 (CYLINDRICAL COMPONENTS)

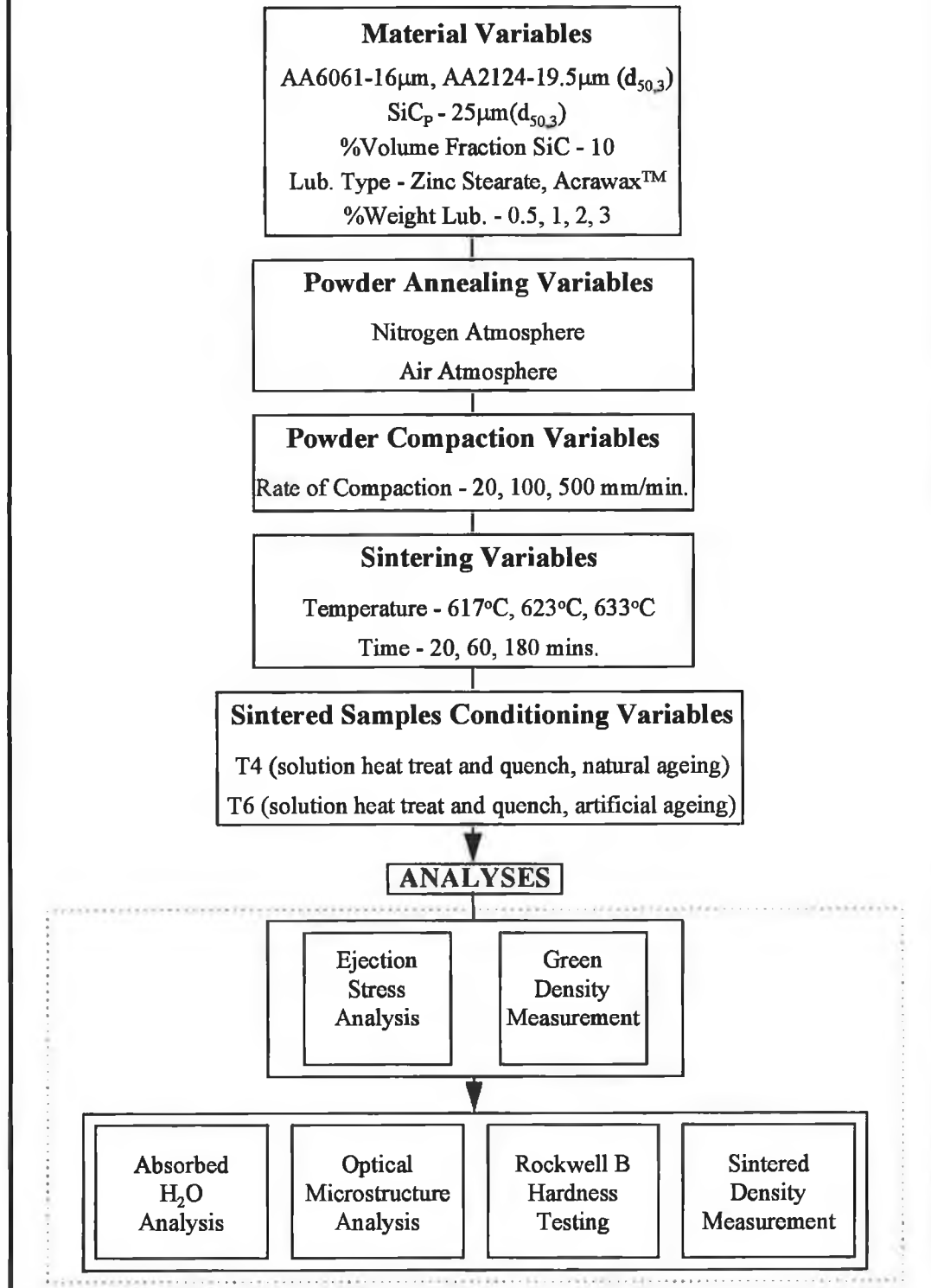


Figure 3.4. Test matrix number 3 flow chart.

TEST MATRIX No. 4

(TENSILE TEST COMPONENTS)

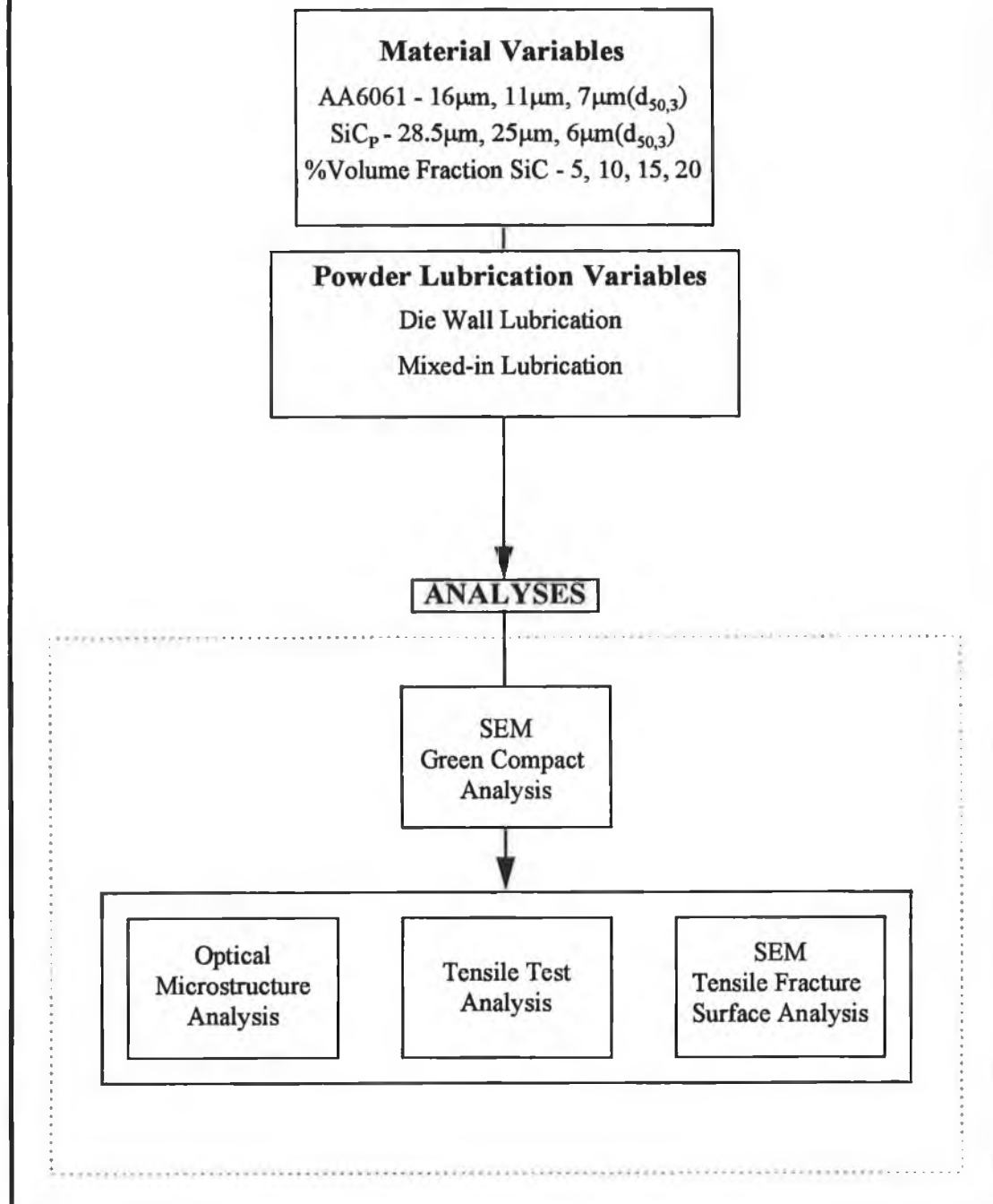


Figure 3.5. Test matrix number 4 flow chart.

3.1 MATERIAL SELECTION

3.1.1 Matrix Material

The aluminium alloys AA6061[†] and AA2124, which have been selected as matrix materials for the present work, are both regularly used in engineering applications [18]. AA6061 is a common medium strength heat treatable alloy and the AA2124 alloy is an advanced high strength alloy. These alloys were selected on the basis of availability, cost, heat-treatable characteristics [148], SiC compatibility [37,209] and suitability to PM processing [20].

The nominal chemical composition by weight of both AA6061 and AA2124 can be seen in table 3.1. Also, table 3.2 lists various material properties of these alloys. A variety of powder sizes, including 7 μm ($d_{50,3}$)[‡] 11 μm ($d_{50,3}$), 16 μm ($d_{50,3}$) and 19.5 μm ($d_{50,3}$) have been used. These argon atomised prealloyed powders, shown in figure 3.6, can be described as nodular and irregular. All powders were produced and supplied by the Aluminium Powder Company, England.

Table 3.1. Nominal chemical composition by weight of AA6061 & AA2124.

	Aluminium	Magnesium	Silicon	Copper	Chromium	Iron	Manganese
AA6061	97.6%	1.01%	0.75%	0.30%	0.18%	0.16%	0.00%
AA2124	94.0%	1.43%	0.01%	4.01%	0.00%	0.18%	0.37%

Table 3.2. Physical properties of monolithic AA6061, AA2124 & SiC_P [14,35,83].

	Density (g/cm ³)	Solidus/Liquidus (°C)	U.T.S. (MPa)	Elastic Modulus (GPa)
AA6061	2.7	552-652	310-380 (PM)	70 (PM)
AA2124	2.77	530-640	474 (PM)	73.1 (PM)
SiC _P	3.2	-	>3000	450

[†] AA refers to the Aluminium Association specification.

[‡] $d_{50,3}$ refers to the statistical median particle size based on the cumulative frequency size distribution (quantity type = 3, RRSB distribution) [17].

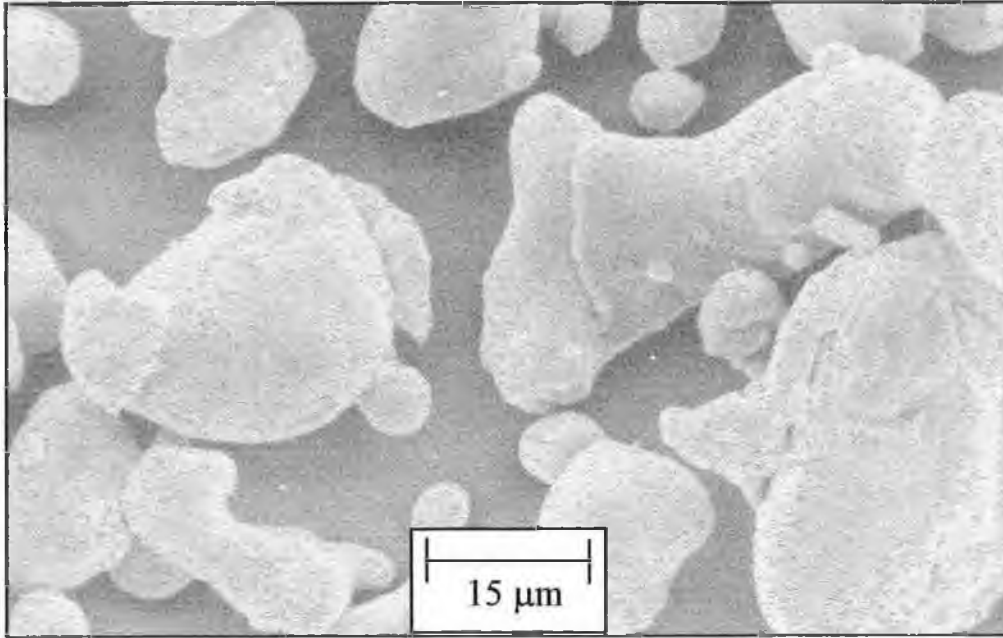


Figure 3.6. SEM micrograph of the argon atomised 16µm ($d_{50,3}$) AA6061 used in the present experimental research, Mag. x 1120.

3.1.2 Reinforcement

SiC particulate was selected as the reinforcement material for the present investigations. These ceramic particles are commonly used as abrasive grit in polishing, grinding and cutting applications and are therefore widely available in a variety of sizes and are also relatively inexpensive (£17/kg for one kilo. purchase).

The SiC used in this work was angular α -SiC particulate with a density of 3.2 g/cm^3 compared to 2.7 or 2.77 g/cm^3 for the matrix materials. The density relationship aims to maximise the specific properties of the final material by only slightly increasing the overall density compared to the density of the matrix material. A range of sizes including $6\mu\text{m}$ ($d_{50,3}$), $25\mu\text{m}$ ($d_{50,3}$) and $28.5\mu\text{m}$ ($d_{50,3}$) were investigated in this research. Table 3.2 lists various nominal material properties of SiC particles. Figure 3.7 shows the angular nature of the SiC particulate.

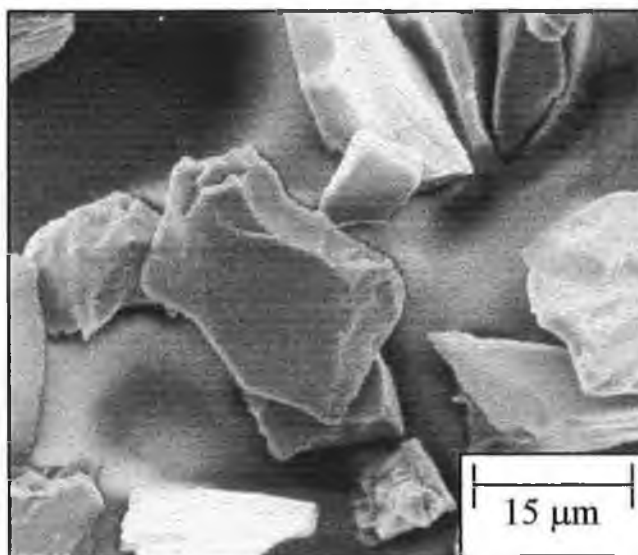


Figure 3.7. SEM micrograph of the as-supplied $25\mu\text{m}$ ($d_{50,3}$) SiC particulate used in the present experimental research, Mag. x 1120.

3.1.3 Lubricant

Zinc stearate powder lubricant was used to reduce die wall friction during sample ejection in the majority of the present research. AcrawaxTM powder lubricant was also investigated. These powder lubricants were either mixed with each blend of composite powder in various quantities including 0.5, 0.75, 1, 2 and 3% by weight or used as die wall lubricants. The solid lubricant was subsequently burnt off from the green components at either 450°C or 415°C. This burn off procedure was incorporated into the presintering stage of the sintering heat treatment process.

Table 3.3. Properties of the zinc stearate and AcrawaxTM solid lubricants [125,126].

Common Name	Softening Temperature (°C)	Melting Temperature (°C)	Density (g/cm ³)	Auto-Ignition (°C)
Zinc stearate	77-110	190	1.09	302
Acrawax TM	99-146	193	NA	310

Note: NA refers to information not available in reviewed literature.

The physical properties of zinc stearate are listed in table 3.3. The particle size of this powder was found by laser diffraction to be approximately 11µm ($d_{50,3}$). The selection of lubricant types was based on their lubricating properties, burn off characteristics and availability [83,125].

3.2 PROCESSING EQUIPMENT AND PROCEDURES

3.2.1 Powder Mixing

Due to the direct relationship between the reinforcement particle distribution at the end of the mixing stage of processing and that of the final composite [116,118], it is of considerable importance that the powder mixing method used produces homogeneously mixed composite powder. In the present work visual and optical qualitative analyses were carried out with the objective of ensuring that the mixed composite powders exhibited reasonable SiC particle distribution. The method referred to as rapid reciprocation used in test matrices no. 2, 3 and 4 was found to provide this desired distribution. However, it should be noted that the qualitative analyses carried out, whilst sufficient for the requirements of the present work, have not in any way quantified the optimum methods or parameters for this complex procedure of powder mixing.

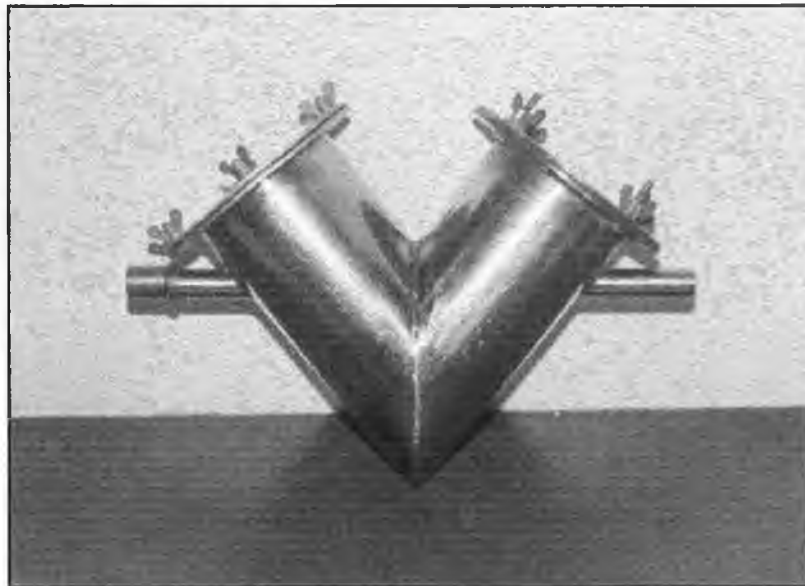


Figure 3.8. V-shaped container used for rotational mixing in test matrix no. 1.

Test Matrix No. 1

Mixing of the powders used in test matrix no. 1 was carried out by mechanical rotation of a V-shaped container shown in figure 3.8. A predetermined charge of aluminium, SiC and zinc stearate powder was placed inside this container. The container was sealed and mounted on a lathe. The rotational speed was set to 36 rpm and the powder blend was rotated at this speed for a duration of 90 minutes. The V-shaped container used was selected on the basis of the use of this container in previous related work [210]. Also, the mixing parameters employed were based on the results of this previous work.

Test Matrices No. 2, 3 and 4

It was observed that the mixing process used in matrix no. 1 resulted in mixtures containing agglomerates of both SiC and zinc stearate. In an attempt to reduce the likelihood of this undesirable inhomogeneity and to reduce the mixing processing time, the mixing of powders for test matrices no. 2, 3 and 4 was carried out by manual rapid reciprocation. In this mixing process predetermined quantities of matrix and reinforcement powders were weighed directly into a transparent plastic container. The container, shown in figure 3.9, was subsequently sealed by fully tightening the screw-on lid. The container was then rapidly reciprocated for approximately three minutes. In the case of test matrix no. 2, the batches of powder which were not annealed after mixing contained a predetermined quantity of lubricant. All other powder mixtures were annealed after mixing. The lubricating powder was then mixed into the heat treated powder by the same reciprocation mixing method unless die wall lubricant was to be used as in the case of test matrix no. 4. Due to the as-supplied agglomerated condition of the lubricant it was necessary to manually break up some large agglomerates with the use of a clean glass rod before adding to the mixture. Under both visual and optical inspection the powder mixtures produced by this method exhibited no sign of either SiC or lubricant agglomeration.

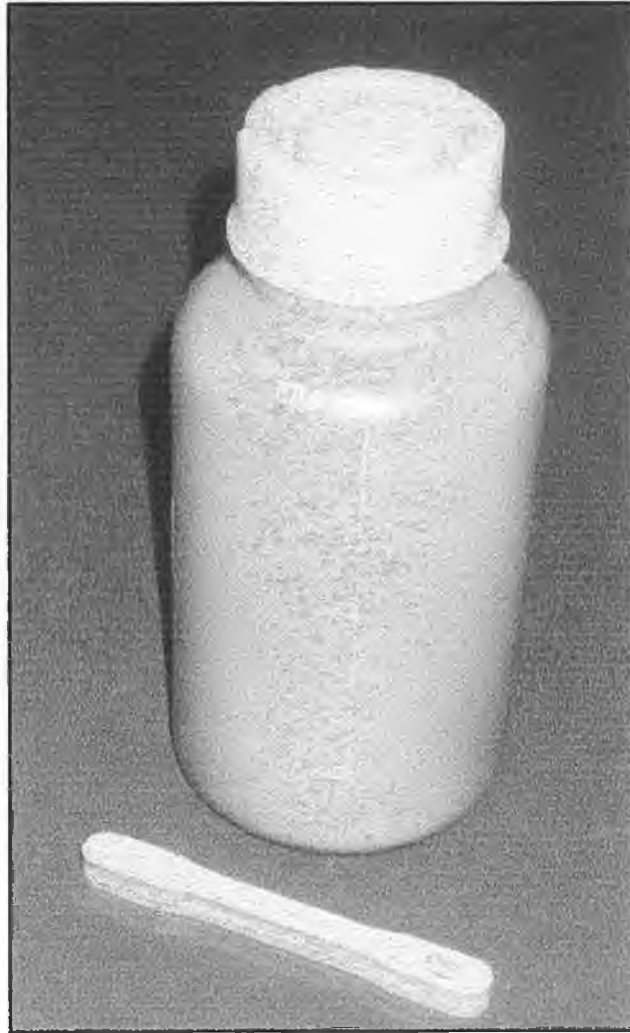


Figure 3.9. Plastic container used for the reciprocation mixing process in test matrices no. 2, 3 and 4.

3.2.2 Powder Conditioning

Test Matrix No. 1

No powder conditioning was carried out on the powders used in test matrix no. 1. Once mixed, these powders were stored in sealed containers awaiting compaction.

Test Matrix No. 2

Based on the results and observations of test matrix no. 1, precompaction annealing was investigated in test matrix no. 2. The concept on which test matrix no. 2 was developed focused on the softening of the rapidly solidified aluminium alloy powders with the aim of increasing compressibility, and reducing the quantity of both the absorbed H_2O in the aluminium powder oxide layer and H_2O on the surface of the SiC particles (SiC_P). Non-annealed powder blends were also processed in this test matrix for comparison.

Annealing of powder blends was conducted at temperatures of 350°C, 415°C and 470°C, and over times of 2 hours and 3 hours in order to investigate various heat treatment conditions. These heat treatment temperatures and times were based on the recommended annealing conditions for AA6061 [148]. The powder blends of AA6061 and SiC_P to be annealed were poured into stainless steel containers and the containers were placed into a mild steel heat treatment unit within a kiln (West 2054 PLC controlled, top-loading Firecraft TLB 34). This mild steel unit was similar in construction to the stainless steel unit shown in figure 3.10.

With the powder blends in place the lid of the mild steel container was placed in position. Industrial nitrogen at a pressure of approximately 1.5 bar was fed to the seal unit at a rate of 14 litres/min for approximately 3 minutes with the lid of the unit unclamped and the gas outlet valve fully closed. This high gas flow rate was used to prime the unit with nitrogen. Following this priming procedure, the gas flow rate was reduced to 3 litres/min, the lid was fully clamped into position and the gas outlet valve was opened. The powder blends were heated to one of the three annealing

temperatures, soaked for either 2 or 3 hours, and cooled to room temperature at a rate of 30°C/hour. Once the annealing cycle was complete the powders were replaced into their original plastic containers, which were immediately sealed. These powder batches were subsequently lubricated prior to compaction.

Test Matrix No. 3

The annealing process used in test matrix no. 3 was based on the results of test matrix no. 2. Due to the flaking and warping of the mild steel unit used in matrix no. 2 this unit was replaced by the high temperature resistant stainless steel unit shown in figure 3.10.

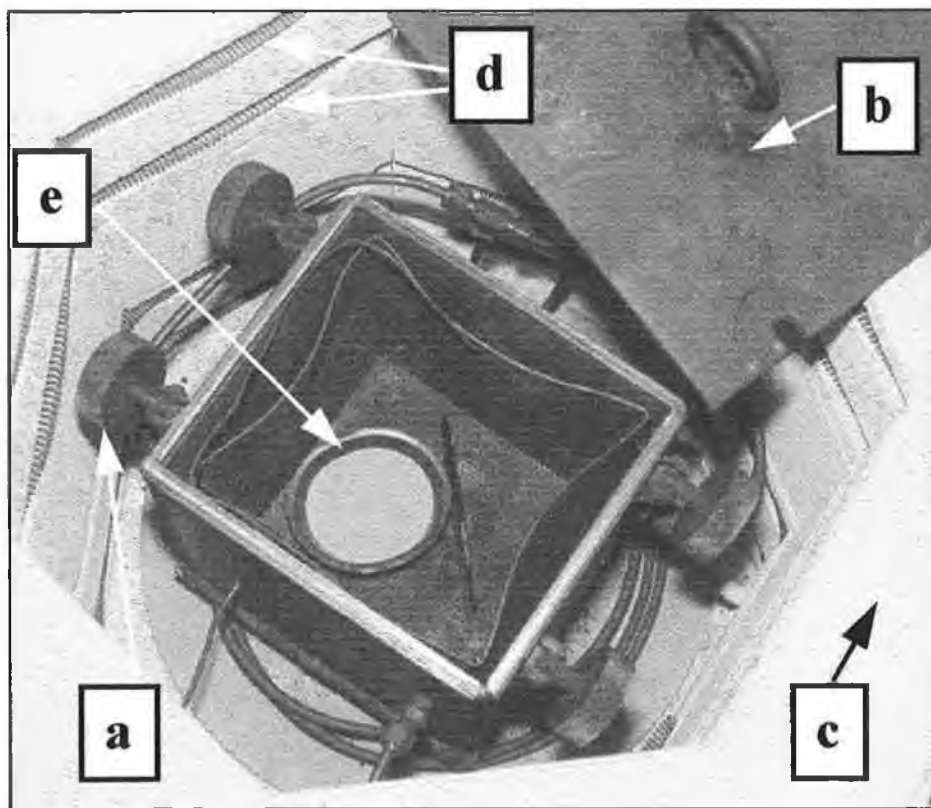


Figure 3.10. Stainless steel heat treating unit within kiln used for powder heat treatment in test matrices no. 3 and 4. (a) one of four knurled nuts used for clamping lid closed, (b) lid of unit, (c) kiln wall, (d) heating elements, (e) single batch of mixed powder within an open stainless steel bowl.

The nitrogen inlet pipe to this unit was constructed so as to circle the unit 3 times within the kiln before entering the unit at two positions. The circling of the unit prior to entry allowed the nitrogen gas to heat up before entering the unit. An annealing temperature of $475^{\circ}\text{C} \pm 2^{\circ}\text{C}$, a heating rate of $130^{\circ}\text{C}/\text{hour}$ and a soak time of 2 hours were employed for all powder blends. However, unlike test matrix no. 2, in order to investigate the effects of different annealing atmospheres this powder heat treatment was carried out in either a nitrogen atmosphere or in air. Again the powders, once at room temperature, were replaced in their containers and these containers were sealed. The powders were subsequently lubricated prior to compaction.

Test Matrix No. 4

The annealing process used in test matrix no. 4 was based on the results of test matrix no. 3. The unit shown in figure 3.10 was used for all the annealing carried out. The powder annealing heat treatment involved heating to a temperature of $480^{\circ}\text{C} \pm 2^{\circ}\text{C}$ at a rate of $130^{\circ}\text{C}/\text{hour}$, soaking for $1\frac{1}{2}$ hours at this temperature, followed by cooling at a rate of $45^{\circ}\text{C}/\text{hour}$ to 100°C . All annealed powder blends were poured into plastic containers and reciprocated for a further 2 minutes to break up any caked powder. Subsequent to annealing, 0.75% by volume zinc stearate powder lubricant was added to 200 grams of batch No. 1 (see appendix D for batch details) of this test matrix. Since die wall lubrication was used for all other powders, no lubricant was added to these powders before compaction.

3.2.3 Powder Pouring

Test Matrices No. 1, 2 and 3 (Cylindrical samples)

Powder pouring was carried out using a funnel positioned on the top of the die. Care must be taken at all times when handling these powders and therefore, during any pouring operation, safety glasses, protective clothing and respiratory protection was worn. Also, over filling, which creates unnecessary dust was avoided. Figure 3.11 shows the funnel in position on the top of the cylindrical die used in test matrices no. 1 and 2 during the pouring operation. This set up was also used in test matrix no. 3.

For each sample produced a predetermined mass of composite powder was measured into a flexible plastic boat (shown in figure 3.12 (a)). With the bottom punch inserted into the die at an appropriate height to suit the quantity of powder, the powder was carefully poured from the flexible boat into the die cavity with the aid of the funnel. The boat, funnel and die body were tapped in order to maximise the quantity of measured powder entering the die cavity and to minimise the quantity of powder on the die wall. Following this pouring procedure the top punch was inserted into the die.

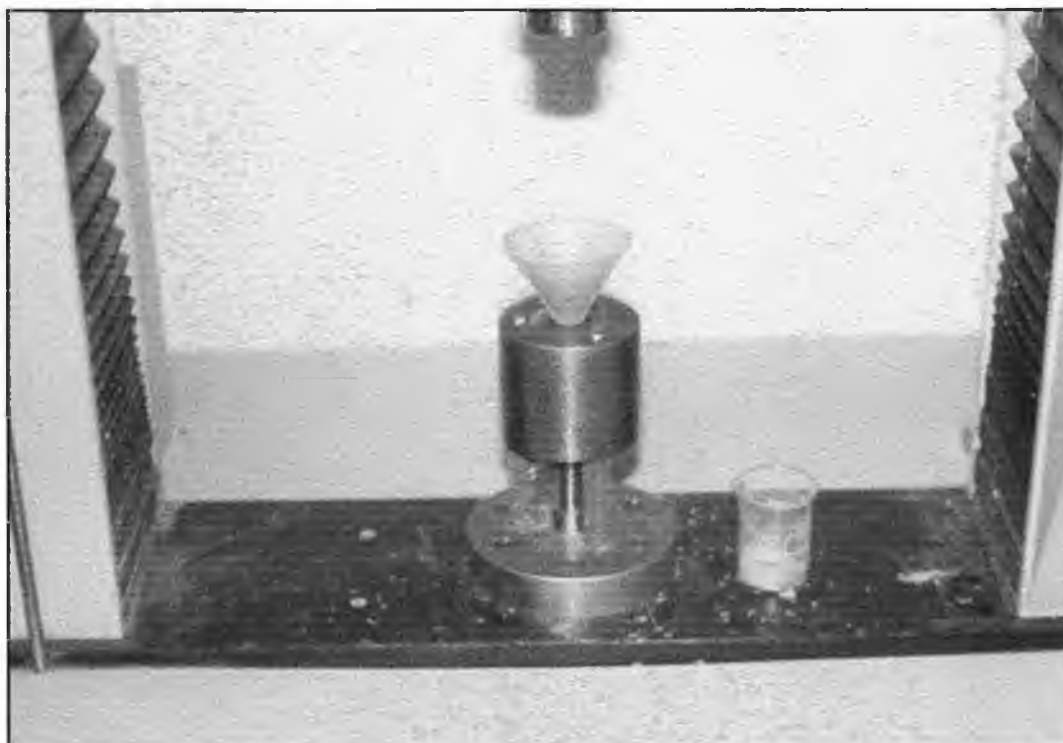


Figure 3.11. Powder pouring set up used in test matrices no. 1, 2 and 3.

Test Matrix No. 4 (Tensile test samples)

Before pouring the powder into the die cavity the bottom punch was inserted. This punch was positioned so that the face of the punch was at a distance from the top face of the fully closed split die to allow the entire predetermined quantity of powder to fit within the cavity. This predetermined mass of powder is dependent on the thickness of sample required. In test matrix no. 4 this thickness was calculated so that if a sintered density of 100 per cent was achieved, each sample would have a thickness of 6.5mm. The nominal mass of powder used for each sample in test matrix no. 4 was 14.5 grams. The exact mass of powder used for each sample depended on the SiC volume fraction of the composite powder from which it was to be made.

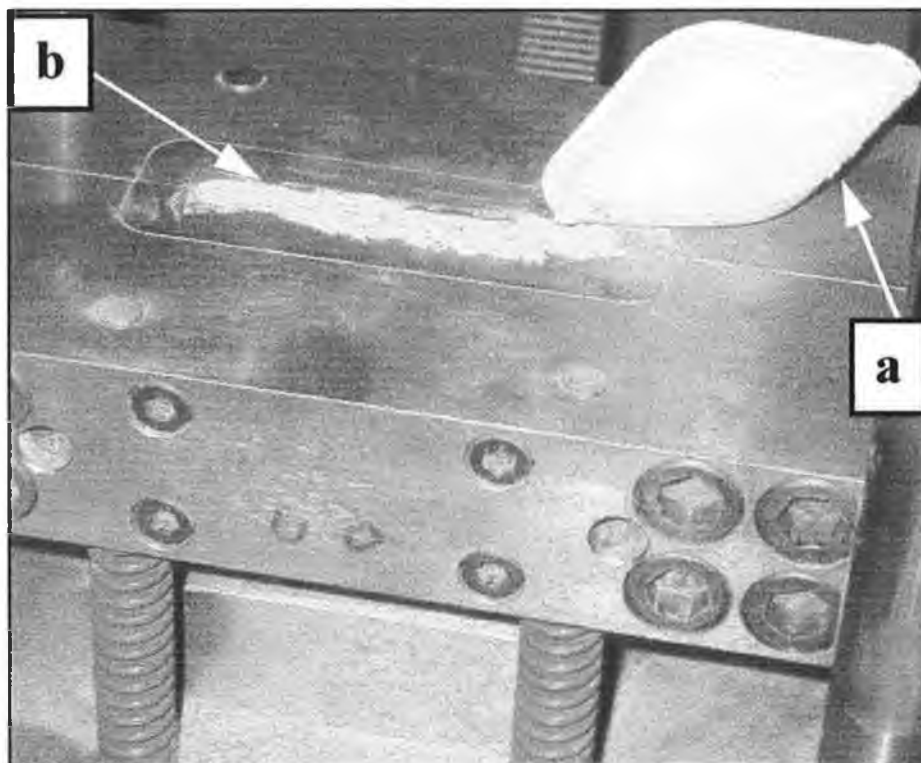


Figure 3.12. Manual powder pouring carried out in matrix no. 4., split die in fully closed position, (a) flexible plastic boat, (b) poured powder within die cavity.

With the bottom punch in place, die wall lubrication was applied by brushing a thin layer of zinc stearate powder lubricant over the die cavity and the punch faces. Where lubricant had been added to the mixture, no die wall lubrication was applied. Powder pouring was carried out by manually pouring the powder mix from a flexible plastic boat into the die cavity, as shown in figure 3.12. Directly after the manual pouring

step the die was tapped to aid powder settling within the die. After this tapping any powder left on the top face of the die was scraped into the cavity. The powder was leveled by tapping, lower die movement and scraping. When the powder was reasonably level and evenly distributed within the die cavity the bottom punch was pulled downward and allowed rest in position for the compaction step. With the bottom in this lower position the die was tapped once more to minimise the quantity of powder on the die walls. Following this pouring procedure the top punch was carefully inserted.

3.2.4 Powder Compaction

Test Matrices No. 1 and 2 (Cylindrical samples)

All compaction of the mixed powders for both test matrix no. 1 and 2 was carried out using the 80mm floating die set shown in figure 3.13. This floating die set was designed and constructed as part of other work [210]. Cylindrical green compacts 17mm in diameter were produced. The height of each compact was dependent on the mass of the powder charged into the die and the compressibility of the powder.

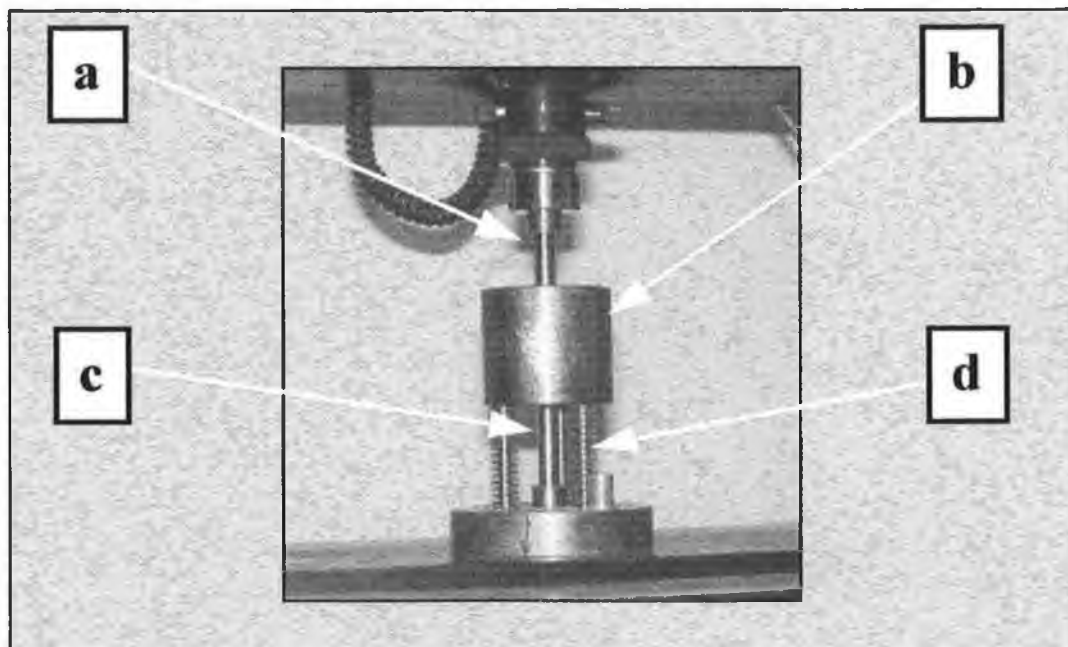


Figure 3.13. Compaction set up used in test matrices no. 1 and 2, (a) top punch, (b) floating die (cavity shape: 17mm diameter cylindrical cavity, 80mm in height), (c) bottom punch, (d) die spring and guide pin (three off).

The die consists of a cylindrical mild steel die body into which two hollow cylindrical tungsten carbide inserts are press fit, so as to meet end to end within the die body. The die rests on three die springs which allow for a floating action to occur during compaction. The vertical movement of the die on the springs is guided by three guide pins located in the centre of each die spring. The die set was mounted on a universal testing machine (INSTRON model 4204), as shown in figure 3.13, with a maximum capacity of 50 kN. This allowed a maximum pressure of 220 MPa to be exerted on

the powder within the die cavity. All green samples were produced by applying this maximum pressure for 10 seconds. The rates of compaction used for test matrix no. 1 and 2 were 10mm/min and 20mm/min respectively. The compaction parameters selected in test matrix no. 1 were based on previous work [210] and in test matrix no. 2 were based on maximising the rate of sample production within the limits of the compaction equipment. During the present work it was found that at rates of compaction above 20mm/min the set pressing load of 50 kN would be overshoot. To avoid this the powder compaction rate was limited to 20mm/min in test matrix no. 2.

In test matrix no. 1 it was notice that galling of the die walls and surface damage of the green compacts occurred frequently due to the carbide insert joint. This damage was avoided in test matrix no. 2 by ensuring that no pressing or ejection would occur in the region of the carbide joint.

Test Matrix No. 3 (Cylindrical samples)

A new die set, shown in figure 3.14, was design and constructed for use in test matrix no. 3. All compaction of the mixed powders for test matrix no. 3 was carried out using this 40mm floating die set. This die set functioned in much the same way as the larger die set (80mm) used in test matrices no. 1 and 2. However, the 40mm die consisted of only one cylindrical tungsten carbide insert. This prevented die wall galling and green compact surface damage from occurring. The height of the die was chosen to allow for a sufficient mass of powder to be charged in the die cavity with the bottom punch in position between 1mm and 2mm inside the die. This location of the bottom punch allowed for maximum die fill and also minimised the distanced over which the green compacts travelled during downward ejection. This downward ejection decreased the time required for compact ejection compared to the upward ejection used in test matrices no. 1 and 2.

Test matrix no. 3 investigated the effect of varying the compaction rate. Compaction rates of 20, 100 and 500 mm/min were investigated. It must be noted that to avoid mechanical damage and personal injury, considerable care was taken when the higher

rates of compaction were used. A compaction pressure of 220 MPa was applied for 10 seconds for each sample produced.

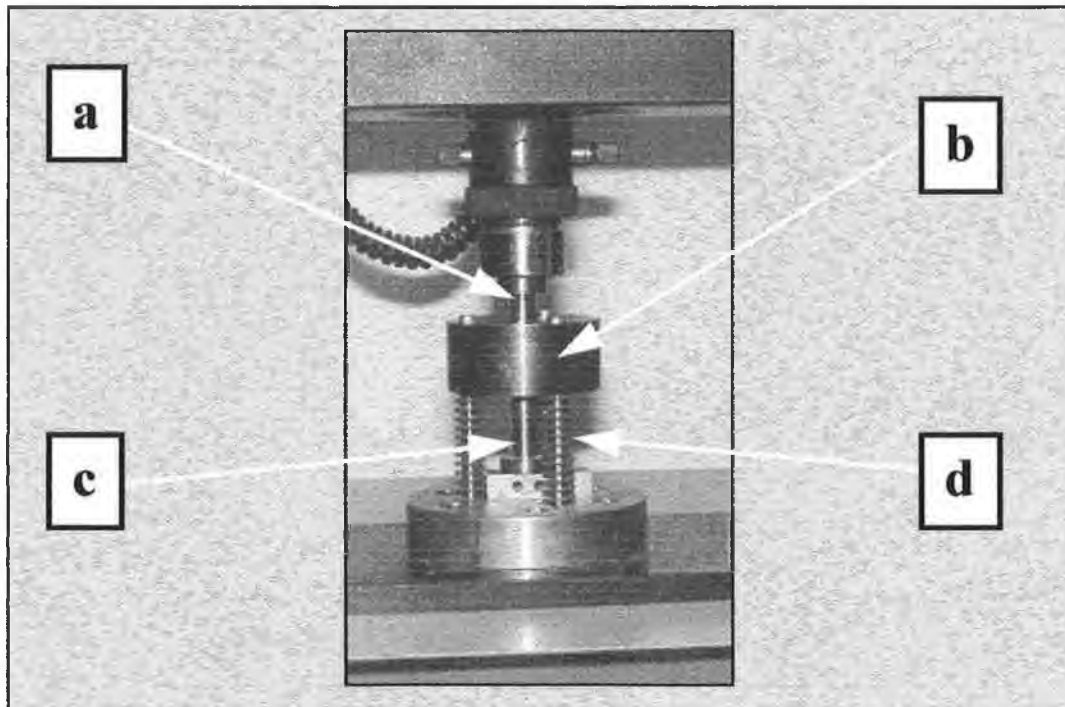


Figure 3.14. Compaction set up used in test matrix no. 3, (a) top punch, (b) floating die (cavity shape: 17mm diameter cylindrical cavity, 40mm in height), (c) bottom punch, (d) die spring and guide pin (three off).

Test Matrix No. 4 (Tensile test samples)

All compaction of the mixed powders for test matrix no. 4 was carried out using the split floating die shown in figure 3.15. The compaction mechanism for this die set is identical to that of the cylindrical die sets used for test matrices no. 1, 2 and 3. The die set was mounted on a manually controlled single action hydraulic press which was fitted with a calibrated load cell and force display unit, a manual direction control switch and a manually operated ram speed control valve.

Great care was taken during the compaction procedure. With the powder within the cavity and the punches aligned and positioned correctly, the top section of the die set was lowered rapidly by operating the direction control switch. As the top section of the die set approached the top of the top punch the ram speed was reduced to a minimum. In the case of the hydraulic press used the minimum speed is approximately 15 mm/min. The direction control switch was kept in the "ram downward" position until the force indicated on the force display unit reached a point below the force required, at which point the direction control switch is released to the neutral position. The difference in force between the point at which the control switch is released and the force required was approximately 15 kN. All of the samples from test matrix no. 4 were compacted using a pressure of $235 \text{ MPa} \pm 5 \text{ MPa}$ and at an average loading rate of 7 MPa/sec. Following the release of the control switch the ram continued to advance slightly. As the ram continues to move downward the force continues to rise slowly. At the required force the direction control switch was toggled to the ram upward position. The speed at which this retraction took place was also kept at a minimum. At a force of approximately 5 kN the control switch was released to the neutral position and each of the die bolts, which hold together the two halves of the die body, were unscrewed by approximately one $\frac{1}{2}$ turn. Whilst the bolts were being released the force on the compacted sample within the die cavity normally increases slightly. To prevent this force from becoming too large the direction control switch must be toggled from the neutral position to the ram upward position and back to the neutral position very rapidly during the bolt release procedure. With all eight die bolts released the two halves of the die were split and simultaneously separated slightly from the sample within. The force on the sample due to the press was now completely

released by fully retracting the ram. With the pressure released the top punch was removed. Although the die was split, the rounded ends of the green compact remained in contact with the die wall. Therefore, it was necessary to eject the sample from within the die. This was carried out by upward ejection of the sample, as discussed in section 3.2.5.

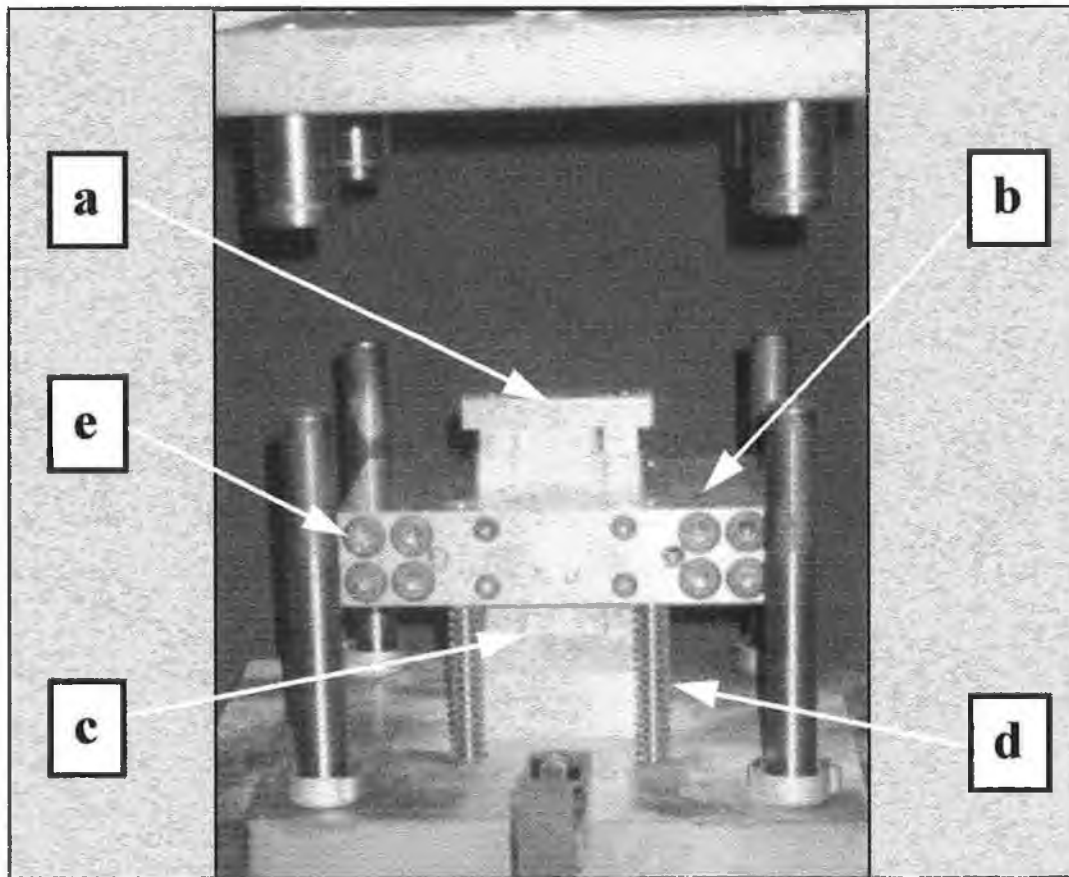


Figure 3.15. Compaction set up used in test matrix no. 4, (a) top punch, (b) split floating die (cavity shape: modified MPIF flat test bar [211], see appendix A), (c) bottom punch, (d) die spring and guide pin (four off), (e) die bolt (eight off).

3.2.5 Ejection

Test Matrices No. 1 and 2 (Cylindrical samples)

The ejection of green compacts carried out in test matrices no. 1 and 2 was achieved by the downward movement of the die relative to the bottom punch (upward ejection). This procedure involved the removal of the top punch from the die and the positioning of a bridging block on the top of the die. The bridging block was shaped so as to allow the green compact to be ejected as shown in figure 3.16. Ejection rates of 20 and 30mm/min were used in test matrix no. 1 and no. 2 respectively.



Figure 3.16. Ejection set up used in test matrix no. 1 and 2, (a) emerging green compact, (b) bridging block. Note: The bottom punch remains within the die during ejection.

Test Matrix No. 3 (Cylindrical samples)

The ejection method used in test matrix no. 3 involved the downward movement of the top punch whilst the die was prevented from moving by positioning three spacing blocks between the base of the die and the die set base (downward ejection). Figure 3.17 shows the ejection set up involved. A centrally positioned sponge on the die set base was used to prevent damage of the green samples on exit from the die.

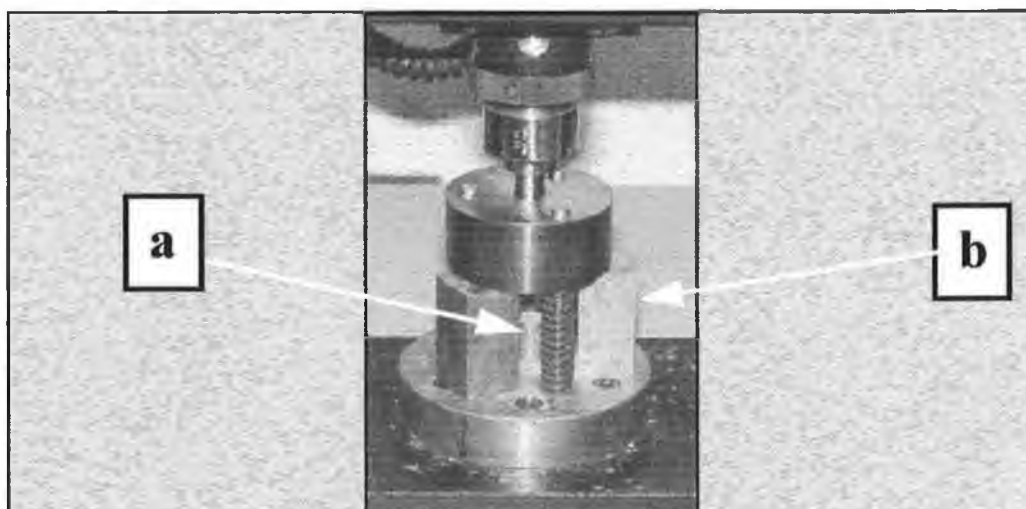


Figure 3.17. Ejection set up used in test matrix no. 3 (a) ejected green compact, (b) spacing block (three off). Note: The top punch remains within the die during ejection.

The rate of ejection was varied manually during ejection in order to decrease the ejection time. This was carried out by setting an initial ejection rate of 20mm/min. Once the compact started to move within the die this rate was increased to 100mm/min. Slight galling occurred during the ejection of a small number of samples. In all cases this galling was accompanied by a distinct increase in ejection force during ejection. In the case of these samples the ejection rate was kept constant at 20mm/min throughout the ejection procedure.

Test Matrix No. 4 (Tensile test samples)

In order to avoid damage of the green tensile test shaped compacts during ejection it was necessary to split the die slightly before ejection. This was achieved by holding the green compact between the top and bottom punch, loosening the die bolts and manually separating the die from the green compact, as described in section 3.2.4. Once the die was split the pressure on the component was released completely, the top punch was removed, spacing blocks were positioned as shown in figure 3.18 and the component was ejected at a rate of approximately 20 mm/min by upward ejection. Figure 3.18 shows the split die separated from the green component and figure 3.19 shows the ejection set up arrangement.

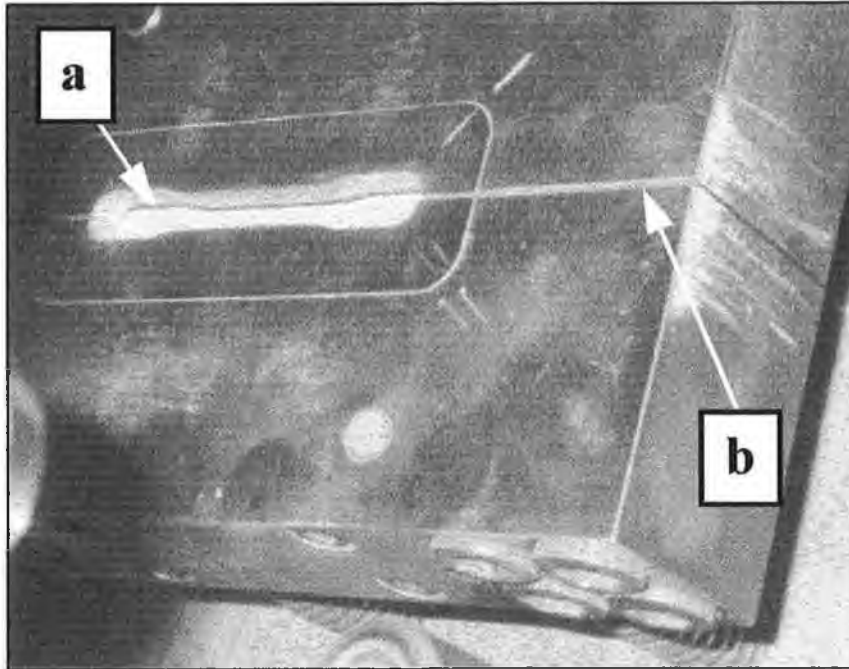


Figure 3.18. Top view of separated split die and green component prior to ejection in test matrix no. 4, (a) green component within die cavity, (b) gap between separated halves of the split die.

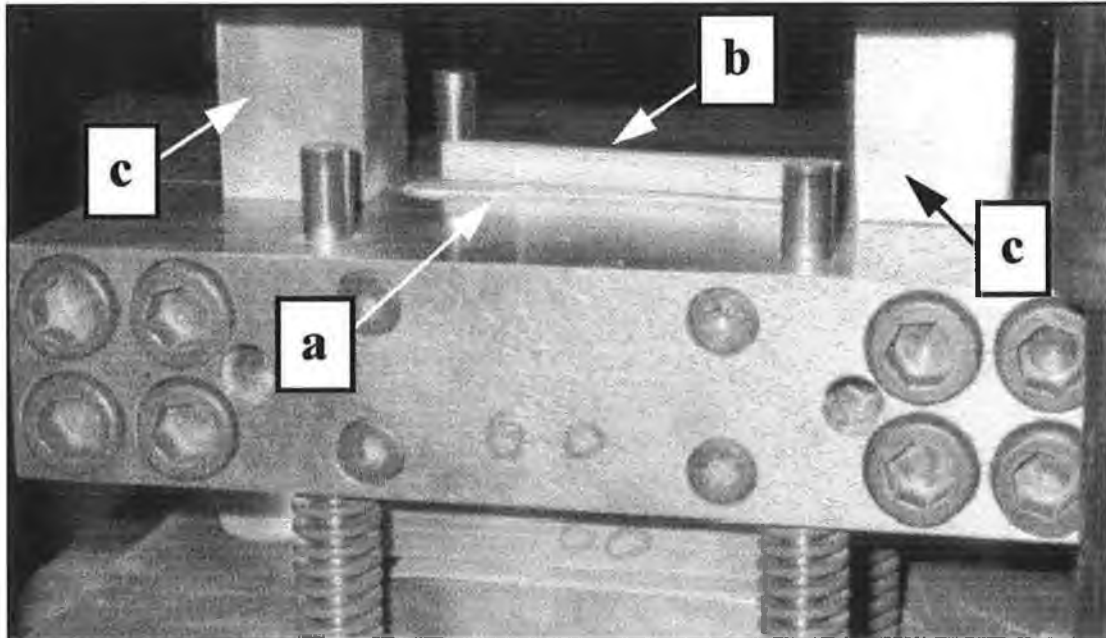


Figure 3.19. Ejection set up used in test matrix no. 4, (a) top face of bottom punch, (b) ejected green component, (c) spacing blocks.

3.2.6 Compact Annealing

Tests were carried out as part of test matrix no. 3 to investigate the effect of green compact annealing and repressing. This annealing process was carried out in air at a temperature of 415°C. It was found that these annealed green compacts could not re-enter the original die for repressing. However, a die was produce with a cavity diameter of 17.1mm to allowed for repressing to be carried out. The results from these analyses show that an increase in green density of up 3 per cent of the theoretical density could be achieved. This repressing of annealed green compacts indicates that this step could be a useful additional step in the consolidation process which could increase green strength, reduce sintering shrinkage and possibly improve the sintering response of the compact. Due to the comparatively complex geometry of the die cavity used in test matrix no. 4 this annealing and repressing procedure was not investigated for the more complex shape.

3.2.7 Sintering

Test Matrix No. 1

The sintering process in test matrix no. 1 was carried out within the temperature controlled kiln shown in figure 3.20. The sintering atmosphere was created by feeding argon gas with 5% hydrogen directly into the kiln. A flow of 3 litres per minute was maintained throughout sintering with the intention of minimising oxidation of the matrix material during the sintering process.

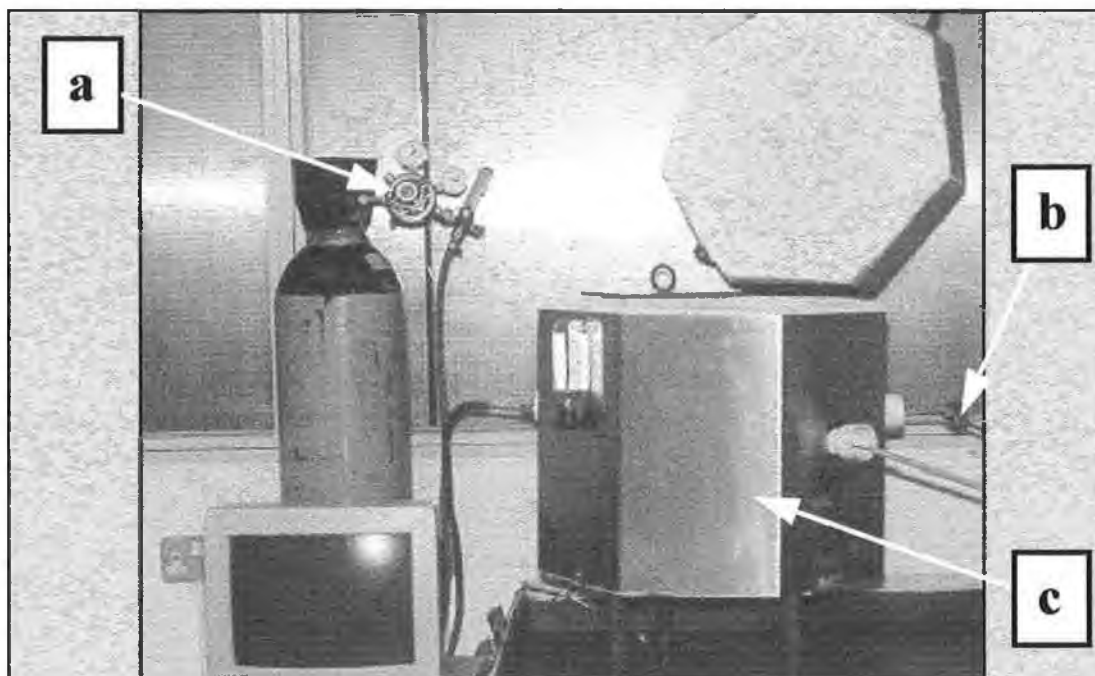


Figure 3.20. Heat treatment system set up, (a) gas supply regulator valve, (b) gas outlet valve, (c) top loading kiln (Firecraft TLB 34).

The green compacts were positioned at the base of the kiln. The gas flow was set to 14 litres/min for approximately 2 minutes in order to prime the kiln with gas and expel the air. With this gas flow applied, the kiln was closed. The flow rate was then reduced to 3 litres/min and the temperature was raised from room temperature to 450°C at a rate of 10°C/min. The temperature was held at 450°C for 30 minutes to allow for burn off of the solid lubricant from within the billets [83]. Following the burn off period the temperature was raised to either 595°C or 625°C, again at

10°C/min. In order to sinter the billets this temperature was maintained for either 60, 105 or 195 minutes. These temperatures and times were chosen based on the results of previous work [210]. Once the sintering stage was complete the kiln was turned off and allowed to cool slowly. During this cooling stage the gas flow was maintained at 3 litres/min and the kiln remained closed

Test Matrix No. 2

The microstructural investigations of the sintered material from test matrix no. 1 indicated that incomplete sintering occurred under the sintering conditions used. Based on these findings and in order to improve control of the sintering atmosphere a mild steel heat treatment unit was designed and constructed to fit within the kiln. This unit was also used for powder heat treatment purposes as described in sub-section 3.3.2 Test Matrix No. 2. The unit was fitted with a thermocouple located within the unit and both an inlet and outlet pipe for gas flow. This mild steel unit was similar in construction to the stainless steel unit shown in figure 3.10. The atmosphere within the unit was created and controlled by feeding pressure controlled and flow regulated industrial grade nitrogen gas directly into the sealed unit through the gas inlet pipe. The unit was sealed by clamping the lid in place using four Inconel set screws.

The experimental procedure for the sintering cycle involved a number of operations. The green billets were placed into a perforated stainless steel container and this container was lowered into the unit at room temperature. The gas outlet valve was closed and the unit was primed with nitrogen. Priming was achieved by setting a high nitrogen flow rate of 14 litres/min whilst securing the lid of the unit. Once the unit was sealed the gas outlet valve was fully opened and the flow rate was reduced to approximately 3 litres/min. This flow rate was maintained throughout the entire cycle and the nitrogen pressure was set at 1.5 bar (gauge) for the complete cycle. Once the unit was primed with nitrogen and sealed the cycle program was initiated. The program initiation procedure, referred to as the module run procedure can be found in appendix B.

The cycle was programmed into the PLC which controlled the kiln temperature throughout the cycle. It was observed during the commissioning of the heat treatment unit that although the kiln temperature followed the programmed temperature closely, when the rate of temperature increase was above 4°C/min, the temperature within the unit would overshoot that of the program. It was also noted that the temperature within the unit lagged behind that of the program. This time lag did not affect the profile of the cycle. However, to avoid the undesirable overshoot, care was taken during programming to ensure that the actual temperature cycle within the unit would follow the required temperature cycle closely. In order to achieve this control the rate of temperature increase was kept below 4°C/min and the temperatures defined in the program were adjusted to suit. The PLC programming procedure for the programming of sintering cycles can be found in appendix B.

The temperature was raised from room temperature to the lubricant burn off temperature of 415°C and this temperature was maintained for a period of 30 minutes. The temperature was then raised to 625°C and held at this temperature for 2½ hours. The temperature was then dropped to 150°C and subsequently raised to the solution heat treatment temperature of 530°C and held at this temperature for approximately 1 hour.

Test Matrix No. 3

Due to the warping and flaking experienced by the mild steel unit used in test matrix no 2 a second heat treatment unit was designed and built. This unit, shown in figure 3.22, was made from stainless steel plate (EN 304) to prevent any degradation. Two gas inlets were positioned on opposite sides at the base of the unit in an attempt to ensure that the gas flow circulated in all areas within the unit and that during priming gas within the unit would be forced from the bottom of the unit and expelled at the top. A quick release mechanism for the lid was also incorporated in this unit to allow easy access during heat treatment. This unit was used in test matrix no. 3.

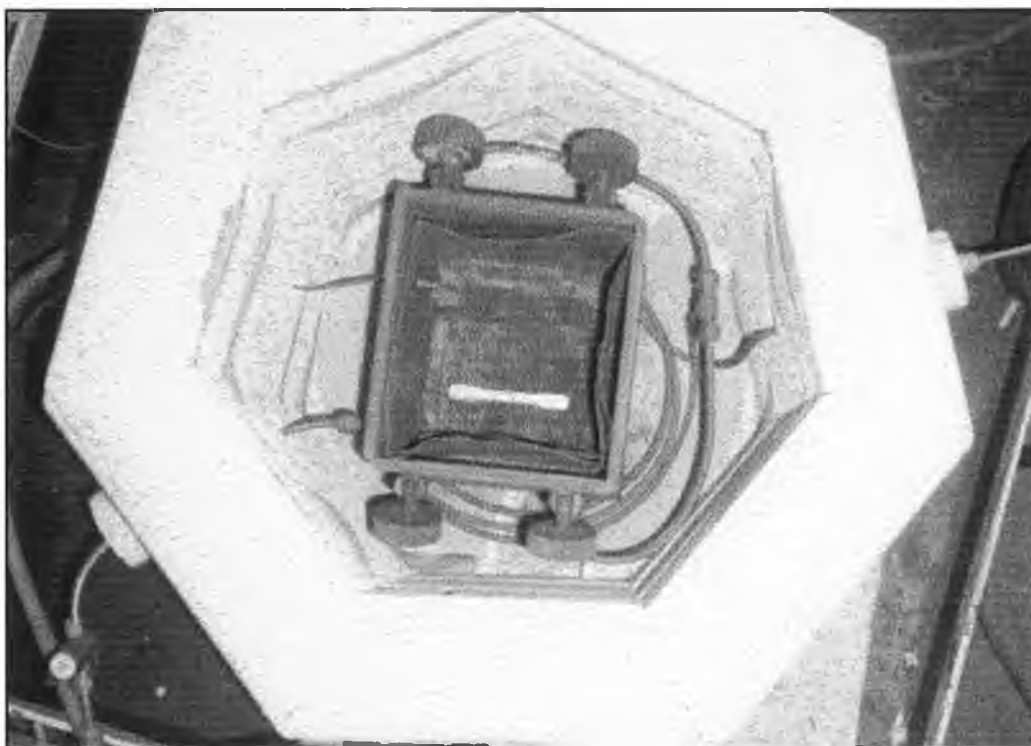


Figure 3.22. Stainless steel heat treatment unit used for test matrix no. 3 and 4.

The sintering cycle employed in test matrix no. 3 was similar to that used in no. 2. Sintering temperatures of 617°C, 623°C and 633°C, and sintering times of 20, 60 and 180 minutes were investigated and all samples were allow to cool to room temperature within the kiln after sintering. After cooling to room temperature the consolidated billets were repressed at a pressure of 220 MPa in the original cylindrical die. Also, to provide the material with either a T4 or T6 heat treatment the samples were batch solution heat treated in air at 515°C, soaked at this temperature, iced water quenched and either allowed to age naturally at room temperature for 10 days before testing (T4), or precipitation hardened at 172°C for 4½ hours (T6).

Test Matrix No. 4

All sintering in test matrix no. 4 was carried out under an industrial nitrogen gas atmosphere using the same stainless steel heat treatment unit as used in test matrix no. 3. The container was continuously supplied with gas at a pressure of 1.5 bar (gauge) and at a flow rate of 3 litres/hour throughout the entire sintering process. Three samples from each of the 12 powder blends tabulated in Table 1 were sintered at a temperature of 617°C ± 2°C for 70 minutes. Also, in order to compare the effect of

mixed-in lubrication with die wall lubrication, ten green samples from batch No. 1 (see appendix D for batch details) containing mixed-in lubricant and two samples of the same powder blend with no mixed-in lubricant were sintered at a temperature of $614.5^{\circ}\text{C} \pm 1^{\circ}\text{C}$ for 50 minutes. All samples were allowed to cool to room temperature within the unit on completion of the sintering cycle.

Geometric deformation of the tensile samples following sintering was very slight, indicating uniform shrinkage. However, all of the sintered components were repressed in the original compaction die at a pressure of $235 \text{ MPa} \pm 5 \text{ MPa}$ to ensure geometric continuity between all the samples produced. Following the repressing procedure all samples were solution heat treated at 515°C , soaked at this temperature for a minimum of 1 hour and quenched in iced water. In order to prevent the initiation of natural ageing after this quench all solution heat treated samples were stored at -18°C until artificial ageing could commence. All samples were artificially aged at $170^{\circ}\text{C} \pm 1^{\circ}\text{C}$. The time held at this temperature depended on the volume fraction SiC content of the samples. Four hours ageing was applied to all samples containing 20% SiC and an additional two hours was allowed for each decrease of 5% SiC. This variation of ageing time was employed in order to approach the T6 peak aged matrix condition for all volume fraction combinations by taking account of the accelerated ageing experienced by the matrix phase caused by the presence of the SiC [149,153,160,163].

3.2.8 Repressing

Test Matrices No. 3 and 4

Post-sintering repressing was not employed in either test matrix no. 1 or no. 2. However, this repressing step was incorporated into the processing route for test matrix no. 3 and no. 4 to coin the samples after sintering. Due to the shrinkage of the samples during sintering it was possible to carry out sintered sample repressing in the original die, from which the samples were pressed. The sintered samples were lightly brushed with powder lubricant and replace in the die. Each sample in test matrix no. 3

was pressed at a rate of 20mm/min and ejected at up to 500mm/min. However, the ejection rate was normally kept below 200mm/min for safety. In test matrix no. 4 the samples were manually removed from the die after repressing.

3.2.9 Precipitation Heat Treatment

Test Matrices No. 2, 3 and 4

The samples produced in test matrix no. 1 were not heat treated after sintering. However, heat treatment was carried out in test matrices no. 2, 3 and 4. The sintered samples taken from the heat treatment unit were in an annealed condition after slow cooling from the sintering temperature. To utilise the precipitation hardening characteristics of the aluminium alloys selected, these materials required heat treatment.

The samples were placed into a perforated stainless steel container and this container was subsequently lowered into the heat treatment unit within the kiln. The samples were heated to a temperature of 515°C in nitrogen and soaked at this temperature for between 1 and 2 hours. Whilst at this temperature, the samples were rapidly removed from the heat treatment unit and placed in iced water. This solution heat treatment was either followed by natural ageing at room temperature for four days or more (T4), or the samples were heated to a temperature between 168°C and 175°C for times of between 4 hours and 5½ hours (T6). All solution heat treatment was carried out in a nitrogen atmosphere and all ageing was carried out in air.

3.3 ANALYSIS EQUIPMENT AND PROCEDURES

3.3.1 Powder Shape

The shape of both the aluminium powders and the SiC particles was analysed using a Philips 505 scanning electron microscope (SEM). To prepare the aluminium powders for observation, samples of powder were fixed using conductive adhesive to a circular platen suitable for use in the SEM. The SiC particulate was mounted in the same way, however due to the low conductivity of SiC it was necessary to gold plate this powder before observation could take place.

3.3.2 Powder Size

Laser diffraction analyses were carried out on all powders. Samples of each batch were sent to the Universität Bremen, Germany, and were analysed. The powders were first dry deagglomerated (Rodos, Co. SYMATHEK), and subsequently analysed using a laser diffraction size analyser (Helos SR 127, Co. SYMATHEK). A statistical representation of the powder size distribution is produced by the equipment.

3.3.3 Mixed Powder Homogeneity

The homogeneity of the powder blends was analysed qualitatively by observation. These observations were made visually and by optical microscopic analysis of the mixed powders. Due to the distinct white colour of the solid lubricant, clusters were easily recognisable by visual analysis. However, to investigate the distribution of the SiC particles throughout the aluminium powders a Reichert MeF3 optical microscope was used. At low magnification it was possible to recognise clusters of SiC particles where they were present. These qualitative analyses provided a comparative indication of the distribution attained from each mixing procedure under investigation.

3.3.4 H₂O Content

The H₂O analysis carried out to investigate the effect of the powder heat treatment on the moisture content of the powder blends was performed on a Mettler DL18. This instrument was used to carry out a Karl Fischer titration [212]. This procedure is a standard chemical analysis. The nominal sample mass of powder analysed in each titration was one gram.

3.3.5 Powder Compressibility

All compressibility tests were carried out using either the cylindrical floating die shown in figure 3.13 or that shown in figure 3.14. The die set was mounted on an Instron 4204 universal testing machine. The compressibility of the mixed powder was measured over a compaction pressure range of 0 MPa to 220 MPa in steps of approximately 44 MPa. A compaction speed of 2mm/min was used. During compressibility testing each pressure step was held for 10 seconds, after which time the pressure was relaxed to 0 MPa. The displacement of the top punch was recorded after each step.

Green compact density was calculated using these readings in conjunction with the diameter of the die and the mass of powder being compressed. After reaching the maximum pressure of 220 MPa each compact was ejected. The mass, diameter and length of each ejected green compact was recorded and the green density (actual density of the green compact) was calculated. The theoretical density of the material was also calculated. The theoretical density calculation for a given powder mix was based on the density of the aluminium alloy, the density of the SiC and the volume fraction of each material. From these calculations the green density could be described as a percentage of the theoretical density. This normalising calculation was carried out to allow comparison to be made between the green density of green compacts produced from different powder mixes. The resulting data was used to compare the compressibility of each powder mix, and to calculate the approximate porosity of the

green samples produced. In all calculations the volume occupied by the lubricant within the green compact was considered as porosity. This compressibility test procedure is a modification of the MPIF test standard 45 [211].

3.3.6 Die Wall Frictional Stress

Die wall frictional stress was calculated to analyse the effects of the lubricant quantity, lubricant type and rate of compact ejection on the magnitude of this ejection stress. To calculate the maximum frictional stress during ejection the maximum ejection force and the green compact length were recorded. The contact area between the green compact and the die wall was calculated using the green compact length and the internal diameter of the die. From these ejection force and contact area readings the maximum die wall friction stress was calculated.

3.3.7 Green Strength (Green compacts)

Diametrical compression testing of brittle green compacts can be used to indicate the green strength of a pressed powder compact [132]. Due to the brittle nature and cylindrical form of the green compacts produced in test matrices no. 1, 2 and 3 it was possible to carry out diametrical compression testing to comparatively analyse the green strength of the these compacts. These tests were carried out on an INSTRON 4204 universal testing machine. Each sample was positioned between the flat platens of the testing machine, as shown in figure 3.23. Using a cross head speed of 2mm/min each sample was tested to fracture, which was accompanied by a dull cracking sound. The fracture force for each sample test was recorded and used to calculate the diametrical compressive green strength G , by applying equation (30) [132],

$$G = \frac{2P}{\pi Dt} \quad (30)$$

where P is the applied load and D and t are the diameter and length of the compact respectively.

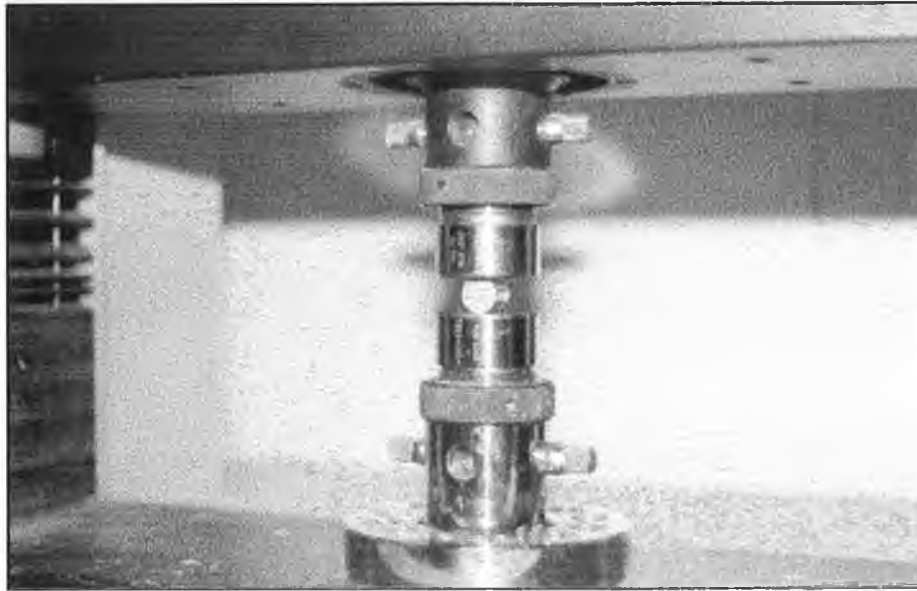


Figure 3.23. Diametrical compression green strength testing set up.

3.3.8 Microstructural (Green compacts)

A morphological investigation of the fracture surfaces of a number of green compacts from test matrix no. 4 was carried out. This investigation was carried out using a Leica (Leo) Stereoscan 440 scanning electron microscope (20kV). The samples investigated were prepared for investigation by fracturing immediately before inserting into the microscope chamber. To minimise the number of loose powders on the fracture surface the sample was gently tapped after fracture. It was found that clear morphological images were obtained from these samples and no sample coating was required.

3.3.9 Diametrical Compressive Strength (Sintered material)

Diametrical compression testing was used for the comparative analysis of the tensile behaviour of the sintered samples in test matrix no. 1. This test was carried out using an Instron 4204 universal testing machine. The test has been found to be comparable with tensile testing [213] in the case of brittle materials, and is also referred to as indirect tensile testing. The sintered samples were held between two flat platens, as in the diametrical green strength testing, and a load was applied. A cross head speed of 0.1 mm/min was employed. The maximum applied load before fracture was used to calculate σ_x (the rupture strength) by applying equation (31) [213],

$$\sigma_x = \frac{2P}{\pi Dt} \quad (31)$$

where P is the applied load and D and t are the diameter and the length of the sintered compact respectively.

It should be noted that the sintered samples tested in test matrix no. 1 were poorly sintered and generally fractured in a brittle manner. However, the well sintered samples produced in test matrices no. 2 and 3 flattened considerably before fracture when diametrically compressed. This flattening invalidates any results of this test. Consequently, no diametrical compressive strength testing was carried out in the subsequent test matrices of this work.

3.3.10 Hardness

Following sintering, Rockwell B macrohardness tests were carried out using an AFFRI 206RT hardness testing machine. Each sample was machined and polished before testing to minimise errors due to either the roughness or the surface oxide layer created during processing. To improve the reliability of this test procedure two readings from each end were taken for all samples. Vickers 30 hardness testing

(Indentec 9045 PKV) was also carried out. However, it was found that less accurate readings were produced by this method due to the irregular indentation shapes created in the composite materials. The Rockwell B testing (1/16" ball, 100 kg) was more reliable and consistent than the Vickers 30 testing. The hardness test procedures carried out were in accordance with the MPIF test standard 43 [211].

3.3.11 Compressive Strength

Material yield strength was assessed using axial compression testing in test matrix no. 2 in order to compare the strength of various compacts. Samples were machined using diamond tooling to a length and diameter of 10mm. Each sample was greased and positioned centrally between ground flat D2 steel platens. This assembly was carefully positioned between the flat platens of an Instron 1196 universal testing machine, as shown in figure 3.24.

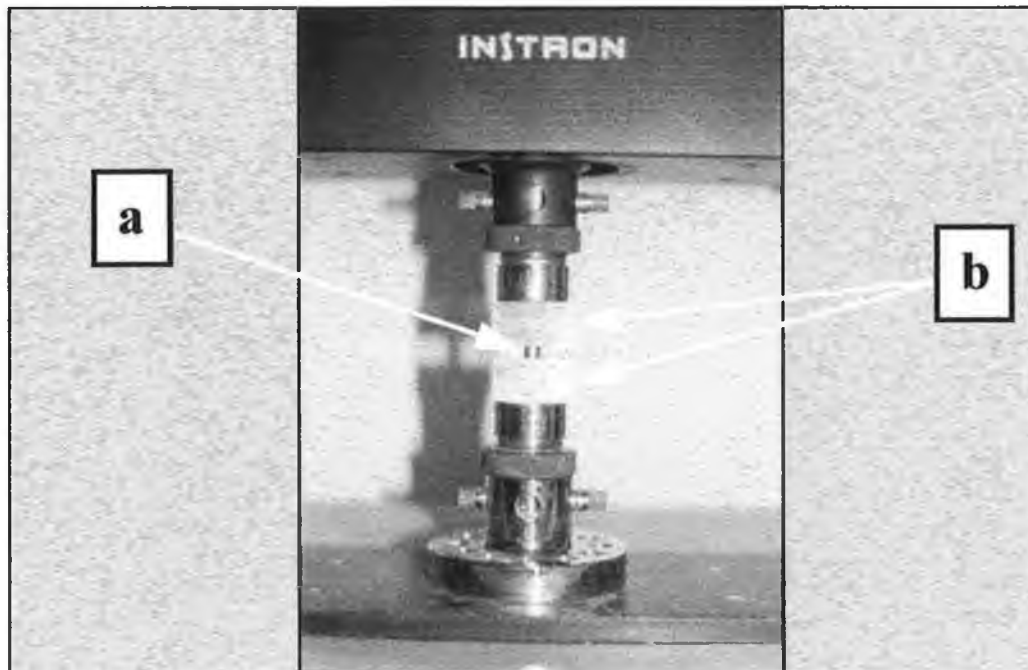


Figure 3.24. Compression testing set up, (a) 10mm dia. x 10mm length cylindrical test sample, (b) flat platens.

A cross head speed of 1mm/min was maintained and each sample was tested to fracture. Material yield strength (0.2% proof stress) was found from the graphical records of force and extension. One sample from each composite batch was tested. Barreling of each sample was observed after yielding occurred. This barreling is due to platen/sample interfacial friction.

3.3.12 Tensile Response

Tensile testing of the samples produced in test matrix no. 4 was carried out on an Instron 4204 universal testing machine at a tensile deformation rate of 1mm/min. The strain measurements were obtained with the use of an Instron extensometer over a gauge length of 25mm. An Instron X-Y recorder was used to record the force and extension during testing. The recorded data was converted manually from this form to the true stress and true strain form. The tensile testing procedure carried out followed the MPIF test standard 10 [211]. The test sample was also based on this standard, however, the sample used in this work was slightly larger than that suggested in the standard. The geometry and dimensions of the die cavity within which these samples were pressed are shown in appendix A.

3.3.13 Microstructural (Sintered material)

Optical Microscopy

Two optical microscopes have been used in this work. The optical micrographs contained in this work were produced using either an Olympus BX 60 M optical microscope (test matrices no. 1 and no. 2) or a Reichert MeF3 optical microscope (test matrix no. 3). Both of these microscopes were fitted with a Sony colour video printer CVP/M3E facility.

The sintered materials in the present work were prepared for optical microscopy by grinding and careful polishing. Grinding and polishing was carried out by hand on a

Stuers DAP-V polishing machine following the Buehler recommended polishing procedure for aluminium SiC composites [214]. Polishing of the samples proved difficult due to the SiC particle pull out experienced. This had the effect of contaminating the polishing surfaces at the fine polishing stages, which in turn caused damage to the surface of the samples.

In order to minimise the possibility of this damage occurring the platen rotation speed was kept between 80rpm and 150rpm. Also, continuous washing of the polishing surface with a spray of water was used to rid the platens of any particles which had been dislodged from the matrix. It should be noted that if particle pull out occurs during the grinding of these materials it may alter the apparent microstructure of the polished sample. To avoid any misleading effects due to grinding and polishing processes great care was taken at all stages of this sample preparation.

A number of composite samples were unsuccessfully prepared by electrolytic polishing in test matrix no. 2. It was found that preferential attack of the matrix / reinforcement interface occurred which resulted in a poor sample surface.

Scanning Electron Microscopy

A morphological investigation of the fracture surfaces of the sintered tensile test samples from test matrix no. 4 was carried out. This investigation was carried out using a Leica (Leo) Stereoscan 440 scanning electron microscope (20kV). It was found that clear morphological fracture surface images were obtained from these samples and no sample coating was required.

CHAPTER 4 EXPERIMENTAL RESULTS AND OBSERVATIONS

The results and observations from the experimental work are described in this chapter. Reference is made throughout the chapter to the test matrices presented in chapter 3 which relate to each set of results and observations. It should be noted that figures 3.2, 3.3, 3.4 and 3.5 detail these test matrices. The information presented in this chapter follows the sequence of the process as closely as possible, starting with the analyses carried out on the as-supplied powders, and ending with the mechanical testing of the fully processed composite samples.

The results presented are categorised on the basis of the experimental investigations carried out. These investigations include powder analyses, compressibility testing, ejection stress analysis, green strength analysis, green compact microstructural analysis, sintered density analysis, diametrical compressive strength analysis, hardness testing, axial compressive strength testing, tensile sample fracture surface analysis and tensile response and sintered sample microstructural analysis. Each of these categories are sub-divided into sections which describe the effects of the parameters investigated in the present work.

The results are based on a large body of experimental work. In total, 255 cylindrical samples and 46 tensile test samples were processed. The main analyses carried out include 234 compressibility tests, 50 ejection stress tests, 36 green strength tests, 19 hardness tests (HRB), eight compressive strength tests, 28 sintered density analyses and 46 tensile tests. In addition, eight particle size analyses were carried out, 10 samples were prepared for scanning electron microscope analyses and 14 samples were prepared for optical microscope analyses.

For clarity, not all data points found are presented in the graphs in this chapter. However for every table and figure, the number of samples tested and the scatter of readings for each set of results presented in this chapter can be found in appendix C. Also, in the interests of traceability the details and results relating to all the individual samples tested throughout this work are listed in appendix D.

4.1 POWDER ANALYSES

4.1.1 Powder Shape

All Test Matrices

Examples of scanning electron micrographs of both the aluminium powders and the SiC particulate are presented in figures 3.6 and 3.7. It has been found that for all powder and particle batches used the aluminium powders are nodular and the SiC particulate are angular. Also, the particles of both materials are irregular in shape.

4.1.2 Powder Size

All Test Matrices

The results of the laser diffraction powder size analyses of the aluminium alloys and ceramic powders are presented in table 4.1.

Table 4.1. Producer specified particle size and particle size analysis results.

Powder	Producer specified particle size	Median particle size ($d_{50,3}$) [†]
AA6061	45 μm MPS	16 μm
AA6061	30 μm MPS	11 μm
AA6061	10 μm MPS	7 μm
AA2124	45 μm MPS	19.5 μm
SiC	75 μm MPS	28.5 μm
SiC	23 μm APS	25 μm
SiC	13 μm APS	13.5 μm
SiC	5 μm APS	6 μm

Note: MPS refers to maximum particle size, APS refers to average particle size.

[†] $d_{50,3}$ refers to the statistical median particle size based on the cumulative frequency size distribution (quantity type = 3, RRSB distribution) [17].

The median particle size values listed are average values calculated using the results of the three analyses carried out for each powder type. The maximum scatter for any powder type was $\pm 0.5\mu\text{m}$. Also, in table 4.1 a comparison is made between these results and the size data supplied by the producer. It can be seen from this comparison that the producer specified size data may be misleading. Ideally, each batch of powder should be supplied with both the median particle size and the particle size distribution specified.

It was also observed that the particle size range is wider in the case of the as-supplied aluminium powder than that of the SiC particulate. It was found that in the case of the $19.5\mu\text{m}$ ($d_{50,3}$) AA2124 powder batch the powder size ranged from $6\mu\text{m}$ to $70\mu\text{m}$, compared to $10\mu\text{m}$ to $46\mu\text{m}$ for the $25\mu\text{m}$ ($d_{50,3}$) SiC particles. The other aluminium powder and SiC particle batches followed similar trends.

4.1.3 Mixed Powder Homogeneity

Test Matrix No. 2

Qualitative optical microscopy analyses were carried out in test matrix no. 2 to compare the rotary and the reciprocation mixing processes. It was observed that the rotary process produced powder mixtures containing numerous undesirable clusters of SiC and powder lubricant agglomerates. The reciprocation process produced mixtures with greater homogeneity, reduced clustering of SiC and an improved distribution of lubricant. An attempt was not made to quantify these improvements.

4.1.4 H₂O Content

Test Matrix No. 3

Karl Fischer titration analyses were carried out on four samples of powder as part of test matrix no. 3 to investigate the effect of powder heat treatment on the H₂O content of the powders. The results of these analyses show a drop in H₂O content

from 0.0424% by weight for the as-supplied powders to 0.0361% by weight for the heat treated powders. Although these results show a distinct drop in H₂O content an analysis involving a larger number of powder samples is required to define the quantitative relationship between heat treatment and H₂O content more accurately.

4.2 COMPRESSIBILITY TESTING

The compressibility of a powder is defined as the ratio between the green density of a compact produced at a specific pressure and the density of a fully consolidated compact (100 per cent theoretical density, 100 %TD) of the same powder. In the following results both compressibility curves and final green density are used to describe compressibility. A full description of the experimental methods carried out to obtain these results is given in section 3.3.5.

It should be noted that the individual compressibility curves and final green density values shown in figures 4.1 to 4.10 are based on the results from single samples only. However, since the maximum scatter recorded for any powder batch tested was no more than $\pm 0.4\%$ TD, these curves and green density values closely represent the compressibility of all samples tested for each batch described in this section.

4.2.1 SiC Content

Test Matrix No. 1

Compressibility tests were carried out in test matrix no. 1 on five powder size mixtures (10%, 20%, 30% SiC for each mixture) to analyse the effect of SiC content variation on the compressibility of these as-supplied powders. Of these five mixtures, three contained $6\mu\text{m}(d_{50,3})$ SiC and two contained $28.5\mu\text{m}(d_{50,3})$ SiC. In the case of the three powder combinations containing the small SiC particles $\{7\mu\text{m}(d_{50,3})$ AA6061 + $6\mu\text{m}(d_{50,3})$ SiC, $11\mu\text{m}(d_{50,3})$ AA6061 + $6\mu\text{m}(d_{50,3})$ SiC and $16\mu\text{m}(d_{50,3})$ AA6061 + $6\mu\text{m}(d_{50,3})$ SiC} increasing the volume fraction of SiC decreased compressibility.

The compressibility curves for the $16\mu\text{m}(d_{50,3})$ AA6061 + $6\mu\text{m}(d_{50,3})$ SiC combinations (10%, 20%, 30% SiC) in figure 4.1 show this relationship between SiC volume fraction and powder compressibility over the full range of pressure used in the present work. The $7\mu\text{m}(d_{50,3})$ AA6061 + $6\mu\text{m}(d_{50,3})$ SiC and the $11\mu\text{m}(d_{50,3})$ AA6061 + $6\mu\text{m}(d_{50,3})$ SiC combinations followed similar trends to that displayed in figure 4.1.

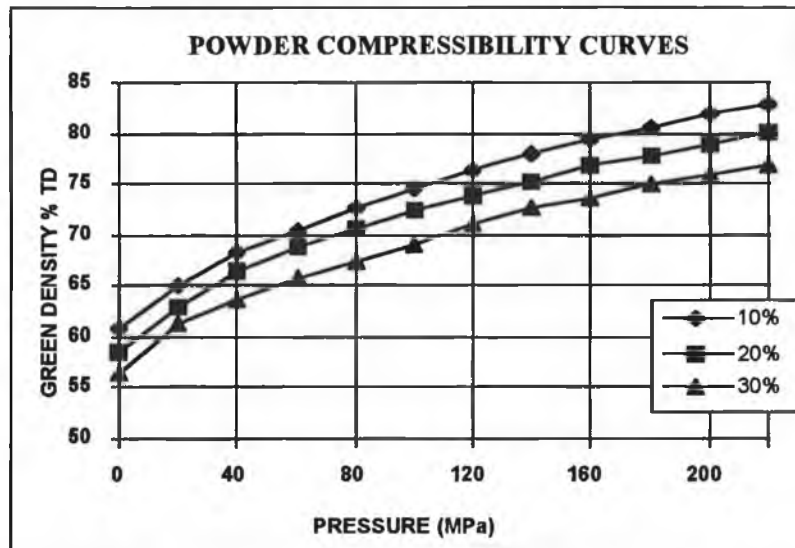


Figure 4.1. Powder compressibility curves for $16\mu\text{m}(d_{50,3})$ AA6061 + $6\mu\text{m}(d_{50,3})$ SiC, test matrix no. 1.

The compressibility results obtained for the remaining two powder combinations containing larger SiC particles $\{7\mu\text{m}(d_{50,3})$ AA6061 + $28.5\mu\text{m}(d_{50,3})$ SiC, $11\mu\text{m}(d_{50,3})$ AA6061 + $28.5\mu\text{m}(d_{50,3})$ SiC} displayed a less distinct and opposite trend. For these powder combinations it was found that an increase in the SiC volume fraction of these large particles caused a slight increase in compressibility.

These five sets of results show that the effect of SiC content on compressibility of these as-supplied powders is dependent on the SiC particle size. In the case the powder combinations containing small SiC particles $\{6\mu\text{m}(d_{50,3})$ SiC} compressibility decreases with increasing volume fraction and in the case of the large particles $\{28.5\mu\text{m}(d_{50,3})$ SiC} compressibility increases with increasing volume fraction. The final percentage TD (compacted at 220 MPa) of all the samples tested for the above as-supplied powder combinations are listed in appendix D.

Test Matrix No. 2 {all $16\mu\text{m}(d_{50,3})$ AA6061 + $25\mu\text{m}(d_{50,3})$ SiC}

Compressibility test results from both the annealed and as-supplied (non-annealed) powder blends {all $16\mu\text{m}(d_{50,3})$ AA6061 + $25\mu\text{m}(d_{50,3})$ SiC} in test matrix no. 2 showed that the compressibility reduces with an increase in SiC volume fraction for

this powder size combination in the annealed and non-annealed conditions. In total ten non-annealed and two annealed samples from each batch type were tested. The final percentage TD (compacted at 220 MPa) of all the samples tested are listed in appendix D. The large difference in compressibility between the annealed and non-annealed powders shown in this figure is discussed in section 4.2.4.

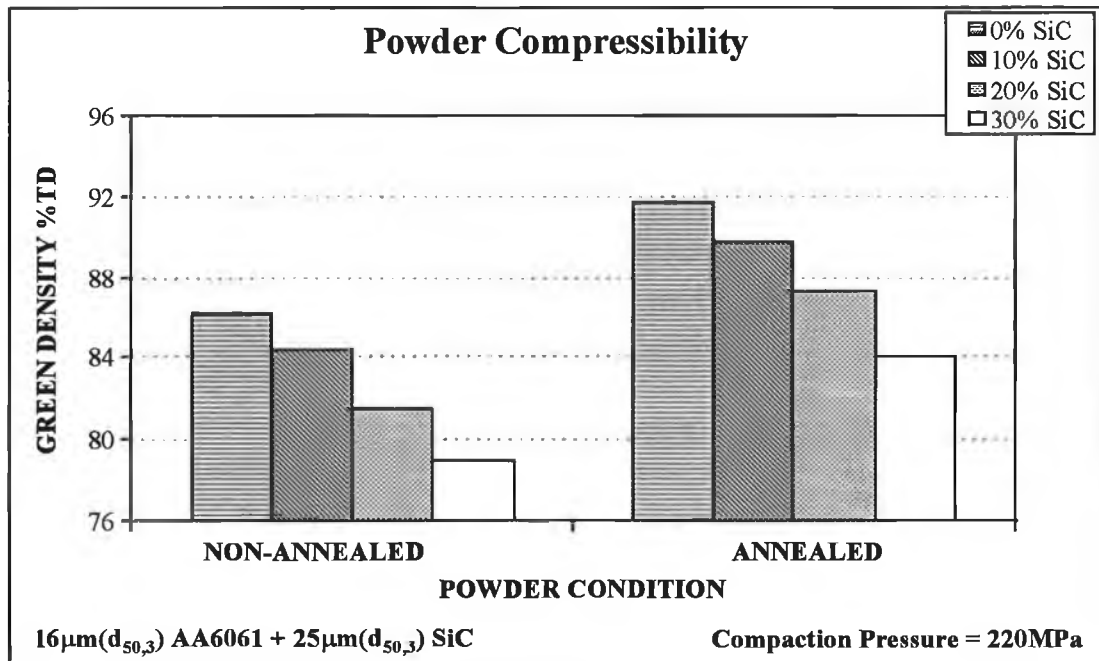


Figure 4.2. Effect of SiC content on compressibility, test matrix no. 2.

4.2.2 Aluminium Powder and SiC Particle Size

Test Matrix No. 1

Compressibility tests carried out in test matrix no. 1 on powder mixtures containing various combinations of powder sizes indicate a strong relationship between both matrix and reinforcement size and the compressibility of a powder mixture. An increase of powder size in the case of either SiC or aluminium has the affect of increasing compressibility.

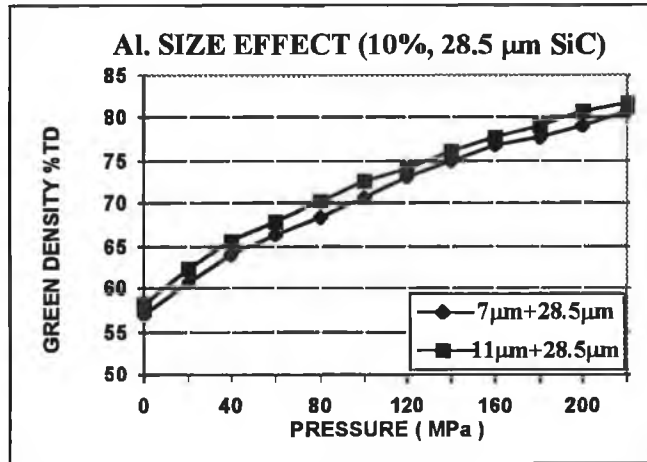


Figure 4.3. Effect of aluminium powder size on compressibility, 10% 28.5μm($d_{50,3}$) SiC, test matrix no. 1.

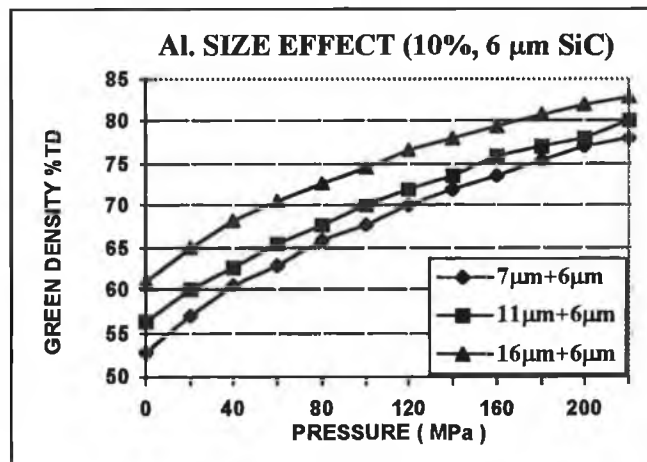


Figure 4.4. Effect of aluminium powder size on compressibility, 10% 6μm($d_{50,3}$) SiC, test matrix no. 1.

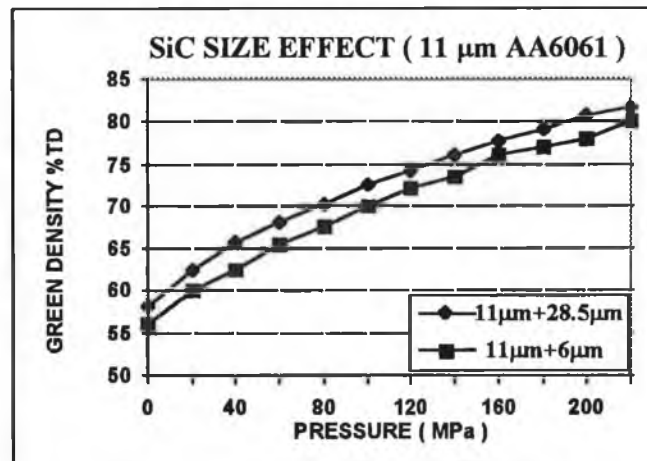


Figure 4.5. Effect of SiC particle size on compressibility, 10% SiC, 11μm($d_{50,3}$) AA6061, test matrix no. 1.

Figures 4.3 and 4.4 for the 10% SiC powder mixtures tested are indicative of this trend, showing that for a constant SiC particulate size and varying matrix powder size, compressibility increases with an increase in matrix powder size. In addition, figure 4.5 shows that holding the matrix powder size constant and varying the size of the reinforcement, compressibility increases with an increase in SiC particle size. The trends presented for the 10% SiC case in these three figures were also observed in the cases of the 20% and 30% SiC powders tested. The quantitative extent to which compressibility varies with either a variation of SiC or aluminium powder size is not distinct from the results.

The compressibility results for all three volume fractions test in test matrix no. 1 are presented graphically in figures 4.6, 4.7 and 4.8 for the cases of 10%, 20% and 30% SiC respectively. Also, the final percentage TD recorded for each sample is listed in appendix D.

In this section the compressibility results from test matrix no. 1 are presented in the context of the relationship between compressibility and both the absolute aluminium powder size and the absolute SiC particle size. However, these results may also be presented in the context of the relationship between compressibility and the aluminium powder size to SiC particle size ratio. This approach is of particular importance due to the strong influence of size ratio on the homogeneity of the SiC distribution (see section 4.11.2). Therefore, these results are presented separately in the following section (section 4.2.3). However, it must be emphasised that this ratio relationship is simply a different way of describing the result that as particle size increases compressibility increases.

4.2.3 Aluminium Powder to SiC Particle Size Ratio

Test Matrix No. 1

The results from the compressibility tests carried out in test matrix no. 1 indicate that, holding the aluminium powder size constant at 16 μ m, 11 μ m or 7 μ m, the relative size of the SiC particles compared to the size of the aluminium powder with which they are blended affects compressibility. These results are presented in the context of the relationship between powder compressibility and absolute particle size in section 4.2.2. However, as mentioned in that section, these results may also be presented in the context of the relationship between compressibility and the aluminium powder size to SiC particle size ratio.

The compressibility results for all powder batches tested in test matrix no. 1 are presented in figures 4.6, 4.7, and 4.8. An analysis of the 20% SiC case (figure 4.7) shows that increasing the size ratio from 1:0.4 to 1:1.8 (both 16 μ m aluminium), from 1:0.625 to 1:2.5 (both 11 μ m aluminium) and from 1:1 to 1:4 (both 7 μ m aluminium) has the affect of increasing compressibility. The same trend is observed in the cases of the 11 μ m and 7 μ m aluminium powder combinations containing 10% SiC and 30% SiC shown in figure 4.6 and 4.8 respectively. These results indicate that increasing the relative size of the SiC particles compared to the aluminium powder size causes increased compressibility within the range of both the aluminium powder sizes tested (7 μ m-16 μ m) and the SiC volume fractions investigated (10%-30%).

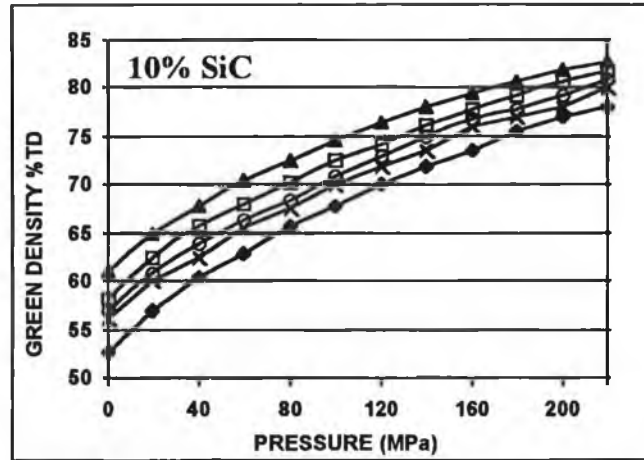
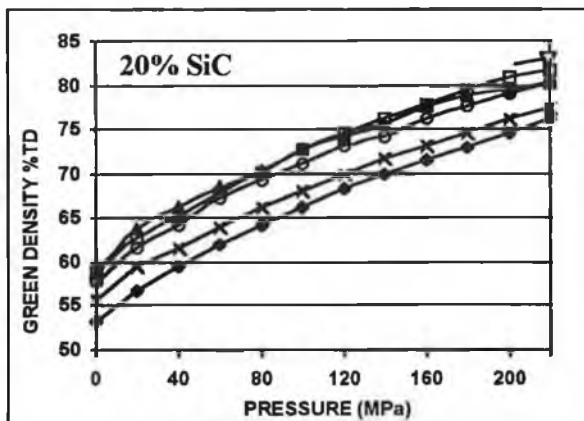


Figure 4.6. Effect of size combinations, 10% SiC, test matrix no. 1.



Al + SiC	Size Ratio $d_{50,3}$
—◆— $7\mu\text{m}+6\mu\text{m}$	1:1
—○— $7\mu\text{m}+28.5\mu\text{m}$	1:4
—×— $11\mu\text{m}+6\mu\text{m}$	1:0.625
—□— $11\mu\text{m}+28.5\mu\text{m}$	1:2.5
—▲— $16\mu\text{m}+6\mu\text{m}$	1:0.4
—▽— $16\mu\text{m}+28.5\mu\text{m}$	1:1.8

Figure 4.7. Effect of size combinations, 20% SiC, test matrix no. 1. In the case of the powder combination $16\mu\text{m}$ AA6061 + $28.5\mu\text{m}$ SiC the green density after compaction at 220 MPa was recorded in the 20% SiC case only.

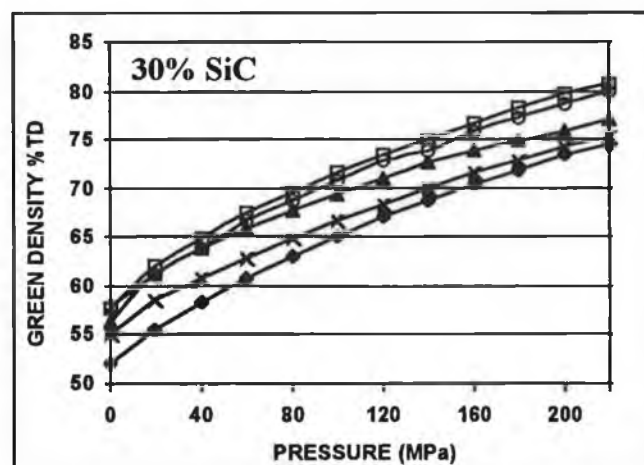


Figure 4.8. Effect of size combinations, 30% SiC, test matrix no. 1.

4.2.4 Powder Heat Treatment Temperature/Time

Test Matrix No. 2 {all $16\mu\text{m}(d_{50,3})$ AA6061 + $25\mu\text{m}(d_{50,3})$ SiC}

Analyses carried out to investigate the effects of powder blend heat treatment (annealing/normalising) on compressibility have shown that the powder compressibility improves considerably with all heat treated powder blends tested compared to non-annealed powders. Figure 4.9 shows that increases of up to 6.19% TD have been achieved, and that green densities of over 89% TD were recorded for samples containing 10% SiC. In addition to the results presented in figure 4.9, the results presented in figure 4.2 show that the absolute increase in compressibility due to the heat treatment is independent of the volume fraction of reinforcement between 0% SiC and 30% SiC.

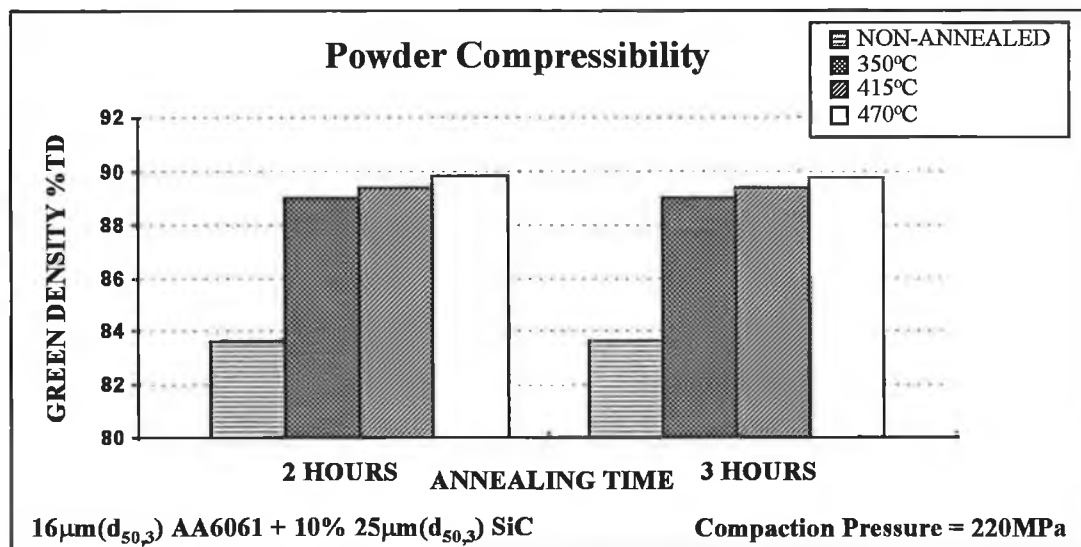


Figure 4.9 Annealed V's non-annealed compressibility results, test matrix no. 2.

Compressibility was found to increase with an increase in annealing temperature. However, this temperature is limited to approximately 470°C due to the occurrence of powder caking[†] at and above this temperature. Heat treatment time was also varied and was seen to have little affect on the powder compressibility. These observations were consistent for all volume fractions tested.

[†] Caking is define as a coalesced mass of unpressed metal powder [83].

4.2.5 Powder Heat Treatment Atmosphere

Test Matrix No. 3

The effects of varying the annealing atmosphere on composite powder compressibility can be seen in figure 4.10. The annealing atmosphere directly affects the powder compressibility. Nitrogen annealing of the powder increases the compressibility by approximately 1% TD compared to powder annealing within air. This has been found to be the case regardless of the compaction rate applied (see section 4.2.8), the lubricant type or the lubricant quantity used.

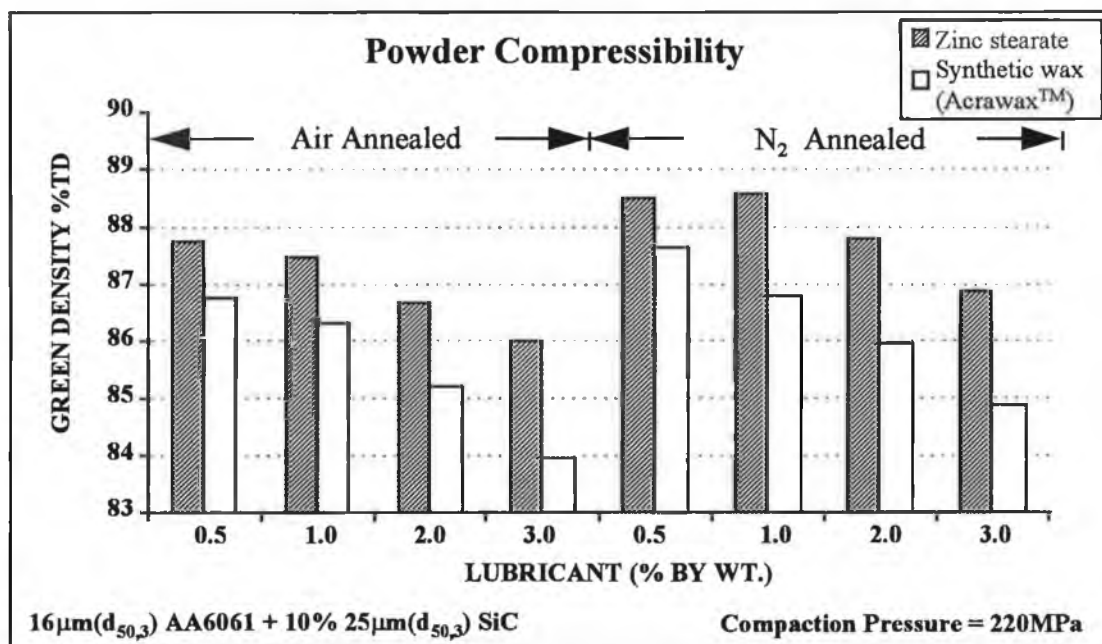


Figure 4.10. Compressibility results for 10% SiC/AA6061 composite powder, effects of annealing atmosphere, lubricant type and lubricant quantity, test matrix no. 3.

It has also been observed that air annealing tends to promote undesirable caking of the powder batches at lower temperatures than for nitrogen annealing. This has the effect of increasing the difficulty of both safe and effective die filling.

4.2.6 Lubricant Type and Quantity

Test Matrix No. 3

It was observed that zinc stearate powder solid lubricant increases compressibility compared to the synthetic wax AcrawaxTM irrespective of lubricant quantity, as shown in figure 4.10. This increase was as large as 2% TD in the case of the 3% lubricant by weight powder mixtures. Also, in the case of both lubricants investigated, the quantity of lubricant has a definite affect on compressibility. In all combinations of annealing atmosphere and lubricant type it is seen (figure 4.10) that as the lubricant quantity increases from 0.5% to 3%, the powder compressibility decreases by approximately 2% TD. This decrease in compressibility can be directly attributed to the larger volume occupied by the greater quantity of lubricant.

4.2.7 Aluminium Alloy Type

Test Matrix No. 2

Attempts to press AA2124 as-supplied powder based powder blends were made in test matrix no. 2. However, the pressed green compacts experienced extensive damage during ejection. Therefore, no valid compressibility test results are available for powder blends containing as-supplied AA2124.

Test Matrix No. 3

Composite powder compressibility tests were carried out on identically processed powder blends of 10% SiC/AA6061 and 10% SiC/AA2124 (0.5% zinc stearate powder lubricant). The effect of alloy type on the compressibility of these nitrogen annealed (475°C) powders indicates a marginally greater compressibility of the AA6061 based powder, compared to the higher strength Al-Cu alloy AA2124 based composite powder. The AA6061 based powder was compressible to an average of 88.12 %TD, which is only very slightly greater than the 87.85 %TD average recorded for the AA2124 based material. It should also be noted that the high compressibility and good quality of the heat treated AA2124 based powder blends compared to the

extremely poor quality of the AA2124 as-supplied based powder blends in test matrix no. 2 highlights the importance of the powder heat treatment process.

4.2.8 Compaction Rate

Test Matrix No. 3

Tests were carried out on 10% SiC/AA6061, nitrogen and air annealed powders, both mixed with 0.5% zinc stearate powder lubricant to investigate the effect of compaction rate on the compressibility of the powders. These investigations show no significant relationship between compaction rate and compressibility over a range from 20mm/min. to 500mm/min for any of the powders tested. It should be noted that these tests were carried out so that in the case of the 20mm/min rate, the powder was compacted at this rate from 0MPa to 220MPa. However, in the case of the higher rates the preset load on the testing equipment was set lower than the required maximum pressure (220MPa) to allow for the load over shoot which occurs at rates of compaction greater than 30mm/min. Also, extreme care was taken during high compaction rate pressing in order to avoid mechanical damage or personal injury.

4.3 EJECTION STRESS ANALYSIS

4.3.1 Lubricant Type and Quantity

Test Matrix No. 3

An investigation into the effects of lubricant type and quantity on the die wall frictional forces was carried out in test matrix no. 3. Figure 4.11 presents the maximum ejection stress recorded for each batch type tested.

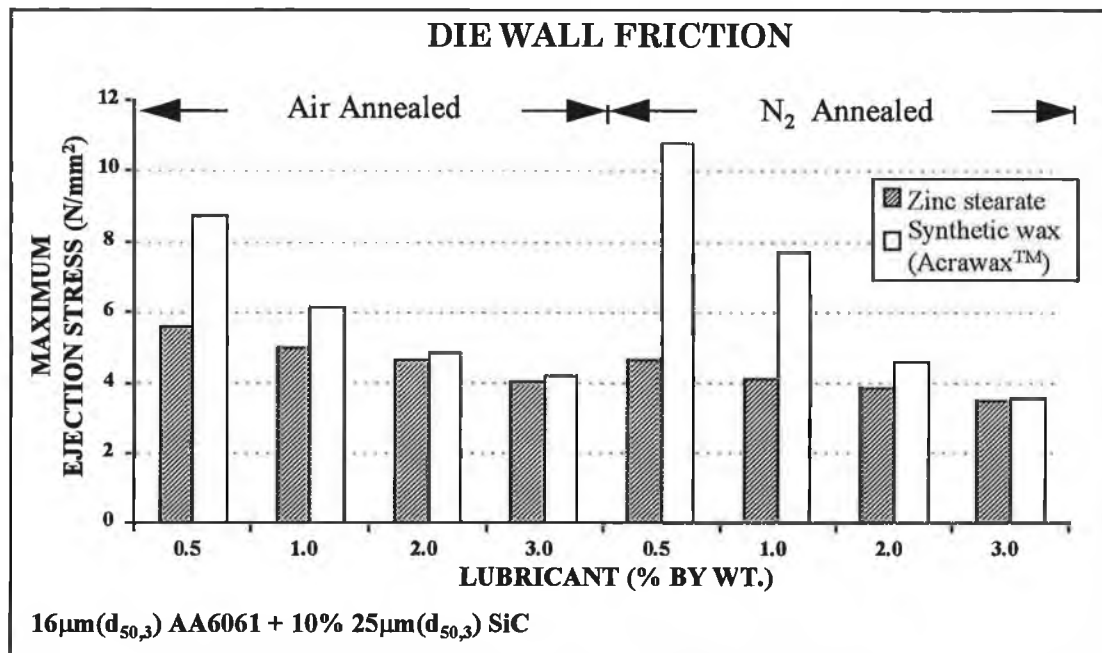


Figure 4.11. Die wall frictional stress results for 10% SiC/AA6061 composite, test matrix no. 3.

The results clearly indicate the expected reduction in die wall friction corresponding to an increase in lubricant quantity for both lubricant types. However, it was found that the zinc stearate lubrication provides sufficient friction reduction to avoid compact damage during ejection over the full range of quantities examined. Conversely, the synthetic wax Acrawax™ can only provide adequate levels of lubrication at higher quantities. Adequate lubrication is essential in order to prevent both galling of the die wall and surface damage of the green compacts during ejection. However, the quantity of lubricant must be kept to a minimum to promote high

compressibility, as discussed in section 4.2.6. The tests have show that 0.5% (by weight) zinc stearate can meet these requirements.

4.3.2 Powder Heat Treatment Atmosphere

Test Matrix No. 3

As shown in figure 4.11, in the case of the zinc stearate lubricated powders the nitrogen heat treated composite powder exhibited marginally lower values of die wall friction compared to the air annealed material. In the case of synthetic wax lubricated powders no consistent relationship between ejection stress and annealing atmosphere was observed.

4.3.3 Compaction Rate

Test Matrix No. 3

Ejection tests were carried out in test matrix no. 3 to investigate the relationship between compaction rate and ejection stress. These tests indicate that within the range from 20mm/min to 500mm/min die wall frictional stress is independent of the rate at which a compact is pressed.

4.4 GREEN STRENGTH ANALYSIS

4.4.1 Powder Heat Treatment

Test Matrix No. 2

Diametrical green strength testing was carried out on green compacts produced from both heat treated (one sample tested per batch) and as-supplied (two samples tested per batch) powders. The results for the 10% SiC case can be seen in figure 4.12. These results clearly indicate that the green compacts produced from heat treated powders exhibit green strength up to three times greater than that of the as-supplied material compacts.

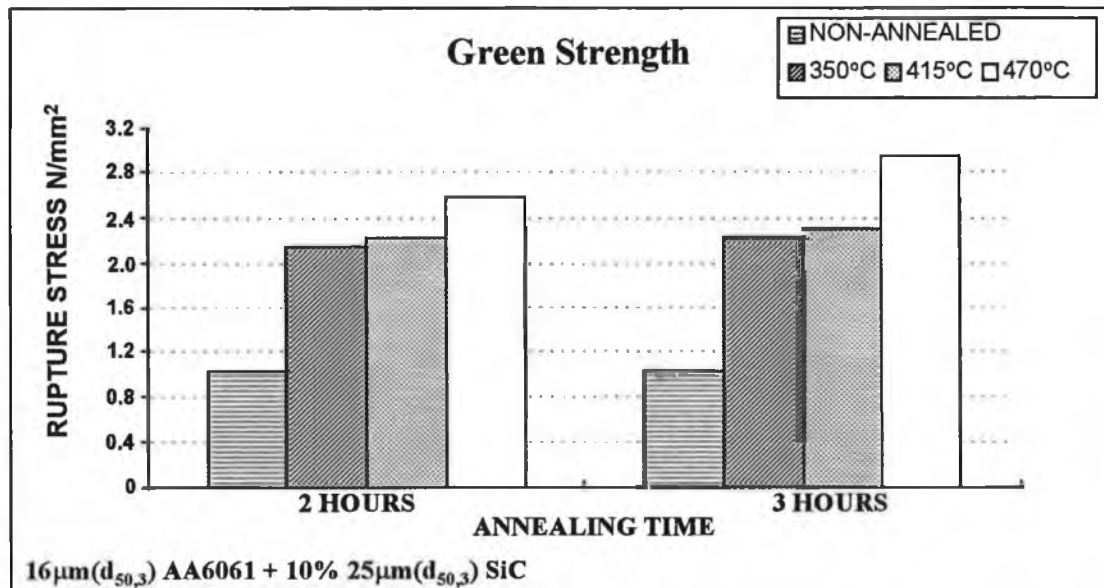


Figure 4.12. Green strength results, test matrix no. 2. Non-annealed results shown indicate the average rupture stress based on two samples tested.

As in the case of compressibility, the highest annealing temperature of 470°C produced the greatest increase in green strength. However, annealing time also has a distinct affect on the green strength of the compacts. The longer annealing time investigated of 3 hours and higher temperature of 470°C provided green compacts

with the highest green strength. These trends were observed for all volume fractions tested including 0% SiC. The full set of results for these tests can be found in appendix D.

4.4.2 Heat Treatment Atmosphere and Lubricant Type

Test Matrix No. 3

Green strength testing was carried out as part of test matrix no. 3. This investigation examined the relationships between compact green strength and both heat treatment atmosphere and lubricant type. The results obtained show little difference between the green strength of the samples tested. These test results indicate no distinct relationship between these factors and compact green strength. However, further detailed investigation may be required in this area. The results of these tests can be found in appendix D.

4.5 GREEN COMPACT MICROSTRUCTURAL ANALYSIS

Test Matrix No. 4

The oxide layer which naturally occurs on the surface of aluminium powders normally acts as a hindrance to the sintering of aluminium green components. Scanning electron microscope investigations of the fracture surface of a green component from batch No. 5 in test matrix no. 4 have shown that the surface of many aluminium powders are penetrated by the rigid angular SiC particles during the compaction of the composite powder. Figure 4.13 clearly illustrates this powder surface layer penetration in the form of both powder indentation and grooving.

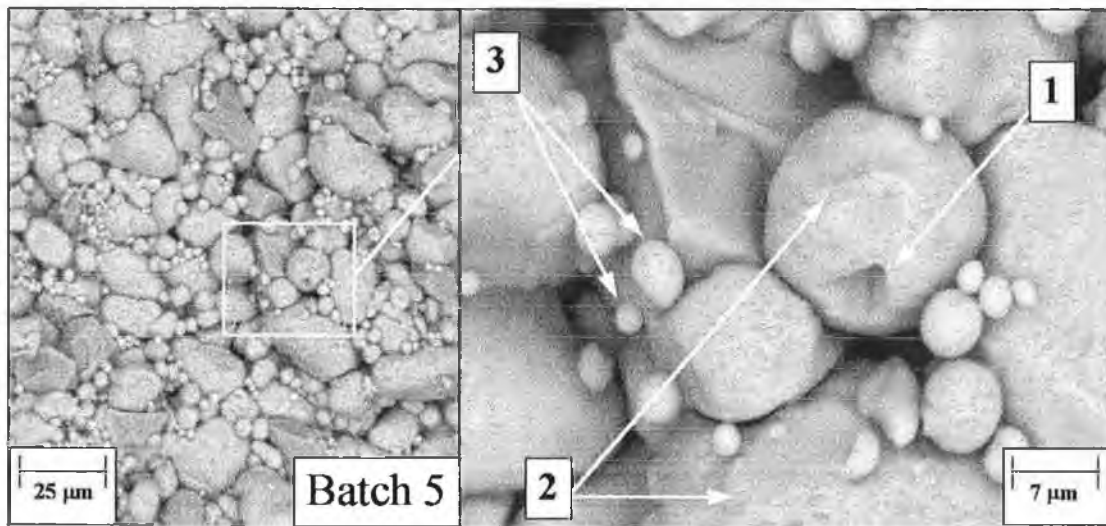


Figure 4.13. Scanning electron micrograph of the fracture surface of a green component from batch No. 5 illustrating the penetration of the aluminium powder surface oxide layers by indentation (1) and grooving (2), and also showing undeformed small aluminium powders (3), test matrix no. 4.

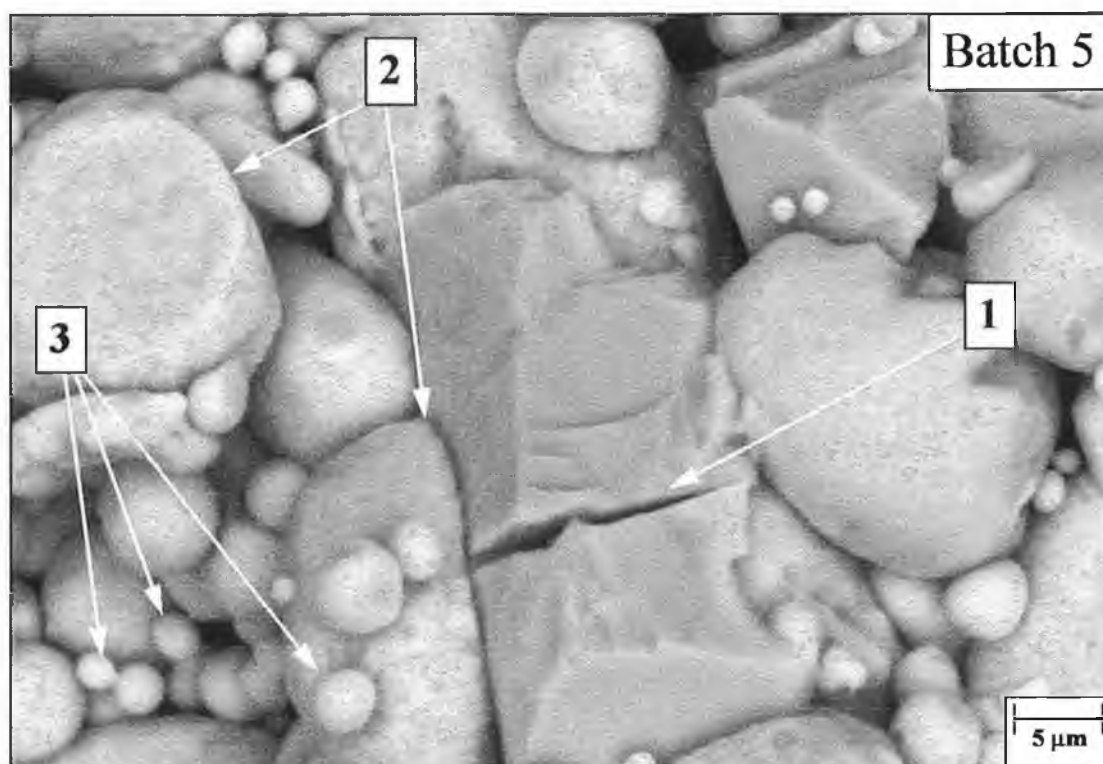


Figure 4.14. Scanning electron micrograph of the fractured surface of a green component from batch No. 5 illustrating the fracture of a SiC particle (1), and both the deformation of large aluminium powders (2) and undeformed small powders (3), test matrix no. 4.

The analysis of the fracture surface of this green component has also revealed fractured SiC particles (figure 4.14), small undeformed aluminium powders (figure 4.13 & 4.14) and has highlighted the wide size distribution range of the 16μm aluminium powder batch.

4.6 SINTERED DENSITY ANALYSIS

4.6.1 Sintering Temperature

Test Matrix No. 3

{16 μ m(d_{50,3}) AA6061 + 25 μ m(d_{50,3}) SiC}

Green compacts containing 10% SiC particulate in an AA6061 matrix were sintered at temperatures of 617°C, 627°C and 633°C for 1 hour as part of test matrix no. 3. The processing histories of the samples chosen for this investigation were identical and the variance in green density for each sample was recorded and found to be ± 0.25 %TD around their nominal average density. These sintered cylindrical samples were repressed directly after sintering and the oxide layers on both flat faces of each sample were machined away. The sintered density of each sample was recorded after machining and the thickness of the circumferential oxide layer was examined.

Figure 4.15 details the results of the sintered density tests. The densities of all the samples tested are within the range from 97.1% TD to 97.9% TD for the AA6061 alloy based composite, indicating no distinct trend due to the sintering temperature. It was also found that the oxide layer thickness was no more than 50 μ m in all cases and that this oxide layer thickness increases with sintering temperature.

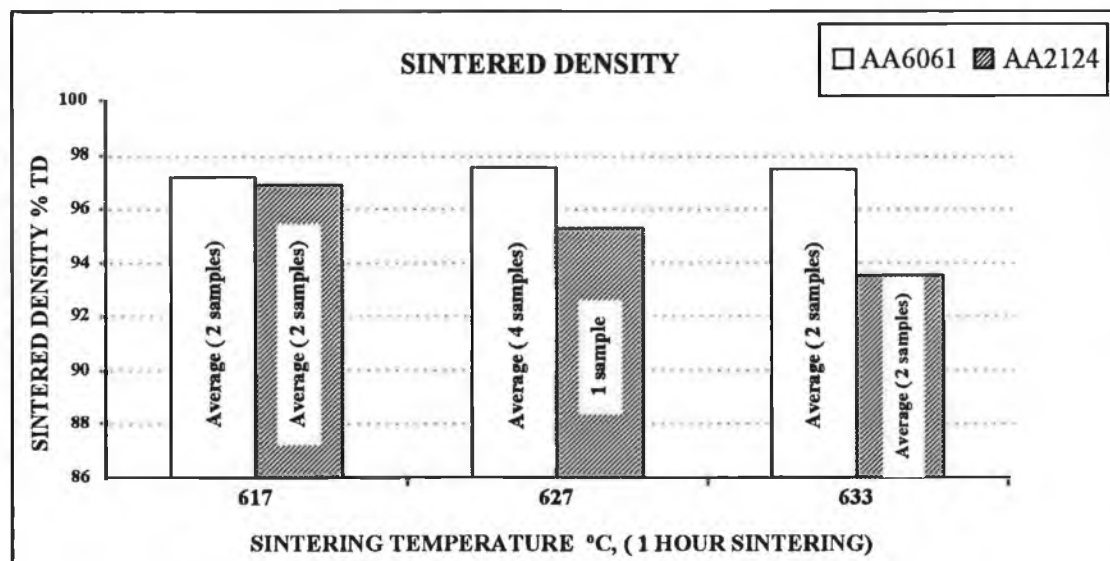


Figure 4.15. Sintered density results, test matrix no. 3.

{19.5 μm ($d_{50,3}$) AA2124 + 25 μm ($d_{50,3}$) SiC}

The tests carried out for the AA6061 composites were also carried out on the AA2124 based material. The results shown in figure 4.15 indicate that the sintered density of the AA2124 composite decreases as the sintering temperature increases. In addition, the higher temperature sintering caused the formation of thick porous oxide layers which were not visible in the case of the low temperature sintered composites.

4.6.2 Sintering Time

Test Matrix No. 3

{16 μm ($d_{50,3}$) AA6061 + 25 μm ($d_{50,3}$) SiC}

Tests were carried out on 10% SiC/AA6061 composites to investigate the effects of sintering time on the final sintered density. The sintering of the test samples was carried out at 617°C and sintering times of 60 and 180 minutes were investigated. The test results shown in figure 4.16 indicate no difference due to sintering time at this temperature.

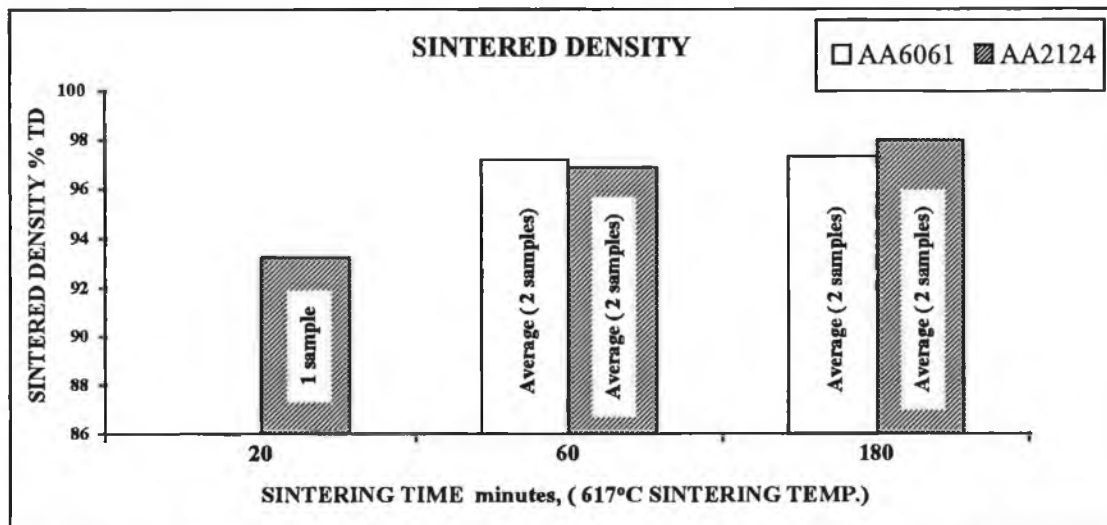


Figure 4.16. Effect of sintering time on sintered density, test matrix no. 3.

{19.5 μm ($d_{50,3}$) AA2124 + 25 μm ($d_{50,3}$) SiC}

Tests were also carried out on AA2124 based composites to investigate the effects of sintering time on sintered density. The sintering of the test samples was also carried out at 617°C and sintering times of 20, 60 and 180 minutes were investigated. The test results shown in figure 4.16 indicate that sintering time is an important parameter in the sintering of the AA2124 alloy based composite. The longest sintering time of 180 minutes produced highly densified material. The highest density recorded in this case was 98.2% TD. The shorter sintering times of 20 and 60 minutes produced composite material of 93.2% and 97% TD respectively. It should also be noted that all of the AA2124 based samples sintered at this temperature exhibited surface oxide layers in the order of 20 μm .

4.6.3 Sintering Atmosphere

Test Matrix No. 1

The sintering carried out in test matrix no. 1 produced material exhibiting very low density. The sintered material densities recorded ranged from 73% TD to 85% TD. In the majority of cases the final density was very close to the original green density. Also, the microstructural investigation of these materials indicated little or no sintering and considerable oxidation. It was realised after the completion of test matrix no. 1 that the atmospheric conditions within the kiln during sintering were not adequately controlled and considerable quantities of oxygen were available within the kiln during sintering. The argon and hydrogen gas mixture used should have created an atmosphere virtually oxygen free. However, this gas mixture was simply allowed to flow into the kiln which was not adequately sealed from the ambient air. These observations of poor sintering and the recognition that a potentially explosive hydrogen/oxygen gas mixture was present within the kiln led to the development of the sealed heat treatment units used in test matrices no. 2, 3 and no. 4.

Test Matrices No. 2, 3 & 4

40 samples were produced from non-annealed powder and sintered within the sealed heat treatment unit as part of test matrix no. 2. Although these samples all exhibited large oxide layers it was found that, unlike the samples produced in test matrix no. 1, consolidation had occurred at the centre of each sample. Also, coupled with the increase in compact green density caused by the annealing of the powder blends, the controlled atmosphere created by the sealed heat treatment units used in test matrices no. 2, 3 and 4 had the affect of increasing the sintered density from approximately 80% TD to a nominal value of approximately 97% TD for 10% SiC composites. Therefore, the close control of the atmospheric conditions during sintering is recognised as being of paramount importance.

4.6.4 Powder Heat Treatment

Test Matrix No. 2

The density of the sintered material produced from both annealed and as-supplied powders was recorded in test matrix no. 2. The test results (based on single samples per batch) obtained are presented in table 4.2.

Table 4.2. Theoretical density (%) of sintered materials, test matrix no. 2.

Vol. %SiC	0%	10%	20%	30%
Non-annealed	99.6	98.9	96.3	91.5
Annealed	96.9	97.1	95.7	88.4

However, the results obtained are misleading due to the very large oxide layer which developed in the case of the materials produced from the non-annealed powders. Aluminium oxide has a density of 3.9 g/cm^3 which is greater than that of the aluminium alloy (2.7 g/cm^3). The large oxide layer causes an increase in the mass of the compacts which leads to the apparent increase in percentage theoretical density in the case of the material produced from the non-annealed powders.

An accurate comparative investigation between these materials is difficult due to this excessive oxidation. However, due to the extremely poor condition of the non-annealed materials further investigations in this area were not pursued.

4.7 DIAMETRICAL COMPRESSIVE STRENGTH ANALYSIS

Test Matrix No. 1

The diametrical strength tests carried out on sintered compacts in test matrix no. 1 aimed to provide data which could be used to indicate the tensile characteristics of these samples. The sintered material responded to the diametrical compressive testing in a brittle manner. However, after further investigation of this material it was found that inadequate sintering had occurred due to the sintering atmospheric conditions described in section 4.6.3.

This situation was rectified and the sintering process was improved for test matrix no. 2. It was then found that the sintered composite material produced tended to flatten at the initial stages of diametrical testing. Since this test method is only valid for the analysis of brittle material this plastic deformation invalidated these test results from test matrix no. 2.

4.8 HARDNESS TESTING

All of the hardness test results presented in this section are based on the average of four hardness readings taken per sample and one sample per batch.

4.8.1 Hardness Test Methods

Test Matrix No. 2

Both Rockwell B and Vickers 30 macrohardness testing was carried out on the sintered material produced in test matrix no. 2. The deformation associated with indentation in the Vickers method caused difficulty in identifying the diagonal distances necessary for the calculation of hardness by this method. This deformation is due to the inhomogeneous macrostructure of the composite. However, the Rockwell B hardness test indentation covers a large area of the composite and is reasonably regular in shape, as shown in figure 4.32. Also, the readings from this method were found to be consistent and repeatable. Therefore, in the case of the composites being tested the more accurate method of hardness testing is the Rockwell B test.

4.8.2 SiC Content

Test Matrix No. 2

Before hardness tests could be carried out on the samples from test matrix no. 2 it was necessary to machine off the oxide layers on the surface of these samples. The machined surfaces were also ground and polished before testing. All samples tested were in the T6 condition. The results shown in figure 4.17 indicate an increase in macrohardness with an increase in volume fraction of SiC in all cases with the exception of the 30% SiC composite produced from heat treated powders. This phenomena is due to the high level of porosity present within this composite compared to the other composites produced from the annealed powders (table 4.2).

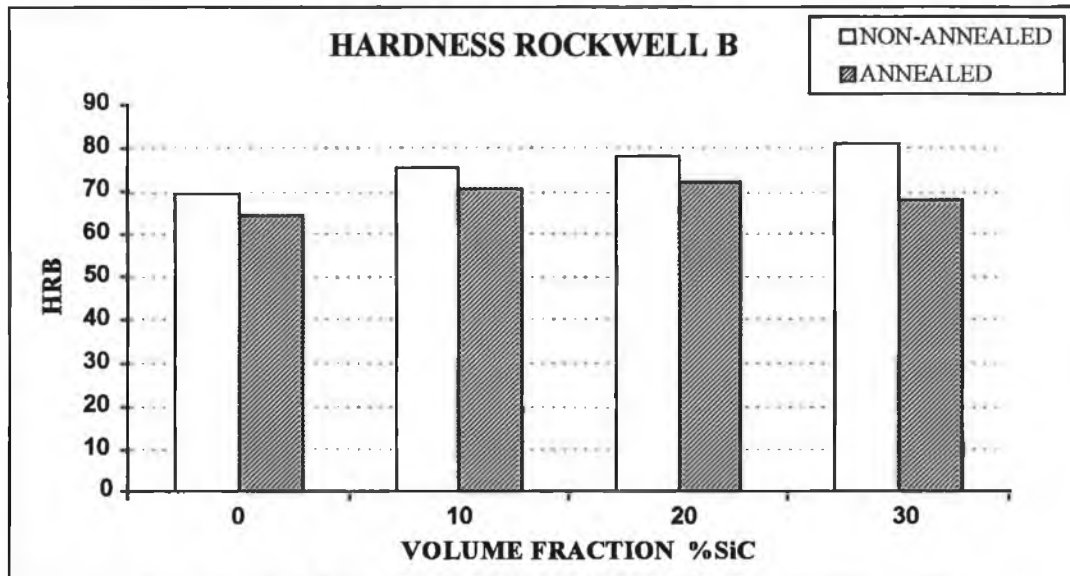


Figure 4.17. Rockwell B hardness test results, test matrix no. 2.

4.8.3 Powder Heat Treatment

Test Matrix No. 2

Figure 4.17 compares the macrohardness of material produced from annealed and non-annealed powders. The sintered material produced from the heat treated powders exhibits lower hardness values compared to the as-supplied powder composites. This was found to be the case for all volume fractions.

4.8.4 Sintering Temperature

Test Matrix No. 3

Macrohardness tests were carried out on both AA6061 and AA2124 based composites in test matrix no. 3. The AA6061 sintered composites were tested in the T4 and T6 heat treatment conditions and the AA2124 composites were tested in the naturally aged condition only (T4). Various sintering parameters were used to produce these samples. The sintering temperatures investigated were 617°C, 627°C

and 633°C. The results displayed in figure 4.18 show the variance in macrohardness related to the sintering temperatures examined.

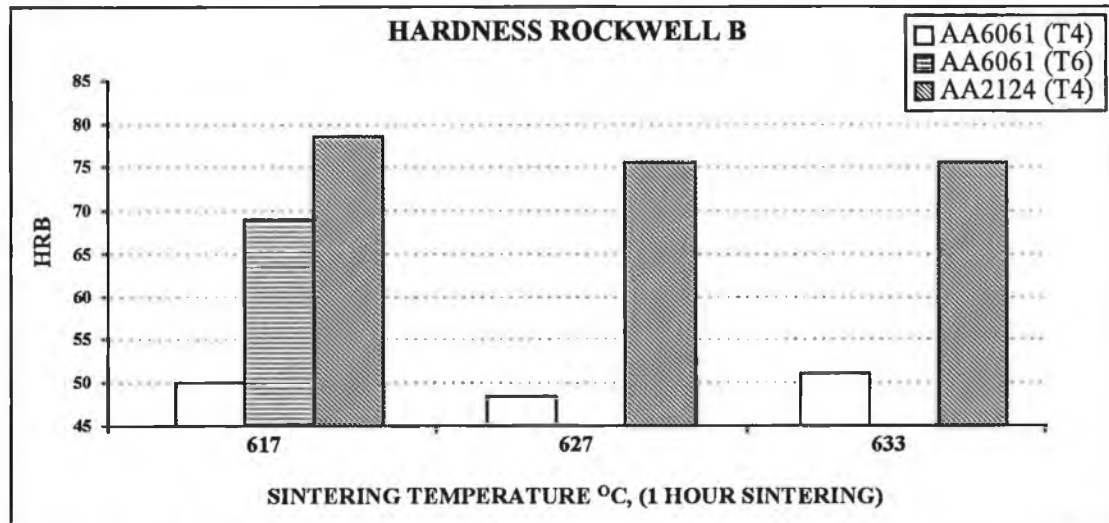


Figure 4.18. Effect of sintering temperature on macrohardness, test matrix no. 3.

The results presented in figure 4.18 indicate that the AA6061 composites in the T4 condition vary slightly around a nominal value of 50 HRB. However, no distinct trend relating to sintering temperature is observed. The AA6061 T6 based material displays a considerable increase in hardness compared to the T4 condition (69HRB recorded for AA6061+10%SiC T6). In the case of the AA2124 material values of 78 HRB were recorded for the samples which were sintered at 617°C for 1 hour. A slight decrease in hardness was recorded for the samples which were sintered at the higher temperatures of 627°C and 633°C. However, as with the AA6061 material no distinct trend relating hardness and sintering temperature was observed.

4.8.5 Sintering Time

Test Matrix No. 3

Macrohardness tests were carried out in test matrix no. 3 to investigate the effect of the sintering time on both AA6061 and AA2124 based composites. As with the sintering temperature investigations described in section 4.8.4 the AA6061 sintered composites were tested in the T4 and T6 heat treatment condition and the AA2124

was tested in the T4 condition. The sintering times investigated were 20, 60 and 180 minutes. The results displayed in figure 4.19 show the variation in macrohardness of these samples.

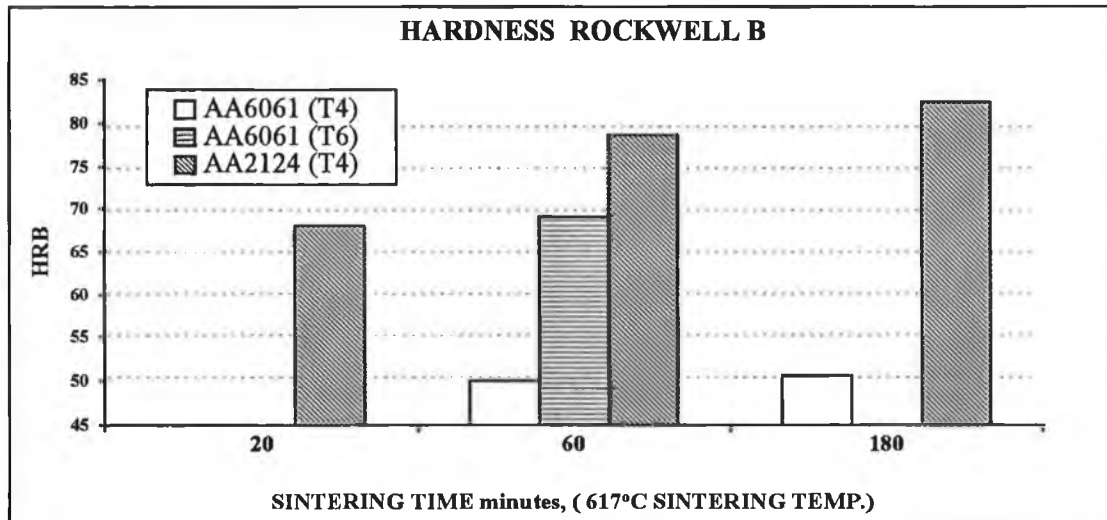


Figure 4.19. Effect of sintering time on macrohardness, test matrix no. 3.

The AA6061 T4 based samples were sintered for either 60 minutes or 180 minutes. Very little difference was recorded between the hardness of these samples. However, the AA2124 T4 samples indicate a distinct relationship between hardness and sintering time. In this case the composite samples sintered for 180 minutes displayed average macrohardness values of 82.5 HRB. This value decreased to 78 HRB for 60 minutes sintering and 67.5 HRB for 20 minutes.

4.9 AXIAL COMPRESSIVE STRENGTH TESTING

4.9.1. SiC Content

Test Matrix No. 2

Compression tests were carried out on composite samples containing various quantities of SiC. Material containing volume fractions of 0%, 10%, 20% and 30% were investigated. The results of these investigations are shown in figure 4.20. The yield strength increases with an increase in SiC content between 0% and 20% SiC. The 30% SiC material exhibits strength values lower than the 20% SiC composites. This phenomena is explained by the extensive porosity within the 30% SiC samples (see table 4.2).

In the cases of the 0%, 10% and 20% SiC for annealed and non-annealed each increase of 10% SiC produced a yield strength increase of approximately 50 N/mm^2 , the maximum value of 456 N/mm^2 being recorded in the case of 20%SiC produced from non-annealed powders.

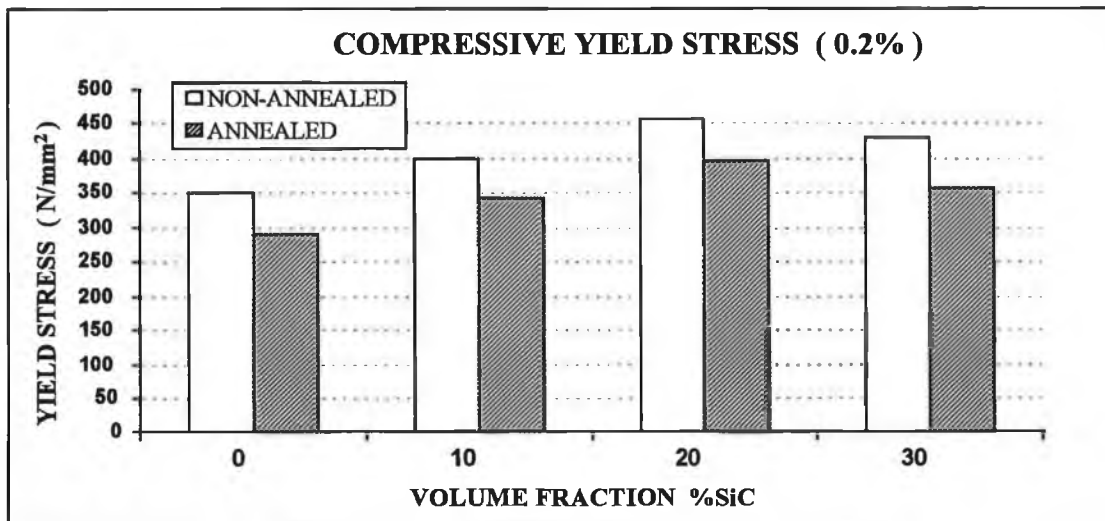


Figure 4.20. Yield strength results based on single samples, test matrix no. 2.

4.9.2 Powder Heat Treatment

Test Matrix No. 2

The samples processed in test matrix no. 2 were produced from both annealed and non-annealed powders. Figure 4.20 compares the yield strengths recorded for these samples. The results show that the materials produced from non-annealed powders exhibit yield strengths approximately 60N/mm^2 greater than the samples produced from annealed powders for all volume fractions tested.

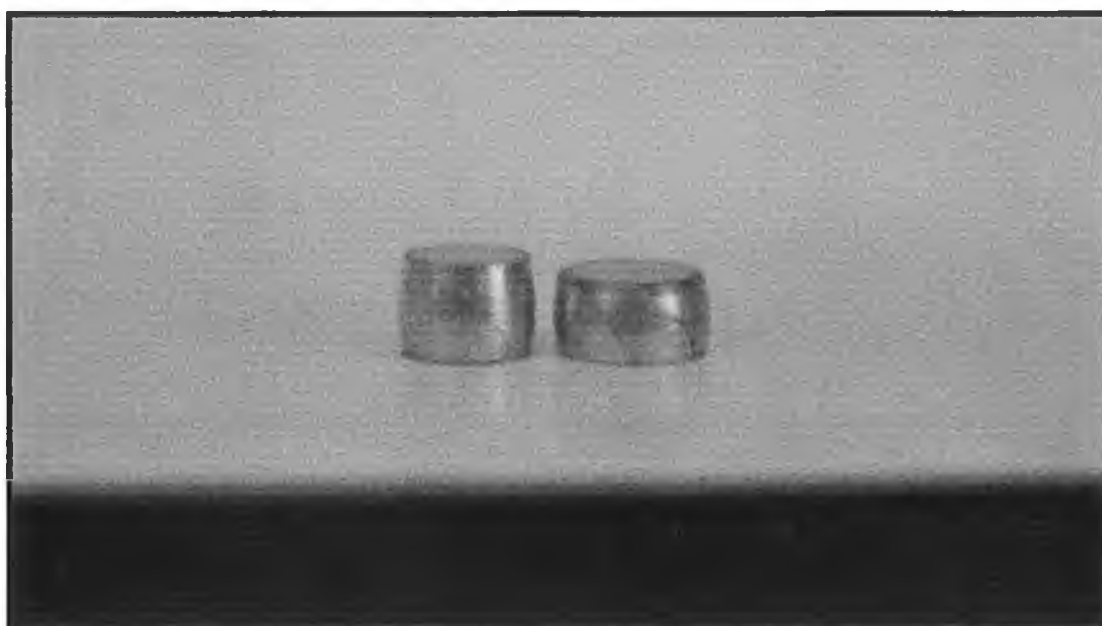


Figure 4.21. Left: Compression sample produced from non-annealed powders. Right: Compression sample produced from annealed powders. (Both 30% SiC).

These compression tests did not provide qualitative results for the ductility of the materials tested. However, the materials produced from annealed powders have exhibited greater ductility than the non-annealed powder based material at all volume fractions of SiC. Figure 4.21 compares the deformation experienced up to the point where cracking occurred for materials produced from both the non-annealed and the annealed powders.

4.10 FRACTURE SURFACE DEFECTS AND TENSILE RESPONSE

4.10.1 Fracture Surface Defects

Test Matrix No. 4 (All AA6061 based)

Following the tensile testing of the tensile test samples (figure 4.22) produced in test matrix no. 4 the fracture surface of each sample was inspected in order to ascertain the cause of fracture. Three distinct defect features were observed on the fracture surfaces of many of the samples. Examples of these features are illustrated in figure 4.23 and are described as SiC pockets, outer layers and localised semi-sintered layers.

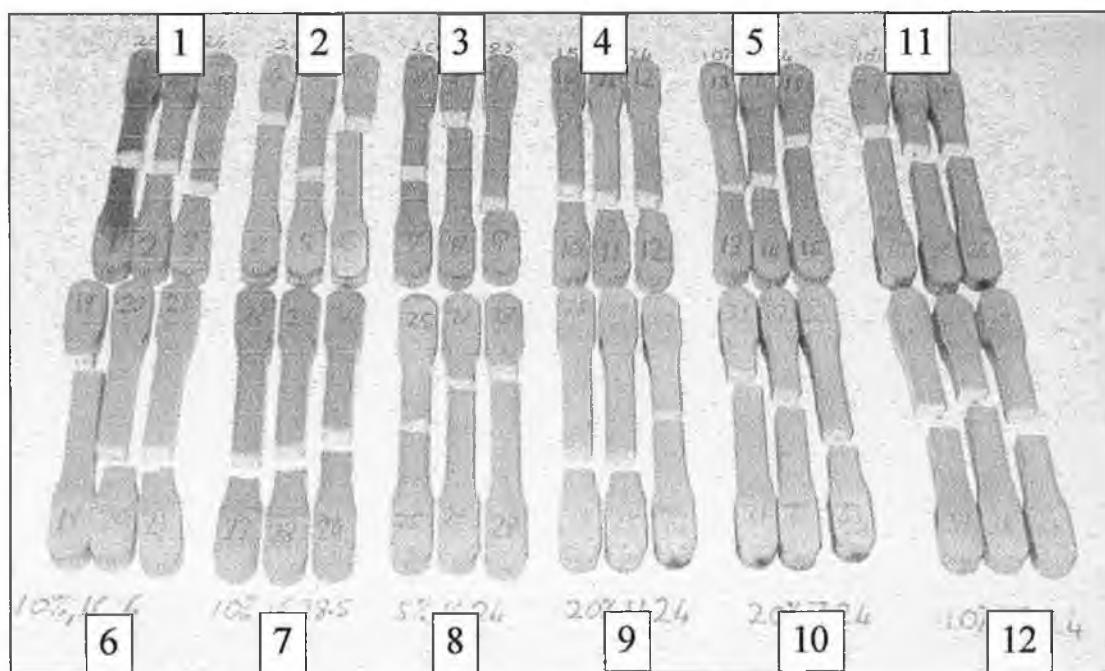


Figure 4.22. Net shape tensile samples produced in test matrix no. 4 using die wall lubrication and labelled according to the batch reference number (see appendix D).

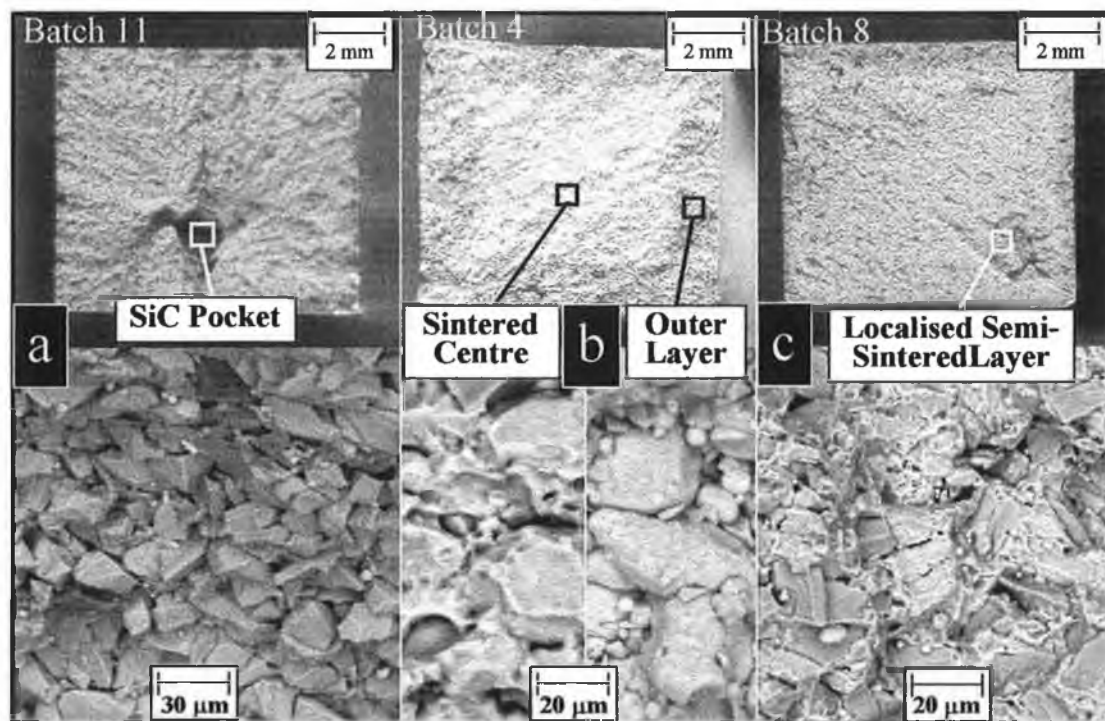


Figure 4.23. Fracture surface defects, test matrix no. 4.

The feature described as a SiC pocket, shown in figure 4.23a, was observed on the fracture surface of 14 samples out of the total 46 samples tested. These pockets consist of a thin layer of SiC particles within which no sintering has occurred. Therefore, this feature acts as a point of weakness in the material and a probable position for the initiation of tensile failure. Figure 4.23a illustrates one such case, where crack propagation proceeded radially from the SiC pocket.

The outer layer shown in figure 4.23b consists of unsintered powders which exhibit a morphology very similar to that of the green compact shown in figures 4.13 & 4.14. The thickness of this layer varied from approximately 50μm (figure 4.24a) to 2mm (figure 4.24b) and was found to be strongly dependent on the aluminium powder size, increasing in depth with increasing powder size. Unfortunately, due to the irregularity of the oxide layer thickness on the majority of the samples produced from the larger aluminium powders it was not possible to quantitatively describe this relationship.

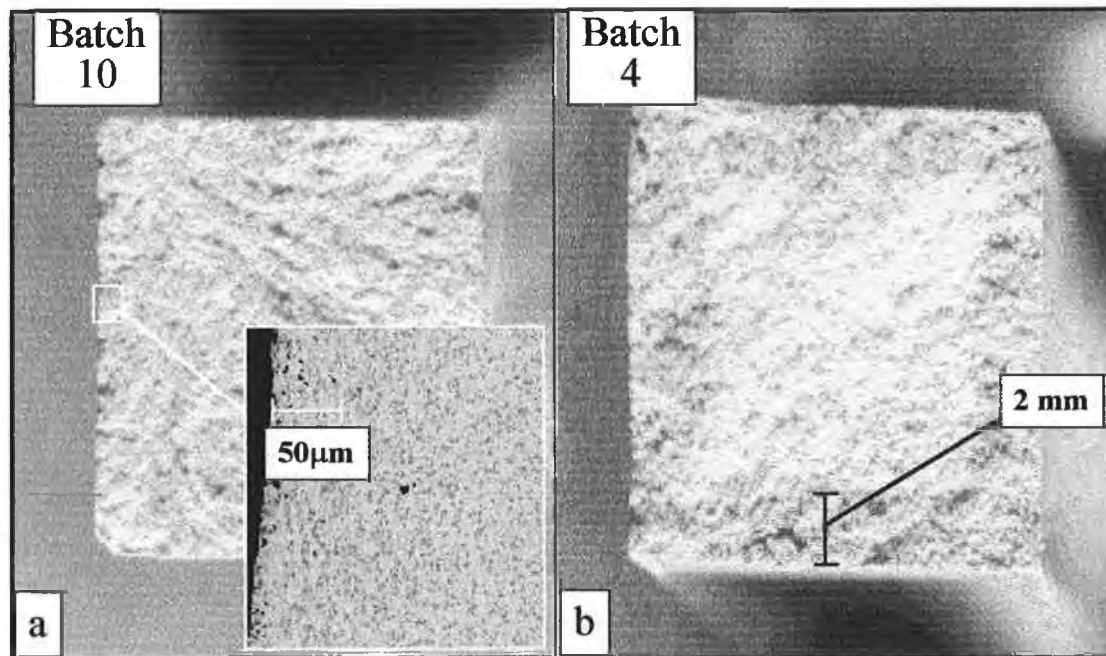


Fig. 4.24. (a) Photograph and micrograph of the fracture surface and polished surface of samples from batch No. 10 consisting of 7µm aluminium powder, and (b) a sample from batch No. 4 consisting of 16µm aluminium powders, showing the large difference in outer layer thickness between batches.

The deepest layers were observed on samples consisting of the largest aluminium powders (16µm). Samples consisting of the smaller aluminium powders (7µm & 11µm) exhibit very shallow outer layers, which in the case of batch No. 10 (figure 4.24a) were only visible under high magnification. It was also observed that the layer thickness decreased with increasing volume fraction in the case of these small aluminium powder samples and the samples consisting of 16µm aluminium with 6µm SiC (batches No. 2 & 6). No such volume fraction related trend was observed for the samples consisting of the larger aluminium powders combined with either 25µm or 28.5µm SiC. The microscopy analyses of the samples indicate that these layers are due to poor sintering response, followed by the reoxidation of any powders previously penetrated by SiC during compaction. Out of the 46 samples investigated 34 samples exhibited significant outer layers.

Figure 4.23c illustrates an example of a localised semi-sintered layer. This layer was observed on the fracture surface of only four samples and consisted of a semi-sintered

layer penetrating radially from a point on the surface of each of the four samples to a depth of between 1mm and 3mm. The morphology of these layers indicate that partial sintering of this area may have been followed by oxidation. All of the localised semi-sintered layers observed were oriented parallel to the cross sectional plane of the samples and therefore had a considerable affect on the tensile response of these samples. The shape of the layers indicates that they may have been caused by the partial fracture of the sintered sample during repressing, followed by fracture surface oxidation during the solution heat treatment of the samples.

In total, out of the 46 samples processed and investigated four samples exhibited no obvious fracture surface defects.

4.10.2 Tensile Response

Test Matrix No. 4 (All AA6061 based)

The tensile response of the samples varied considerably between batches and was also greatly affected by the presence of outer layers and internal defects discussed in section 4.10.1. Figure 4.25 shows both the variation in ultimate tensile strength (UTS) between the batches, and the scatter of results for each powder combination.

The large scatter observed in most batches is directly attributable to the existence of SiC pockets and localised semi-sintered layers in samples from these batches. In the case of all batches consisting of 16 μ m aluminium powder, including the samples produced using mixed-in lubrication, the UTS records follow no obvious trends regarding SiC content or size. Also, no distinct difference was observed between the UTS of the samples produced using mixed-in lubricant and that of the same batch produced using die wall lubricant. In addition, the slight differences between the sintering temperatures and times used for the sintering of identical samples from batch No. 1 did not result in consistent differences of UTS between these samples. However, the samples produced from the smaller aluminium powders exhibited reasonable UTS, with maximum values as high as 324 MPa.

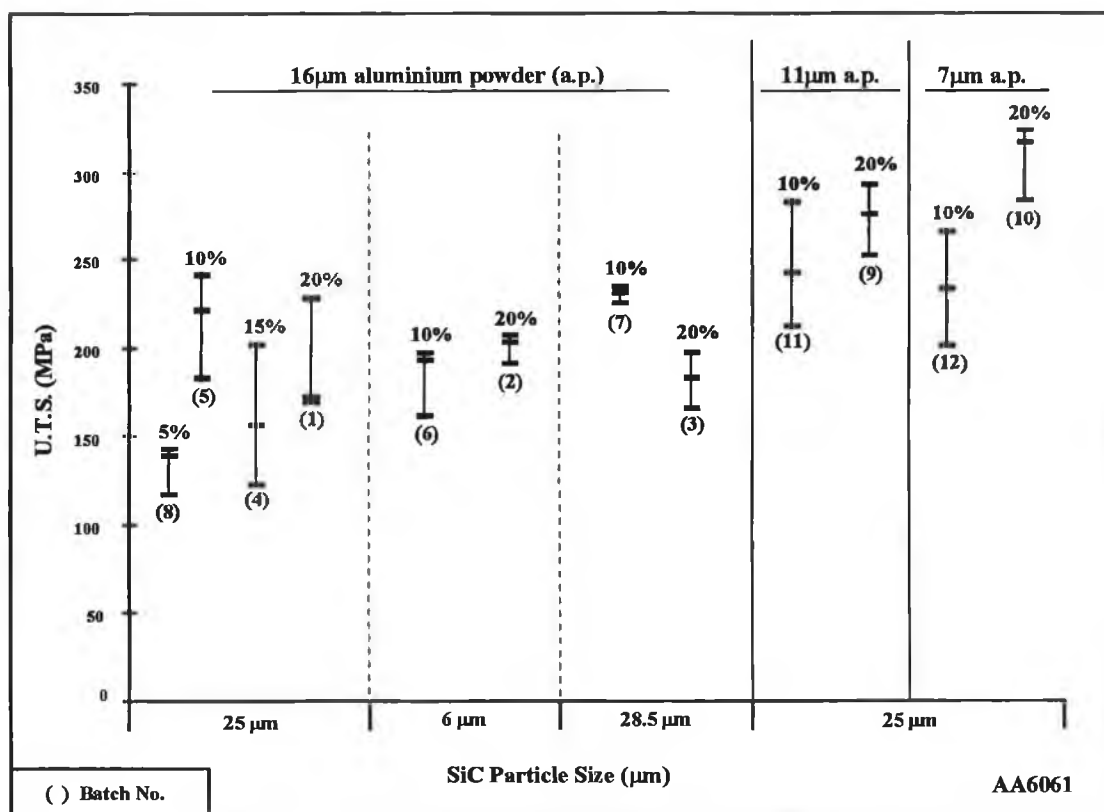


Figure 4.25. Ultimate tensile strength (UTS) variation recorded between batches and the effect of the SiC volume fraction on the average UTS values.

The flow curves recorded during the testing of the samples displaying the maximum tensile strength from each batch are illustrated in figure 4.26. The tensile response of the samples consisting of the smaller 11µm and 7µm aluminium powders (batches 9-12) are superior to those of the samples containing the larger aluminium powders. The ductility recorded for the materials is low with a maximum of approximately 0.8% elongation to fracture recorded for a sample from batch No. 11. However, the extensometer readings taken during the tensile testing may have been adversely affected by the existence of the brittle outer layers on these net shape samples.

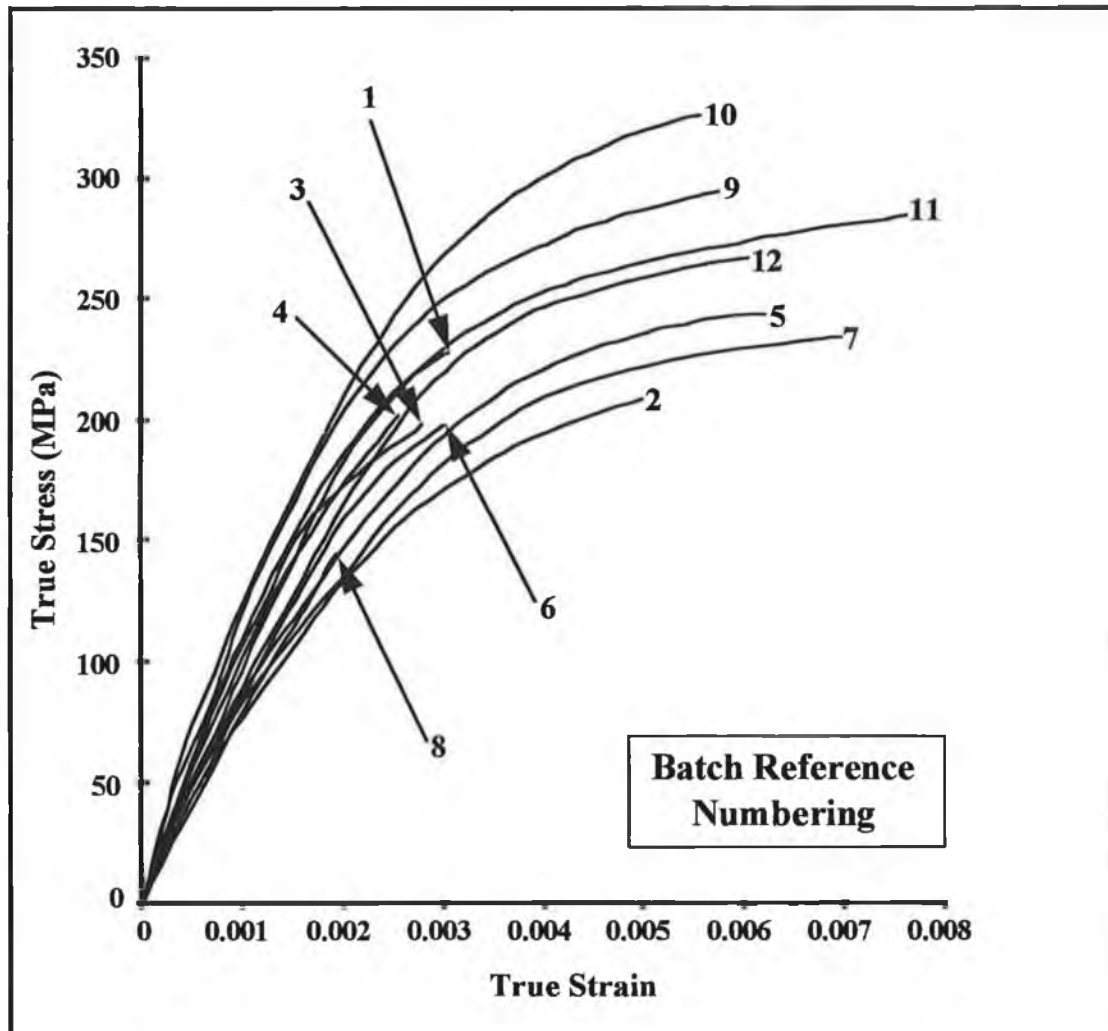


Figure 4.26. Flow curves recorded during the testing of the samples displaying the maximum tensile strength recorded from each batch.

4.11 SINTERED SAMPLE MICROSTRUCTURAL ANALYSIS

4.11.1 Sintering Atmosphere

Test Matrix No. 1

The microstructural analyses of the samples from test matrix no. 1 show the incomplete sintering which occurred due to the inadequate sintering atmosphere control. An example of this partial sintering is shown in figure 4.27. This micrograph shows that only partial sintering has occurred (A). The black lines (B) denote the previous particle boundaries of the aluminium powders. The black areas (C) denote the SiC particles with surrounding porosity.

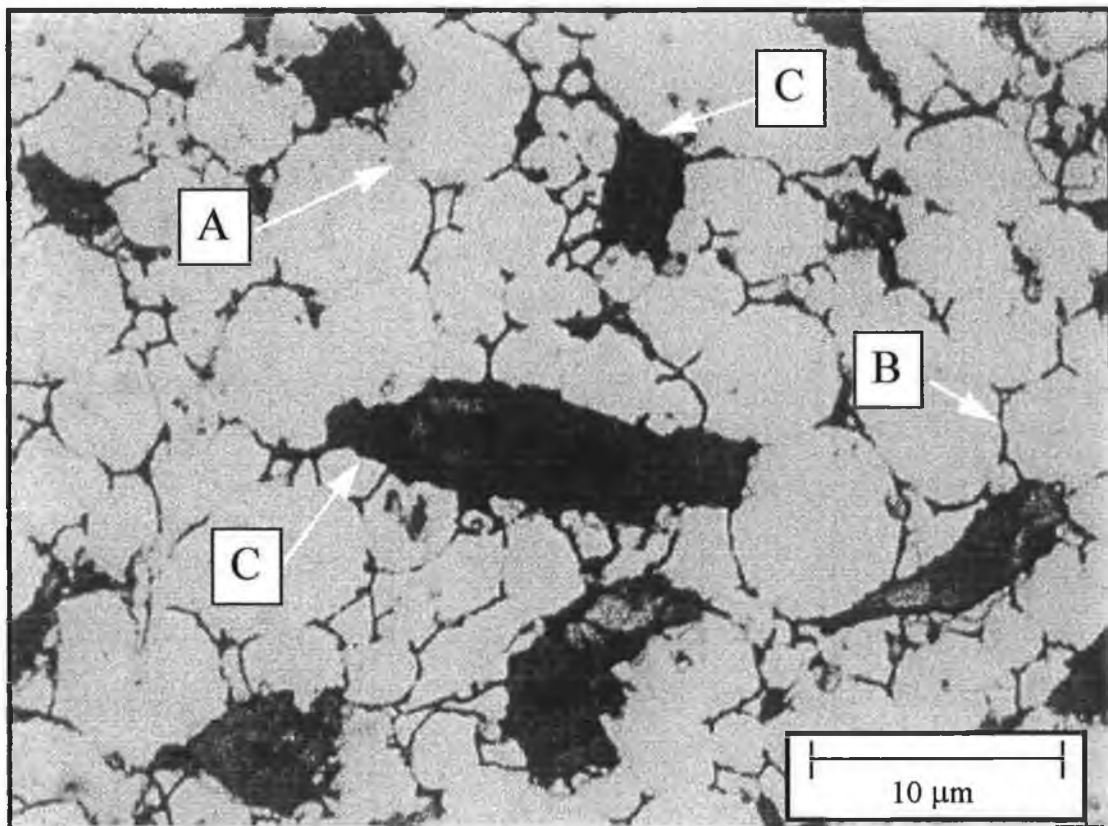


Figure 4.27. Incomplete sintering. $7\mu\text{m}(d_{50,3})$ AA6061 + 10% $6\mu\text{m}(d_{50,3})$ SiC .
test matrix no. 1. Mag. x 2500.

Test Matrices No. 2 & 3

The qualitative analyses carried out on the samples from both test matrix no. 2 and 3 indicate that the control of the sintering atmosphere is of paramount importance. The improved sintering can be seen in figure 4.28.

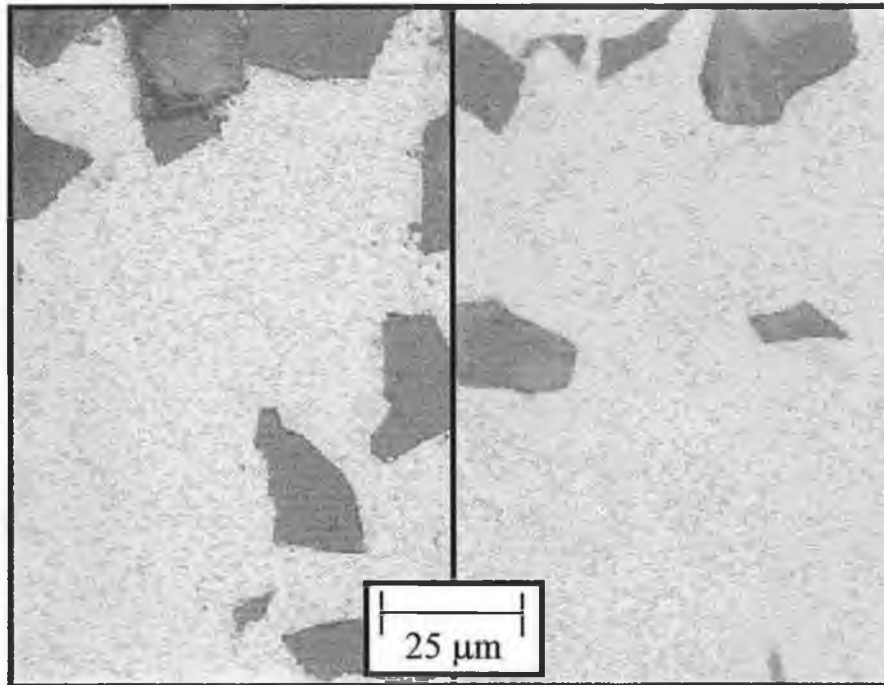


Figure 4.28. Complete sintering. Left: AA6061/10% SiC, test matrix no. 2.

Right: AA2124/10% SiC, test matrix no. 3. Mag. x 750.

4.11.2 Powder Size

Test Matrix No. 1

Although incomplete sintering occurred with the samples in test matrix no. 1 the micrographs of these materials indicate the importance of the correct combination of SiC particulate size and aluminium powder size. Figure 4.29 shows an example of the gross clustering which occurred with mixtures of $5\mu\text{m}$ SiC and $45\mu\text{m}$ AA6061. The small SiC particles become clustered in the relatively large areas between the adjoining aluminium powders.

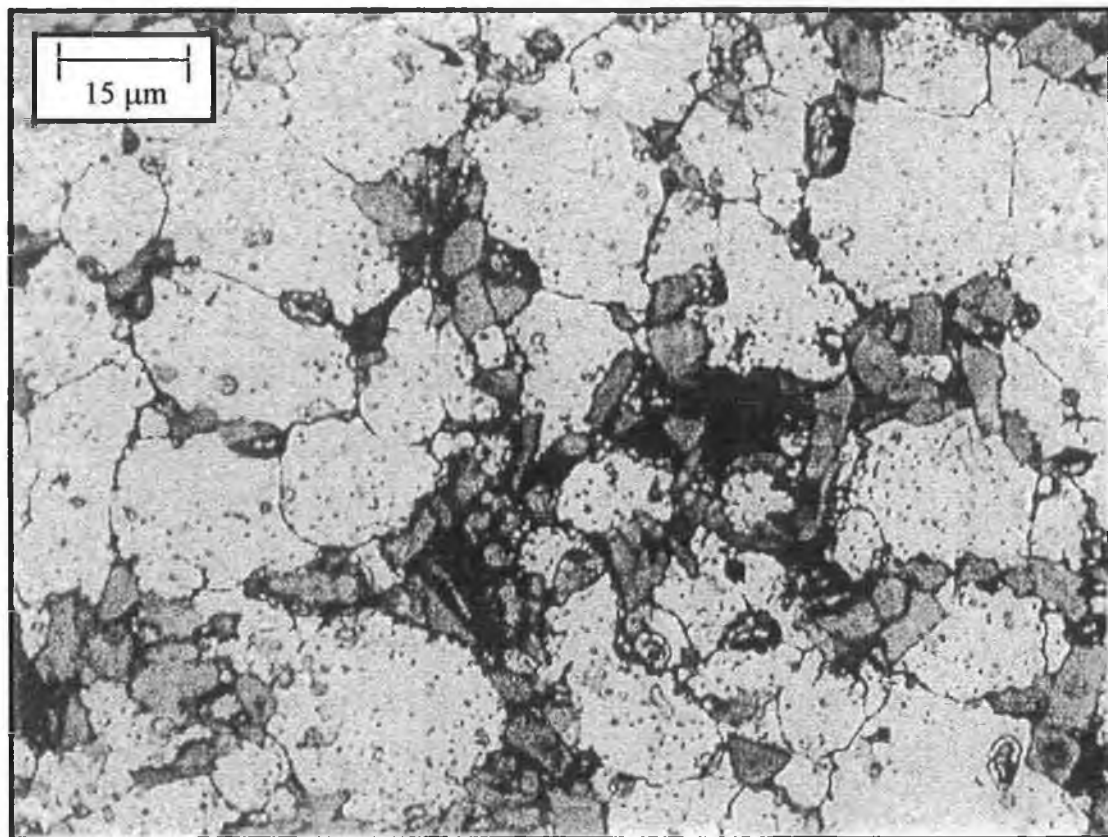


Figure 4.29. SiC clustering. $16\mu\text{m}(d_{50,3})$ AA6061 + 30% $6\mu\text{m}(d_{50,3})$ SiC.
test matrix no. 1. Mag. x 1250.

Test Matrices No. 2 & 3

Two similar SiC/aluminium powder size ratio were investigated in test matrices no. 2 and 3, as discussed in section 4.2.3. Based on the median particle size ($d_{50,3}$) the ratio

of the mixed powders was approximately 1:1.6 ($16\mu\text{m}$ AA6061: $25\mu\text{m}$ SiC) for the AA6061 based material and 1:1.3 ($19.5\mu\text{m}$ AA2124: $25\mu\text{m}$ SiC) for the AA2124 based material. These powder size combinations provided the basis for homogeneous composite materials exhibiting very little clustering. An example of the homogeneity of the material produced in test matrices no. 2 and 3 is presented in figure 4.30. However, it should be noted that the homogeneity of the composites also depends on the distribution of the SiC during mixing which may vary depending on the mixing method employed, as described in section 4.1.4.

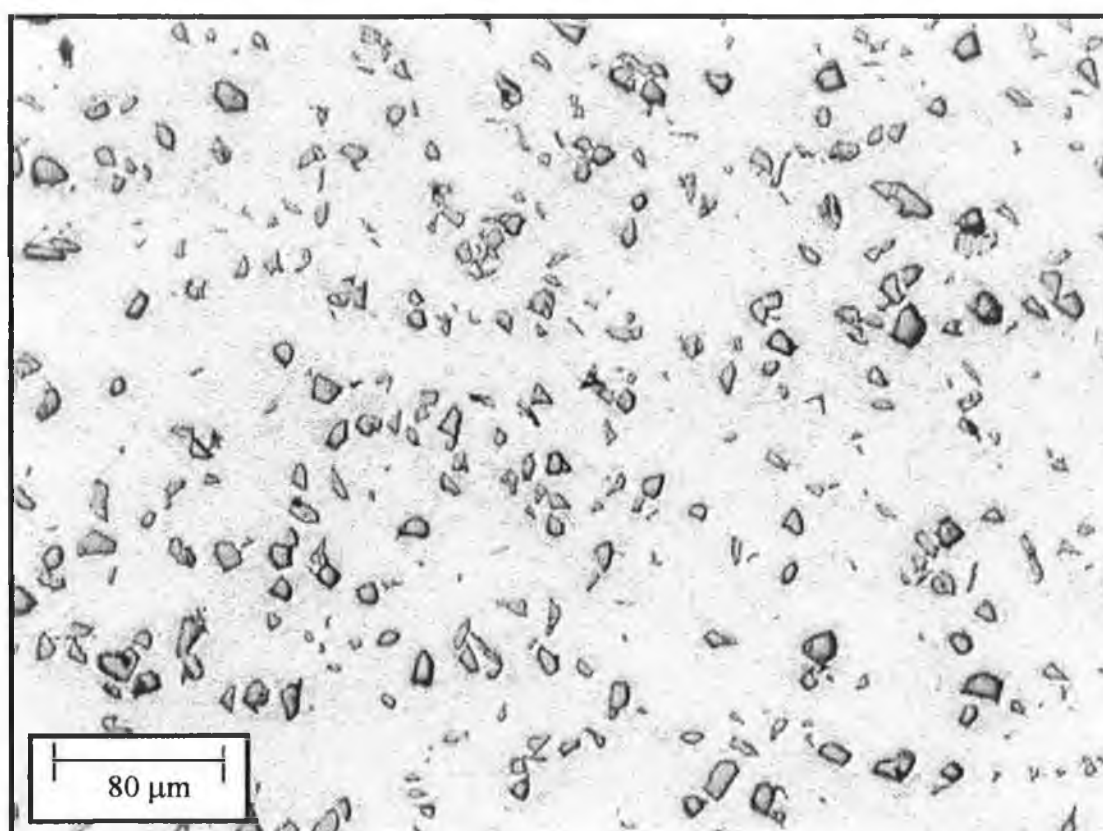


Figure 4.30. Homogeneous distribution. $19.5\mu\text{m}(d_{50,3})$ AA2124 + 10% $25\mu\text{m}(d_{50,3})$ SiC. test matrix no. 3. Mag. x 250.

4.11.3 SiC Content

Test Matrix No. 2

The porosity of the material investigated in test matrix no. 2 increases with an increase in SiC content. The micrographs in figure 4.31 are typical of this progressive increase in porosity for composites containing 0%, 10%, 20% and 30% SiC.

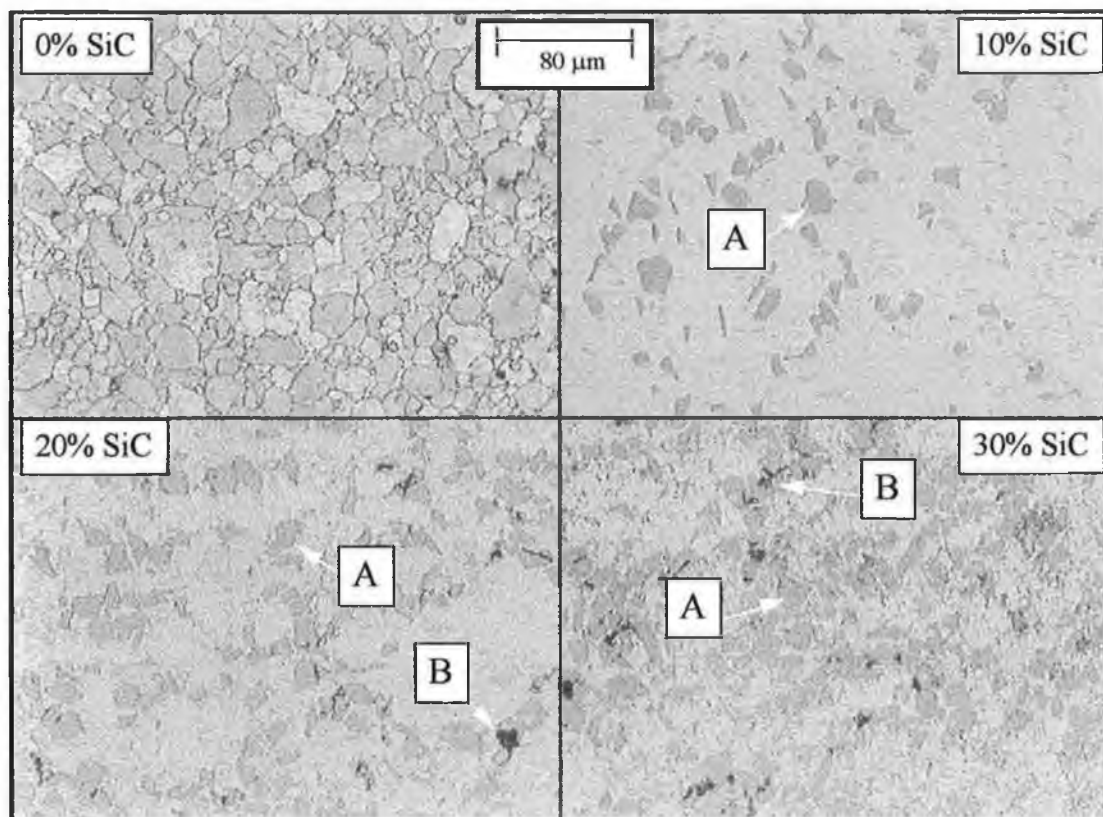


Figure 4.31. Effect of SiC (A) content on porosity (B). AA6061/ 0%, 10%, 20% & 30% SiC. test matrix no. 2. Mag. x 250.

4.11.4 Hardness Testing

Test Matrix No. 3

An example of an indentation caused by the Rockwell B macrohardness test is shown in figure 4.32. The micrograph shows that the size of the indentation compared to the size of the SiC particles eliminates the possibility of an inaccurate hardness reading

due to an individual particle. Conversely, analyses carried out on indentations made during Vickers macrohardness testing have shown that the indentation geometry can be adversely affected by both individual particles and clusters leading to difficulties in obtaining reliable and consistent results.

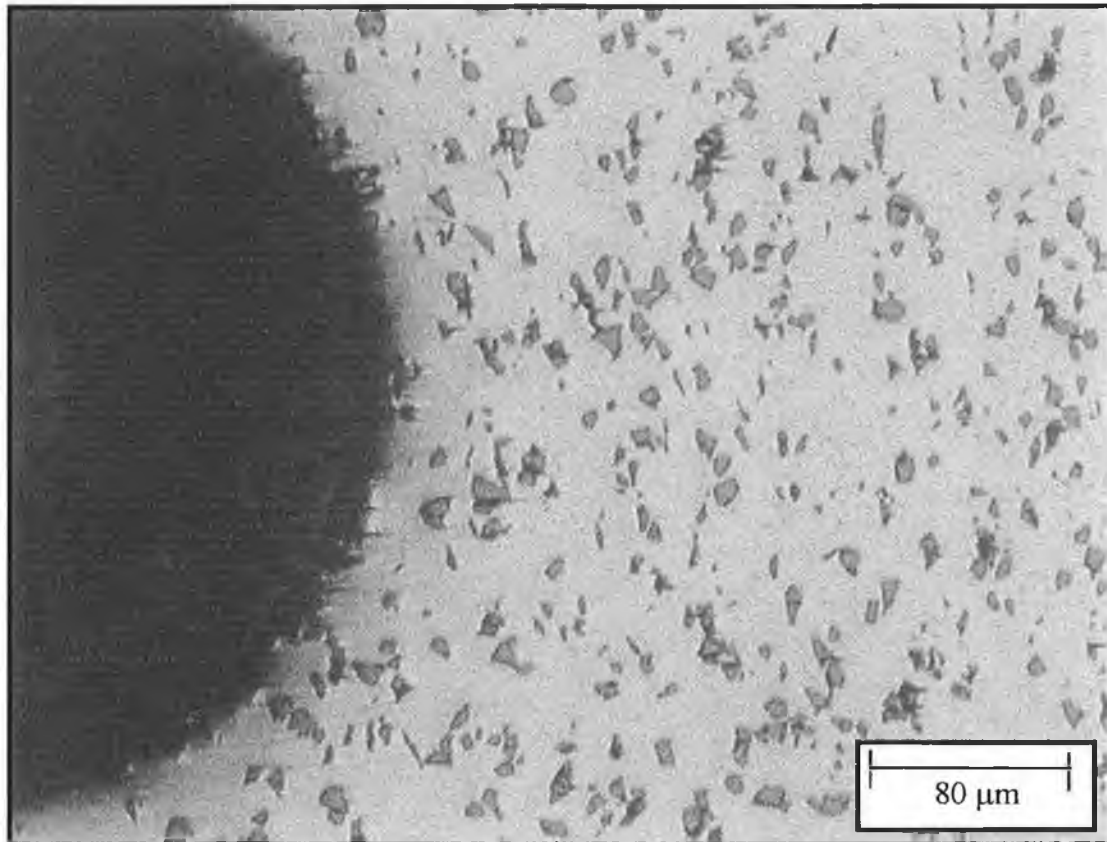


Figure 4.32. Scale of Rockwell B indentation. test matrix no. 3. Mag. x 250.

4.11.5 Sintering Time

Test Matrix No. 3

The effect of the sintering time on the porosity of the composites is illustrated by comparison of the material in figure 4.30 with that of figure 4.32. Both materials are identical in composition. However, the material in figure 4.30 (sintered for 180 minutes) exhibits very little porosity compared to noticeable porosity in figure 4.32 (sintered for 20 minutes). The density measurements carried out quantitatively confirmed these observations by finding the density of the sample in figure 4.32 to be 93.2% TD and the sample in figure 4.30 to be 98.2% TD.

4.11.6 Interfacial Bonding

Test Matrices No. 2 & 3

Complete interfacial bonding has been observed in composites produced in test matrix no. 2 and 3. Figure 4.33 shows a high magnification micrograph of a AA2124/10%SiC composite produced in test matrix no. 3. This material was produced using annealed powders and was sintered at 617°C for 180 minutes. The micrograph clearly exhibits the complete interfacial bonding between the aluminium alloy and the SiC particles. Similar observations were made in the case of the AA6061 based composites produced in test matrices no. 2 and 3. To achieve this good interfacial bonding in the case of the AA6061 based materials the samples should be produced using annealed powders and should be sintered within a controlled atmosphere at 617°C-633°C for between 20 minutes and 3 hours. To achieve the same quality in the case of the AA2124 based material the sintering temperature should be 617°C with a sintering time of 3 hours.

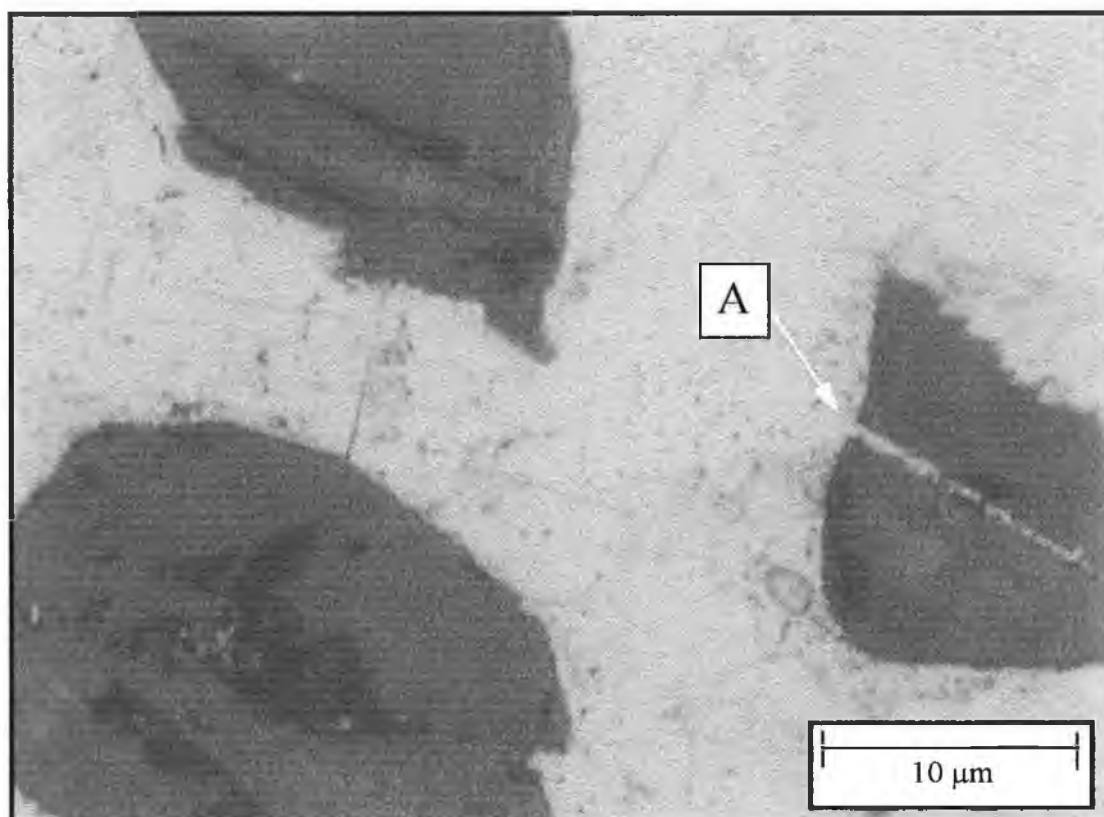


Figure 4.33. Interfacial bonding and cracked particle infiltration (A). test matrix no. 3.
Mag. x 2500.

4.11.7 Cracked Particle Infiltration

Test Matrix No. 3

The crack shown in figure 4.33, which is approximately $0.4\mu\text{m}$ at its widest, is completely infiltrated by aluminium. The microstructural analyses of the materials produced in test matrix no. 3 indicate that SiC particle cracks which occur during compaction may be completely infiltrated during sintering and therefore eliminate undesirable microcracks within the material.

Figure 4.34 shows a fractured SiC particle (A) in 98.2% TD AA2124/10%SiC sintered at 617°C for 180 minutes. The crack infiltration by the aluminium alloy is complete. However, crack infiltration is dependent on the sintering time used. Figure 4.35 shows examples of poor crack infiltration (A) in 93.2% TD AA2124/10%SiC composite material, sintered at 617°C for 20 minutes.

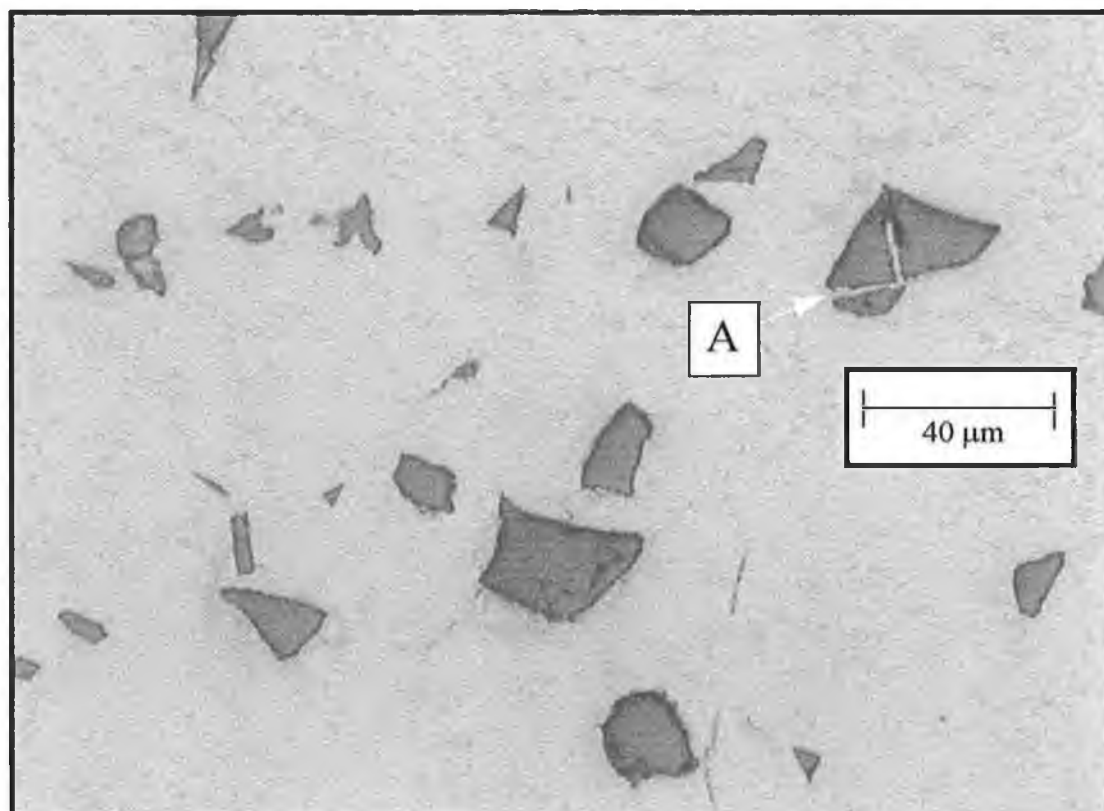


Figure 4.34. Cracked SiC particle infiltration. test matrix no. 3. Mag. x 500.

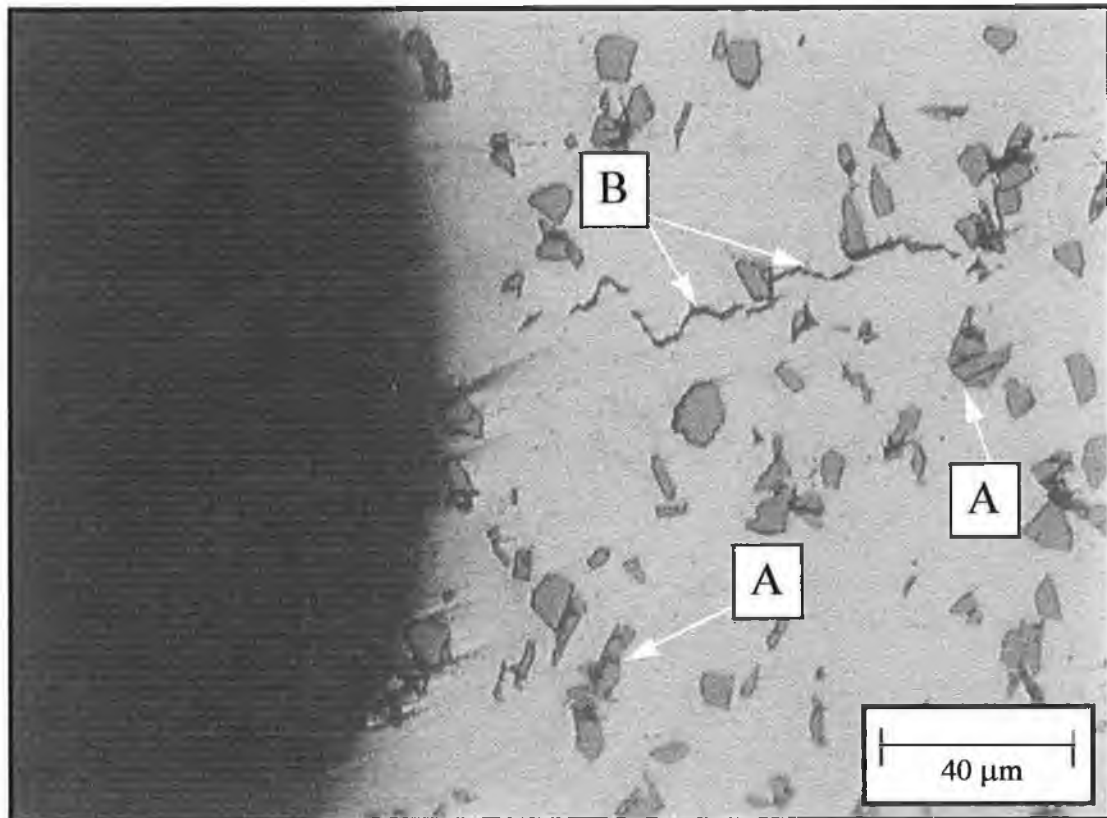


Figure 4.35. Poor infiltration (A) and crack propagation (B). test matrix no. 3.

Mag. x 500.

4.11.8 Fracture Surface Analyses

Test Matrix No. 4

The fracture surface analyses of the tensile samples produced in test matrix no. 4 reveal that the microstructures of the materials vary greatly between batches produced in this test matrix, as illustrated by the micrographs in figure 4.36. The micrograph of the inner region of the sample from batch No. 5 (figure 4.36 (5)) shows that the smaller aluminium powders within this 16 μ m aluminium powder batch which remained undeformed during compaction (d), fail to become structurally incorporated within the material due to insufficient sintering of the surrounding powders. By increasing the SiC content from 10% in figure 4.36 (5) to 15% and 20% in figure 4.36 (4) and figure 4.36 (1) respectively, improved sintering occurred. This improved consolidation corresponds to the high levels of aluminium powder penetration within the green compacts containing larger quantities of SiC.

Figure 4.36 (1a) shows fractured SiC particles on the fracture surface surrounded by matrix material which has fractured through ductile failure (figure 4.36 (1b)). In contrast to figure 4.36 (1), figure 4.36 (6) displays a SiC-free fracture surface. Therefore, in both batch No. 1 and No. 6 the aluminium and SiC have formed an adequate bond to prevent interfacial decohesion. However, the large SiC particles of batch No. 1 are more susceptible to fracture than the small particles of batch No. 6. Also, as shown in figure 4.36 (3) and figure 4.36 (7) many areas within these materials were poorly sintered.

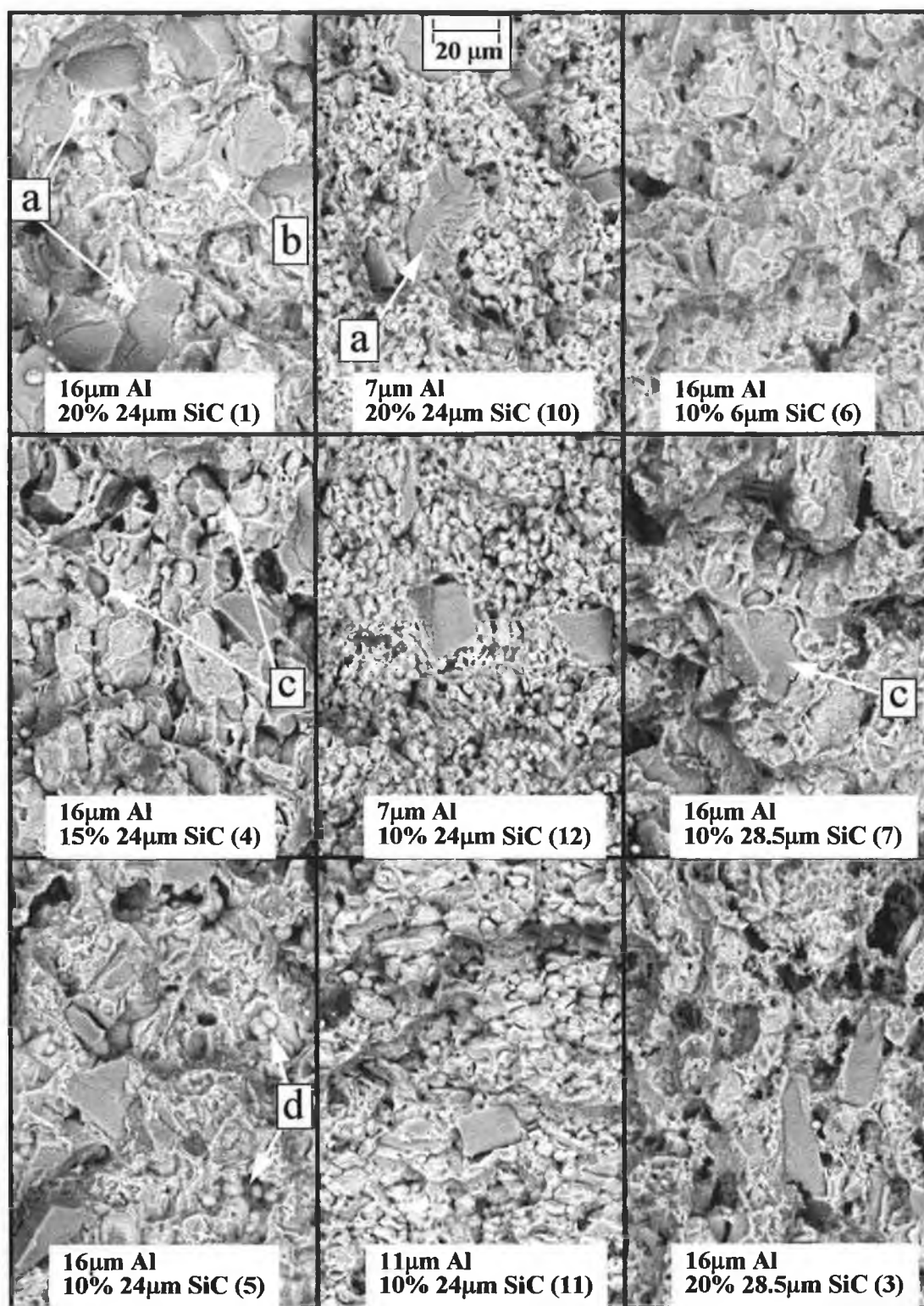


Figure 4.36. Fracture surface morphologies of tensile samples. (a) Fractured SiC particle, (b) Ductile failure of matrix, (c) Poorly sintered areas, (d) Unsintered small powders. Parentetical numbering refers to the batch from which each sample was produced. See appendix D for batch details.

The effect of aluminium powder size on the material microstructure is highlighted by the morphological variation between (10), (11) and (12) in figure 4.36, and the samples consisting of 16 μ m aluminium powder ((1), (3)-(7)). The fine networks of sintered aluminium powders provided adequate strength to achieve a UTS of 324 MPa in the case of the sample displayed in figure 4.36 (10). SiC particle fracture was frequently observed on the fracture surfaces of all the samples consisting of these smaller aluminium powders. This indicates that good interfacial bonding is achieved during sintering. It was also observed that these materials exhibit considerable levels of porosity compared to that of the materials produced using the larger aluminium powders. However, although the samples produced using the 16 μ m aluminium powders generally exhibited less porosity, the tensile properties recorded for the materials produced using the smaller powders were superior in all cases.

4.12 SUMMARY

The results and observations presented highlight the primary material selection and processing factors which affect the cold uniaxial pressing and sintering production of particle reinforced aluminium matrix composites. These factors include the absolute size of both the reinforcement particles and aluminium powders and the ratio between these sizes, the mixing method used, the powder heat treatment carried out, the lubricant type and quantity and the sintering atmosphere, temperature and time. This systematic experimental work also demonstrates that with the correct selection of raw materials and processing parameters this near conventional powder metallurgical pressing and sintering route can be used to produce well formed net shape composite components which exhibit a homogeneous distribution of reinforcement, low porosity and reasonable material properties.

CHAPTER 5 MODELLING WORK

The present modelling work is described in this chapter. This work consists of the development and use of a new micromechanical model for use in the theoretical investigation of discontinuously reinforced composite materials which exhibit a random distribution of randomly oriented reinforcement particles. The primary objectives of this work are to design a model which allows for the isolation of various important parameters including reinforcement particle volume fraction, size, distribution and orientation and can predict the elastic/plastic response of a real composite.

This chapter consists of an overview of the modelling design considerations based on the literature discussed in section 2.6, a full description of the present geometric model and a presentation of both the modelling analyses carried out and the results of these analyses. The results of these analyses and both the capabilities and limitations of the present model are discussed separately in chapter 6.

5.1 MODEL DESIGN CONSIDERATIONS

Industrial interest in the use of discontinuously reinforced metal matrix composites (DRMMCs) continues to grow due to the attractive properties exhibited by these materials [19,35,37,43,45,82,89,99,101,103,215]. However, this growth has been restricted by factors such as the low ductility and low fracture toughness normally exhibited by these composites. A greater understanding of the micromechanics governing the composite material properties is required in order to overcome these undesirable characteristics and further expand the application range of DRMMCs.

A wide range of variables have been recognised through both experimental and modelling research as factors which may affect the final properties of DRMMCs. These factors include the properties and quantities of the constituent materials, the reinforcement particle size, geometry, orientation and distribution, the thermal coefficient mismatch between the constituent materials and the composite processing history [2,14,76,205,206,216]. Also, the main strengthening mechanisms associated with DRMMCs are based on the load transfer from the matrix to the reinforcement, the increased dislocation and precipitate density throughout the matrix material, the constrained plastic flow of the ductile matrix and the residual stresses due to the thermal contraction mismatch occurring during thermal processing [63,198]. Due to the complexity of these materials it is extremely difficult to isolate individual parameters experimentally. In an attempt to quantify the effects of individual parameters considerable research has focused on the development of models of composite behaviour.

Due to the inherent restriction of analytical models to analytically tractable geometric forms (discussed in section 2.6.3) and material linearities [14,216], many recent DRMMC modelling studies have turned to numerical methods of modelling to accommodate geometric complexities and material non-linearities. The majority of these numerical models employ finite element method (FEM) procedures [217,218] to spatially discretise a unit cell model into numerically manageable elements.

The development of this unit cell normally relies on the assumption that the composite material can be described as a matrix material containing a regular and perfectly periodic array of identical particles [195]. Subsequently, it is generally assumed that this composite model can be divided into an array of regular hexagonal cylinders, each containing one reinforcement particle. This allows the entire composite to be described by a single hexagonal cylinder. To reduce the complexity further this hexagonal cylinder can be approximated by a circular cylinder in order to allow axisymmetry and plane symmetry to apply. The product of these assumptions and approximations is an over simplified model of a highly complex material. Importantly, regarding the isolation of crucially important parameters such as reinforcement

particle distribution, reinforcement orientation, reinforcement size distribution and particle shape this unit cell modelling approach has very limited capabilities.

Real DRMMCs do not consist of regular arrays of aligned uniform reinforcement particles. The present modelling work involves the development and use of a new continuum mechanics based quantitative numerical model capable of predicting the elastic/plastic response of a composite system containing a random distribution of randomly oriented elastic discontinuous particles surrounded by a ductile matrix. This plane stress model facilitates the isolation of variables such as volume fraction and particle size, and allows for the varying of particle orientation and distribution. The modelling analyses carried out in the present study involve a thermal strain loading simulation followed by a uniaxial stress loading step on models containing 20 μ m particles in volume fractions of 5%, 10%, 15% and 20% reinforcement. A model containing 10 μ m particles in a volume fraction of 5% was also investigated under the same loading conditions. In both cases the particle size dimension refers to the across corners hexagonal dimension. The properties attributed to the matrix and reinforcement materials are those of a powder metallurgical aluminium alloy AA6061 (T6) and SiC particles respectively.

5.2 GEOMETRIC MODEL

In the present work the microstructural geometry of a DRMMC is represented by the three dimensional (3D) model shown in figure 5.1. The model consists of a cubic solid containing a variable volume fraction of reinforcement particles. These reinforcement particles are short regular hexagonal cylinders or plates. The cylindrical axis of each plate is parallel with the z-axis as shown, and both the position and the radial orientation of these plates are random throughout the cubic solid. Furthermore, these particles do not overlap one another or protrude the boundary surface of the model. These two conditions ensure consistency of particle size and allow for tractable boundary conditions (BCs) in the numerical model.

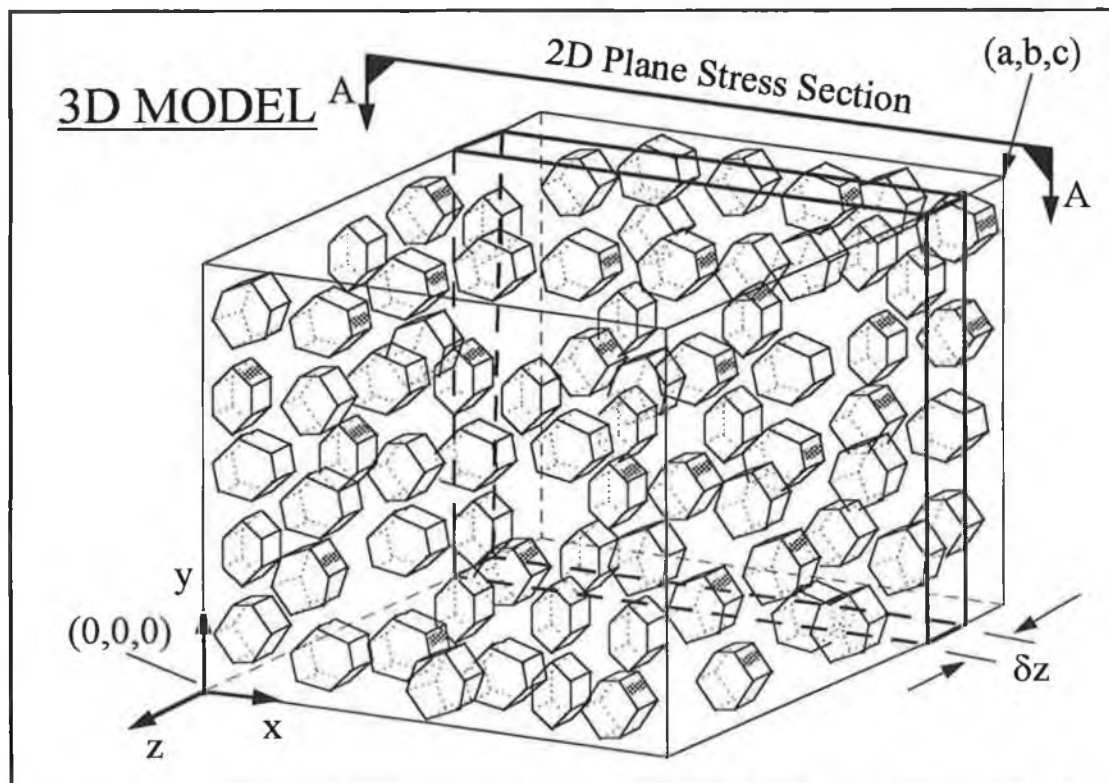


Figure 5.1. Micromechanical representative 3D model of DRMMCs developed in the present modelling work.

In order to reduce the complexity of this model a plane stress approximation was made. It should be noted that for this approximation to be considered reasonable every possible plane stress section (A-A) through the three dimensional model must

exhibit a constant area fraction of particles. In addition, this area fraction must be equivalent to the volume fraction of particles within the entire model, that is,

$$A_{P_i} = K \quad \text{for} \quad 0 \leq i \leq c \quad (32)$$

and,

$$\int_{0 \rightarrow c} A_{P_i} a b \delta z = A_{P_i} a b c \quad \text{therefore,} \quad A_{P_i} = V_P \quad (33)$$

where A_{P_i} is the area fraction of hexagonal particles at any incremental position i along the z axis, K is a constant, V_P is the volume fraction of plates within the entire 3D model and a , b and c are the outer dimensions of this 3D model as shown in figure 5.1.

As a consequence of the two dimensional approximation made the model is restricted to the prediction of the response of composite component shapes which conform to the conditions of plane stress. The derived two dimensional composite model and the boundary conditions applied during the load of the model are shown in figure 5.2. The random distribution of the hexagonal areas in the two dimensional model was achieved by the superimposition of a 200 x 200 point uniform grid on the model. Each point on this grid represents a possible centre position for the hexagonal areas. To avoid both excessive stress concentration at the edges of the model during loading and model inconsistency, a region 20 points in width was excluded from the perimeter of the grid. The remaining 160 x 160 point grid had 25,600 possible centre positions, each of which was then numbered sequentially. In the present work the selection of centre positions was based on the use of random digits, and was performed manually [219]. The number of centre positions selected depended on the particle volume fraction and the average particle size to be represented. In the case of the 20 μ m particle models the inclusion of 15 hexagonal areas represented a volume fraction of five per cent reinforcement. However, the 10 μ m particle model required 60 hexagons to represent the same volume fraction. The resulting models had side lengths of 279.2 μ m as shown in figure 5.2.

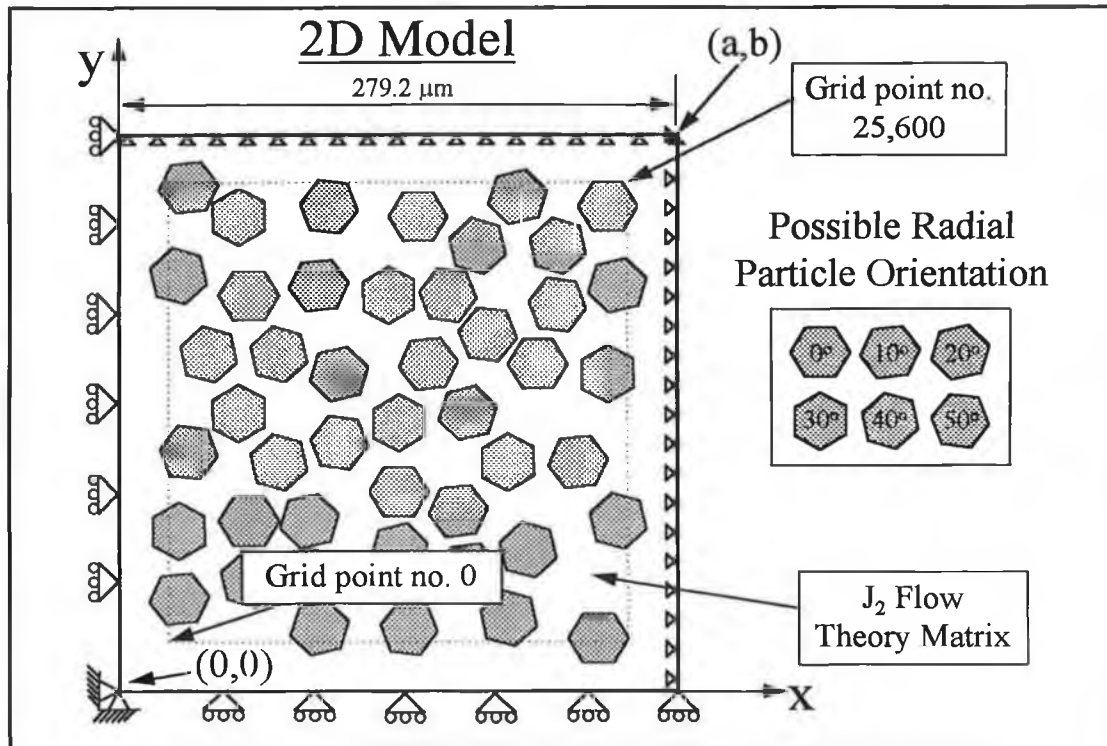


Figure 5.2. Plane stress geometrical model derived from the 3D model (figure 5.1) and the boundary conditions applied to the model during loading.

In order to conform with the model description given above, no area overlap was permitted during the selection of particle centre position. Also, the predetermined composite volume fraction under analysis was represented by the equivalent area fraction of hexagons. The orientation of these areas was also determined manually using random digits [219]. Six possible radial orientations (0° , 10° , 20° , 30° , 40° & 50°) are considered in the present model, as shown in figure 5.2. The size of the hexagonal areas used in each model depended on the particle size to be represented and was based on the diametrical corner to corner dimension of the hexagons.

5.3 MODELLING ANALYSIS INPUT

The numerical analyses were performed using the finite element package ANSYS® 5.3. (University). The element type selected for all models was a plane stress triangular element with midside nodes (ANSYS element code, Plane 2) [218]. Meshing of each model was carried out using the automatic meshing and the smart-size (basic 2) facilities [218] in order to avoid the generation of poorly shaped elements. Table 5.1 lists the number of elements generated for each model.

Table 5.1. Number of elements generated with the use of the automatic meshing and the smart size (basic 2) facilities for each model.

	Model Description				
	5%SiC 20µm	10%SiC 20µm	15%SiC 20µm	20%SiC 20µm	5%SiC 10µm
No. of Elements	1776	3200	5038	7590	5768

To achieve quantitative analyses and geometric consistency it was necessary to maintain consistency of dimensional and loading quantities and also to control the deformation of the model during loading. The boundary conditions applied to the models to avoid inconsistencies were,

$$\frac{du_x}{dt} = 0 \quad \text{on} \quad x = 0 \quad (34)$$

$$\frac{du_y}{dt} = 0 \quad \text{on} \quad y = 0 \quad (35)$$

$$u_x = U_x \quad \text{on} \quad x = a \quad (36)$$

$$u_y = U_y \quad \text{on} \quad y = b \quad (37)$$

where u_x represents individual nodal displacements in the x direction, u_y represents individual nodal displacements in the y direction, t represents time, U_x is the overall displacement at the boundary $x = a$ and U_y is the overall displacement at the boundary

$y = b$. These conditions ensure that the perimeter of the model remains in the form of a right rectangle during loading. This is equivalent to the three dimensional model remaining in the shape of a right parallelepiped during loading and therefore implies geometric consistency for this model. The geometry and boundary conditions of the five models analysed in the present work can be seen in figures 5.3, 5.4, 5.5, 5.6 and 5.7. The first four models contain $20\mu\text{m}$ hexagonal areas in 5%, 10%, 15% and 20% respectively and are used to investigate the effect of reinforcement volume fraction. The last model (figure 5.7) contains 5% $10\mu\text{m}$ hexagonal areas for comparison with the 5% $20\mu\text{m}$ model to investigate the effect of particle size.

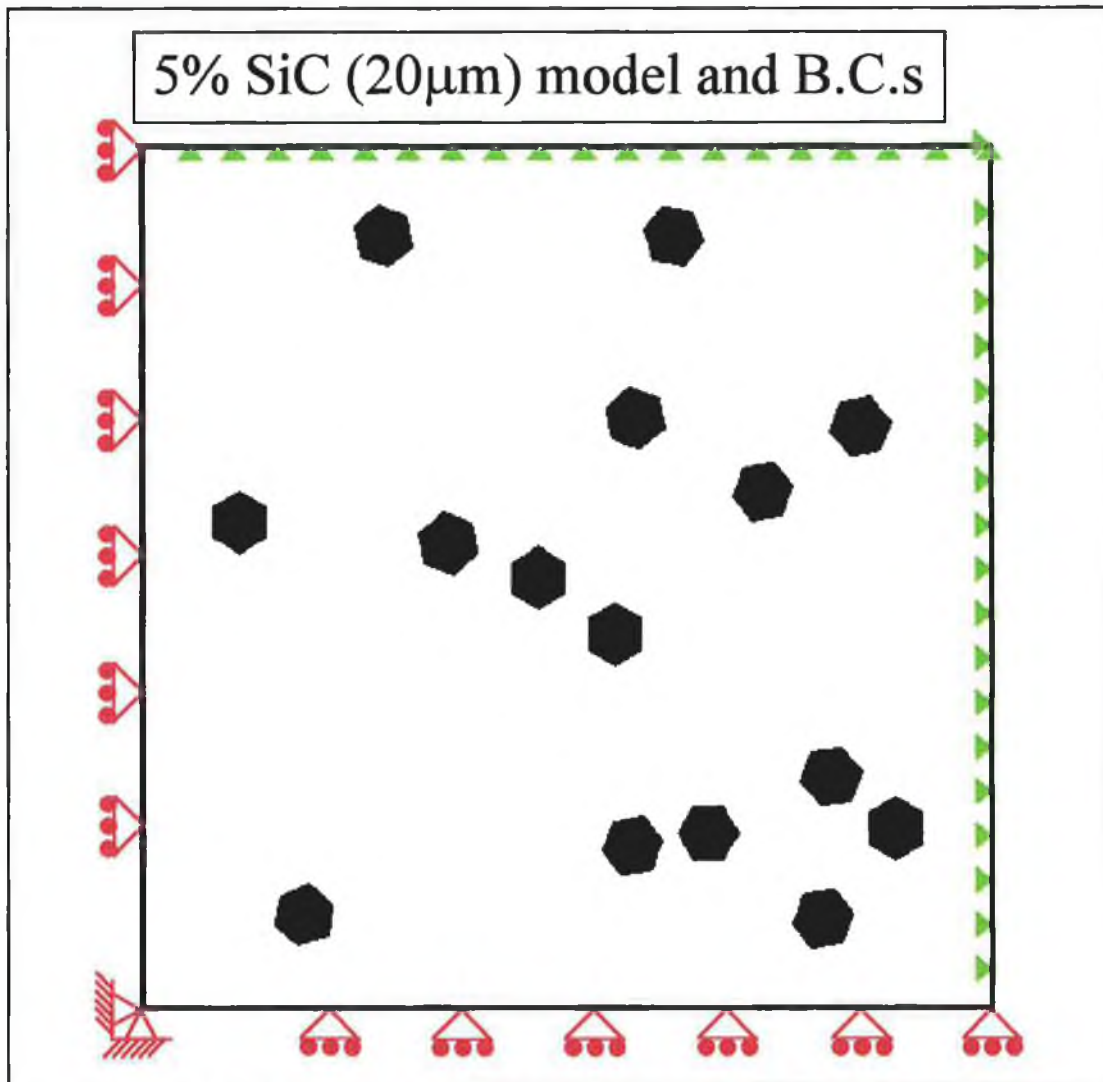


Figure 5.3. Geometric model of DRMMC containing 5% SiC ($20\mu\text{m}$) and the boundary conditions applied for the present analyses.

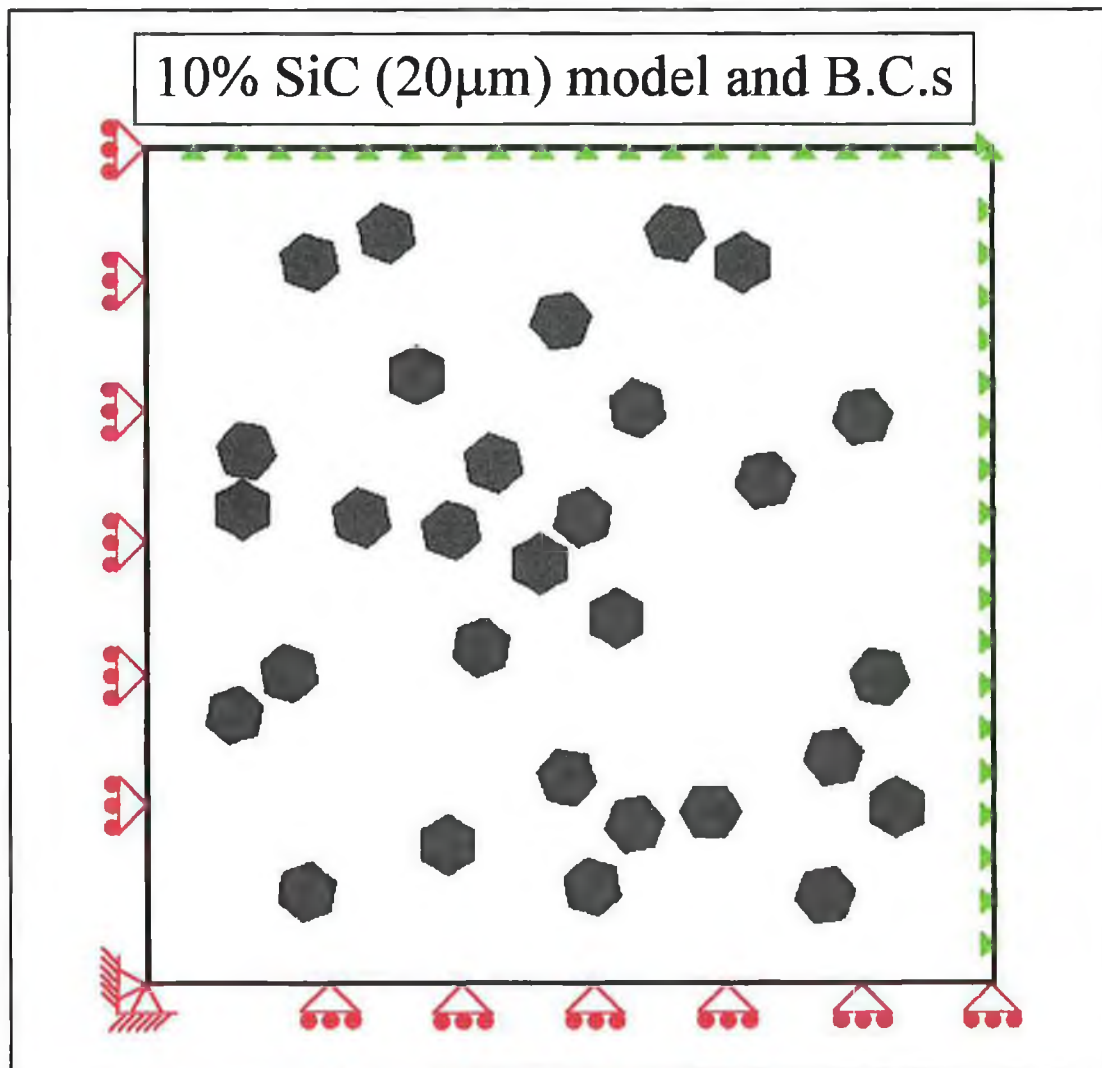


Figure 5.4. Geometric model of DRMMC containing 10% SiC (20 μ m) and the boundary conditions applied for the present analyses.

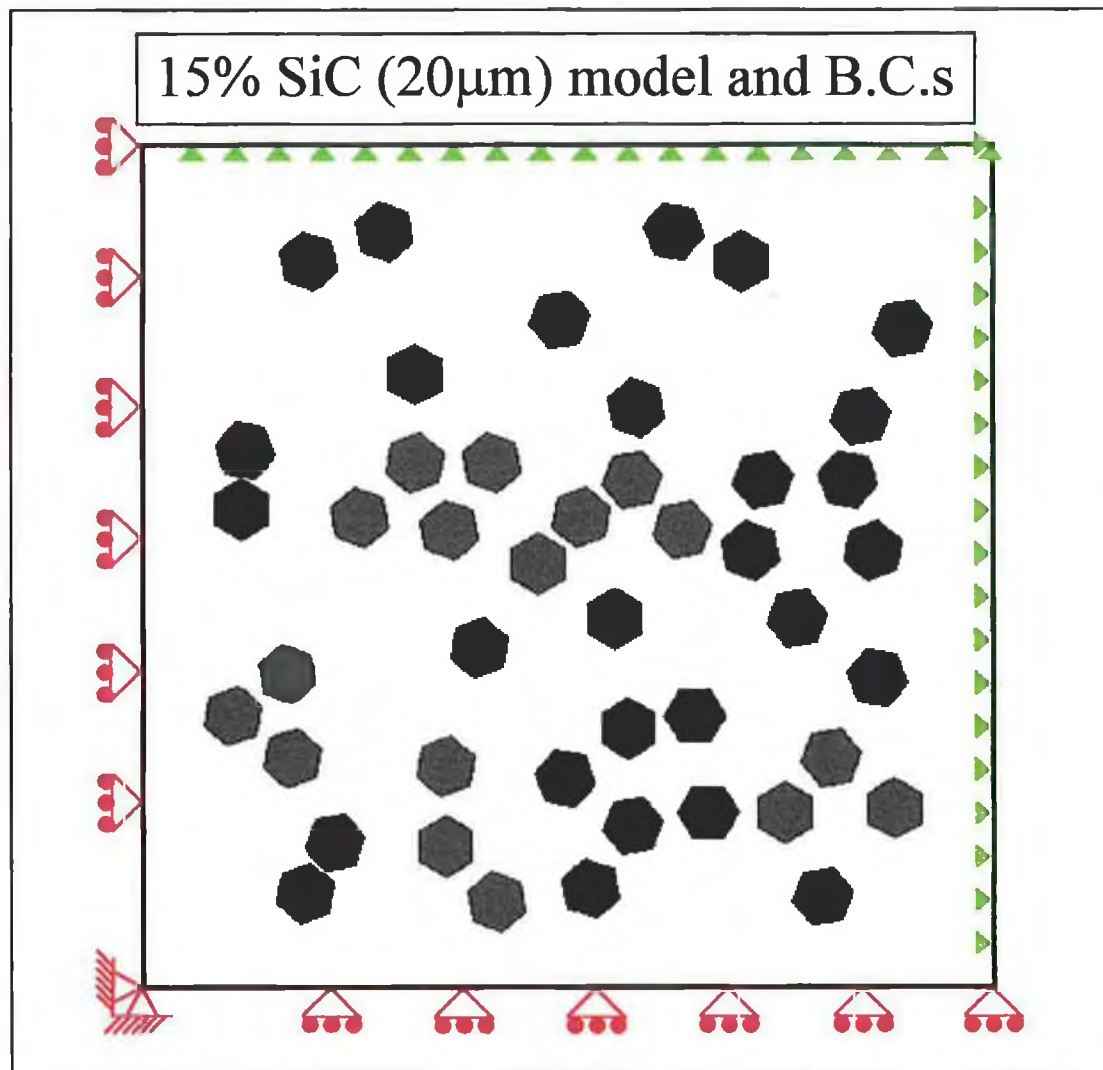


Figure 5.5. Geometric model of DRMMC containing 15% SiC (20 μ m) and the boundary conditions applied for the present analyses.

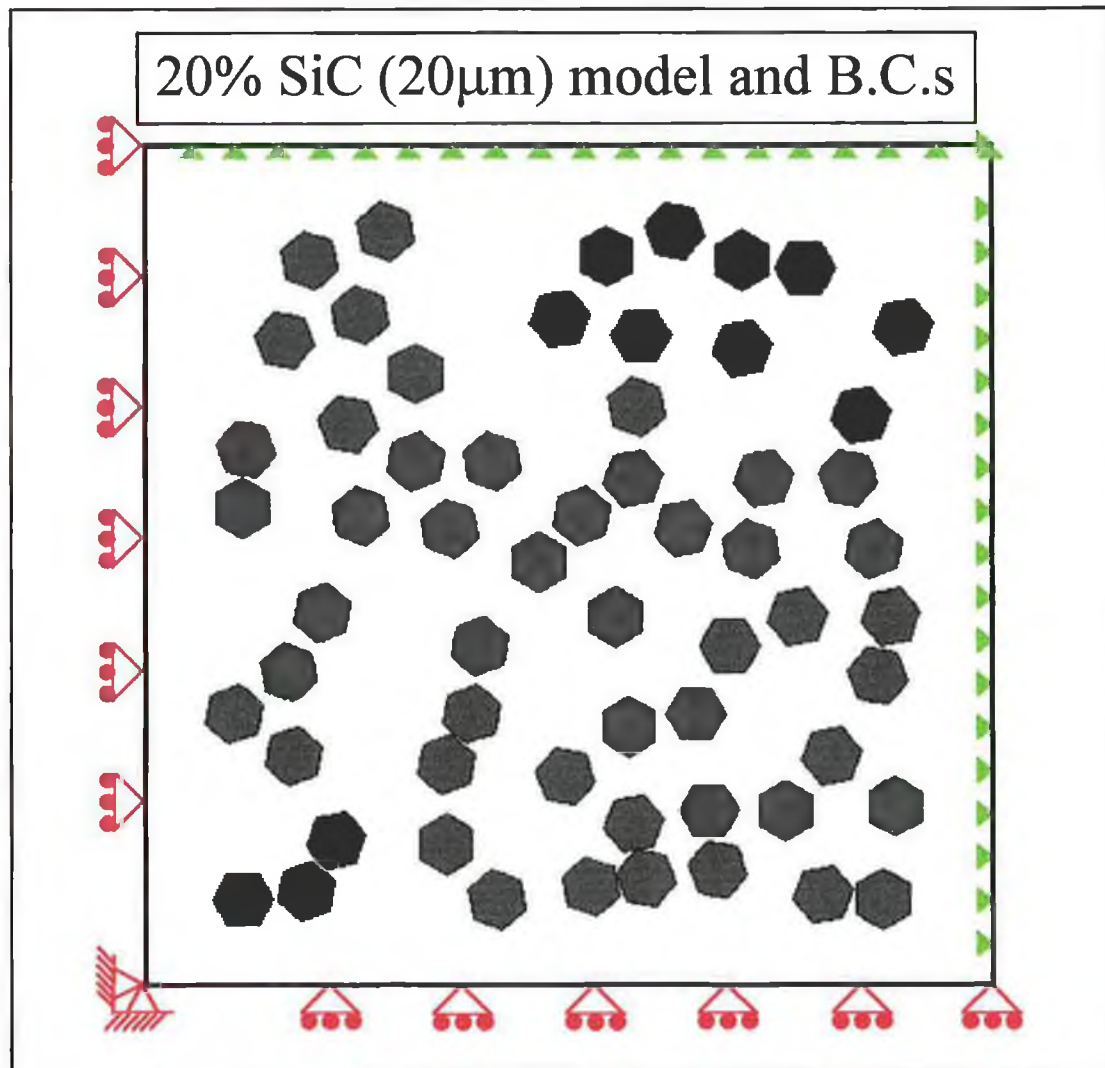


Figure 5.6. Geometric model of DRMMC containing 20% SiC (20 μ m) and the boundary conditions applied for the present analyses. Note: No particle contact occurs in this model.

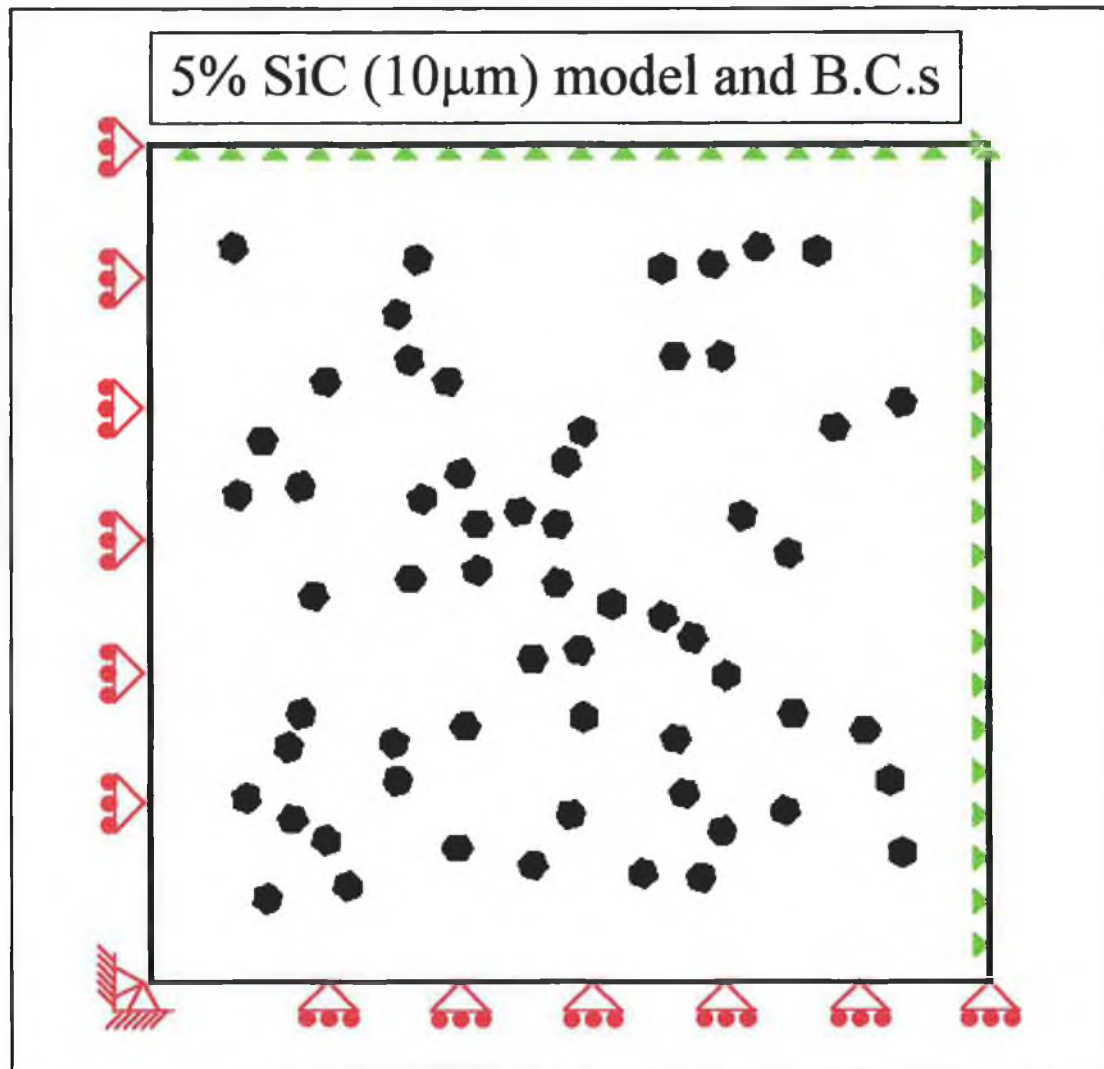


Figure 5.7. Geometric model of DRMMC containing 5% SiC (10 μ m) and the boundary conditions applied for the present analyses.

A geometric model containing 10% 10 μ m hexagonal areas was also designed and constructed. However, meshing of this model was not possible due to the nodal limitations of the finite element analysis software used and was therefore abandoned.

In all of the analyses carried out the matrix material was defined as an elastic/isotropically hardening rate independent plastic solid, and the hexagonal plates were considered to be purely elastic. The uniaxial tensile (constitutive) response of the aluminium alloy AA6061 (T6) produced using a powder metallurgical route [103,167,220] was used to describe the model matrix material, and the material data for SiC particles [14] was used to describe the model reinforcement. The matrix material tensile data was defined by Hooke's law (equations 38) up to the point of yield and by the power law relationship defined in equation 39 [220] beyond yield,

$$\sigma = E\varepsilon \quad \text{for} \quad \varepsilon \leq \varepsilon_0 \quad (38)$$

$$\sigma = \sigma_0[\varepsilon^p/\varepsilon_0 + 1]^N \quad \text{for} \quad \varepsilon \geq \varepsilon_0 \quad (39)$$

where σ is the true stress, E is the modulus of elasticity, ε is the true strain, σ_0 and ε_0 are the yield stress and true strain at yield respectively, ε^p is the true plastic strain and N is the reciprocal of the strain hardening exponent. The material properties used for the aluminium matrix and the SiC reinforcement are,

$$\begin{aligned} \text{AA6061 Data: } E &= 72.3 \text{ GPa}, \sigma_0 = 330 \text{ MPa}, N = 0.1, \\ v &= 0.3, \varepsilon^f = 0.101, \alpha = 23.6 \times 10^{-6}/^\circ\text{C} [103,167,220]. \end{aligned}$$

$$\text{SiC Data: } E = 450 \text{ GPa}, v = 0.17, \alpha = 4.0 \times 10^{-6}/^\circ\text{C} [14].$$

where v is the Poisson's ratio, ε^f is the total strain at fracture and α is the coefficient of thermal expansion. The non-linear tensile characteristic curve of the matrix material produced with the use of equations 38 and 39 was included in the model using the multi-linear isotropic function available within ANSYS® 5.3 (University). The material properties were kept constant during the thermal strain loading simulation step. Also, it was assumed that a perfect bond existed between the SiC and the aluminium alloy and that no reinforcement particle fracture existed before loading or occurred during the analyses.

The initial loading imposed on the models consisted of a thermal strain, equivalent to a sudden drop in temperature from 170°C to 24°C. The thermal contraction load step was incorporated in the analyses to simulate the internal stress condition within the composite material due to the thermal processes which are normally carried out during DRMMC processing. Due to the small extent of the inelastic deformation which occurred within the model during this load step it was not necessary to divide the temperature drop loading step into incremental substeps.

The thermal loading step was followed by a uniaxial tensile stress step. This stress was applied to either the surface at $y = b + u_{yt}$ or to the surface $x = a + u_{xt}$. u_{yt} is the linear translation due to the thermal load step of the nodes originally positioned at $y = b$ and u_{xt} is the linear translation due to the thermal load step of the nodes originally positioned at $x = a$. The solution for the application of stress in both the x and y directions provided tensile response results for two random distributions using just one geometric model. This was carried out to allow comparison between the tensile response of two random distributions of the same area fraction and size of reinforcement. The tensile stress loading step was divided into 20 substeps and the numerical results for each substep was recorded for analysis.

The maximum applied stress for a given model was equal to a uniaxial stress level approximately 1 MPa lower than that which would prevent the numerical solution from converging. This may be interpreted as the stress preceding a level which would cause any matrix material element within the model to experience failure. In the present analyses the true strain at this maximum applied stress is taken to be representative of the true strain at failure for the composite. However, it should be noted that since particle fracture and interfacial debonding mechanisms are not incorporated in the present models, this failure criteria may not predict the composite material failure with great quantitative accuracy.

Details of the standard computational methods used by the software during mesh generation and analysis may be found in reference [218].

5.4 NUMERICAL RESULTS

The objective of the thermal loading step ($170^{\circ}\text{C} \rightarrow 24^{\circ}\text{C}$) is to simulate the thermal strain normally experienced by an AA6061/SiC composite during processing. The von Mises stress maps (nodal values) for the thermal load step for each of the models analysed are shown in figures 5.8 to 5.12. These stress maps show the distribution of the residual stress within each composite model resulting from the thermal contraction.

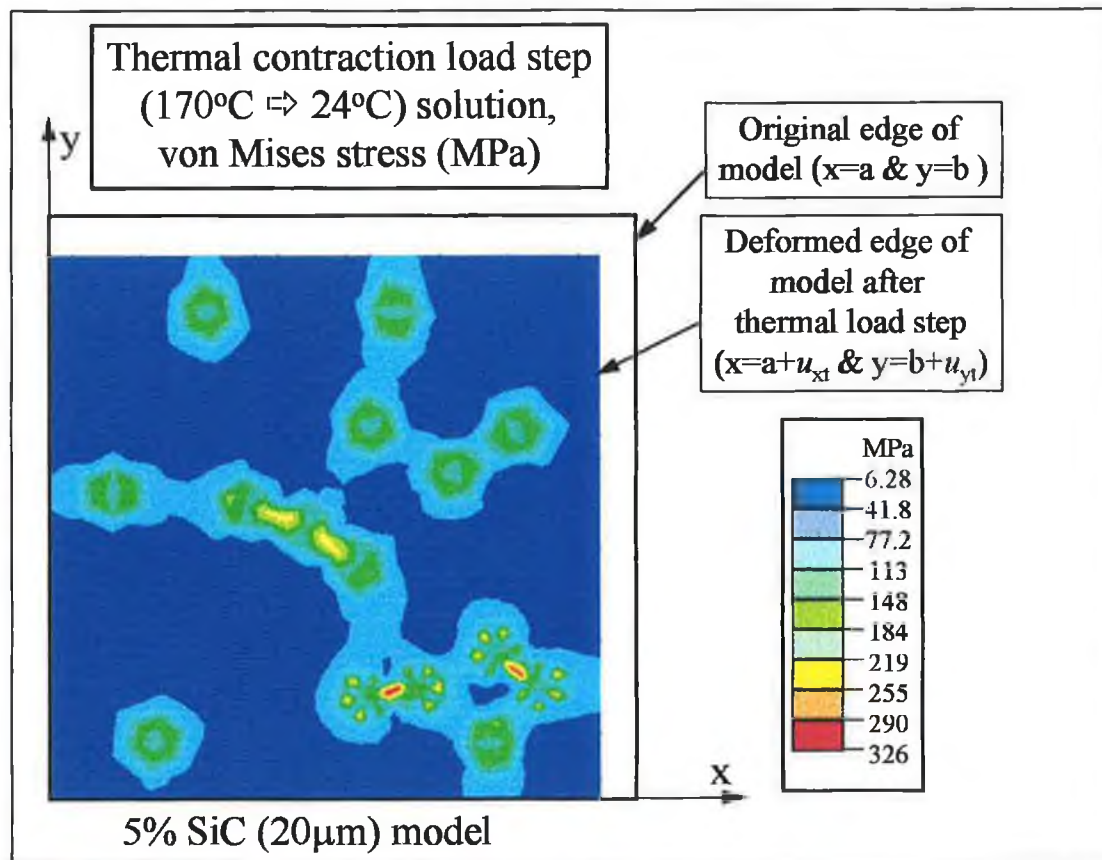


Figure 5.8. Thermal residual stress map solution for 5% SiC ($20\mu\text{m}$) model.

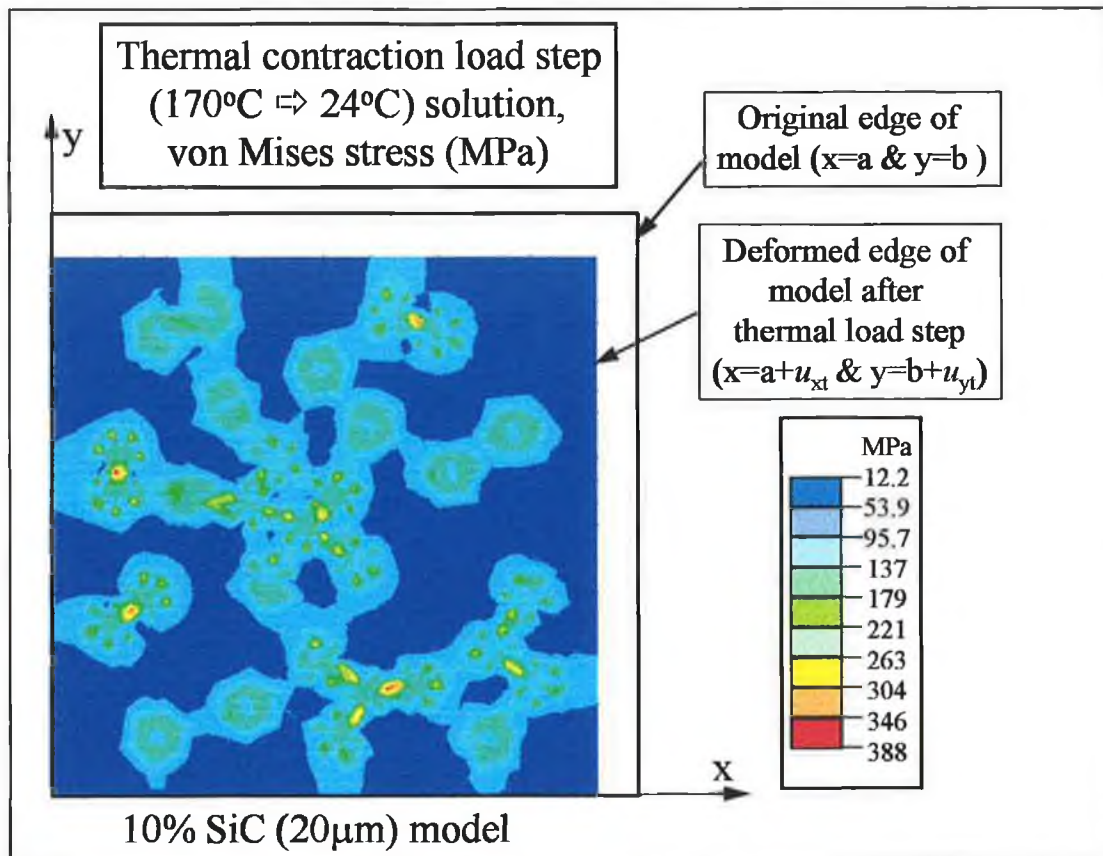


Figure 5.9. Thermal residual stress map solution for 10% SiC (20μm) model.

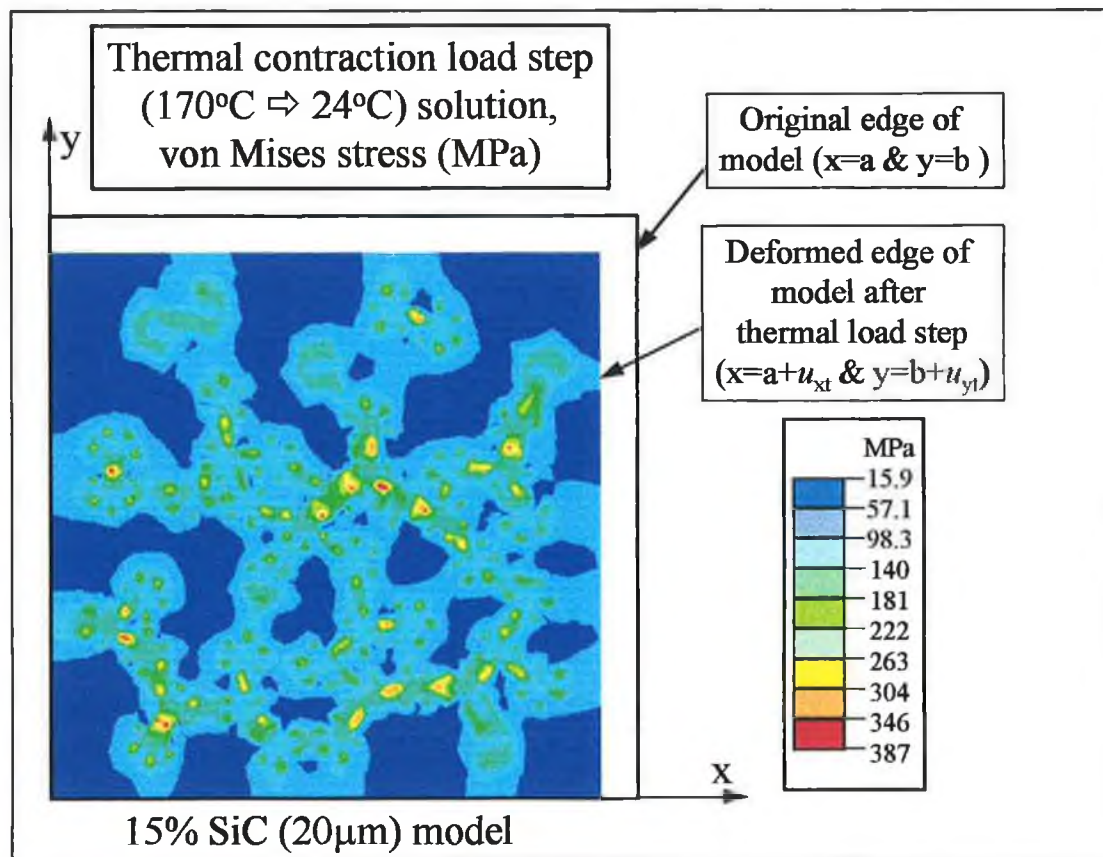


Figure 5.10. Thermal residual stress map solution for 15% SiC (20μm) model.

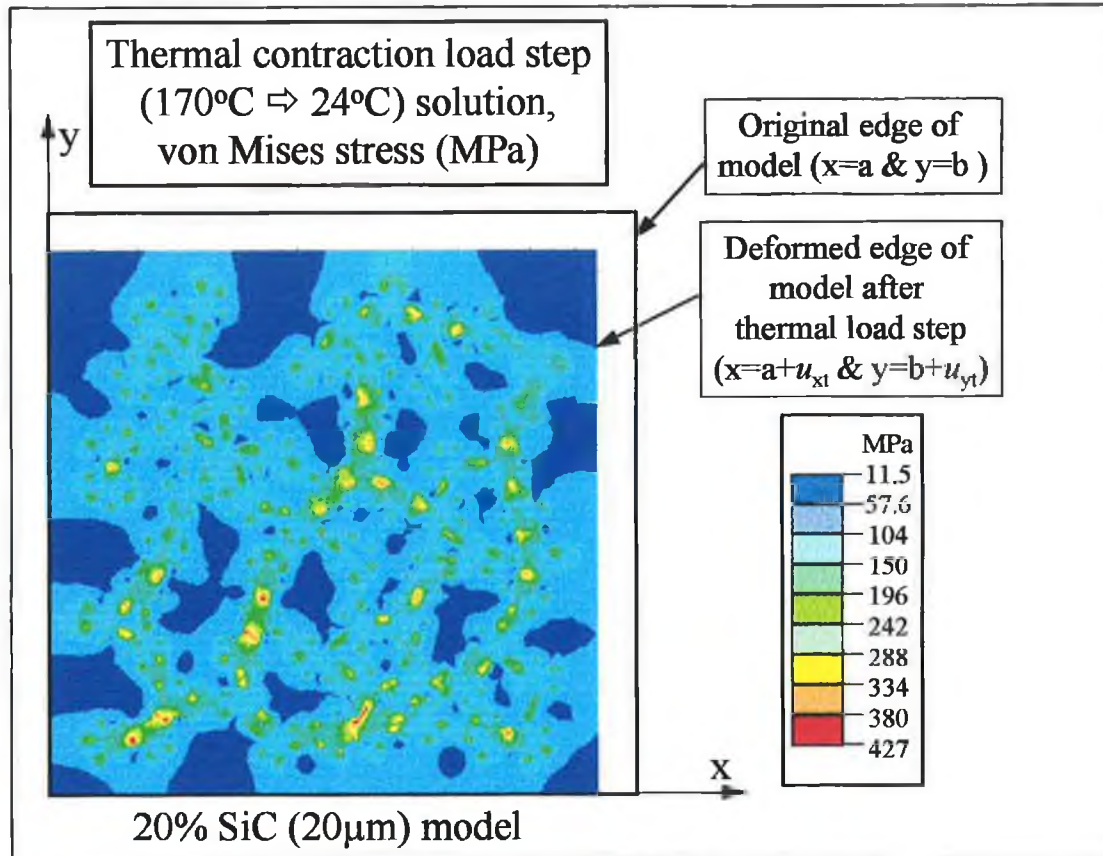


Figure 5.11. Thermal residual stress map solution for 20% SiC (20µm) model.

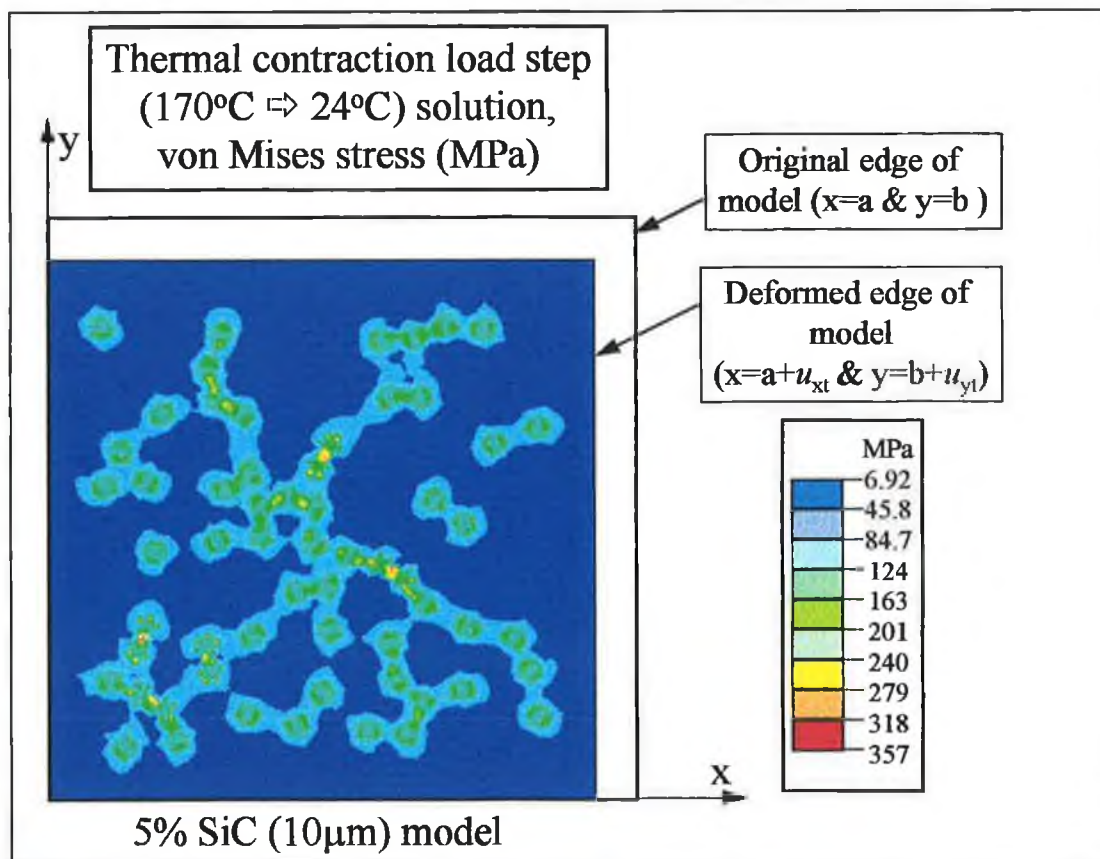


Figure 5.12. Thermal residual stress map solution for 5% SiC (10µm) model.

Analysis of the stress maps shown in figures 5.8 to 5.12 indicates a tendency for high levels of stress to occur at localised regions between closely positioned reinforcement particles. Also, a comparison between the first four stress maps show that the number of highly stressed regions increase with an increase in volume fraction.

A detailed analysis of the individual nodal stress results within the matrix material regions surrounding the particles in the thermally strained models was carried out. This detailed analysis shows that the distribution of stress around isolated particles is uniform compared with the distribution recorded around particles in close proximity to each other. The matrix material surrounding these close particles exhibit high stress in two specific regions, the region between the particles as mentioned above and the also the regions immediately surrounding the corners of the hexagonal areas. The maximum nodal values of von Mises equivalent thermal stress recorded for each model is listed in table 5.2.

Table 5.2. Maximum nodal values of von Mises equivalent thermal stress recorded.

Volume fraction	5%	10%	15%	20%
20 μ m SiC	326MPa	388MPa	387MPa	427MPa
10 μ m SiC	357MPa	-	-	-

Matrix properties: Yield stress = 330MPa, Stress at failure = 450MPa [103,169,220].

The listed values in table 5.2 show that the maximum residual thermal stress tends to increase both as the volume fraction of reinforcement increases and with a drop in reinforcement size. These values also indicate that plastic deformation of matrix material between closely positioned particles is predicted to occur during the temperature drop from 170°C to 24°C for all models with the exception of the 5% 20 μ m SiC model. However, no matrix failure is predicted for this thermal loading.

Following the thermal loading step each thermally strained model was duplicated. The two resulting thermally strained models derived from each original model type provided for tensile analyses to be carried out in both the x and y directions. Each model was then subjected to a load step which consisted of a tensile load applied to either the surface at $y = b + u_{yt}$ in the positive y direction or to the surface at $x = a + u_{xt}$ in the positive x direction. The difference between the results obtained from the y direction analyses and the x direction analyses was found to be negligible. Therefore, only the results obtained from the tensile analyses in the y direction are presented.

In order to achieve reasonable numerical accuracy, obtain a record of the development of the stress condition within the models during loading and provide the results required for the construction of stress/strain flow curves for these models, the tensile load steps were applied iteratively. The results from each iteration (substep) were recorded and analysed. The development of the von Mises stress distribution within each model is shown in figures 5.13 to 5.17. These results were obtained for the substep representing half full tensile load for each model. It must be noted that since both the stress condition prior to tensile loading and the final applied tensile stress differ between models no quantitative comparisons should be made between these nodal results. However, an analysis of these figures show that as the tensile load is applied in the y direction the distribution of stress in the matrix material around the particles alters considerably compared to the thermally strained model. The nodal stress values in the matrix material regions between particles in close proximity in the y direction are generally lower than the values observed for the same regions after thermal loading. Conversely, the regions between particles in close proximity in the x direction exhibit higher stress levels than that recorded after thermal loading. In addition, the stress decreases in regions above and below isolated particles and increases on both the right and left sides of these particles. These trends occur in all five models.

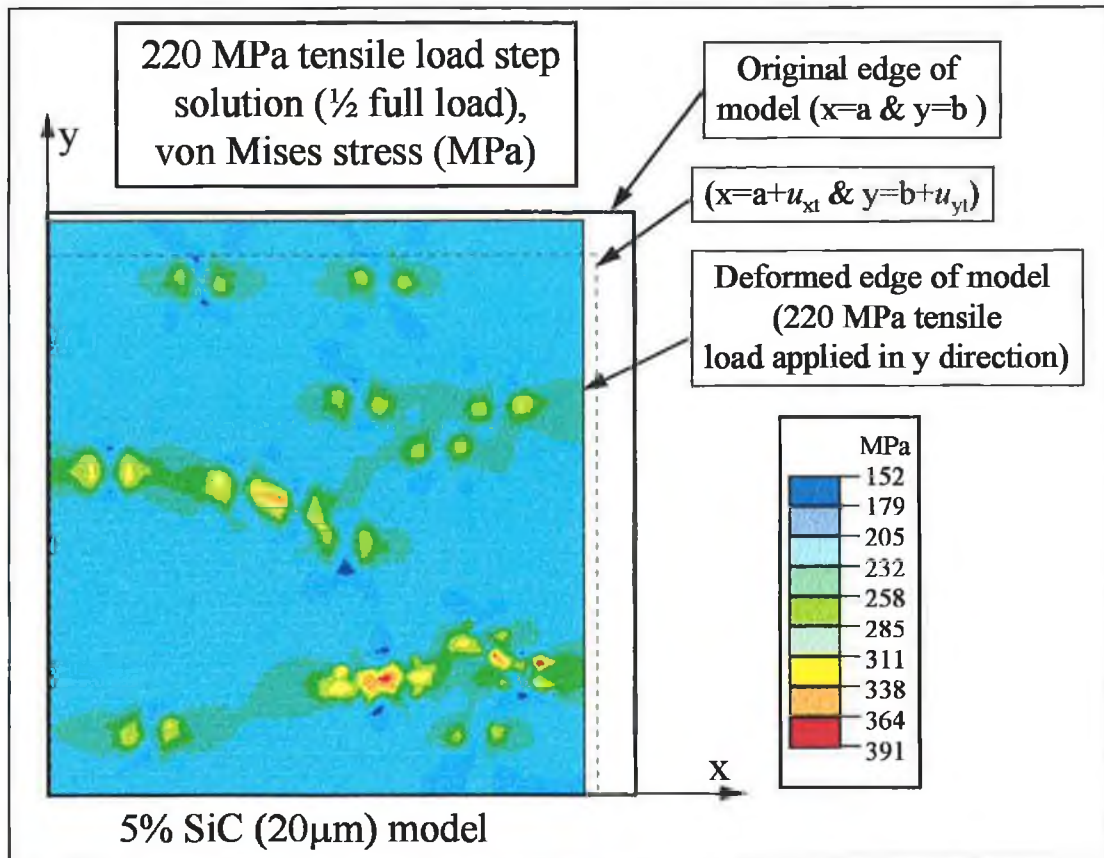


Figure 5.13. Stress map solution for 5% SiC (20 μ m) model at half full load.

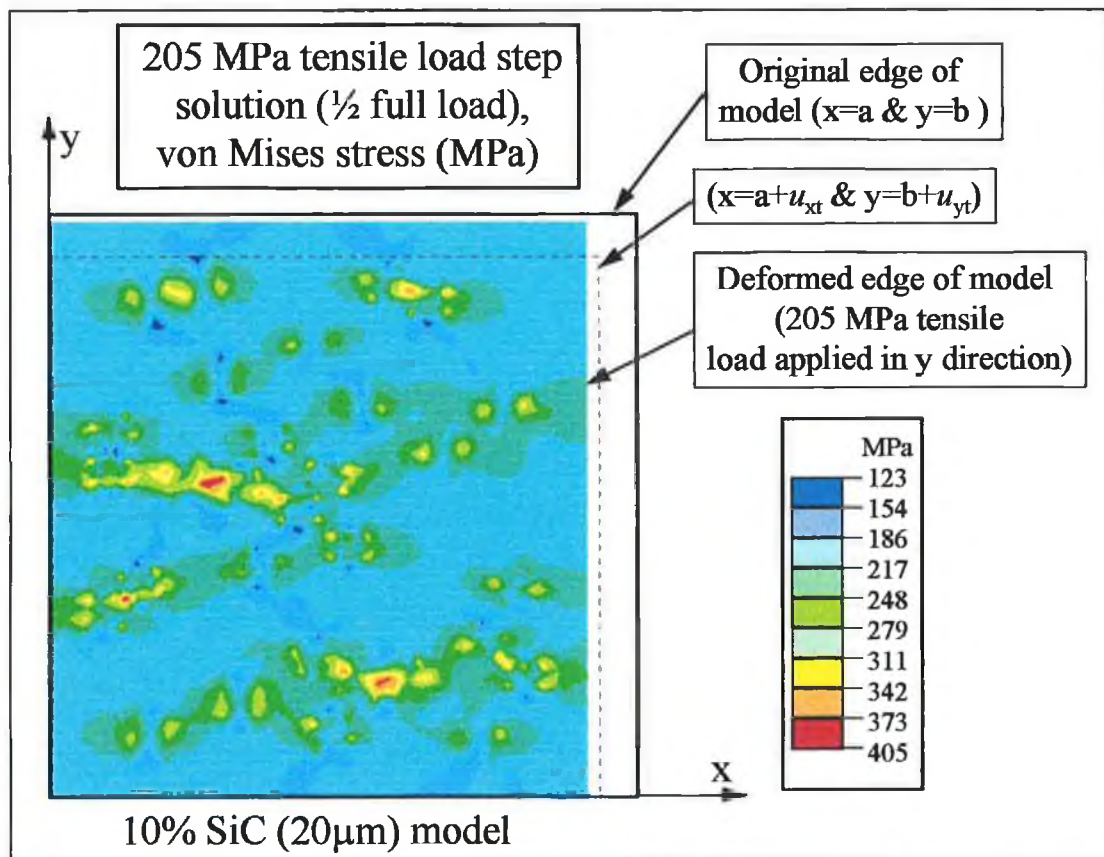


Figure 5.14. Stress map solution for 10% SiC (20 μ m) model at half full load.

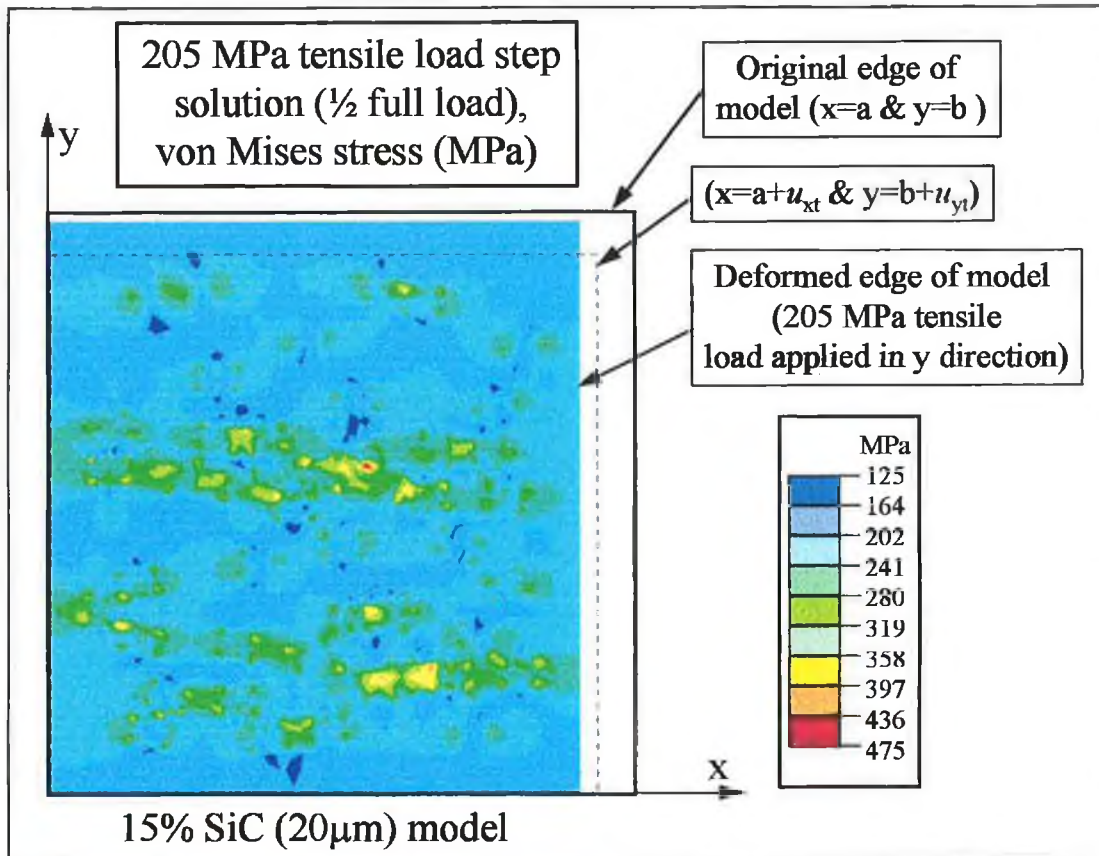


Figure 5.15. Stress map solution for 15% SiC (20 μ m) model at half full load.

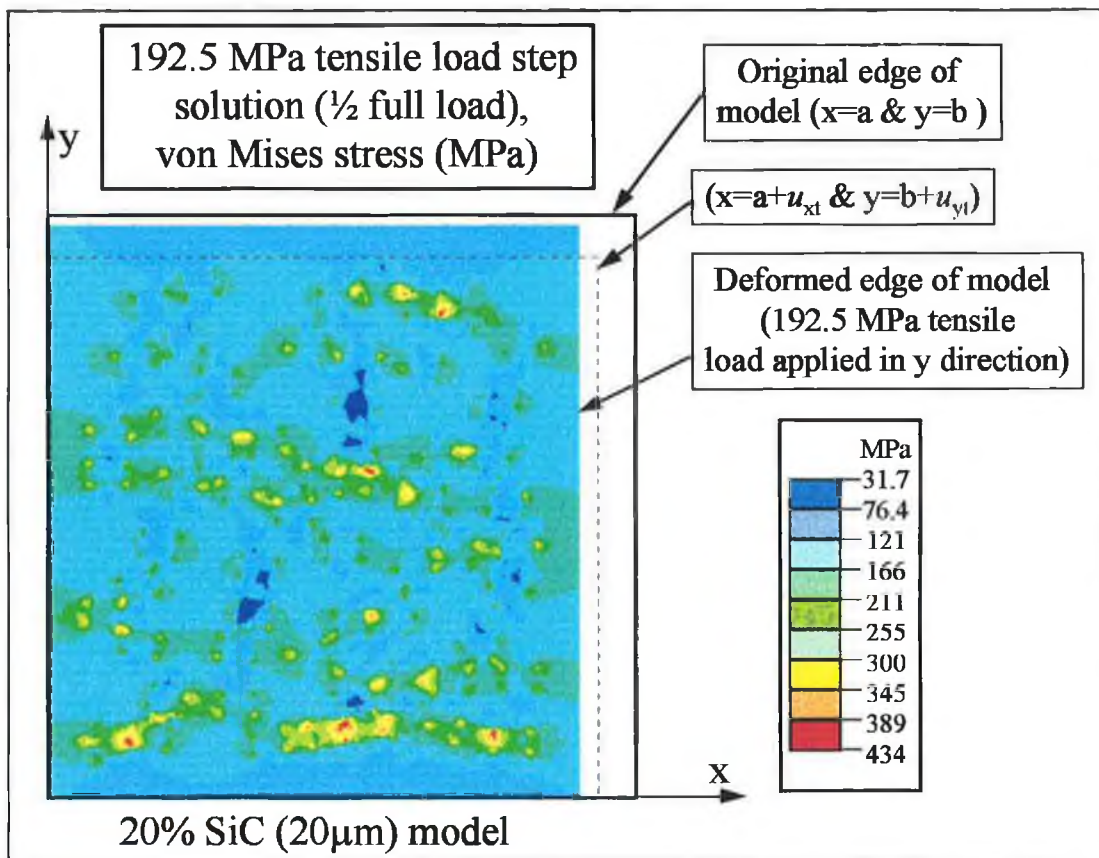


Figure 5.16. Stress map solution for 20% SiC (20 μ m) model at half full load.

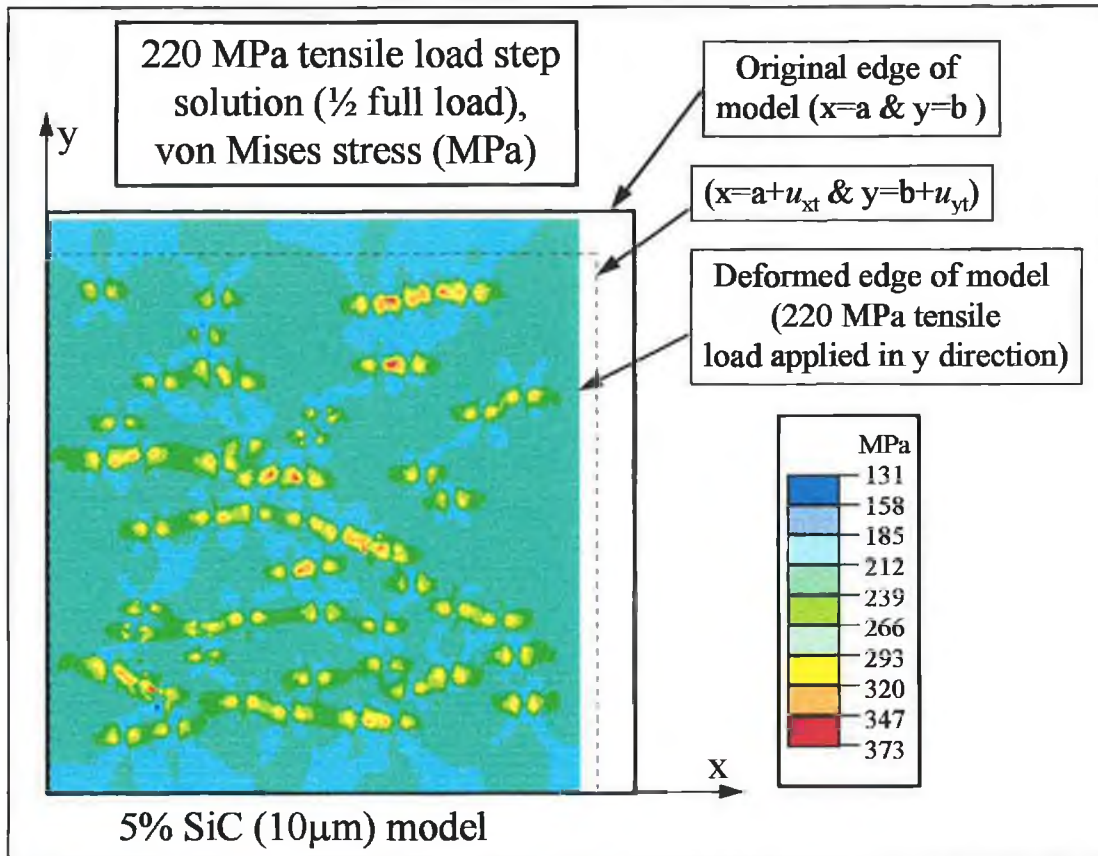


Figure 5.17. Stress map solution for 5% SiC ($10\mu\text{m}$) model at half full load.

The results obtained for each model at the final substep representing full tensile load are shown in von Mises stress map form in figures 5.18 to 5.22. These stress maps show the effect of the full tensile load on the thermally stressed model stress distribution within each composite model. Again, it must be noted that since both the stress condition prior to tensile loading and the final applied tensile stress differ between models no quantitative comparisons should be made between these nodal results. It can be seen from these figures that the trends previously described in relation to the stress development at half full load also apply at full load. The maximum stress is observed in matrix material regions between particle in close proximity in the x direction.

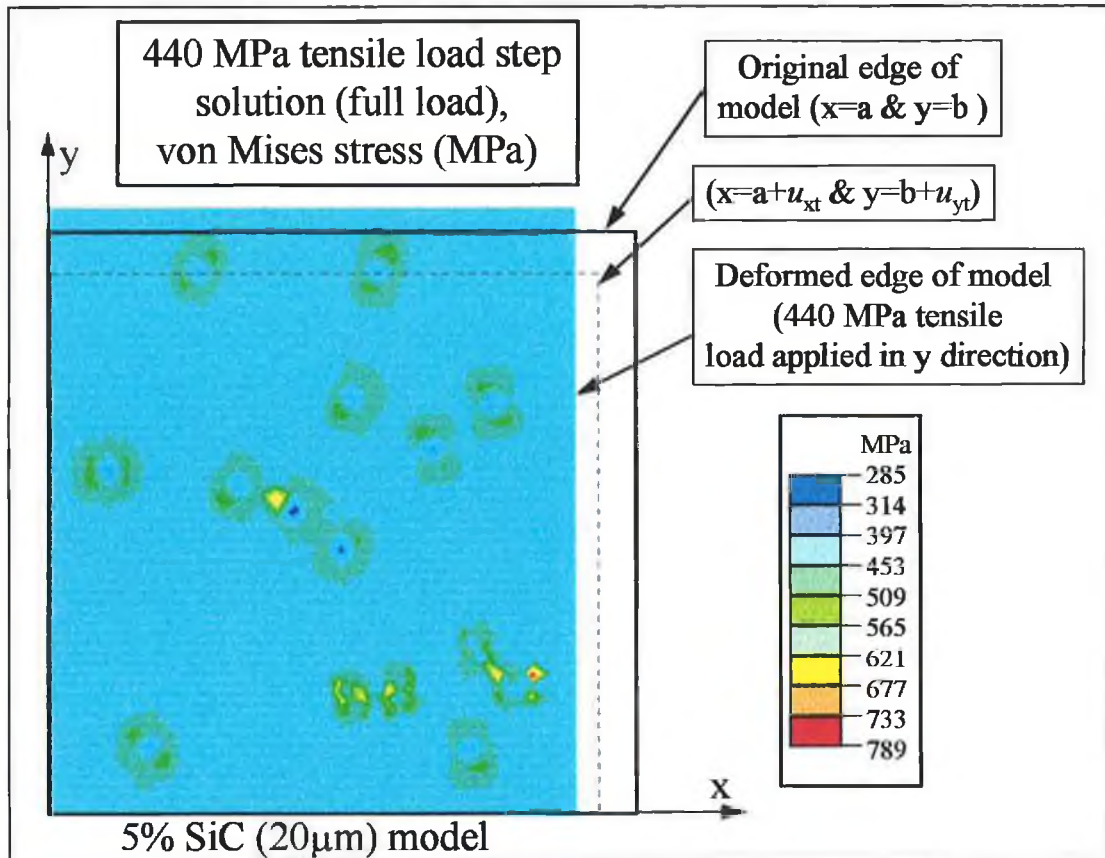


Figure 5.18. Stress map solution for 5% SiC (20 μ m) model at full load.

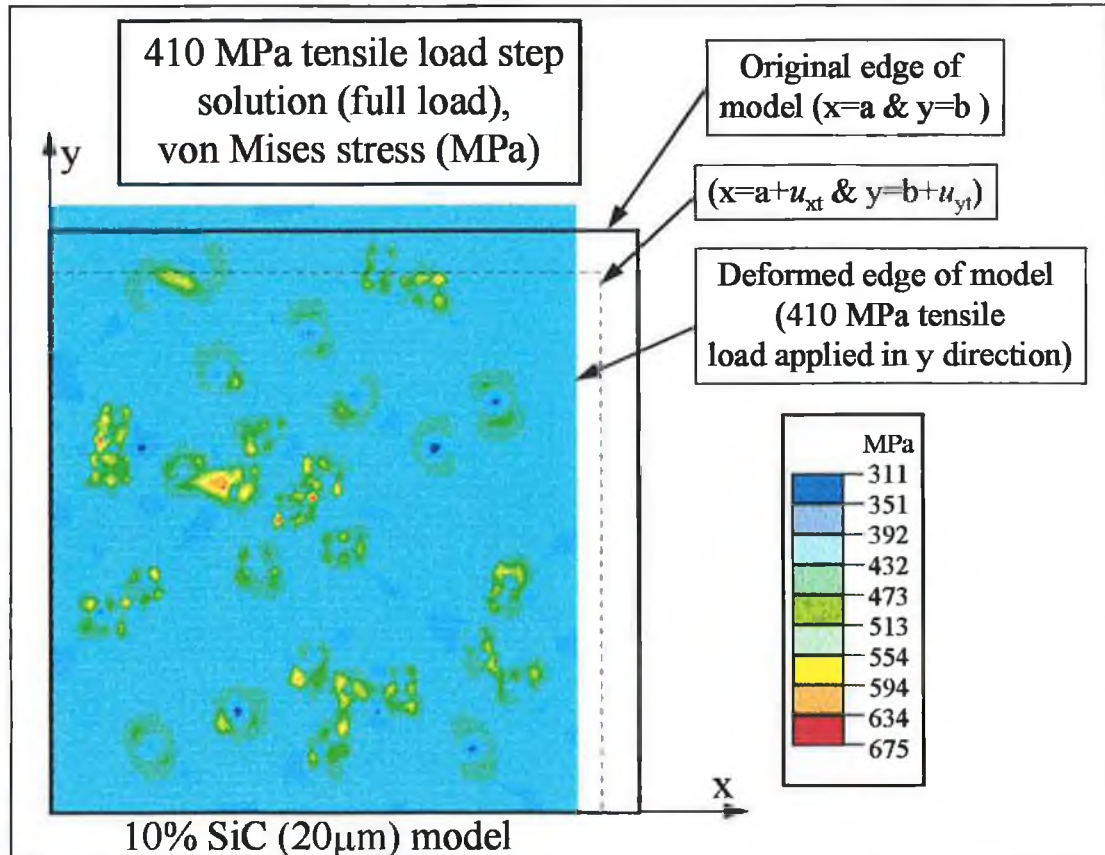


Figure 5.19. Stress map solution for 10% SiC (20 μ m) model at full load.

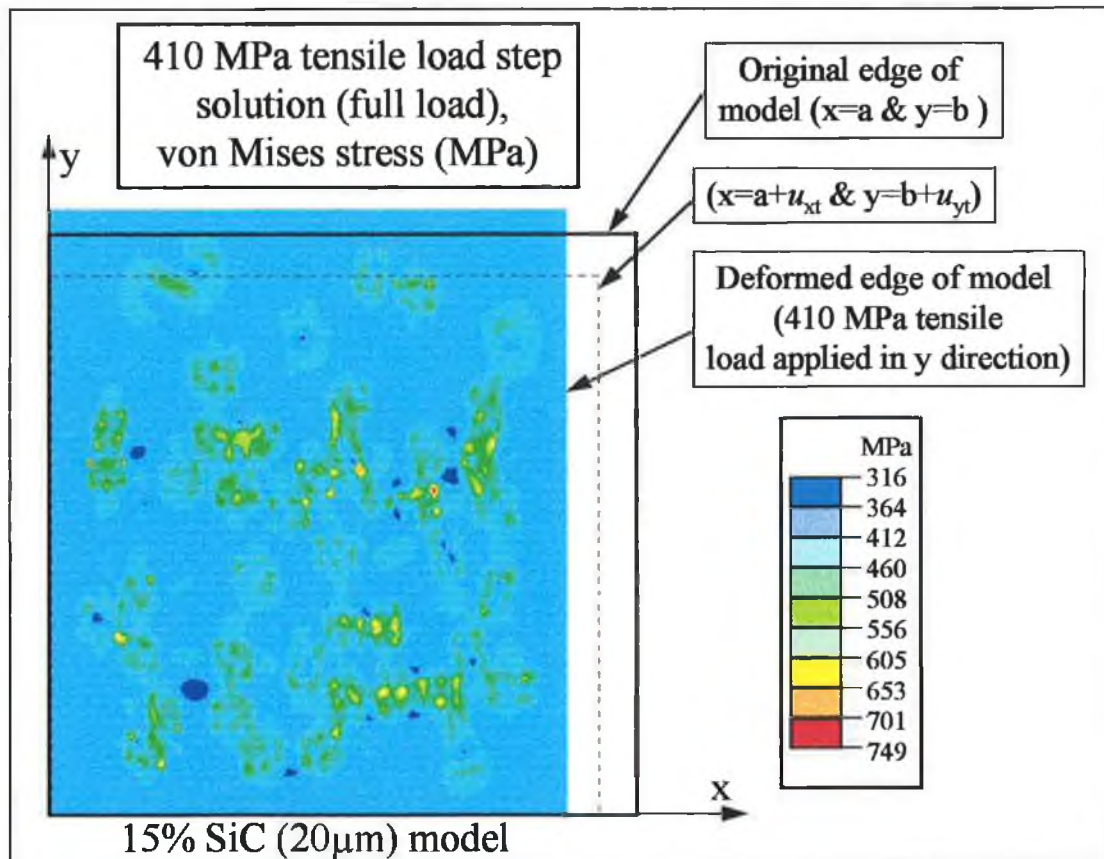


Figure 5.20. Stress map solution for 15% SiC (20 μ m) model at full load.

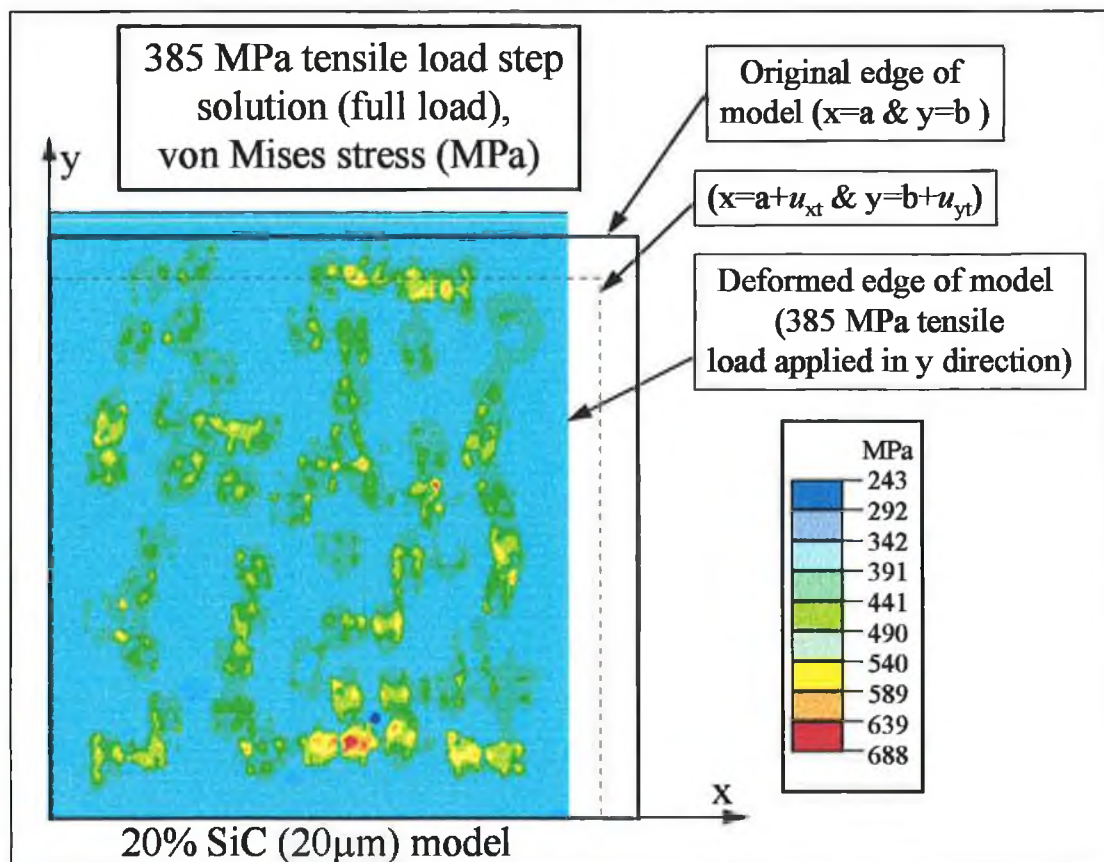


Figure 5.21. Stress map solution for 20% SiC (20 μ m) model at full load.

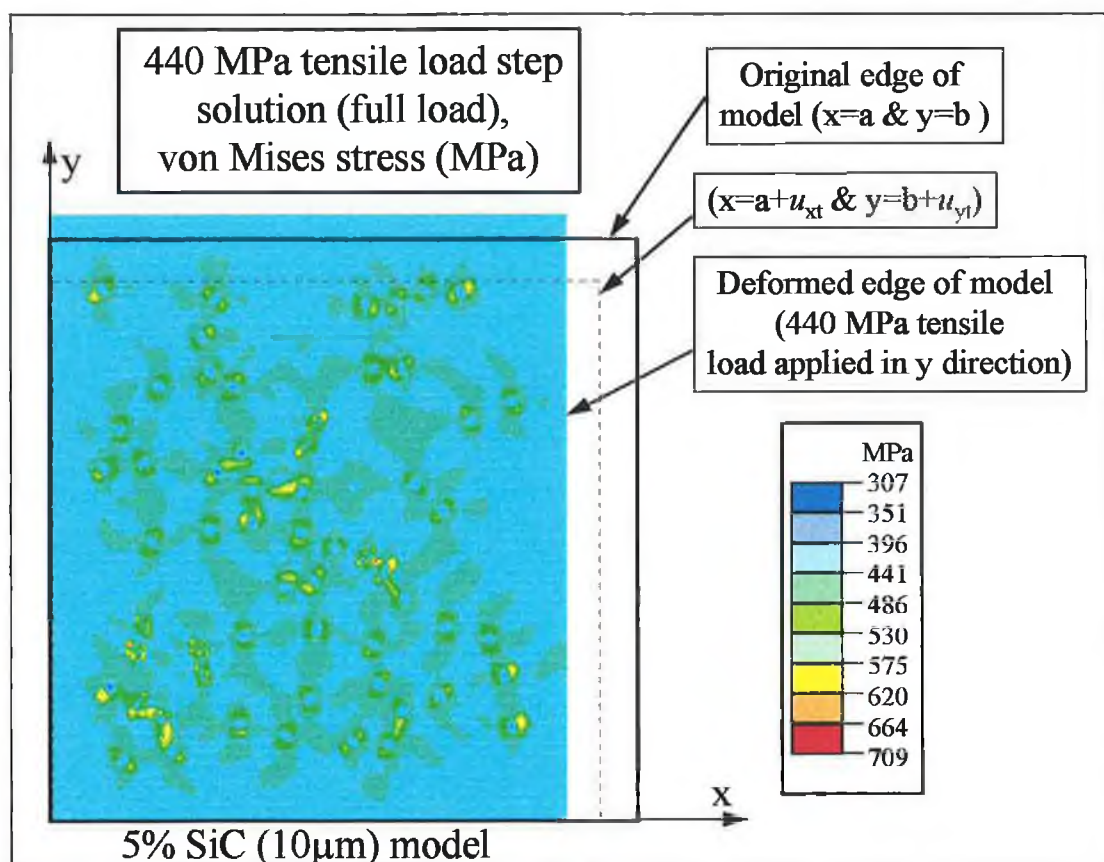


Figure 5.22. Stress map solution for 5% SiC (10 μ m) model at full load.

The complete true stress/true strain response of the thermally strained models (stress applied in the y direction) derived from the substep results can be seen in figure 5.23. The results shown in figure 5.23 indicate that an increase in volume fraction of SiC has the effect of increasing the stiffness, strain hardening and the flow strength of the model material. Also, this increase in volume fraction has the effect of reducing the predicted elongation to fracture down to as little as 0.01 (true strain) in the case of 20% SiC (20 μ m). The elongation to failure predicted by the analyses are listed in table 5.3.

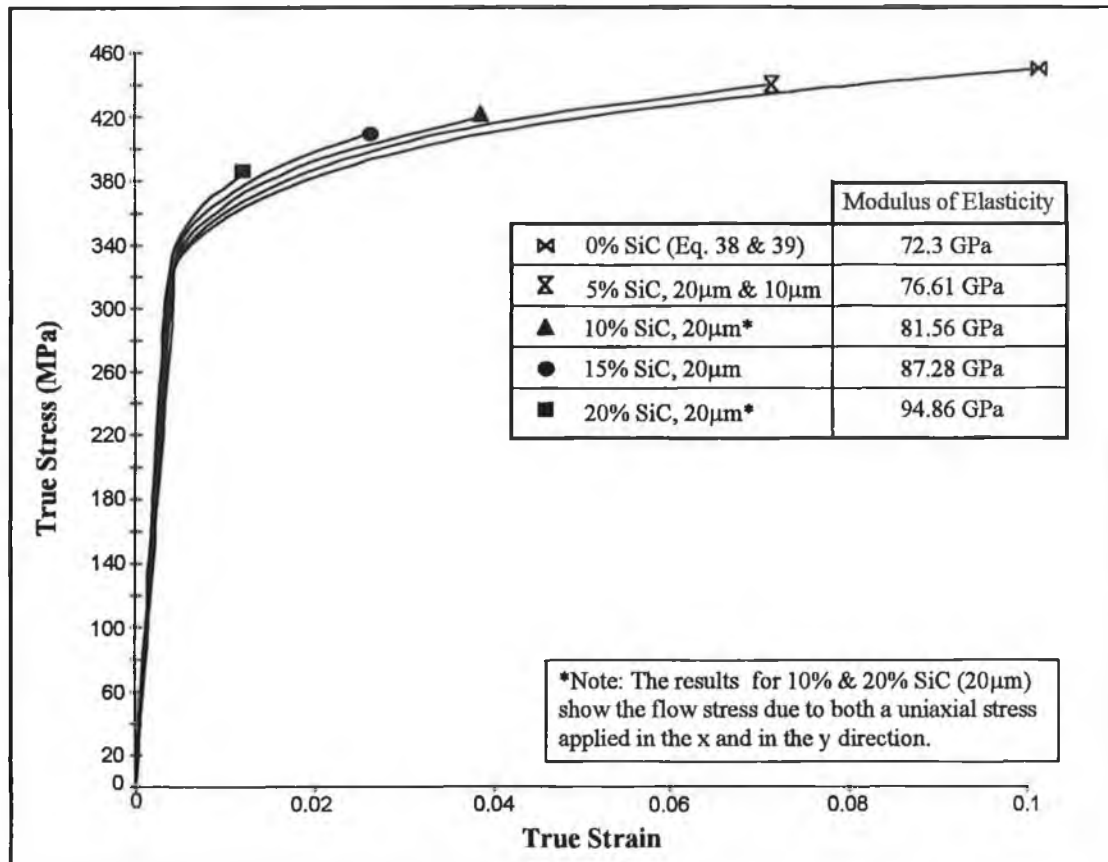


Figure 5.23. Numerically predicted true stress/ true strain response of the five DRMMC models investigated in the present modelling work.

Table 5.3. Predicted % elongation to failure results.

Volume fraction	0%	5%	10%	15%	20%
20µm	10.15%	7.12%	3.06%	2.63%	1.21%
10µm	10.15%	7.11%	-	-	-

Analysis of the stress distribution maps shown in figures 5.18 to 5.22 indicates that the matrix tends to fail in regions both between reinforcement particles which are in close proximity in the x direction and in regions surrounded by a cluster of particles.

CHAPTER 6 DISCUSSION

The findings derived from the results of the present experimental and modelling investigations (chapter 4 and 5 respectively) are presented and discussed in this chapter. The chapter consists of three main sections including process optimisation, numerical modelling and material development.

The process optimisation discussion primarily relates to the findings of the experimental work and follows the sequence of the processing route. This section draws on both the observations made during the present processing work and the related powder metallurgical and particle reinforced aluminium matrix composite (PRAMC) processing literature reviewed (sections 2.4 and 2.5 respectively). The three main objectives of this first section are to elucidate the effects of the material and processing parameters, to highlight the salient mechanisms involved at each stage of the process and to quantitatively define the optimum parameters for the production of PRAMCs by the cold uni-axial pressing and sintering powder metallurgical route.

The numerical modelling discussion details both the present model design and the capabilities and limitations of the present model. This discussion also describes the findings derived from the results and observations of the modelling analyses (presented in chapter 5). The final section of this chapter describes the primary contributions arising from the present work in the context of the present and further development of PRAMCs.

6.1 PROCESS OPTIMISATION

The processing work described in chapter 3 and the experimental results presented in chapter 4 highlight the predominant factors which affect the processing steps and the final condition of PRAMCs produced through this novel application of the cold uni-axial pressing and sintering powder metallurgical route. These factors include both material and processing parameters.

The salient material parameters highlighted include aluminium alloy type, reinforcement quantity, reinforcement as-supplied condition and shape, aluminium powder and reinforcement particle size, and lubricant type. The salient processing parameters include mixing method, powder heat treatment procedure, lubrication method, lubricant quantity (for mixed-in method), compaction parameters, sintering procedure, repressing and final material heat treatment. In addition to these predominant factors a number of other factors can also influence the process and the final material, albeit to a lesser extent. These factors include die filling, green compact ejection and green compact handling.

In the following sections the above mentioned findings are discussed in the context of the optimisation of the present processing route applied to PRAMC production. The order of these sections follows the investigated processing route as closely as possible. In addition to these discussions which relate directly to the present experimental findings, a number of factors which are not explicitly investigated in the present work are also discussed. These factors, which include reinforcement material selection, as-supplied powder and particulate purity, and green compact density distribution, are included in the present discussion due to their obvious importance in the process. The discussion related to these factors is primarily based on reviewed literature.

6.1.1 Material Selection

The present investigations show that the aluminium alloy type and reinforcement quantity selected, and both the reinforcement as-supplied condition (agglomeration) and reinforcement particle shape affect the sintering parameters and final condition of PRAMCs processed by the cold pressing and sintering route. In addition, it is intuitively obvious that the reinforcement material type selected and the purity of both the aluminium powders and reinforcement particles can influence the processing route and the condition of the final material.

Aluminium Alloy Selection

It is reported that the selection of aluminium alloy type for a particular PRAMC application is primarily based on the mechanical properties required [19,20,37] and the processing method used [38]. Other considerations affecting the selection of the matrix material include the chemical compatibility between the aluminium alloy and the selected reinforcement material [35], the corrosion and thermal properties required for the particular application [19,29,38], and both the material cost [38] and alloy availability [52].

In the case of the present experimental work the matrix materials selected are AA6061 and AA2124. These alloys were selected on the basis of availability, cost, heat-treatable characteristics [148], reported SiC chemical compatibility [37,209] (SiC was selected as reinforcement) and suitability to other powder metallurgical PRAMC processing methods [20].

The micrographs shown in figures 4.28, 4.30, 4.33 and 4.34 indicate that good bonding between the reinforcement and the matrix is achieved in the case of both alloys. In addition to these qualitative observations, the quantitatively analysed green compact and final material characteristics show the suitability of the AA6061 and AA2124 alloys to the present process. These quantitative results include the high green densities achieved in the case of both alloy types (approximately 88% TD for 10%SiC, section 4.2), the high sintered densities achieved (maxima of 97.9% TD for AA6061 and 98.2% TD for AA2124, both 10% SiC, section 4.6), the high hardness

recorded (maxima of 82.5HRB for AA2124+10%SiC (T4) and 69HRB for AA6061+10%SiC (T6), section 4.8) and the reasonable compressive and tensile properties recorded for the AA6061 based composites in test matrices no. 3 and no. 4 (sections 4.9 and 4.10 respectively).

It is widely accepted that in order to produce PRAMCs through high temperature processing such as casting without the generation of undesirable interfacial reaction products the aluminium alloy must be carefully selected [38,84] or the reinforcement material must be treated [221]. However, the present process, like other PRAMC spray and PM based processes [38], does not demand alloy adjustment or reinforcement treatment. This is due to the low temperature of the sintering process which is below that which would promote the generation of interfacial compounds such as Al_4C_3 [130,209].

However, the present processing investigations also show that to achieve optimum sintered density the sintering temperature and time must be adjusted to suit the aluminium alloy selected. The results of the sintered density analyses carried out in test matrix no. 3 show that in order to obtain the maximum sintered density in the case of AA6061+10%SiC the green compact should be sintered at 627°C for 60 minutes (appendix D). In addition, it was found that for these AA6061 composites a variation in either sintering temperature or time has only a small effect on the final density. However, in the case of the AA2124 alloy based composites the maximum sintered density is achieved by sintering at 617°C for 3 hours (appendix D). In contrast to the AA6061 composites, the final densities recorded for the AA2124 composites are significantly affected by both sintering temperature and time. In this case the sintered density decreased with either an increase in temperature (in the range 617°C to 633°C) or a decrease in sintering time (in the range 20 minutes to 3 hours). The green compacts used in these sintering investigations were similarly processed and exhibited very similar green densities. Therefore, the differences in sintering response between these two materials must be related to the alloy composition. However, further experimental investigation is required to fully describe this relationship between sintering response and alloy composition.

It must be noted that the compressibility of any heat treatment sensitive aluminium alloy atomised powder can be increased by the pre-compaction powder heat treatment process introduced in the present work (sections 4.2.4 and 4.2.5) and that this increased compressibility leads to good sintering response and therefore, good final material properties. On the basis of the present work it is reasonable to assume that any as-supplied or heat treated aluminium alloy powders which exhibit high compressibility are suited to this processing method. However, it is likely that the optimum processing parameters would vary for each alloy type used.

Reinforcement Selection

The selection of the reinforcement material type mainly depends on chemical compatibility with the selected alloy, the required mechanical properties of the composite and both cost and availability [20,35]. Due to the availability and low cost of abrasive grade SiC particles this high strength ceramic is commonly selected for the purpose of reinforcement. This material is also reported to be chemically compatible with a wide range of readily available aluminium alloys [37].

The present investigations deal with the processing of aluminium alloys reinforced with SiC particles only. Therefore, the influence of reinforcement material type on the present processing route has not been investigated. However, the micrographs shown in figures 4.28, 4.30, 4.33 and 4.34 indicate that good bonding between the SiC and the aluminium is achieved. Also, these micrographs show no undesirable reaction products such as Al_4O_3 . Therefore, the present work indicates that SiC particulate material is suitable for use in the cold uni-axial pressing and sintering route. It is reasonable to assume that other reinforcement materials such as Al_2O_3 , Si_3N_4 , TiC and B_4C commonly used in PRAMCs (see section 2.2.2, Discontinuous Reinforcement) are also compatible to the present processing route.

Reinforcement Quantity

It is reported that the quantity of reinforcement to be combined with a matrix is dictated by the strengthening required, the minimum acceptable level of ductility and the process used [19,20]. The present investigations show that in the case of the cold pressing and sintering processing route, as the quantity of reinforcement increases the compressibility decreases (section 4.2.1) and both the final material hardness and compressive strength increase (sections 4.8.2 and 4.9.1 respectively). However, the relationships between reinforcement quantity and both hardness and compressive strength are only true up to a level of 20% reinforcement volume fraction. Above this level the sintered material exhibits considerable porosity (>10% porosity for AA6061+30%SiC, table 4.2 and figure 4.31). This poor sintering response and the poor mechanical properties can be attributed to an initial low green density of the compacts containing 30% reinforcement volume fraction (84% TD, figure 4.2). Therefore, the present experimental work indicates that the maximum quantity of reinforcement which can be successfully introduced into a matrix material by the present method is 20% by volume. This maximum level of reinforcement quantity is comparable to the levels of reinforcement commonly used in PRAMCs (table 2.8).

Purity

It is intuitively obvious that the selected aluminium powder, reinforcement particles and solid lubricant must not contain any undesirable contaminants. Contaminants within these particulate materials are not easily extracted and can affect the properties of the final composite material. Therefore, an analysis of each material used should be carried out before processing. A chemical analysis of the supplied material is normally available on request from the supplier. Also, care must be taken to ensure that no impurities are introduced during processing. The material used in the present work did not exhibit any effects of undesirable impurities.

Agglomerates

In test matrix no. 4 the fracture surface analyses reveal that many of the tensile samples tested contained large pockets of SiC, an example of which is shown in figure 4.23a. Due to the large size of these pockets it may be assumed that they are not created during mixing, compaction or sintering. Therefore, these pockets must be caused by large agglomerates within the supplied material. These inhomogeneities could be avoided by sieving the supplied particles. This sieving procedure should also be carried out on the supplied aluminium powders and solid lubricant. This would ensure that inhomogeneity within the final material does not occur due to aluminium powder agglomerates and that the solid lubricant used is as effective as possible.

Shape

The present investigations indicate that the shape of both the reinforcement particles and the aluminium powders affect the penetration of the aluminium powder oxide layer during compaction (shown in figure 4.13), and therefore also affects both green strength and sintering response. The resulting physical interlocking between the aluminium powders and the particles due to this penetration can increase the green strength of the green compacts. The penetration also affects the sintering response of a green compact by exposing oxide free aluminium. In order to promote the penetration of the aluminium powders by the reinforcement particles the particles should be angular in shape and exhibit reasonably sharp edges and corners.

Also, it is reported that irregularly shaped metallic powders provide optimum green strength by creating a network of mechanically interlocked powders during compaction [83,126]. Therefore, in the case of the present process angular reinforcement particles and irregular aluminium powders must be selected to promote high green strength and good sintering response. The argon atomised aluminium powders and the abrasive grade SiC particles used in the present work (figures 3.6 and 3.7 respectively) are suitably shaped to meet these requirements.

Overview

The present work indicates that any of the aluminium alloy types and reinforcement material types commonly used for PRAMCs can be processed by the cold pressing and sintering method. However, it is important to ensure that the selected materials do not contain any undesirable contaminants or agglomerates and are suitably shaped to promote both powder interlocking and powder penetration during compaction. Also, this processing method is limited to the processing of composites containing no more than 20% volume fraction reinforcement.

6.1.2 Powder and Particle Size Selection

The present work shows that the aluminium powder size, reinforcement particle size and the size ratio between these materials can affect reinforcement distribution, compressibility, sintering response and reinforcement particle fracture.

Reinforcement Distribution

Many researchers have reported strong links between reinforcement distribution and the mechanical properties of PRAMCs [10,35,37,84,98,124]. It has been reported that reinforcement inhomogeneity causes poor strength, low ductility and poor fracture toughness. The present experimental work shows that to minimise the possibility of inhomogeneity in the case of powder metallurgical processing, careful consideration must be given to the selection of both the aluminium powder size and the reinforcement particle size.

The results and observations of test matrix no. 1 show that the aluminium powder size to reinforcement particle size ratio greatly affects final composite homogeneity, as presented in section 4.11.2. In order to promote homogeneity the median size of the reinforcement particles should be of the same order or larger than the median size of the aluminium powder. If the reinforcement particles are small compared to the aluminium these reinforcement particles will form clusters in the interstitial regions between the matrix powders, as shown in figure 4.29. These observations are in

agreement with the findings of other researchers who report high levels of reinforcement clustering with the use small reinforcement particle and relatively large aluminium powders in the case of various PM processes [35,43,95,98,124].

The two size ratios, 1:1.6 and 1:1.3 (Al:SiC), selected for the 10% SiC materials produced in test matrices no. 2 and no. 3 resulted in final materials which exhibited well dispersed reinforcement. An example of this homogeneity can be seen in figure 4.30. However, in the case of the 1:1.6 size ratio material investigated in test matrix no. 2 an increase in reinforcement volume fraction gives rise to reinforcement distribution inhomogeneity. This relationship can be seen in figure 4.31. Therefore, the size ratio required to optimise reinforcement homogeneity is dependent on the volume fraction. Qualitative analyses of the material produced in the present work indicate that in order to maintain reinforcement homogeneity as reinforcement volume fraction increases the size ratio must also increase. Therefore, for a given reinforcement size, as the volume fraction is increased the aluminium powder size must be reduced to maintain homogeneity. It is proposed that this relationship is primarily based on the fact that as the reinforcement volume fraction increases for a given reinforcement particle size the average distance between the particles decreases. Therefore, to prevent these particles from having to come into contact with each other, the aluminium powder must be suitably small. This important dependence between the size ratio and the volume fraction has not been reported before.

It is reported that inhomogeneities can be improved upon by secondary processing including rolling and extrusion of the consolidated composite [14,35]. However, in the case of net shape or near net shape processing such as the cold pressing and sinter route, it is often impossible to perform secondary processing which would provide sufficient material deformation to affect the homogeneity of the reinforcement distribution. Also, secondary processing can damage the consolidated composite material by generating cracked particles and interfacial voids within the material [2] and should be avoided where possible. Therefore, rather than attempting to correct inhomogeneities in the final material by the use of a secondary process,

inhomogeneities should be minimised by the selection of the correct powder to particle size ratio for the given volume fraction.

The present work shows that with the correct selection of aluminium powder size and reinforcement particle size composite material exhibiting homogeneously distributed reinforcement can be produced by the cold uni-axial pressing and sintering route. In comparison with the inhomogeneous distribution exhibited by many AMCs produced by liquid matrix solidification processing (casting) [14,35,36,44,84,88,122, 124,128,222] and by various PM routes [130,223], the distribution exhibited by the composite material produced in test matrices no. 2, no. 3 and no. 4 (figures 4.24, 4.30 and 4.32) can be considered superior.

The powder to particle size ratios investigated in the present work which were observed to result in good distribution of reinforcement include 1:1 10% SiC (test matrix no. 1, figure 4.27), 1:1.6 10% SiC (test matrix no. 2 and 3, figures 4.31 and 4.32 respectively), 1:1.3 10% SiC (test matrix no. 3, figure 4.30) and 1:3.5 20% SiC (test matrix no. 4, batch 10, figure 4.24a). It should be noted that the dominance of suitable size ratios for the 10% SiC volume fraction stated here are directly related to the fact that the present processing investigations mainly focused on the processing of composites containing this volume fraction. Further investigations are required to define the range of suitable size ratios for all volume fractions.

Compressibility

The results of the compressibility tests performed in test matrix no. 1 indicate a strong influence of powder and particle absolute size on compressibility. Compressibility drops considerably with a reduction in either matrix powder or reinforcement particle size. This decreased compressibility can be attributed to a number of factors including the increase in specific surface area of the smaller powders and, in the case of the pre-alloyed powders investigated in this work, the increased resistance to plastic deformation due to powder refinement [17,126]. The relatively large specific surface area of the smaller powders increases the frictional resistance to powder movement during compaction. As mentioned, the small matrix powders offer more resistance to

plastic deformation than relatively large powders. This is due to the high strength of these rapidly solidified powders [178]. It must be noted that the powders investigated in test matrix no. 1 were all tested in the as-supplied atomised condition.

The annealing heat treatment of the powders in test matrices no. 2 and no. 3 (16 μ m AA6061, 19.5 μ m AA2124) provided increases in compressibility of up to 6.2% theoretical density due to the reduced resistance to plastic deformation of these relatively soft large powders. Also, both the tensile investigations and scanning electron microscopy carried out in test matrix no. 4 indicate that the use of annealed small matrix powders (7 μ m, 11 μ m, batches 9, 10, 11 and 12) leads to well consolidated sintered material which exhibits reasonable tensile properties (see figures 4.25 and 4.26 for tensile response and figure 4.36 for micrographs). Therefore, incorporation of the powder heat treatment stage into the cold pressing and sintering route can allow both large and small aluminium powders to be compacted to adequate levels of green density leading to well sintered material. Further research must be carried out to quantitatively define the increase in compressibility achieved by heat treatment of these small powders.

The heat treatment effects discussed above refer to the softening of the aluminium powder. However, the heat treatment process should always be carried out after mixing to avoid mixing difficulties arising from caked aluminium powders. Therefore, the SiC particles are present during the heat treatment procedure. Although present, this heat treatment should not influence the mechanical properties of the reinforcement. Consequently, the relationship between SiC size and compressibility recognised in test matrix no. 1 should also be considered in the case of heat treated powders. The compressibility tests carried out in test matrix no. 1 also reveal a relationship between compressibility and powder to particle size ratio. The results from this test matrix show that for all aluminium powder sizes and reinforcement volume fractions tested, as the size ratio increases the compressibility increases. However, as described in sections 4.2.2 and 4.2.3, this relationship is simply a different way of describing the result that as particle size increases compressibility increases.

The present work indicates that in order to optimise the compressibility and therefore the green density of the green compacts produced by cold uni-axial pressing, both the aluminium powder size and reinforcement particle size (or size ratio) selected must be maximised. This work also shows that the use of powder heat treatment can widen the size range of aluminium powder which can be compacted to acceptable levels of green density.

Sintering Response

Both the powder and particle size, and size ratio are recognised as factors which may influence the response of a green compact to sintering conditions. The size ratio affects the penetration of the aluminium powder by the SiC particles and the aluminium and reinforcement sizes affect the surface contact area within the green compact. Both of these factors influence sintering response.

The effect of the size ratio on the extent of aluminium powder oxide layer penetration must be considered when selecting the powder and particle sizes. If the reinforcement particles are considerably smaller than the aluminium powders the particles will tend to form clusters in the interstitial regions between the aluminium powders, as seen in figure 4.29. These clustered particles may not significantly impinge on the matrix powder surface layer. Conversely, if the SiC particles are of the same order or larger than the aluminium powders the reinforcement will tend to become surrounded by the relatively soft powders during compaction and will penetrate the surface oxide layer of these powders. Examples of this oxide layer penetration can be seen in figure 4.13. This penetration provides oxide free aluminium which in turn promotes consolidation during sintering. The phenomena of improved consolidation due to mechanical deformation of the matrix powder oxide layer has been reported by a number of researchers [17,36,143,224,225] investigating various PM processing routes and is regarded as a significant processing consideration. Therefore, the size ratio selected must promote oxide layer penetration which will in turn optimise the sintering response of the green compact.

The second relationship described is based on the reported relationship between sintering response and powder contact area within green compacts where the increased powder contact area within green compacts produced from small powders is believed to enhance sintering [17]. Therefore, to optimise sintering response on the basis of powder contact area, the powder and particle sizes selected must be kept to a minimum. This is in direct conflict with the need to maximise sizes for good compressibility, which indicates that a balanced approach to size selection is required.

Reinforcement Particle Fracture

The present experimental work shows that the fissures created by particle fracture during cold compaction (figure 4.14) can be fully infiltrated by aluminium during sintering (figures 4.33 and 4.34). This fissure infiltration is obviously more desirable than residual cracks within the sintered material. However, the present modelling work shows that a material containing particles in close proximity will experience high localised stress within these regions. Therefore, since a cracked and infiltrated particle can be considered to be two or more smaller particles in close proximity (a small cluster), particle fracture during cold pressing should be avoided. It has been reported that large reinforcement particles ($>20\mu\text{m}$) tend to fracture more readily than small particles [35,95,226]. Therefore, in order to minimise the possibility of particle fracture during either processing or service the particle size selected must be kept to a minimum.

Overview

Based on both the present experimental work and the reviewed literature the following aluminium powders sizes, reinforcement particle sizes and powder to particle size ratios may be considered for selection for use in the processing of PRAMCs by the cold uni-axial pressing and sintering route.

Reinforcement particle mean sizes: $5\mu\text{m} - 20\mu\text{m}$ ($d_{50,3}$)

Aluminium powder mean sizes: $3\mu\text{m} - 20\mu\text{m}$ ($d_{50,3}$)

Size ratios: 1:1 - 1:3.5 (ratio base on aluminium size to reinforcement size ($d_{50,3}$))

Also, it should be noted that small powders and particles are inherently difficult to handle (transport, mix and die fill) and are generally more expensive than larger materials. These factors must be considered when selecting suitable materials.

6.1.3 Mixing Method[†]

It has been reported that the homogeneity of fully consolidated PM AMCs primarily depends on the particle size selection and also the effectiveness of the powder mixing stage [35,43,116]. The primary objective of the mixing stage is to homogeneously distribute the SiC particles throughout the matrix powder. This is only possible if a correct combination of aluminium powder and reinforcement particle size is selected, as discussed in section 6.1.2.

In test matrix no. 2 identical powder combinations were mixed by both rotation and reciprocation based mixing methods. The qualitative analyses of the resulting mixtures indicate that composite powder mixing by rapid reciprocation within a cylindrical container improves the distribution of the reinforcement particle throughout the matrix compared to rotational mixing within a V-shaped container. The rotary action of the V-shaped container does not tend to break up agglomerates. It has been reported that some regions of a powder charge within a rotational mixing container may not experience forces with the capacity to overcome the interparticle bonds which exist throughout the powder [116]. Conversely, the rapid reciprocation of the composite powders used in test matrix no. 2, no. 3 and no. 4 causes the powder to impact on the walls of the mixing container. This impact tends to break up any loose powder agglomerates and allows random and independent movement of individual powders and particles resulting in mixtures exhibiting well distributed reinforcement. All of the mixing processes described in the reviewed literature relate to rotational type mixing. No literature on reciprocation mixing has been found.

[†] **Mixing Safety:** It should be noted that small aluminium powders ($< 5\mu\text{m}$) are explosive [83]. In order to prevent the generation of dust clouds from the mixing process, and therefore potential explosion, all powder mixing should be carried out within a sealed container and mixed batches must be allowed to settle after mixing. Also, extreme care must be taken when loading and unloading powder charges to avoid spillage and dust clouds and both respiratory protection and protective clothing must be used at all times. Non-compliance with these respiratory and skin protection directives can result in serious lung and skin irritation, and will increase the possibility of ingestion.

6.1.4 Powder Heat Treatment

The present work clearly shows that the pre-compaction heat treatment of composite powder blends greatly improves compressibility, compact green strength and the sintered condition of PRAMCs produced by the cold pressing and sintering route.

Compressibility

It has been reported that the rapid solidification which occurs during the atomisation of pre-alloyed aluminium increases the strength of these powders [17,83,178]. This increased strength hinders powder compressibility. It was the hypothesis of the author that the heat treatment (annealing/normalising) of this powder can reduce the powder's resistance to deformation and therefore increase compressibility. Test matrix no. 2 has revealed that powder heat treatment carried out in a nitrogen atmosphere can increase the powder compressibility by approximately 6.2% TD for AA6061 powders blended with 0%, 10%, 20% and 30% SiC (see figure 4.2), as compared to the as-supplied rapidly solidified powders. This absolute increase in compressibility due to powder heat treatment is predominantly independent of the SiC content within the range investigated. Also, in test matrix no. 2 attempts were made to press AA2124 as-supplied powder based powder blends. In this case the pressed green compacts experienced extensive damage during ejection. This is attributable to the very high strength of the rapidly solidified AA2124 powders. In contrast to these observations the AA2124 based powder blends processes in test matrix no. 3 (all produced with heat treated powder) resulted in very well formed high density green compacts. These results are presented in sections 4.2.1, 4.2.4 and 4.2.7.

It has also been found that an increase in the heat treatment temperature increases the powder compressibility. However, the heat treatment temperature is limited by the powder caking which occurs at temperatures above 470°C. This caking is primarily due to interparticle bridging caused by oxide formation and powder interlocking caused by slight deformation of the powders at elevated temperatures. Caking of the powder inhibits subsequent powder pouring and die filling. In test matrix no. 3

powders were heat treated at 475°C in air resulting in gross powder caking. These air annealed powders also exhibited poor compressibility and high die wall friction during ejection compared to the nitrogen annealed powders.

The heat treatment times investigated in the present work were chosen based on the recommended annealing and normalising times for AA6061 and AA2124 [148]. It was found that the powder compressibility did not vary between powder blends heat treated for times of 2 hours and 3 hours. However, a more extensive investigation may reveal a relationship between the heat treatment duration and the powder compressibility.

Green Strength

The green strength analyses carried out in test matrix no. 2 compared the green strength of the compacts produced from both as-supplied and heat treated powder blends. The green strength of the compacts produced from heat treated powders was found to be up to three times greater than that of the as-supplied powder compacts, as presented in section 4.4. This is due to increased powder interlocking, larger interparticle contact area and may also be influenced by the penetration of the SiC particles into the aluminium powders (figure 4.13, also discussed in section 6.1.2 sintering response). These factors are obviously directly related to the high levels of compressibility which can be achieved. The results presented in section 4.4 (figure 4.12) clearly show that in order to maximise green strength the highest possible heat treatment temperature must be employed. It was also found that although there was no distinct relationship between heat treatment time and compressibility, an increase in heat treatment time from 2 hours to 3 hours caused an increase in green strength.

The increase in compact green strength due to the powder heat treatment greatly improved the condition of the green compacts and the ease with which they could be handled. Handling of the green compacts produced from as-supplied powders caused breakage of sharp corners and flaking on the compact surface. However, if reasonable care is taken during handling this damage does not occur in the case of the compacts produced from heat treated powders.

Sintered Material

The very poor condition of the sintered compacts (maximum sintered density = 86% TD) produced from as-supplied powder blends produced in test matrix no. 1 allowed no valid quantitative comparison between these materials and the sintered compacts produced from the heat treated powders, as indicated in sections 4.6.3, 4.6.4 and 4.7. However, it should be noted that the composite material produced from heat treated powders in test matrices no. 2, no. 3 and no. 4 exhibited high sintered density (up to 98.2% TD) and reasonable mechanical properties (UTS=324 MPa, HRB=82.5 and compressive yield strength=456 MPa).

In test matrix no. 2 samples were produced from both heat treated and as-supplied powders. It was found that although the sintered compacts produced from as-supplied powders experienced far greater sintering within the centre of each compact compared to the material produced in test matrix no. 1, these samples exhibited very large outer layers (up to 4mm). The large brittle outer layers made these materials structurally useless. In contrast to these poor materials, the sintered compacts produced from heat treated powders exhibited very small outer layers (<50 μ m, see figure 4.24a).

The results presented in figure 4.17 shows that the hardness of the sintered material produced from as-supplied powders (hardness tests carried out in the well sintered centre portion of these samples) is slightly greater than that of the sintered material produce from heat treated powders. Similar trends were observed for the compressive yield strength of these materials (see figure 4.20). These superior material properties indicate that the rapidly solidified as-supplied powders provide increased strength in the final material. However, these superior material properties are negligible considering the very large brittle outer layer exhibited by the material.

Ejection

In both test matrix no. 1 and 2 it was noticed that in a number of cases compacts produced from as-supplied powders cracked during ejection. This fracture occurs due

to the low level of compaction achieved and the high level of residual stress caused by the compaction of these highly stressed rapidly solidified powders. No green compact cracking occurs for heat treated powder compacts. This is attributable to the increased level of compaction and the relatively soft condition of the compacts.

H₂O Content

The Al₂O₃ surface layer that exists on aluminium powders is known to absorb small quantities of H₂O [17,83,96,107,108,129]. In order to decrease the quantity of this absorbed H₂O and also minimise the quantity of air and other undesirable elements aluminium powder is normally treated by applying a costly canning and degassing process before primary consolidation [35,43,83,107,108,129]. Preliminary tests were carried out as part of the present work to investigate the effect of powder heat treatment on the H₂O content of the composite powder blends, as described in section 4.1.4. These investigations indicate that the heat treatment process slightly reduces the H₂O content of the powder blends. As reported in the case of aluminium powder degassing, this reduction in H₂O content may be due to the evaporation of physically absorbed H₂O within the oxide layer of the powders [227].

Overview

The incorporation of the powder heat treatment stage in the processing of AMCs by cold pressing and sintering is essential. This heat treatment has a significant positive impact on powder compressibility, compact green strength and sintering response. Based on the present experimental work, heat treatment must be carried out in a non-reactive atmosphere (industrial grade nitrogen is suitable) at the highest temperature possible which does not cause excessive caking (approximately 480°C) for a period of between two and three hours (three hours to maximise green strength). It is important to note that this heat treatment stage must be carried out after mixing to avoid mixing difficulties arising due to agglomerated aluminium powders (from caking).

This new powder heat treatment stage may also be very advantageous in the processing of PRAMCs by other PM routes and could be of benefit in the processing of monolithic aluminium powder metallurgical components.

6.1.5 Lubrication

In order to prevent galling during compact ejection it is necessary to either add solid lubricant to the composite powder blends before compaction or coat the die wall with lubricant before die filling. Two common lubricant types, zinc stearate and the synthetic wax AcrawaxTM, in various quantities (0%, 0.5%, 1%, 2% and 3% by weight mixed-in lubrication and zinc stearate brushed die wall lubrication) have been investigated in this work, as presented in sections 4.2.6 and 4.3.1.

In the case of mixed-in lubrication zinc stearate provides improved lubrication during ejection compared to the synthetic wax and can provide adequate lubrication at levels as low as 0.5% by weight. However, the superiority of the zinc stearate observed may be due to the agglomerated form of the AcrawaxTM powder used in this work.

High levels of lubrication reduces powder compressibility and therefore, the quantity of lubricant should be kept as low as possible. It should also be noted that the lubricant dispersed throughout the green compact must be burnt off before the sintering stage. Consequently, in order to minimise the undesirable residual combustion products both within the sintered compact and on the surface of the material the quantity of lubricant should be kept at a minimum.

The results of the present work indicate that the avoidance of mixed-in lubrication is desirable in order to achieve maximum green density, eliminate residual combustion products and avoid both the lubricant mixing and burn off processing stages. In test matrix no. 4 no lubricant was mixed in with the powders before compaction. In this case lubrication was provided by brushing the die walls and the punches with zinc stearate powder prior to compaction. This method of lubrication prevented any galling from occurring. It was also found that the surface of the samples process in test matrix no. 4 exhibited very little residue.

Overview

Based on the present experimental work, optimum lubrication can be achieved with the use of zinc stearate solid lubricant in the form of die wall lubrication. Alternatively, adequate lubrication is provided by the use of 0.5% by weight mixed-in zinc stearate lubrication.

6.1.6 Powder Pouring

The procedures used in the present work for die filling described in section 3.2.3 are adequate for use in the present research work. However, with particular reference to the slow manual die filling procedure used in test matrix no. 4 for the production of tensile test samples, an automated or semi-automated die filling procedure could increase the rate of production and provide a very uniform distribution of powder within the die cavity. Many conventional die filling techniques would suit this process.

6.1.7 Compaction

The primary objective of the compaction procedure in the present process is to produce powder compacts with adequate green strength, green density and green density distribution for further processing. The compact must be sufficiently strong to withstand the forces encountered during ejection and handling and should be compressed to a density which will allow adequate sintering to occur. Also, the distribution of density throughout the compact must not be so large to cause either localised poor sintering or excessive shrinkage during sintering.

Pressure

The main factor which influences the compaction process is the compressibility of the powder to be pressed. As compressibility decreases the compaction pressure required to produce a given density increases. This relationship is intuitively obvious and was not quantitatively investigated in the present work. The cylindrical samples produced

in this work were compacted at a pressure of 220 MPa. This pressure was the maximum safe pressure which could be applied to these compacts with the available equipment. The green compacts produced in test matrix no. 4 were pressed at $235 \text{ MPa} \pm 5 \text{ MPa}$. It should be noted that the maximum size of component which can be produced by the cold uni-axial pressing and sintering route is primarily limited by the compressibility of the powder used and the maximum pressing force available.

Rate

An investigation was carried out as part of test matrix no. 3 in order to examine the relationship between the rate of compaction and green compact characteristics. It has been found that a variation in the rate of compaction over the range from 20 mm/min to 500 mm/min does not affect compact green density or ejection stress. In order to produce cylindrical green compacts safely and in reasonable time a compaction rate of 30 mm/min may be used.

Density Distribution

Due to the density gradient created during the floating die single action uni-axial pressing operation the compact inevitably shrinks unevenly during sintering. In the present work the shrinkage experienced by the compacts produced from heat treated powders was acceptably minor. However, in all cases it was necessary to repress the sintered compacts to regularise their geometric form. This simple repressing operation can be carried out at a rate of 20 mm/min with a maximum pressure of 220 MPa. No investigations were carried out in the present work to find the limiting compact height for this process.

Compact Annealing and Pre-sintering Repressing

As described in section 3.2.6, the green density of the compact can be increased by annealing the green compact followed by pre-sintering repressing. This additional stage could be useful for processing PRAMCs with higher volume fractions than 20% and also reducing the density gradient of the green compact. However, since this process requires a second die and an expensive heat treatment procedure it should be avoided if possible.

Overview

The present experimental work indicates that adequately compressed green compacts can be produced by applying a compaction pressure of 220 MPa at the maximum safe rate of compaction available. In the case of the equipment used in the present work the maximum safe rate of compaction is 30mm/min. In addition, the die must be designed to withstand the applied compaction pressure and the surface finish of the die walls should be sufficiently smooth to avoid excessive die wall friction either during compaction or ejection.

6.1.8 Ejection

Cylindrical Compacts

The present work indicates that ejection of green compacts containing 0.5% mixed-in zinc stearate may be carried out at an initial rate of 20 mm/min followed by a rate of 100 mm/min. The rate of ejection should only be increased after the green compact is in motion within the die. Also, in order to avoid green compact damage during downward ejection the compact should be prevented from impacting on the die set base after exit from the die. This may be achieved by the use of sponge padding. The die set should be designed so as to minimise the distance over which the compact must travel during ejection. This has the affect of minimising ejection time and the possibility of die and green compact damage during ejection.

Tensile Samples

The time consuming ejection procedure described in section 3.2.5 can be used to successfully remove a geometrically complex compact from within a die. However, it may be possible to avoid this lengthy procedure by minimising the clearance fit between the ejecting punch and the die, and relieving the die wall on the exit side of the die. This relief may be in the form of a gradual taper which would reduce the stresses experience by the green compact during exit from the die.

6.1.9 Green Compact Handling

Handling of green compacts can cause damage and should be minimised and carried out with extreme care when handling is unavoidable. A useful aid for the handling of green compacts recognised during the present work is a sponge padded tongs. This tongs allows only a very slight force to be applied to the green compact.

6.1.10 Sintering

The objective of the sintering stage in the present process is to transform the green compact from a low strength powder compact to a structurally useful material by maximising consolidation. The control of the sintering processing is of paramount importance in the present processing route. The results of the present sintering investigations shows that the main sintering parameters which affect the characteristics of the sintered material include the sintering atmosphere, time and temperature.

Atmosphere

The control of the sintering atmosphere is of particular importance to the final material condition. In test matrix no. 1 the green compacts were sintered within a poorly controlled atmosphere resulting in sub-standard material. However, the PRAMCs produced in test matrices no. 2, no. 3 and no. 4 were sintered within a closely controlled atmosphere resulting in many well sintered compacts. Sintering must be carried out within a sealed container which can not be affected by the ambient atmosphere. The present work shows that an atmosphere of industrial nitrogen within a sealed unit can provide adequate atmospheric protection at temperatures up to 630°C, above which substantial compact oxidation occurs due to the presence of large quantities of liquid aluminium. Sintering temperatures above 630°C should also be avoided to prevent gross geometric deformation due to melting.

Sintering Time and Temperature

As reported in sections 4.6.1 and 4.6.2, very high levels of consolidation (98.2% TD) can be achieved by sintering AA2124 + 10%SiC at 617°C for 180 minutes. At higher temperatures the surface oxide layer thickness increases and at shorter sintering times sintered material porosity increases. AA6061 + 10%SiC can be sintered at temperatures of 617°C for a range of times from 20 minutes to 180 minutes achieving levels of consolidation above 97% TD. The surface oxide layer thickness increases at temperatures above 617°C.

High temperature liquid phase sintering processes involve many mechanisms of material transport, as described in section 2.4.6. However, the high sintered density achieved in the present work is primarily attributed to the oxide layer penetration (described in section 4.5) and the high incidence of powder contact due to the high green compact density achieved with the use of heat treated powders (described in sections 4.2.4 and 4.2.5).

Overview

The results of the present investigation into the sintering of cold uni-axially pressed compacts for the production of AMCs indicate that optimum sintering can be achieved by sintering within a controlled industrial nitrogen gas atmosphere at a temperature between 617°C and 633°C for times between 20 minutes and three hours. The present investigations indicate that optimum sintering of AA6061 and AA2124 based composites is achieved by sintering at 617°C for between 20 and 180 minutes and 617°C for 180 minutes respectively. The sintering temperature and time must be kept to a minimum to prevent the development of excessively large outer layers on the samples.

6.1.11 Repressing

Due to the non-uniform shrinkage of the green compacts during sintering the repressing of the sintered components is an essential stage in the processing of AMCs by cold pressing and sintering. This can be carried out by pressing to 220 MPa at a rate of 20mm/min.

6.1.12 Composite Material Heat Treatment

Due to the high temperatures reached and the slow cooling rate used during the sintering process the sintered compacts are soft and weak. These sintered compacts must be heat treated to improve their mechanical properties. The choice of the sintered compact heat treatment times and temperatures used throughout the test matrices in the present work were based on the extensively reported accelerated ageing response of particle reinforced AMCs [101,103,124,150-166], as discussed in section 2.4.7. Solution heat treatment of the present composites can be carried out at 515°C in a nitrogen atmosphere. This may be followed by natural ageing at room temperature (equivalent to a T4 heat treatment) or artificially aged at between 168°C and 175°C for four hours or over. The duration of this artificial ageing is dependent on the aluminium alloy type and the reinforcement volume fraction used. The effects of heat treatment parameter variation were not investigated in the present work.

6.1.13 Outline of the Process Optimisation Work Findings

The PRAMC processing route detailed above can be used to produce highly consolidated green compacts and final material. The results and observations indicate that the process is compatible with any aluminium alloys which can be produced in powder form and the reinforcement particulate material commonly used in PRAMCs. The new powder heat treatment processing stage introduced in this work is an indispensable addition to the conventional pressing and sintering powder metallurgical route which significantly improves green density, green strength, sintering response and final material condition. In addition, the powder and particle size related investigations highlight the considerable importance of both individual sizes and the size ratio between these sizes.

6.2 NUMERICAL MODELLING

In parallel with the processing developments detailed in the previous section (6.1), modelling work was carried out which focuses on particle reinforced aluminium matrix composite (PRAMC) material design. In order to enable the correct selection of materials for a composite to suit a given application the effects of the various material parameters on both the composite processing method and the final composite material properties must be known. The processing investigations carried out in the present work elucidate the effects of the material parameters on each stage of the presently investigated powder metallurgical processing method. To complement this promising processing development the composite material model development provides a mechanism by which the effects of the salient material parameters on the fully processed composite and the constitutive response of a specific composite can be quantitatively defined.

The two objectives of the modelling work are to develop a model which can be used to elucidate the micromechanical effects of individual composite material parameters in isolation, and to predict the macroscopic elastic/plastic response of a specific composite material to both thermal and mechanical loading. The main purpose of the first objective is to provide the facility of parameter isolation which is not possible by experimental means [171,175,216]. The two purposes of the second objective are to allow comparison between the simulated model response of a material and the response of a real composite, and also allow comparison between the responses of different models.

The numerical model design work and modelling analyses described in chapter 5 highlight the main model design considerations and both the capabilities and limitation of this novel modelling approach. In this section each of the design considerations are discussed in detail in the context of the present objectives, the capabilities and limitations of the model, and the relevant composite modelling literature reviewed in section 2.6. The factors considered in the design of the model include the salient

mechanisms and composite material parameters, the geometric model description, the selection of a suitable mechanistic framework and also the selection of a computational method suited to the developed model.

Also, in this section the thermal strain and tensile loading results and observations presented in chapter 5 are discussed. It should be noted that although the present work focuses on the development of the processing and modelling of PRAMCs, the modelling work is also relevant to similar discontinuously reinforced metal matrix composites (DRMMCs).

6.2.1 Model Design Considerations

Salient Mechanisms and Material Parameters

As discussed in section 2.6, the mechanisms which affect the properties of PRAMCs include matrix to reinforcement load transfer, thermal expansion and stiffness mismatch residual stress development, internal localised stress concentration, refined precipitation strengthening, matrix grain refinement, constrained plastic flow and both interfacial failure and particle fracture [63]. Also, the composite material parameters which influence these mechanisms, and therefore the overall properties of PRAMCs, include the constitutive properties of both the reinforcement and the matrix, the reinforcement quantity (content or volume fraction), reinforcement size and size distribution, reinforcement shape, orientation and surface morphology, reinforcement distribution within the matrix, and the chemical compatibility between the reinforcement and the matrix material [14,84,169,170]. Ideally, all of these variables and mechanisms should be included in a PRAMC model to maximise the accurate and the investigative capabilities of the model.

At present it is not computationally feasible to include all of these material parameters and mechanisms. Also, the inclusion of both material parameters and mechanisms rely on quantitatively accurate analytical or numerical description. Unfortunately, accurate descriptions of many of these factors are not presently available [63]. The selection of

both material parameters and mechanisms to be included in the present model is primarily dictated by the scale of the geometric model, the availability of accurate material and mechanism descriptors, and the computational capacity of both the software and hardware presently available. The selection and exclusion of the salient parameters and mechanisms is discussed in the following sub-sections.

Geometric Description

A geometric model suited to the prediction of the response of a composite material to various stimuli and also to allow geometric and material property parameter isolation must be sufficiently large to both provide a macroscopic constitutive response prediction and allow a range of values for each material parameter to be incorporated in the model. This range of values should avoid interdependency between parameters to facilitate parameter isolation without model boundary condition adjustment, and also facilitate variation of reinforcement distribution, orientation, size distribution and shape.

To allow for all the above mentioned conditions a representative microstructural based geometric model is proposed in the present work (figure 5.1). This model is a cubic solid consisting of matrix material containing discrete reinforcement particles in the form of aligned identical short hexagonal cylinders. These cylinders are aligned parallel to one axis of the cubic solid and are randomly distributed in the plane normal to this axis. Also, each reinforcement particle is randomly oriented about its own axis. The hexahedron (cubic solid) geometry is selected to allow spatial consistency of the model during deformation through the use of manageable boundary conditions (section 5.3 for boundary conditions applied in present plane stress modelling analyses and [206] for similar plane strain boundary conditions in three dimensions). The hexagonal reinforcement description is selected to both avoid excessively high stress concentration associated with sharp cornered particles such as parallelepiped shaped reinforcement [63] and allow particle orientation variation which is not possible with a spherical description of reinforcement shape. However, the present geometric approach can easily accommodate any regular prismatic polyhedron shaped reinforcement. The alignment and prismatic form of the reinforcement particles are

selected to facilitate plane stress description of the full three dimensional model (see equations (32) and (33) in section 5.2).

In this geometric model the particles are described as discrete. This is achieved during the particle position random selection procedure described in chapter 5 by preventing particle overlap, particle contact and model boundary penetration. The discrete positioning of the particles avoids inconsistencies of reinforcement description. Examples of these possible inconsistencies can be found in the literature [203-206], where reinforcement overlap and contact is permitted in random distribution models. In these cases three inconsistencies can occur including the generation of large size reinforcement (two or more reinforcement regions acting as one or a reinforcement area penetrating a model boundary), reinforcement shape inconsistency (two or more regions combined giving a new reinforcement shape) and inaccurate volume fraction description (due to overlap of reinforcement regions).

To allow quantitative prediction the size scale of the geometric model must be defined. The size scale of the geometric model shown in figure 5.1 is primarily dependent on the maximum particle size limit and the minimum volume fraction resolution required. Based on both the finding of the present experiment investigations (section 6.1.2) and the reviewed literature [35,170,226] the maximum size selected for inclusion in the present model was 20 μ m (across corners hexagonal dimension). A minimum of three particles was selected to represent one per cent reinforcement volume fraction (based on the maximum particle size of 20 μ m). This allows a minimum volume fraction increment of $\frac{1}{3}\%$ between models containing 20 μ m particles. This is in excess of the resolution used in any existing random distribution models described in the reviewed literature [203-206]. Also, it should be note that as the particle size decreases the volume fraction resolution increases (i.e. for a 10 μ m particle model the minimum volume fraction increment between models is $\frac{1}{12}\%$).

Table 6.1. Number of hexagonal particles required for various composites.

Particle Size μm	Nominal Percentage Volume Fraction (%)					
	5	10	15	20	25	30
20	15	30	45	60	75	90
15	27	53	80	107	133	160
10	60	120	180	240	300	360
5	240	480	720	960	1200	1440

This selection of the maximum particle size and minimum volume fraction resolution defines the size scale of the model. Therefore, considering the size scale in two dimensions only, the area of a $20\mu\text{m}$ hexagonal area is $259.8\mu\text{m}^2$ and this area represents $\frac{1}{3}\%$ (minimum resolution) area fraction of the two dimensional model.

Consequently, the present three dimensional geometric model is $21.764 \times 10^{-3}\text{mm}^3$ in volume, that is, each side is $279.2\mu\text{m}$ in length (note equation (32) and (33) in chapter 5). Table 6.1 lists the number of hexagonal particles required to describe volume fractions ranging from 5% to 30% for particle sizes of $20\mu\text{m}$, $15\mu\text{m}$, $10\mu\text{m}$ and $5\mu\text{m}$ in this geometric model.

Selection of Mechanistic Framework

Due to the size scale of the geometric model defined above, dislocation and precipitate related mechanisms cannot be explicitly described in the present model. Therefore, the mechanistic framework suited to the present model is that of continuum mechanics. Consequently, the mechanisms which can be included must be suited to continuum mechanics description.

Composite Material Mechanisms

The mechanisms which can be described by continuum mechanics include load transfer, mismatch related residual stress development, internal stress concentration, constrained plastic flow, interfacial failure and particle fracture. However, in order to reduce the computational complexity of the present model, the matrix and reinforcement are considered perfectly bonded (no interfacial failure) and the

reinforcement particles are described as non-fracturing solids. These assumptions are commonly made in order to reduce the computational complexity of continuum mechanics based composite models [76,202,206,228]. Obviously, these simplifications affect the accuracy of the model. However, it is reported that a strong bond exists between the reinforcement particles and matrix in well processed SiC reinforced AMCs [37,209]. It is also important to note that due to the reported proportionality between particle size and incidence of particle fracture [169,170] the accuracy of the model will increase as the particle size selected decreases.

Due to the size scale of the geometric model and these interfacial strength and particle fracture related assumptions, the present model is limited to constitutive response and micromechanical predictions based on the mechanisms of load transfer, mismatch related residual stress development, internal stress concentration and constrained plastic flow. It is proposed that the inclusion of these mechanisms coupled with an accurate empirical description of the subcontinuum strengthening mechanisms permits reasonable accuracy up to the point of fracture initiation.

The assumptions that no particle fracture and no interfacial debonding can occur restricts the mechanisms on which failure prediction can be based to those relating to failure of the matrix material only. However, in the case of well processed (good interfacial bonding) and small particle size PRAMCs it is reported that fracture occurs predominantly through the matrix [169,170]. In the analyses carried out in the present work composite failure was described by the point at which non-convergence of the model solution occurred. This may be interpreted as the macroscopic true stress and true strain level which would cause a region of matrix material within the model to experience failure. Since a localised matrix material failure of this type (constrained microcrack in a ductile material) does not define macroscopic composite failure this criteria must underestimate the overall composite failure. However, unlike many composite models described in the reviewed literature that are restricted to analyses that are within a range that excludes the possibility of failure [193,202] or that completely ignore failure prediction [45,199,229] the present model allows

quantitative comparison of composite material failure between different variations of this model.

Material Parameters

Within the continuum mechanics framework the material parameters which can be described include the constitutive properties of both the reinforcement and the matrix (the accuracy of which depends on the accuracy of the phenomenological description selected and the material constants used), the reinforcement volume fraction, reinforcement size and size distribution, reinforcement shape, orientation and surface morphology and reinforcement distribution within the matrix. The chemical compatibility between the reinforcement and the matrix material cannot be explicitly described by continuum mechanics. However, due to the assumption of perfect matrix to reinforcement bonding this chemical compatibility parameter is irrelevant. The inclusion of the above listed material parameters in the present model compares favourably with the capabilities of the existing models described in the reviewed literature.

Computational Method

Due to the complexity and size of the model a numerical computational method is required. The numerical method selected for the present model is the finite element method (FEM). This selection is based primarily on the suitability of the method to the developed model in the context of mechanism inclusion and both material parameter inclusion and variation. The selection of the finite element method is also based on the availability of both suitable computational software and hardware. As stated in section 2.6, the majority of recent composite modelling research has focused on continuum mechanics based modelling using the FEM for solution computation due to the versatility of this method.

6.2.2 Modelling Analyses

In the present work the developed numerical model is used to investigate the evolution of thermal strain induced internal residual stress for the five AA6061(T6)+SiC models defined in chapter 5. In addition to these illuminating investigations, analyses are carried out to investigate both the internal stress development and the macroscopic constitutive response during tensile loading of thermally strained PRAMCs. The five model solutions obtained in the thermal strain investigations were used to describe the initial thermally strained models for the tensile loading investigations. The composite parameters investigated in these analyses include reinforcement volume fraction, size and distribution. The parameters kept constant for these analyses include matrix and reinforcement material constitutive response, and reinforcement size distribution, shape, orientation (although randomly selected) and surface morphology. It must be noted that the reinforcement distribution analyses results showed very little difference between the two random distributions analysed for each of the five models under tensile investigation. Therefore, the tensile loading discussion will only consider the results obtained from the tensile loading in the y direction.

In the following discussion regular reference is made to von Mises stress and both the maximum and minimum principal stresses. For clarity these terms are defined. The nodal von Mises stress is calculated based on the predicted nodal principal stresses as follows. Note that a plane stress approach is used. Therefore,

$$\sigma_e = \left(\frac{1}{2} \left[(\sigma_1)^2 + (\sigma_2)^2 + (\sigma_1 - \sigma_2)^2 \right] \right)^{1/2} \quad (40)$$

where,

σ_e = nodal von Mises stress

σ_1 = nodal algebraic[†] maximum principal stress

σ_2 = nodal algebraic minimum principal stress

[†] The term algebraic is used here in the same context as in reference [175], that is, the σ_1 value will be closer to $+\infty$ than the σ_2 value.

Thermal Strain

The von Mises stress map solutions for the thermal strain analyses carried out in the present work are shown in figures 5.8 to 5.12. Figure 5.8 (5% SiC 20 μ m) shows that the model predicts a reasonably uniform von Mises stress distribution within and surrounding positionally isolated reinforcement particles (for example, particle at bottom left hand corner, see figures 5.3 and 5.8). The von Mises stress within these isolated particles ranges from 129MPa at the centre up to 174.5MPa at the periphery (both von Mises). The principal stress results obtained indicate that these particles are in compression.

The compression of the particles due to a thermal contraction is expected due to the difference (mismatch) in coefficient of thermal expansion between the particle material and the surrounding matrix material ($4 \times 10^{-6}/^{\circ}\text{C}$ and $23.6 \times 10^{-6}/^{\circ}\text{C}$ respectively). As the temperature drops the aluminium contracts. However, an area occupied by the more rigid SiC material will not contract by the same amount as it would if this area consisted of the same aluminium matrix. Therefore, after a temperature drop the aluminium surrounding a hexagonal SiC particle imposes a near pure hydrostatic compressive stress condition on that particle.

For equilibrium, the compressed condition of the particle must be opposed by an equal and opposite compressive stress within the aluminium surrounding the particle. An analysis of the nodal stress conditions within the matrix material surrounding isolated particles shows that for each node the minimum principal stress (σ_2) is compressive and aligned with the line described by the node and the centre of the particle. The orthogonal maximum principal stress (σ_1) is tensile and obviously aligned tangentially to the particle perimeter. Also, this nodal analysis shows that the absolute magnitude of σ_1 is greater than that of σ_2 , and that both are small in comparison to the yield stress of the matrix (330MPa). For example, a typical nodal stress condition in such a region is $\sigma_1 = +33.7\text{MPa}$ and $\sigma_2 = -19.2\text{MPa}$ (von Mises stress = 46.38MPa).

For the same stress map solution (figure 5.8), the particles which are not isolated show a deviation from the uniform stress distribution observed in the case of isolated

particles, both within the particle and in the surrounding matrix material. In the centre of the model two high stress matrix material regions (maximum nodal von Mises stress = 246.7MPa left region, 237.9MPa right region) can be seen in the interstices between pairs of closely positioned particles (three particles at the centre of the model, see figure 5.3 and figure 5.8). As in the case of the isolated particles, these particles exhibit a general compressive stress condition and the surrounding matrix material exhibits compressive stress in the radial direction and tensile stress in the tangential direction (relative to the closest particle). Obviously, the matrix material interstices also follow a similar trend to the rest of the surrounding matrix material. However, in these regions two particles strongly influence the reaction of the matrix material to the thermal strain and therefore, a condition of high compressive stress develops in the direction described by the shortest interstitial distance.

The maximum von Mises stress levels recorded (up to 326MPa) for this analysis (5% SiC 20 μ m) occur in the interstices of two pairs of particles located in the bottom right hand corner of the model as shown in figure 5.8 (also refer to figure 5.3 for particle positions). The shortest interstitial distance between particles in the case of both of these pairs is approximately half that of the particles in the centre of the model discussed above (see figure 5.3 to compare). These high interstitial stresses are also accompanied by a change in the stress distribution both within the individual particles and in the surrounding matrix material. The results show that the stress distribution is not uniform, but is concentrated at both the interstice and the matrix material surrounding all the particle corners (figure 5.8). Analysis of the stress state at individual nodes in these regions indicates that these high concentrations of stress in the particle corner regions may be due to the reaction of the particles to the very high levels of stress in the interstices. Also, the principal stress results recorded show that the direction of the numerical maximum principal stresses (the principal stresses with the highest absolute numerical value, in this case σ_2) for the nodes at the particle corners tend strongly towards alignment with the direction of the line which describes the shortest interstitial distance. Obviously, the numerical maximum principal stresses in the interstice also follow this direction. Therefore, these particles which are in close proximity (localised clustering) not only cause the development of high compressive

4.2.6 Lubricant Type and Quantity

Test Matrix No. 3

It was observed that zinc stearate powder solid lubricant increases compressibility compared to the synthetic wax AcrawaxTM irrespective of lubricant quantity, as shown in figure 4.10. This increase was as large as 2% TD in the case of the 3% lubricant by weight powder mixtures. Also, in the case of both lubricants investigated, the quantity of lubricant has a definite affect on compressibility. In all combinations of annealing atmosphere and lubricant type it is seen (figure 4.10) that as the lubricant quantity increases from 0.5% to 3%, the powder compressibility decreases by approximately 2% TD. This decrease in compressibility can be directly attributed to the larger volume occupied by the greater quantity of lubricant.

4.2.7 Aluminium Alloy Type

Test Matrix No. 2

Attempts to press AA2124 as-supplied powder based powder blends were made in test matrix no. 2. However, the pressed green compacts experienced extensive damage during ejection. Therefore, no valid compressibility test results are available for powder blends containing as-supplied AA2124.

Test Matrix No. 3

Composite powder compressibility tests were carried out on identically processed powder blends of 10% SiC/AA6061 and 10% SiC/AA2124 (0.5% zinc stearate powder lubricant). The effect of alloy type on the compressibility of these nitrogen annealed (475°C) powders indicates a marginally greater compressibility of the AA6061 based powder, compared to the higher strength Al-Cu alloy AA2124 based composite powder. The AA6061 based powder was compressible to an average of 88.12 %TD, which is only very slightly greater than the 87.85 %TD average recorded for the AA2124 based material. It should also be noted that the high compressibility and good quality of the heat treated AA2124 based powder blends compared to the

magnitude of this stress depends on both the proximity and the relative orientation of the particles. It is found that two separate pairs of particles which exhibit a similar shortest interstitial distance may develop different stress levels. The higher interstitial stress levels are found between pairs of particles whose closest facets include particle corners. The lower stress levels are recorded in the cases where the closest facets are the sides of the particles (i.e. the sides are close to parallel).

In the case of the 10 μ m particle model (5% SiC 10 μ m, figure 5.12), similar stress directionality trends to those observed for the 20 μ m models are predicted. However, this model solution also indicates that the distance between particles can be far smaller before a high stress interstitial region develops, compared to that for the 20 μ m cases. By comparing both the interstitial distance and the nodal stress results in the region of the interstices between pairs of 20 μ m particles with those for pairs of 10 μ m particles, a general relationship was found. This analysis indicates that for pairs of particles with similar relative particle orientations and similar levels of interstitial stress, the interstitial distance in the case of a 10 μ m pair is approximately half that for a 20 μ m pair. This relationship is expected since the coefficient of thermal expansion is based on a temperature difference and a relative length parameter.

Table 5.2 shows that the 10 μ m model predicts plastic deformation within this 5% SiC model due to the thermal strain. Two regions within this model exhibit von Mises stress levels above the yield stress of the matrix material (maximum stresses of 357MPa and 335MPa). Both of these high stress interstitial regions are between particles which are in very close proximity (compare stress map in figure 5.12 with geometric model in figure 5.7).

The continuum mechanics based numerical results discussed above predict that thermal strain can cause localised internal plastic deformation within a PRAMC and that the extent of this plastic deformation is related to the reinforcement volume fraction, the particle size, the proximity of reinforcement particles and the relative orientation of the particles in close proximity. These numeric predictions also show that the plastic deformation is mainly due to the development of high compressive

stress in the interstitial matrix material between particles in close proximity and that the direction of these high interstitial stresses follow the direction of the shortest interstitial distance between particles.

The magnitude of the thermal strain applied to these models, from 170°C to 24°C, was based on the artificial ageing heat treatment temperature normally applied to achieve a T6 condition and standard room temperature. However, considering the larger temperature drop experienced during the solution heat treatment step which is carried out before ageing (approximately 515°C to 0°C) it must be assumed that the model underestimates the magnitude of the thermal strain induced residual stress. Therefore, these composites may experience localised matrix failure and possibly particle fracture (for large particles) during heat treatment processing. The resulting microcracks in the composite may be a contributing factor to the general low ductility exhibited by many PRAMCs.

Tensile Loading

The five thermally strained models discussed above were used to describe the initial internal stress conditions for the tensile loading investigations (loading in the y direction). A detailed analysis of the predicted nodal stresses at each sub-step of the tensile loading simulation was carried out for all five models. It was found that similar internal stress related trends occur in all five models. It should be noted that as the tensile load increases during the simulation, the orientation of the principal stresses tend towards alignment with the Cartesian axes. Therefore, in the following discussion reference is made to the stress related to the Cartesian axes.

The nodal analyses indicate that as the tensile load is applied to these thermally strained materials the initial compressive stress within the particles begins to increase (i.e. the stress increases toward a state of tensile stress) in both the x direction and the y direction. However, the stress in the y direction increases by a far greater amount for each sub-step compared to the small stress increase in the x direction.

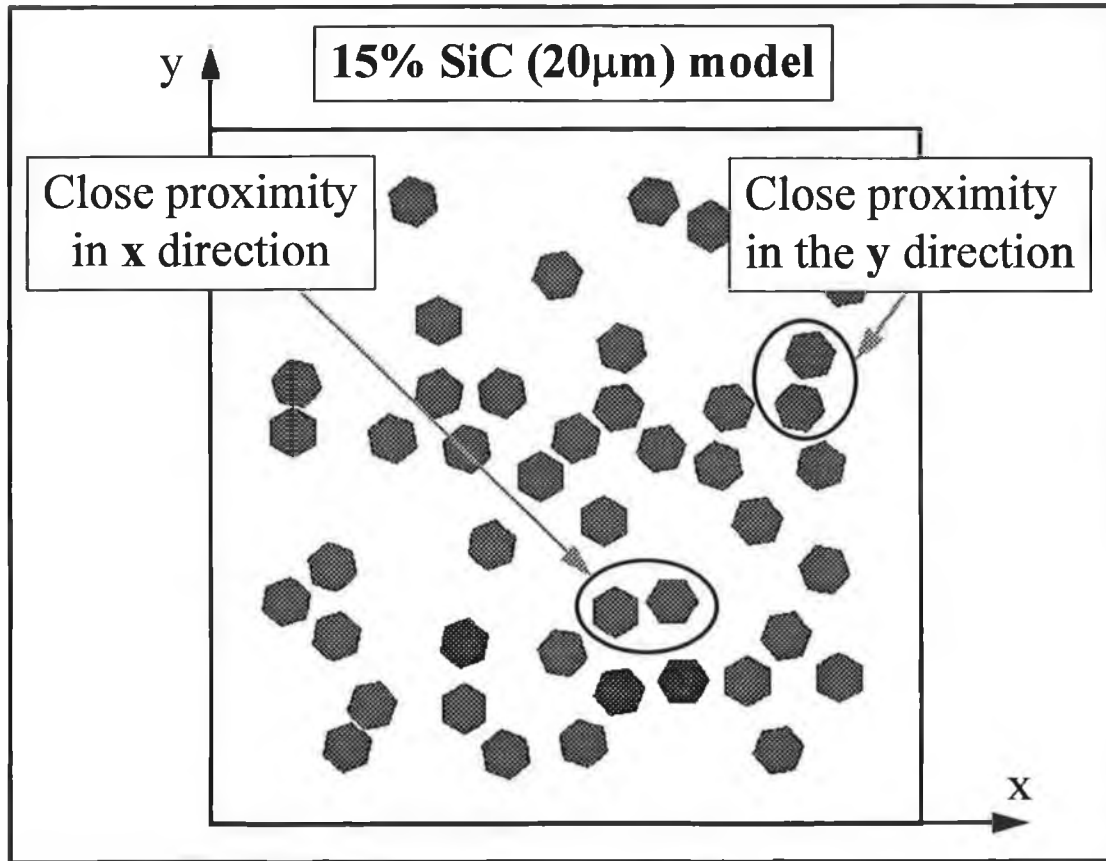


Figure 6.1. Examples of particles in close proximity in both x and y direction.

The internal stress within the matrix material also follows a specific trend. In the case of the matrix material the high stress interstitial regions between particles which are in close proximity in the x direction (see figure 6.1), exhibit increasing von Mises stress levels during the entire tensile loading simulation. However, the interstitial regions between particles which are in close proximity in the y direction initially exhibit decreasing von Mises stress levels followed by increasing levels during loading. Examples of the interstitial nodal stress development during tensile loading for both cases are quantitatively presented in figure 6.2. Also, these trends can be seen by comparing the initial von Mises stress distribution for each model (figures 5.8 - 5.12) with the predicted von Mises internal stress distribution at half full load (figure 5.13 - 5.17). In these half full load stress maps the high stress regions tend towards alignment with the x axis. The most clear example of this can be seen in the case of the 5% SiC 10 μ m model (compare figures 5.12 and 5.17).

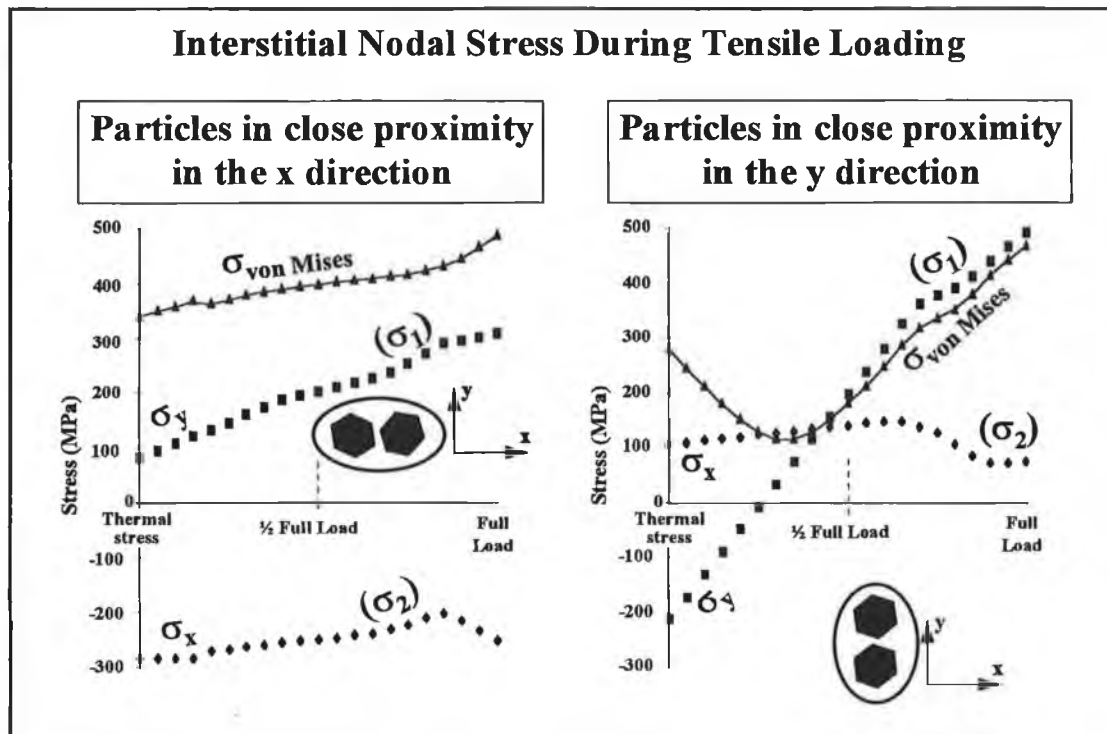


Figure 6.2. Examples of the interstitial nodal stress results for pairs of particles in close proximity in the x (left) and y (right) directions.

Although localised plastic deformation is predicted within the matrix material of all five models at half full tensile load, the macroscopic response of the models is elastic (see flow stress curves in figure 5.23). As the tensile analysis progresses from the half full load towards full loading the model begins to exhibit not only localised plasticity in the interstitial regions between particles in close proximity in the x direction, but also plastic deformation in the entire matrix material. As this overall plastic deformation occurs the internal stress distribution tends to change. This change in stress distribution does not follow very specific trends. However, in general the model indicates that the high stress interstitial regions predicted in the half full load stage continue to become more highly stressed and also a number of matrix material regions in close proximity to particle corners on either the left or right hand sides of particles begin to exhibit high levels of stress (figures 5.18 - 5.22). In all cases the maximum von Mises stress recorded in the final sub-step of the tensile analyses occurs in either an interstitial region (between particles in close proximity in the x direction) or around a particle corner on the left or right of a particle.

Detailed analyses of the nodal stress development in these critical regions elucidate the micromechanical mechanisms which occur during the tensile loading. These analyses indicate that as the tensile load increases, the directionality of the principal stresses within these regions become aligned with the x and y axes. The algebraic minimum principal stress (σ_2) at each node tends towards alignment with the x axis as the tensile load is applied in the y direction. However, the magnitude of this principal stress does not change by a large amount (remains at a high level of compressive stress, figure 6.2). Conversely, the algebraic maximum principal stress (σ_1) tends towards alignment with the y axis (direction of tensile loading) and increases substantially during loading. Consequently, the difference between σ_1 and σ_2 within the interstices increases by a greater amount in these regions compared to any other region within the model. This difference in principal stress is directly related to the magnitude of the von Mises stress (see equation (40) and figure 6.2). This explains the increase of the von Mises stress levels within these regions during tensile loading.

In the case of the previously high stressed interstitial regions between particles which are in close proximity in the y direction, the high compressive stress (σ_2) due to the thermal strain loading is primarily aligned with the y axis. Also, the algebraic maximum principal stress (σ_1 , which is tensile) in these regions is primarily aligned with the x direction. As the tensile load is applied the high compressive stress in the y direction increases (i.e. the stress increases toward a state of tensile stress) and the tensile stress in the x direction also increases in magnitude. However, the rate of increase in both directions is not equal. The rate of increase in the x direction is far less than the rate of increase in the y direction (figure 6.2). Consequently, the difference between the maximum and minimum principal stress at each node decreases until σ_1 is equal to σ_2 , after which the difference begins to increase. However, this increase occurs too late in the analysis to develop a large difference between the principal stresses before non-convergence of the model (non-convergence used to indicate failure). Therefore, due to the direct relationship between von Mises stress and the difference between the principal stresses these regions exhibit lower stress levels during loading and at full load than the interstitial regions between particles in close proximity in the x direction.

The macroscopic true stress/true strain response of the thermally strained models can be seen in figure 5.23. This figure shows that the model predicts increasing stiffness, strain hardening and flow strength, and decreasing ductility with increased volume fraction reinforcement. These predictions are consistent with experimental evidence. The stiffness is quantified by the modulus of elasticity listed in figure 5.23. Comparison between these predicted values and values obtained by experiment [35,45] shows that although the model predicts the expected trend, the modelling analysis results slightly underestimate the actual increases exhibited by the equivalent experimental composites. This indicates that the increase in stiffness exhibited by well processed composites is not only due to the load bearing effect of the more rigid reinforcement particles. Indirect effects such as the increased dislocation and precipitate density at the particle matrix interface should also increase the stiffness by elevating the modulus of elasticity of the in-situ matrix material [162].

The predicted increasing strain hardening (indicated by the increase in flow curve gradient) and flow strength of the composite material also follow the expected trends [35]. However, no modelling or experimental results are available in the literature to allow quantitative comparison. It should be noted that the predicted ductility and maximum true stress values are based purely on the point at which the numerical model becomes non-convergent. Therefore, these values should be regarded as conservative.

The modulus of elasticity predicted by the model containing the smaller 10 μ m particles was found to be identical to the 20 μ m particle model containing the same volume fraction. This follows the general trend observed by experiment that the modulus of the composite is independent of the reinforcement particle size [45].

Based on these predicted trends the internal stress development during tensile loading of a thermally strained composite depends on the directionality of particle clustering. To avoid the evolution of localised high stressed regions within a real composite undergoing tensile deformation the reinforcement should not be in close proximity in

the plane normal to the direction in which the load is applied. Also, the level of stress within particle clusters may be reduced by the use of particles which do not exhibit sharp corners and edges. Unfortunately, no experimental or modelling analyses of a comparable nature to these present analyses can be found in the literature. Therefore, further work is required in the area to clarify these finds. However, it should be noted that although reinforcement particles which do not exhibit sharp corners and edges are available, the position of reinforcement particles within a matrix material is extremely difficult to control. Based on this technical factor it may be more realistic to suggest that any processing method used for the production of PRAMCs must minimise particle clustering in all planes.

The macroscopic response predicted by the present model can provide useful qualitative indication of PRAMC mechanical properties including stiffness, strain hardening, flow strength and ductility. However, further model development is required in the specific area of composite failure to allow full quantitative description of these quantities. Also, this development must be coupled with experimental work to allow model validation at the macroscopic level.

6.2.3 Outline of the Numerical Modelling Work Findings

The new modelling approach introduced in this work provides a platform for detailed micromechanical simulation of PRAMCs. This model offers many facilities which are not available from the existing modelling approaches. The facilities offered by this model include the capabilities of varying reinforcement particle distribution, particle size and size distribution, volume fraction, particle shape, orientation and morphology, and the constitutive response of both the matrix and reinforcement materials.

The present analyses carried out with this model clearly show how this model may be used to elucidate the individual factors affecting the internal stress development during thermal straining and mechanical loading. The results and observations indicate that a possible contributing factor to the low ductility of PRAMCs can be the existence of internal matrix damage caused during heat treatment. Also, these analyses indicate that relationships exist between the level of internal stress developed and the level of reinforcement used, the proximity, relative orientation (facets in close proximity) and size of particles, and the directionality of particle clustering.

6.3 MATERIALS DEVELOPMENT

The contributions to PRAMC materials development arising from this work come from both the process optimisation and numerical modelling work. The novel application of the conventional pressing and sintering powder metallurgical processing route to the processing of PRAMCs introduced and described in this work provides an attractive processing method for the production of net shape and near net shape PRAMC components. Also, the new modelling approach introduced provides a method of analysing the effects of various individual parameters on the micromechanical and macroscopic response of fully processed PRAMCs to thermal and mechanical loading. The versatility of both the processing method and the modelling approach provides a basis for systematic further development of these composite materials.

The mechanical properties of a number of aluminium alloys and PRAMCs are listed in table 6.2 for comparison to the composites produced in the present work. This table shows that the processing route investigated and developed in this work can be used to produce composite material which exhibits improved mechanical properties compared to the monolithic material and comparable properties to PRAMCs produced by both casting and spray deposition. However, unlike PRAMC casting processes, the temperatures involved in the present sintering process never exceed the melting temperature of the aluminium alloy. This low temperature avoids undesirable interfacial reaction and allows the use of a wide range of reinforcement and aluminium alloys. Compared to the spray deposition process the present pressing and sintering route provides a means to produce net shape and near net shape components which cannot be spray processed. Also, the specialised canning, degassing and isostatic pressing processing stages carried out in most other powder metallurgical PRAMC processes are avoided in the present near conventional process. Therefore, the process development work carried out provides an attractive alternative to the existing processing routes for the production of net shape and near net shape small to medium size components.

Table 6.2. Mechanical properties of PRAMCs produced in the present work and the properties of relevant monolithic aluminium alloys and PRAMCs produced by other processing methods.

Material, (Heat Treat.), Process	Hardness HRB	Density (TD)	Yield Strength MPa	UTS MPa	Ref.
AA6061 10%SiC, (T6)	69	97%-98%	340-400 Compressive	284-324 20%SiC	†
AA2124 10%SiC, (T4)	68-82.5	93%- 98.2%	-	-	†
AA6061, (T6), Wrought	47-72	92.5%- 96.8%	303-317	303-345	[99]
AA2024, (T6), Wrought	74.5-83.5	92.5%- 96.8%	386-414	393-434	[99]
AA6061, (T6), PM-Ext.	-	91.1%- 96%	237-241	241-252	[71]
AA2124, (T6), PM-Ext.	-	91%-97%	339-354	343-356	[71]
AA6061 10%SiC, (T6), Cast-Ext.	-	-	345	375	[125]
AA2124 10%SiC, (T6), Spray Depos.	-	-	437	484	[55]
AA6061 20%SiC, (T6), PM-Ext.			415	498	[20]

† Refers to the PRAMCs produced in the present research.

The present continuum based modelling approach also compares well with existing modelling approaches. This modelling method is limited only by the accuracy of the continuum based phenomenological material descriptions and the computational capacity of the hardware available.

CHAPTER 7 CONCLUSIONS, CONTRIBUTIONS AND PROPOSED FURTHER RESEARCH

7.1 CONCLUSIONS

- The cold pressing and sintering powder metallurgical processing method can be used to produce well consolidated small to medium size net shape and near net shape PRAMC components containing up to 20% reinforcement with careful design of equipment to ensure temperature and atmosphere control during processing. In the present work PRAMCs exhibiting ultimate tensile strength of 324 MPa, hardness of 82.5 HRB and compressive yield strength of 456 MPa have been produced by this method.
- The novel powder heat treatment processing stage introduced in the present work is of paramount importance to the success of the process. The heat treatment increases powder compressibility by up to 6.2% theoretical density, allows green densities of up to 89% be achieved (10%SiC, 220MPa), increases compact green strength by up to 200% compared to as-supplied powder compacts, and reduces powder H₂O content.
- The homogeneity of reinforcement distribution within the final composite primarily depends on the reinforcement particle size, the matrix powder size and the effectiveness of the mixing method used. For good reinforcement distribution similar reinforcement and matrix sizes should be selected and rapid reciprocation mixing should be used. Matrix powder within the range from 3µm to 20µm and reinforcement particulate within the range from 5µm to 20µm can be used.
- Sintering must be carried out in a oxidation inhibiting atmosphere, and sintering temperature and time must be carefully controlled to both avoid the development

of large outer layers and promote maximum consolidation during sintering. The optimum sintering time and temperature can depend on the alloy used. In the case of AA2124 and AA6061 based composites respectively: 98.2% TD can be achieved by sintering at 617°C for 180 minutes and 97% TD can be achieved by sintering at 617°C for between 20 and 180 minutes.

- The penetration of aluminium powder by reinforcement particles must occur during compaction to promote good consolidation during sintering.
- The new PRAMC model developed in the present work provides a method of investigating the effects of many composite parameters on both the microscopic and macroscopic response of a composite material.
- The model indicates that high stress levels develop both in interstitial regions between reinforcement particles in close proximity and at particle corners during cooling and tensile loading. Therefore, particle clustering in real composites must be minimised to avoid high internal stress development. Also, sharp cornered reinforcement should be avoided.

7.2 CONTRIBUTIONS

- The process developed in the present work provides a new near conventional powder metallurgical based method of producing PRAMC components without the need for expensive powder canning, degassing or isostatic pressing.
- The model developed in the present work provides a new versatile method of analysing the effects of individual parameters on the micromechanical and macroscopic response of fully processed PRAMC material to thermal and mechanical loading.

7.3 PROPOSED FURTHER RESEARCH

It is proposed that the following research and development would further contribute to the present field of study.

Processing

- A systematic processing investigation using various combinations of narrow size distribution reinforcement particles and matrix powders to elucidate further the effects of powder size, reinforcement size, size ratio and reinforcement volume fraction on composite homogeneity, compressibility and final material condition.
- An analysis of the effects of warm uniaxial pressing on green compact characteristics and final composite material condition.
- An investigation of the relationships between final composite heat treatment time and temperature and the mechanical properties of the heat treated composites.
- The development of a sintering facility which allows sample removal during sintering without affecting the sintering atmosphere or temperature. This facility should also allow very close control over sintering temperature, time and atmosphere. This equipment should allow detailed investigations of the composite material during sintering at various temperatures and times.
- The development of an automated die wall lubrication system to eliminate the need for mixed-in lubrication.
- The incorporation of a sieving system to eliminate powder and particle clusters before mixing.

- The development of an automated die filling system to increase the rate at which green samples can be produced.

Modelling

- The extension of the present modelling approach to allow plane strain analyses and to incorporate a self-consistent boundary.
- The refinement of the composite failure prediction capabilities of the present model.
- The development of a facility to allow automatic random particle position and orientation selection.
- Quantitative validation of the present modelling approach by means of a combined experimental and modelling investigation.

REFERENCES

- [1] Kay E., Solid Thin Films, Annual Review of Materials Science, Vol. 1, pp 289-312, 1971.
- [2] Suresh S., Mortensen A., Needleman A., Fundamentals of Metal Matrix Composites, Butterworth-Heinemann, ISBN 0-7506-9321-5, 1993.
- [3] Composites, Vol. 1, ASM International, Engineering Materials Handbook, American Society For Metals, Metals Park, Ohio 44073, ISBN 0-87170-279-7 (v. 1), 1989.
- [4] Froes F.H., Advanced Metals for Aerospace and Automotive Use, Materials Science and Engineering, Vol. A184, pp 119-133, 1994.
- [5] Hull M., Commercial Success for MMCs, Powder Metallurgy, Vol. 41, No. 1, pp 25-26, 1998.
- [6] Zeuner T., On Track with MMC Brake Disks, Materials World, Vol. 6, No. 1, pp 17-19, 1998.
- [7] Curran G., MMCs: The Future, Materials World, Vol. 6, No. 1, pp 20-21, 1998.
- [8] Baker C., Metal Matrix Composites VI, Materials World, Vol. 6, No. 1, pp 22-23, 1998.
- [9] Gurganus T.B., Gilliland R.G., Hunt W.H., Composite Technology - Parameters Influencing Production, Properties and Use:1, Industrial Heating, pp 46-50, February, 1990.
- [10] Chou T.W., Kelly A., Okura A., Fibre-Reinforced Metal Matrix Composites, Composites, Vol. 16, No. 3, pp 187-206, July, 1985.
- [11] Bhagat R.B., Emerging P/M Metal Matrix Composites, Advances in Powder Metallurgy & Particulate Materials-1992, Vol. 9, pp 139-146, ISBN 1-878954-28-8, 1992.

- [12] Torralba J.M., da Costa C.E., Cambronero L.E.G., Ruiz-Prieto J.M., P/M Aluminum Composite Reinforced with Ni_3Al , Key Engineering Materials, Vol. 127-131, pp 929-936, 1997.
- [13] Schmid E., German Patent No. 425452, 1924. (in German)
- [14] Clyne T.W., Withers P.J., An Introduction to Metal Matrix Composites, Cambridge University Press, ISBN 0-521-41808-9, 1993.
- [15] Pickens J.R., Aluminium Powder Metallurgy Technology for High-Strength Applications, Journal of Materials Science, Vol. 16, pp 1437-1457, 1981.
- [16] Nembach E., Particle Strengthening of Metals and Alloys, John Wiley & Sons Inc., ISBN 0-471-12072-3, 1997.
- [17] Thümmel F., Oberacker R., Introduction to Powder Metallurgy, eds. Jenkins I. and Wood J.V., The Institute of Materials, ISBN 0-901716-26-X, 1993.
- [18] Properties and Selection: Nonferrous Alloys and Special-Purpose Materials, Vol. 2, ASM International, Metals Handbook, American Society For Metals, Metals Park, Ohio 44073, IBSN 0-87170-378-5 (v. 2), 1990.
- [19] Eliasson J., Sandström R., Applications of Aluminium Matrix Composites, Key Engineering Materials, Vol. 104-107, pp 3-35, 1995.
- [20] Srivatsan T.S., Ibrahim I.A., Mohamed F.A., Lavernia E.J., Processing Techniques for Particulate-Reinforced Metal Matrix Composites, Journal of Materials Science, Vol. 26, pp 5965-5978, 1991.
- [21] Degischer H.P., Schulz P., Lacom W., Properties of Continuous Fibre Reinforced Al- and Mg- Matrix Composites Produced by Gas Pressure Infiltration, Key Engineering Materials, Vol. 127-131, pp 99-110, 1997.
- [22] Warriar S.G., Majumdar B.S., Miracle D.B., Interface Effects on Crack Deflection and Bridging During Fatigue Crack Growth of Titanium Matrix Composites, Acta Metallurgica, Vol. 45, pp 4969-4980, 1997.
- [23] Dève H.E., Compressive Strength of Continuous Fiber Reinforced Aluminum Matrix Composites, Acta Metallurgica, Vol. 45, pp 5041-5046, 1997.
- [24] Trumper R.L., Metal Matrix Composites - Applications and Prospects, Metals and Materials, Vol. 3, pp 662-667, November, 1987.

- [25] Millière C., Suéry M., Fabrication and Properties of Metal Matrix Composites based on SiC Fibre Reinforced Aluminium Alloys., *Materials Science and Technology*, Vol. 4, pp 41-51, January, 1988.
- [26] Hunt W.H. Jr., Cook C.R., Sawtell R.R., Cost-Effective High Performance P/M Aluminum Matrix Composites for Automotive Applications, *International Congress and Exposition, Detroit, Michigan, USA, SAE Technical Paper Series, 910834*, pp 1-11, February-March, 1991.
- [27] Allison J.E., Davis L.C., Jones J.W., Metal Matrix Composites by Design, *Proc. of ICCM-10, Whistler, BC, Canada, Part 2*, pp 345-352, August, 1995.
- [28] Sundararajan S., Mahadevan R., Dwarakadasa E.S., Particulate Metal Matrix Composite Material Development for I.C. Engine Piston Application, in *Proc. of ICCM-10, Whistler, BC, Canada, Part 2*, pp 831-838, August, 1995.
- [29] Mohn W.R., Vukobratovich D., Recent Applications of Metal Matrix Composites in Precision Instruments and Optical Systems, *Journal of Materials Engineering*, Vol. 10, pp 225-235, 1988.
- [30] Divecha A.P., Fishman S.G., Karmarkar S.D., Silicon Carbide Reinforced Aluminum - A Formable Composite, *Journal of Metals*, pp 12-17, September, 1981.
- [31] Divecha A.P., Fishman S.G., Progress in the Development of SiC/Al Alloys, *SAMPE Quarterly*, pp 40-42, April, 1981.
- [32] Webster D., Effect of Lithium on the Mechanical Properties and Microstructure of SiC Whisker Reinforced Aluminum Alloys, *Metallurgical Transactions A*, Vol. 13A, pp 1511-1519, August, 1982.
- [33] Arsenault R.J., The Strengthening of Aluminium Alloy 6061 by Fibre and Platelet Silicon Carbide, *Materials Science and Engineering*, Vol. 64, pp 171-181, 1984.
- [34] Ham-Su R., Wilkinson D.S., The Role of Platelet Orientation on the Creep Behaviour of Al₂O₃/SiC Composites, *Key Engineering Materials*, Vol. 127-131, pp 885-888, 1997.
- [35] Lloyd D.J., Particle Reinforced Aluminium and Magnesium Matrix Composites, *International Materials Reviews*, Vol. 39, No.1, pp 1-23, 1994.

- [36] Hunt W.H. Jr., Rodjom T.J., Discontinuously Reinforced Aluminium Materials by Powder Metallurgy Processes, *Advances in Powder Metallurgy & Particulate Materials-1992*, Vol. 9, pp 21-32, ISBN 1-878954-28-8, 1992.
- [37] Nair S.V., Tien J.K., Bates R.C., SiC-Reinforced Aluminium Metal Matrix Composites, *International Metals Reviews*, Vol. 30, No.6, pp 275-288, 1985.
- [38] McKimpson M.G., Scott T.E., Processing and Properties of Metal Matrix Composites Containing Discontinuous Reinforcement, *Materials Science and Engineering*, Vol. A107, pp 93-106, 1989.
- [39] McDanel D. L., Analysis of Stress-Strain, Fracture, and Ductility Behavior of Aluminum Matrix Composites Containing Discontinuous Silicon Carbide Reinforcement, *Metallurgical Transactions A*, Vol. 16A, pp 1105-1115, June, 1985.
- [40] Clyne T.W., Bader M.G., Cappleman G.R., Hubert P.A., The Use of a δ -Alumina Fibre for Metal-Matrix Composites, *Journal of Materials Science*, Vol. 20, pp 85-96, 1985.
- [41] Thomas M.P., King J.E., Effect of Thermal and Mechanical Processing on Tensile Properties of Powder Formed 2124 Aluminium and 2124Al-SiC_p Metal Matrix Composites, *Materials Science and Technology*, Vol. 9, pp 742-753, September, 1993.
- [42] Preet M.S., Lewandowski J.J., Effects of Heat Treatment and Reinforcement Size on Reinforcement Fracture During Tension Testing of a SiC_p Discontinuously Reinforced Aluminium Alloy, *Metallurgical Transactions A*, Vol. 24A, pp 2531-2543, November, 1993.
- [43] Xiaomin N., Maclean M.S., Baker T.N., Design Aspects of Processing of Aluminium 6061 Based Metal Matrix Composites via Powder Metallurgy, *Materials Science and Technology*, Vol. 10, pp 452-459, June, 1994.
- [44] Karnezis P.A., Durrant G., Cantor B., Palmiere E.J., Mechanical Properties and Microstructure of Twin Roll Cast Al-7Si/SiC_p MMC's, *Materials Science and Technology*, Vol. 11, pp 741-751, August, 1995.
- [45] Shyong J.H., Derby B., The Deformation Characteristics of SiC Particle-Reinforced Aluminium Alloy 6061, *Materials Science and Engineering*, Vol. A197, pp 11-18, 1995.

- [46] Pagounis E., Lindroos V.K., Processing and Properties of Particulate Reinforced Steel Matrix Composites, *Materials Science and Engineering*, Vol. A246, pp 221-234, 1998.
- [47] Lee D.M., Suh B.K., Kim B.G., Lee J.S., Lee C.H., Fabrication, Microstructures, and Tensile Properties of Magnesium Alloy AZ91/SiC_p Composites Produced by Powder Metallurgy, *Materials Science and Technology*, Vol. 13, pp 590-595, July, 1997.
- [48] Liu J., Shi Z., Gu M., Di Zh., Wu R., An G., Study on the Behaviors of Antifriction and Wear Resistance of Silicon Particulates Reinforced Zinc Matrix Composites, *Proc. of AMPT98*, Kuala Lumpur, Malaysia, eds. Hamouda A.M.S., Sulaiman S., and Ahmadun M., Vol. 1, pp 451-457, August, 1998.
- [49] Abkowitz S., Weihrauch P., Trimming the Cost of MMC's, *Advanced Materials & Processes*, pp 31-34, 7/1989.
- [50] Flom Y., Arsenault R.J., Interfacial Bond Strength in an Aluminium Alloy 6061-SiC Composite, *Materials Science and Engineering*, Vol. 77, pp 191-197, 1986.
- [51] Flom Y., Arsenault R.J., Deformation in Al-SiC Composites Due to Thermal Stresses, *Materials Science and Engineering*, Vol. 75, pp 151-167, 1985.
- [52] Erich D.L., Metal-Matrix Composites; Problems, Applications, and Potential in the PM Industry, *Metal Powder Report*, pp 418-423, June, 1988.
- [53] Brazil D., Monaghan J., Aspinwall D.K., Ng E-G, Wear Characteristics of Various Diamond Tooling When Single Point Turning a Particulate Reinforced Metal Matrix Composite, *Proc. of IMC-14*, Dublin, Ireland, eds. Monaghan J. and Lyons C.G., pp 143-152, September, 1997.
- [54] Müller F., Monaghan J., Electro Discharge Machined Surface Characterisation of a Particle Reinforced Metal Matrix Composite, *Proc. of IMC-14*, Dublin, Ireland, eds. Monaghan J. and Lyons C.G., pp 461-470, September, 1997.
- [55] Chadwick G.A., Heath P.J., Machining Metal Matrix Composites, *Metals and Materials*, pp 73-76, February, 1990.
- [56] Gurganus T. B., Aluminium Powder Applications, *Advanced Materials & Processes*, pp 57-59, 8/1995.

- [57] Schwartz M., Composite Materials Handbook 2nd Edition, McGraw-Hill Inc., ISBN 0-07-055819-1, 1992.
- [58] McHugh P.E., Asaro R.J., Shih C.F., Computational Modeling of Metal Matrix Composite Materials-I. Isothermal Deformation Patterns in Ideal Microstructures, *Acta Metallurgica et Materialia*, Vol. 41, pp 1461-1476, 1993.
- [59] Harren S.V., Dève H.E., Asaro R.J., Shear Band Formation in Plane Strain Compression, *Acta Metallurgica*, Vol. 36, pp 2435-2480, 1988.
- [60] Bruzzi M., Eberhardt M., McHugh P.E., Micro-Macro Modelling of the Mechanical Behaviour of MMC's During Cyclic Loading, *Proc. of IMC-14*, eds. Monaghan J. and Lyons C.G., pp 163-172, September, 1997.
- [61] Levin M., Karlsson B., Influence of SiC Particle Distribution and Prestraining on Fatigue Crack Growth Rates in Aluminium AA6061-SiC Composite Material, *Materials Science and Technology*, Vol. 7, pp 596-607, 1991.
- [62] Takao Y., Taya M., The Effect of Variable Fiber Aspect Ratio on the Stiffness and Thermal Expansion Coefficients of a Short Fiber Composite, *Journal of Composite Materials*, Vol. 21, pp 140-156, 1987.
- [63] Christman T., Needleman A., Suresh S., An Experimental and Numerical Study of Deformation in Metal-Ceramic Composites, *Acta Metallurgica*, Vol. 37, No.11, pp 3029-3050, 1989.
- [64] Noguchi M., Takahashi K., Status and Prospects for Metal Matrix Composites in Japan, *Key Engineering Materials*, Vol. 127, pp 153-164, 1997.
- [65] The New Encyclopædia Britannica, Vol. 3, page 518, ISBN 0-85229-605-3.
- [66] Wu G., Zhao Y., Kono N., Watanabe H., Takahashi T., Fabrication of SiC_w-Al₂O_{3p}/6061 Alloy Composite and its Mechanical Properties, *Key Engineering Materials*, Vol. 104-107, pp 467-474, 1995.
- [67] Wu G., Zhao Y., Kono N., Watanabe H., Takahashi T., Strengthening Mechanism of SiC_w-Al₂O_{3p}/6061 Aluminum Alloy Composites, *Key Engineering Materials*, Vol. 104-107, pp 647-654, 1995.
- [68] Chawla K.K., Ceramic Matrix Composites, Chapman & Hall, ISBN 0-412-36740-8, 1993.

- [69] Kishi T., Enoki M., Development of Ceramic Matrix Composites and the Meaning of Microcracks, *Key Engineering Materials*, Vol. 127, pp 63-72, 1997.
- [70] Beesley C.P., The Application of CMCs in High Integrity Gas Turbine Engines, *Key Engineering Materials*, Vol. 127, pp 165-174, 1997.
- [71] Schiroky G.H., Miller D.V., Aghajanian M.K., Fareed A.S., Fabrication of CMCs and MMCs Using Novel Processes, *Key Engineering Materials*, Vol. 127-131, pp 141-152, 1997.
- [72] Bruhn J., Schicker S., García D.E., Janssen R., Wagner F., Claussen N., Novel Reaction-Based Processing of Co-Continuous Ceramic-Metal Composites, *Key Engineering Materials*, Vol. 127-131, pp 73-80, 1997.
- [73] Zedalis M.S., Peltier J.M., Gilman P.S., High Temperature Al-Fe-V-Si Base Matrix Composites: Mechanical Properties and Microstructure, *The Metallurgical Society of AIME*, Warrendale, PA, pp 323-334, 1989.
- [74] Fan Z., Grant P.S., Cantor B., Manufacture of Hoop Reinforced Ti-MMC Rings by Spray/Wind Process, *Key Engineering Materials*, Vol. 127-131, pp 335-342, 1997.
- [75] Güngör S., Ruiz C., Measurement of Thermal Residual Stress in Continuous Fibre Composites, *Key Engineering Materials*, Vol. 127-131, pp 851-860, 1997.
- [76] Christman T., Needleman A., Nutt S., Suresh S., On Microstructural Evolution and Micromechanical Modelling of Deformation of a Whisker-reinforced Metal-Matrix Composite, *Materials Science and Engineering*, Vol. A107, pp 49-61, 1989.
- [77] Vasudevan A.K., Richmond O., Zok F., Embury J.D., The Influence of Hydrostatic Pressure on the Ductility of Al-SiC Composites, *Materials Science and Engineering*, Vol. A107, pp 63-69, 1989.
- [78] Cao L., Jiang C.P., Yao C.K., Lei T.C., Study of the Whisker Rotation in Metal Matrix Composite, *Composites*, No. 2, Vol. 21, pp 127-131, 1990.
- [79] Nakanishi M., Nishida Y., Matsubara H., Yamada M., Tozawa Y., Effect of Thermal Cycling on the Properties of SiC Whisker-Reinforced Aluminium Alloys, *Journal of Materials Science Letters*, Vol. 9, pp 470-472, 1990.

- [80] Voituriez C., Hall I.W., Strengthening Mechanisms in Whisker-reinforced Aluminium Composites, *Journal of Materials Science*, Vol. 26, pp 4241-4249, 1991.
- [81] Komai K., Minoshima K., Yoshida G., Fracture Behavior of SiC Whisker Reinforced Aluminum Alloy under Combined Tension/Torsion Loading at Room and Elevated Temperatures, *Proc. of ICCM-10*, Whistler, BC, Canada, Part 2, pp 815-822, August, 1995.
- [82] Sinclair I., Gregson P.J., Structural Performance of Discontinuous Metal Matrix Composites, *Materials Science and Technology*, Vol. 13, pp 709-726, September, 1997.
- [83] Powder Metallurgy, Vol. 7, *ASM Metals Handbook*, American Society For Metals, Metals Park, Ohio 44073, ISBN 0-87170-013-1, 1990.
- [84] Murphy A.M., Clyne T.W., The Effect of Initial Porosity and Particle Clustering on the Tensile Failure of Cast Particulate MMCs, *Proc. of ICCM-10*, Whistler, B.C., Canada, Part 2, pp 35-42, August, 1995.
- [85] Hashim J., Looney L., Hashmi M.S.J., Particle Distribution in Cast MMCs-Part I, *Proc. of AMPT98*, Kuala Lumpur, Malaysia, eds. Hamouda A.M.S., Sulaiman S. and Ahmadun M., Vol. 1, pp 349-357, August, 1998.
- [86] Skibo M.D., Schuster D.M., Process for Preparation of Composite Materials Containing Nonmetallic Particles in a Metallic Matrix, and Composite Materials Made Thereby, U.S. Patent No. 4,786,467, Nov. 22, 1988. Assignee - Dural Aluminum Composites Corp., San Diego, Calif., USA.
- [87] Skolianos S., Mechanical Behavior of Cast SiC_p-Reinforced Al-4.5%Cu-1.5%Mg Alloy, *Materials Science and Engineering*, Vol. A210, pp 76-82, 1996.
- [88] Lloyd D.J., Lagace H., Mcleod A., Morris P.L., Microstructural Aspects of Aluminium-Silicon Carbide Particulate Composite Produced by a Casting Method, *Materials Science and Engineering*, Vol. A107, pp 73-80, 1989.
- [89] Bhanuprasad V.V., Bhat R.B.V., Kuruvilla A.K., Prasad K.S., Pandey A.B., Mahajan Y.R., P/M Processing of Al-SiC Composites, *The International Journal of Powder Metallurgy*, Vol. 27, No.3, pp 227-235, 1991.

- [90] Hwu B-K., Lin S-J., Jahn M-T., The Interfacial Compounds and SEM Fractography of Squeeze-Cast SiC_p/6061 Al Composites, *Materials Science and Engineering*, Vol. A206, pp 110-119, 1996.
- [91] Chadwick G.A., Squeeze Casting of Metal Matrix Composites Using Short Fibre Preforms, *Materials Science and Engineering*, Vol. A135, pp 23-28, 1991.
- [92] Mortensen A., Interfacial Phenomena in the Solidification Processing of Metal Matrix Composites, *Materials Science and Engineering*, A135, pp 1-11, 1991.
- [93] Singer A.R.E., Metal Matrix Composites Made by Spray Forming, *Materials Science and Engineering*, Vol. A135, pp 13-17, 1991.
- [94] Lugscheider E., Jokiel P., Remer P., Yushchenko K., Borisov Y., Vitiaz P., Steinhäuser S., Hard Particle Reinforced Aluminium-Alloys for Aircraft Applications EWISCO 1993-1994, *Proc. of the 7th National Thermal Spray Conference*, Boston, Massachusetts, pp 79-83, June, 1994.
- [95] Hunt W.H. Jr., Richmond D., Young R.D., Fracture Initiation in Particle Hardened Materials with High Volume Fraction, *Proc. of ICCM-VI*, eds. Matthews F.L. Buskell N.C.R., Hodginson J.M. and Morton J., London, Elsevier Applied Science, pp 2.209-2.223, 1987.
- [96] Šuštaršić B. Kevorkijan V., Kosec L., Morphological and Microstructural Features of Discontinuously Reinforced PM Al/SiC Composites, *Advances in Powder Metallurgy & Particulate Materials*, Vol. 5, Part 16, pp 177-183, 1996.
- [97] Kosec L., Javoric S., Šuštaršić B., Petrovic S., Explosive Compaction of Metal-SiC Composites, *Advances in Powder Metallurgy & Particulate Materials*, Vol. 5, Part 16, pp 185-190, 1996.
- [98] Lewandowski J.J., Liu C., Hunt W.H.Jr., Effects of Matrix Microstructure and Particle Distribution on Fracture of an Aluminum Metal Matrix Composite, *Materials Science and Engineering*, Vol. A107, pp 241-255, 1989.
- [99] Krishnamurthy S., Kim Y-W., Das G., Freos F.H., Applications of RS/PM to the Processing of Metal Matrix Composites, *Metal & Ceramic Matrix Composites: Processing, Modeling & Mechanical Behavior*, eds. Bhagat R.B, Clauer A.H., Kumar P. and Ritter A.M., The Minerals, Metals & Materials Society, pp 145-155, 1990.

- [100] Strangwood M., Hipsley C.A., Lewandowski J.J., Segregation to SiC/Al Interfaces in Al Based Metal Matrix Composites, *Scripta Metallurgica*, Vol. 24, pp 1483-1487, 1990.
- [101] Zhao Z., Zhijian S., Yingkun X., Effect of Microstructure on the Mechanical Properties of an Al Alloy 6061-SiC Particle Composite, *Materials Science and Engineering*, Vol. A132, pp 83-88, 1991.
- [102] Tweed J.H., Manufacture of 2014 Aluminium Reinforced with SiC Particulate by Vacuum Hot Pressing, *Materials Science and Engineering*, Vol. A135, pp 73-76, 1991.
- [103] Bronsveld P.M., Bruinsma P., De Hosson J.Th., Sargent M.A., Alsem W.H.M., Microstructural Analysis of Hot Isostatically Pressed Al-SiC, *Materials Science and Engineering*, Vol. A135, pp 77-81, 1991.
- [104] Niklas A., Froyen L., Delaey L., Buekenhout L., Comparative Evaluation of Extrusion and Hot Isostatic Pressing as Frabrication Techniques for Al-SiC Composites, *Materials Science and Engineering*, Vol. A135, pp 225-229, 1991.
- [105] Tarrant A., Extending the Performance of Particle-Reinforced Aluminium Alloys, *Metallurgia*, pp 137-140, April, 1994.
- [106] Schatt W., Wieters K-P., *Powder Metallurgy Processing and Materials*, EPMA, ISBN 1 899072 05 5, 1997.
- [107] Estrada J.L., Duszczyk J., Degassing of Al-Si-X Powders Assisted by Flushing with Argon or Nitrogen, *Journal of Materials Science*, Vol. 26, pp 3909-3913, 1991.
- [108] Suzuki Y., Watanabe T., Effects of Degassing Treatment on Properties of P/M 7091 Alloy, *Proc. of 1993 Powder Metallurgy World Congress*, pp 575-578, 1993.
- [109] Baugh D.J., *Aluminium Powder Company*, Sutton Coldfield, England, UK, private communication, 1998.
- [110] Lin C-Y., McShane H.B., Rawlings R.D., Structure and Properties of Functionally Gradient Aluminium Alloy 2124/SiC Composites, *Materials Science and Technology*, Vol. 10, pp 659-664, July, 1994.

- [111] Kanetake N., Saiki H., Choh T., Improvement in Mechanical Properties of Aluminium Matrix Composite by Compressive Deformation, Proc. of ICCM-10, Whistler, B.C., Canada, August, Part 2, pp 107-42-114, 1995.
- [112] Carden R.A., Metal Matrix Compositions and Method of Manufacture Thereof, U.S. Patent No. 5,613,189, Sep. 29, 1995. Assignee - Alyn Corporation, Irvine, Calif., USA.
- [113] Mabuchi M., Iwasaki H., Higashi K., Langdon T.G., Processing and Superplastic Properties of Fine Grained $\text{Si}_3\text{N}_4/\text{Al-Mg-Si}$ Composites, Materials Science and Technology, Vol. 11, pp 1295-1299, December, 1995.
- [114] Hong S.J., Kao P.W., SiC-Reinforced Aluminium Composite made by Resistance Sintering of Mechanically Alloyed Powders, Materials Science and Engineering, Vol. A119, pp 153-159, 1989.
- [115] Hong S.J., Kao P.W., Chang C.P., Microstructural Development in Al-SiC Composite Made by Resistance Sintering of Mechanically Alloyed Powders, Materials Science and Engineering, Vol. A158, pp 195-202, 1992.
- [116] Parent J.O.G., Iyengar J., Henein H., Fundamentals of Dry Powder Blending for Metal Matrix Composites, The International Journal of Powder Metallurgy, Vol. 29, pp 353-366, 1993.
- [117] Cooke M.H., Stephens D.J., Bridgwater J., Powder Mixing-A Literature Survey, Powder Technology, Vol. 15, pp 1-20, 1976.
- [118] Parent J.O.G., Iyengar J., Henein H., Powder Blending of Metal-Matrix Composite Systems, Proc. of the 1989 Powder Metallurgy Conference & Exhibition, MPIF, pp 25-37, 1989.
- [119] ter Haar J.H., Duszczek J., Cold compaction of an aluminium/short fibre alumina powder composite, Journal of Materials Science, Vol. 27, pp 6495-6505, 1992.
- [120] ter Haar J.H., Duszczek J., Mixing of Powder Metallurgical Fibre-Reinforced Aluminium Composites, Materials Science and Engineering, Vol. A135, pp 65-72, 1991.
- [121] McGeary R.K., Mechanical Packing of Spherical Particles, Journal of the American Ceramic Society, Vol. 44, No. 10, pp 513-522, 1961.

- [122] Gupta M., Lai M.O., Soo C.Y., Effect of Type of Processing on the Microstructural Features and Mechanical Properties of Al-Cu/SiC Metal Matrix Composites, *Materials Science and Engineering*, Vol. A210, pp 114-122, 1996.
- [123] Gupta M., Mohamed F., Lavernia E., The Effects of Solidification Phenomena on the Distribution of Ceramic Reinforcements During Spray Atomization and Deposition, *Metal & Ceramic Matrix Composites: Processing, Modelling & Mechanical Behavior*, eds. Bhagat R.B., Clauer A.H., Kumar P. and Ritter A.M., The Minerals, Metals & Materials Society, pp 91-106, 1990.
- [124] Lewandowski J.J., Liu C., Hunt W.H. Jr., Microstructural Effects on the Fracture Micromechanisms in 7XXX Al P/M-SiC Particulate Metal Matrix Composites, *Processing and Properties for Powder Metallurgy Composites*, eds. Kumar P., Vedula K. and Ritter A., The Metallurgical Society of AIME, Warrendale, PA, pp 117-137, 1989.
- [125] Moyer K.H., The Burn-Off Characteristics of Common Lubricants In 316L Powder Compacts, *International Journal of Powder Metallurgy*, Vol. 7, pp 33-43, 1971.
- [126] German R.M., *Powder Metallurgy Science*, MPIF, Princeton, New Jersey, ISBN 0-918404-60-6, 1984.
- [127] Dudas J.H., Dean W.A., The Production of Precision Aluminum P/M Parts, *Progress in Powder Metallurgy*, Vol. 25, Metal Powder Industries Federation (MPIF), pp 103-130, 1969.
- [128] Han N., Pollard G., Stevens R., Interfacial Structure and Fracture of Aluminium Alloy A356-SiC Particle Metal Matrix Composite, *Materials Science and Technology*, Vol. 8, pp 184-187, 1992.
- [129] Davis S.J., Miodownik A.P., Watts J.F., Degassing and Surface Analysis of Gas Atomized Aluminium Alloy Powders, *Journal of Materials Science*, Vol. 30, pp 3811-3819, 1995.
- [130] Lee J-C., Byun J-Y., Oh C-S., Seok H-K., Lee H-I., Effect of Various Processing Methods on the Interfacial Reactions in SiC_p/2024 Al Composites, *Acta Metallurgica*, Vol. 45, pp 5303-5315, 1997.
- [131] Hunt M, Pressing Ahead with Powder Metallurgy, *ME*, pp 25-28, August, 1989.

- [132] Claussen N., Jahn J., Green Strength of Metal and Ceramic Compacts as Determined by the Indirect Tensile Test, Powder Metallurgy, Vol. 2, pp 87- 90, 1970.
- [133] Easterling K.E., Thölen A.R., The Role of Surface Energy and Powder Geometry in Powder Compaction, Powder Metallurgy, Vol. 16, pp 112-118, 1973.
- [134] Heckel R.W., An Analysis of Powder Compaction Phenomena, Transactions of the Metallurgical Society of AIME, Vol. 221, pp 1001-1008, 1961.
- [135] Carvalhinhos H., Carvalho M.H., Marcelo T., Comparative Properties of Al 6061/SiC and Al 6061/Al₂O₃ Composites Produced by Sintering and Forging Route, Advances in Powder Metallurgy & Particulate Materials-1992, Vol. 9, pp 157-169, ISBN 1-878954-28-8, 1992.
- [136] James P.J., Particle Deformation During Cold Isostatic Pressing of Metal Powders, Powder Metallurgy, No. 4, pp 199-204, 1977.
- [137] Conaway R. M., Cost-Effective Isostatic Forging, Advanced Materials & Processes, 6/89, pp 35-39, 1989.
- [138] Ferguson B.L., Emerging Alternatives to Hot Isostatic Pressing, MPR, pp 473-483, September, 1985.
- [139] Ferguson B.L., Emerging Alternatives to Hot Isostatic Pressing, The International Journal of Powder Metallurgy & Powder Technology, Vol. 21, pp 201-218, 1985.
- [140] Dudas J.H., Thompson C.B., Improved Sintering Procedures for Aluminium P/M Parts, Modern Developments in Powder Metallurgy, Vol. 5, pp 19-36, 1971.
- [141] Miura S., Machida Y., Hirose Y., Yoshimura R., The Effects of Varied Alloying Methods on the Properties of Sintered Aluminium Alloys, Proc. of 1993 Powder Metallurgy World Congress, pp 571-574, 1993.
- [142] Miura S., Hirose Y., Sato M, Starting Powder for Producing Sintered-Aluminium Alloy, Method for Producing Sintered Parts, and Sintered Aluminium Alloy, U.S. Patent No. 5,466,277, Nov. 14, 1995. Assignee - Showa Denko K.K., Tokyo, Japan.

- [143] Sawtell R.R., Hunt W.H.Jr., Rodjom J., Hilinski E.J., Milsom J.H., Method of Producing Structural Metal Matrix Composite Products from a Blend of Powders, U.S. Patent No. 5561829, Oct. 1, 1996. Assignee - Aluminium Company of America, Pittsburgh, PA.
- [144] Shibli I.A., Davies D.E., Effect of Oxidation on Sintering Characteristics of Al Powder and Effect of Some Minor Metallic Additions, Powder Metallurgy, Vol. 30, No. 2, pp 97-102, 1987.
- [145] Sagar R., Madan P.K., Kumar M., Sachdeva S., Isostatic Compaction of Silicon Carbide Reinforced Aluminium, Advances in Powder Metallurgy & Particulate Materials-1992, Vol. 9, pp 45-56, ISBN 1-878954-28-8, 1992.
- [146] Chang A-J., Rhee S-W., Baik S., Nitridation Characteristics of Floating Aluminium Powder, Journal of Materials Science, Vol. 30, pp 1180-1186, 1995.
- [147] Hayashi T., Takeda Y., Nitrogen-Combined Aluminium Sintered Alloys and Method of Producing the Same, U.S. Patent No. 5,460,775, Oct. 24, 1995. Assignee - Sumitomo Electric Industries, Ltd., Osaka, Japan.
- [148] Heat Treating, Vol. 4, ASM International, Engineering Materials Handbook, American Society For Metals, Metals Park, Ohio 44073, ISBN 0-87170-379-3, 1991.
- [149] Appendino P., Badini C., Marino F., Tomasi A., 6061 Aluminium Alloy-SiC Particulate Composite: a Comparison Between Aging Behaviour in T4 and T6 Treatments, Materials Science and Engineering, Vol. A135, pp 275-279, 1991.
- [150] Nieh T.G., Karlak R.F., Aging Characteristics of B₄C-Reinforced 6061-Aluminum, Scripta Metallurgica, Vol. 18, pp 25-28, 1984.
- [151] Rack H.J., Age Hardening Behavior of SiC Whisker Reinforced 6061 Aluminium, Proc. ICCM-VI, eds. Matthews F.L. Buskell N.C.R., Hodginson J.M. and Morton J., London, Elsevier Applied Science, pp 2.382-2.389, 1987.
- [152] Nutt S.R., Carpenter R.W., Non-Equilibrium Phase Distribution in an Al-SiC Composite, Materials Science and Engineering, Vol. 75, pp 169-177, 1985.
- [153] Dutta I., Allen S.M., Hafley J.L., Effect of Reinforcement on the Aging Response of Cast 6061 Al-Al₂O₃ Particulate Composites, Metallurgical Transactions A, Vol. 22A, pp 2553-2563, 1991.

- [154] Starink M.J., Gregson P.J., S' and δ' phase precipitation in SiC_p Reinforced Al-1.2wt.%Mg-xLi Alloys, *Materials Science and Engineering*, Vol. A211, pp 54-65, 1996.
- [155] Papazian J.M., Effects of SiC Whiskers and Particles on Precipitation in Aluminium Matrix Composites, *Metallurgical Transactions A*, Vol. 19A, pp 2945-2953, 1988.
- [156] Knowles D.M., King J.E., The Influence of Ageing on Fatigue Crack Growth in SiC-Particulate Reinforced 8090, *Acta Metallurgica Mater.*, Vol. 39, pp 793-806, 1991.
- [157] Shakesheff A.J., Ageing and Toughness of Silicon Carbide Particulate Reinforced Al-Cu and Al-Cu-Mg Based Metal-Matrix Composites, *Journal of Materials Science*, Vol. 30, pp 2269-2276, 1995.
- [158] Dutta I., Bourell D.L., Influence of Dislocation Density and Distribution on the Aging Behavior of 6061 Al-SiC_w Composites, *Acta Metallurgica et Materialia*, Vol. 38, pp 2041-2049, 1990.
- [159] Zhao Z., Yingkun X., Wenduo W., Zhuangqi H., Effect of Matrix Microstructure on Mechanical Properties of 2124 Aluminium Alloy-SiC Particle Composite, *Materials Science and Technology*, Vol. 7, pp 592-595, 1991.
- [160] Chawla K.K., Esmaeili A.H., Datye A.K., Vasudevan A.K., Effect of Homogeneous / Heterogeneous Precipitation on Aging Behavior of SiC_p/Al 2014 Composite, *Scripta Metallurgica et Materialia*, Vol. 25, pp 1315-1319, 1991.
- [161] Dunand D., Mortensen A., Thermal Mismatch Dislocations Produced by Large Particles in a Strain-Hardening Matrix, *Materials Science and Engineering*, Vol. A135, pp 179-184, 1991.
- [162] Prangnell P.B., Stobbs W.M., The Effect of Internal Stress on Precipitation Behavior in Particulate Reinforced Al Matrix MMCs, *Proc. of the 12th Risø Inter. Symp. on Metallurgical and Materials Science*, Roskilde, Denmark, pp 603-610, 1991.

- [163] Prangnell P.B., Stobbs W.M., The Effect of SiC Particulate Reinforcement on the Ageing Behavior of Aluminium Based Matrix Alloys, Proc. of ICCM-VII, pp 573-578, 1989.
- [164] Wu Y., Lavernia E.J., Spray-Atomised and Codeposited 6061 Al/SiC_p Composites, JOM, pp 16-23, 1991.
- [165] Humphreys F.J., Deformation and Annealing Mechanisms in Discontinuously Reinforced Metal-Matrix Composites, Proc. of the 9th Risø Inter. Symp. on Metallurgical and Materials Science, Roskilde, Denmark, pp 51-74, 1988.
- [166] Christman T., Suresh S., Microstructural Development in an Aluminium Alloy-SiC Whisker Composite, Acta Metallurgica et Materialia, Vol. 36, pp 1691-1704, 1988.
- [167] Sargent M.A., Rensen C., Alsem W.H.M., The Structure and Properties of Particulate-SiC/Aluminium Alloy 6061 Metal-Matrix Composite Manufactured via Hot Isostatic Pressing, Metal & Ceramic Matrix Composites: Processing, Modeling & Mechanical Behavior, eds. Bhagat R.B, Clauer A.H., Kumar P. and Ritter A.M., The Minerals, Metals & Materials Society, pp 137-144, 1990.
- [168] Sritharan T., Xia K., Heathcock J., Mihelich J., Matrix/Reinforcement Development for Aluminium-based Composites, Metal & Ceramic Matrix Composites: Processing, Modeling & Mechanical Behavior, eds. Bhagat R.B, Clauer A.H., Kumar P. and Ritter A.M., The Minerals, Metals & Materials Society, pp 13-22, 1990.
- [169] Roebuck B., Lord J.D. Plane Strain Fracture Toughness Test Procedures for Particulate Metal Matrix Composites, Materials Science and Technology, Vol. 6, pp 1199-1209, 1990.
- [170] Manoharan M., Lewandowski J.J., Effect of Reinforcement Size and Matrix Microstructure on the Fracture Properties of an Aluminum Metal Matrix Composite, Materials Science and Engineering, Vol. A150, pp 179-186, 1992.
- [171] Aikin R.M. Jr., Christodoulou L., The Role of Equiaxed Particles on the Yield Stress of Composites, Scripta Metallurgica et Materialia, Vol. 25, pp 9-14, 1991.
- [172] Arsenault R.J., Fisher R.M., Microstructure of Fiber and Particulate SiC in 6061 Al Composites, Scripta Metallurgica, Vol. 17, pp 67-71, 1983.

- [173] Kamat S.V., Hirth J.P., Mehrabian R. Mechanical Properties of Particulate-Reinforced Aluminium-Matrix Composites, *Acta Metallurgica*, Vol. 37, No. 9, pp 2395-2402, 1989.
- [174] Lilholt H., Aspects of Deformation of Metal Matrix Composites, *Materials Science and Engineering*, Vol. A135, pp 161-171, 1991.
- [175] Dieter G.E., *Mechanical Metallurgy*, 3rd edition, ISBN 0-07-016893-8, 1986.
- [176] Chawla K.K., Metzger M., Initial Dislocation Distributions in Tungsten Fibre-Copper Composites, *Journal of Materials Science*, Vol. 7, pp 34-39, 1972.
- [177] Miller W.S., Humphreys F.J., Strengthening in Particulate Metal Matrix Composites, *Scripta Metallurgica et Materialia*, Vol. 25, pp 33-38, 1991.
- [178] Lavernia E.J., Ayers J.D., Srivatsan T.S., Rapid Solidification Processing with Specific Application to Aluminium Alloys, *International Materials Reviews*, Vol. 37, pp 1-44, 1992.
- [179] Gensamer M., Pearsall E.B., Pellini W.S., Low J.R. Jr., The Tensile Properties of Pearlite, Bainite, and Spheroidite, *Transactions of the American Society for Metals*, Vol. 30, pp 983-1020, 1942.
- [180] Movchan B.A., Structural Conditions for Maximum Ductility of Two-phase Polycrystalline Materials, *Materials Science and Engineering*, Vol. 72, pp 109-117, 1985.
- [181] Liaw P.K., Gregg J.G., Logsdon W.A., Microstructural Characterisation of a Silicon Carbide Whisker Reinforced 2124 Aluminium Metal Matrix Composite, *Journal of Materials Science*, Vol. 22, pp 1613-1617, 1987.
- [182] Needleman A., Finite Elements for Finite Strain Plasticity Problems, *Proc. of Research Workshop (Plasticity of Metals at Finite Strain: Theory, Computation and Experimental)*, Stanford University, USA, June 29, 30, July 1, 1981, eds. Lee E.H. and Mallett R.L., pp 387-436, ISBN 0-9609992-0-5, 1982.
- [183] Eshelby J.D., The Determination of the Elastic Field of an Ellipsoidal Inclusion, and Related Problems, *Proc. Roy. Soc. London, Series A*, pp 376-396, 1957.
- [184] Clyne T.W., A Simple Development of the Shear Lag Theory Appropriate for Composites with a Relatively Small Modulus Mismatch, *Materials Science and Engineering*, Vol. A122, pp 183-192, 1989.

- [185] Wakashima K., Tsukamoto H., Mean-field Micromechanics Model and its Application to the Analysis of Thermomechanical Behaviour of Composite Materials, *Materials Science and Engineering*, Vol. A146, pp 291-316, 1991.
- [186] Yu N., Ravisankar M.V.S., Hsu D.K., Liaw P.K., Elastic and Elastic-Plastic Properties of Silicon Carbide Aluminium Matrix Composites, *Inelasticity and Micromechanics of Metal Matrix Composites*, eds. Voyiadjis G.Z. and Ju J.W., Elsevier Sc. B.V., pp 83-96, ISBN 0-44481800-6, 1994.
- [187] Yu N., Ravisankar M.V.S., Liaw P.K., The Effective Elastoplastic Behaviour of Silicon Carbide Particulate Reinforced Metal Matrix Composites, *Key Engineering Materials*, Vol. 104-107, pp 837-844, 1995.
- [188] Warner T.J., Stobbs W.M., Modulus and Yield Stress Anisotropy of Short Fibre Metal-Matrix Composites, *Acta Metallurgica*, Vol. 37, pp 2873-2881, 1989.
- [189] Roatta A., Bolmaro R.E., An Eshelby Inclusion-Based Model for the Study of Stresses and Plastic Strain Localization in Metal Matrix Composites I: General Formulation and its Application to Round Particles, *Materials Science and Engineering*, Vol. A229, pp 182-191, 1997.
- [190] Roatta A., Bolmaro R.E., An Eshelby Inclusion-Based Model for the Study of Stresses and Plastic Strain Localization in Metal Matrix Composites II: Fiber Reinforcement and Lamellar Inclusions, *Materials Science and Engineering*, Vol. A229, pp 192-202, 1997.
- [191] Roatta A., Turner B.A., Bertineti M.A., Bolmaro R.E., An Iterative Approach to Mechanical Properties of MMCs at the Onset of Plastic Deformation, *Materials Science and Engineering*, Vol. A229, pp 203-218, 1997.
- [192] Sørensen N.J., Suresh S., Tvergaard V., Needleman A., Effects of Reinforcement Orientation on the Tensile Response of Metal-Matrix Composites, *Materials Science and Engineering*, Vol. A197, pp 1-10, 1995.
- [193] Davis L.C., Flow Rule for the Plastic Deformation of Particulate Metal-Matrix Composites, *Computational Materials Science*, Vol. 6, pp 310-318, 1996.
- [194] Fang D., Qi H., Tu S., Elastic and Plastic Properties of Metal-Matrix Composites: Geometrical Effects of Particles, *Computational Materials Science*, Vol. 6, pp 303-309, 1996.

- [195] LLorca J., González C., Microstructural Optimization of Discontinuously-Reinforced Metal-Matrix Composites, *Key Engineering Materials*, Vol. 127-131, pp 111-122, 1997.
- [196] Povirk G.L., Needleman A., Nutt S.R., An Analysis of Residual Stress Formation in Whisker-Reinforced Al-SiC Composites, *Materials Science and Engineering*, Vol. A125, pp 129-140, 1990.
- [197] Povirk G.L., Needleman A., Nutt S.R., An Analysis of the Effect of Residual Stresses on Deformation and Damage Mechanisms in Al-SiC Composites, *Materials Science and Engineering*, Vol. A132, pp 31-38, 1991.
- [198] Tvergaard V., Analysis of Tensile Properties for a Whisker-Reinforced Metal-Matrix Composite, *Acta Metallurgica et Materialia*, Vol. 38, No. 2, pp 185-194, 1990.
- [199] Zahl D.B., McMeeking R.M., The Influence of Residual Stress on the Yielding of Metal Matrix Composites, *Acta Metallurgica et Materialia*, Vol. 39, No. 6, pp 1117-1122, 1991.
- [200] Biner S.B., A Finite Element Method Analysis of the Role of Interface Behavior in the Creep Rupture Characteristics of a Discontinuously Reinforced Composite with Sliding Grain Boundaries, *Materials Science and Engineering*, Vol. A208, pp 239-248, 1996.
- [201] Teply J.L., Dvorak G.J., Bounds on Overall Instantaneous Properties of Elastic-Plastic Composites, *J. Mech. Phys. Solids*, Vol. 36, No. 1, pp 29-58, 1988.
- [202] Jain M., MacEwen S.R., Wu L., Finite Element Modelling of Residual Stresses and Strength Differential Effect in Discontinuously Reinforced Metal Matrix Composites, *Materials Science and Engineering*, Vol. A183, pp 111-120, 1994.
- [203] Neti S., Vijayshankar M.N., Ankem S., Finite Element Method Modeling of Deformation Behavior of Two-Phase Materials Part I: Stress-Strain Relations, *Materials Science and Engineering*, Vol. A145, pp 47-54, 1991.
- [204] Neti S., Vijayshankar M.N., Ankem S., Finite Element Method Modeling of Deformation Behavior of Two-Phase Materials Part II: Stress and Strain Distributions, *Materials Science and Engineering*, Vol. A145, pp 55-64, 1991.

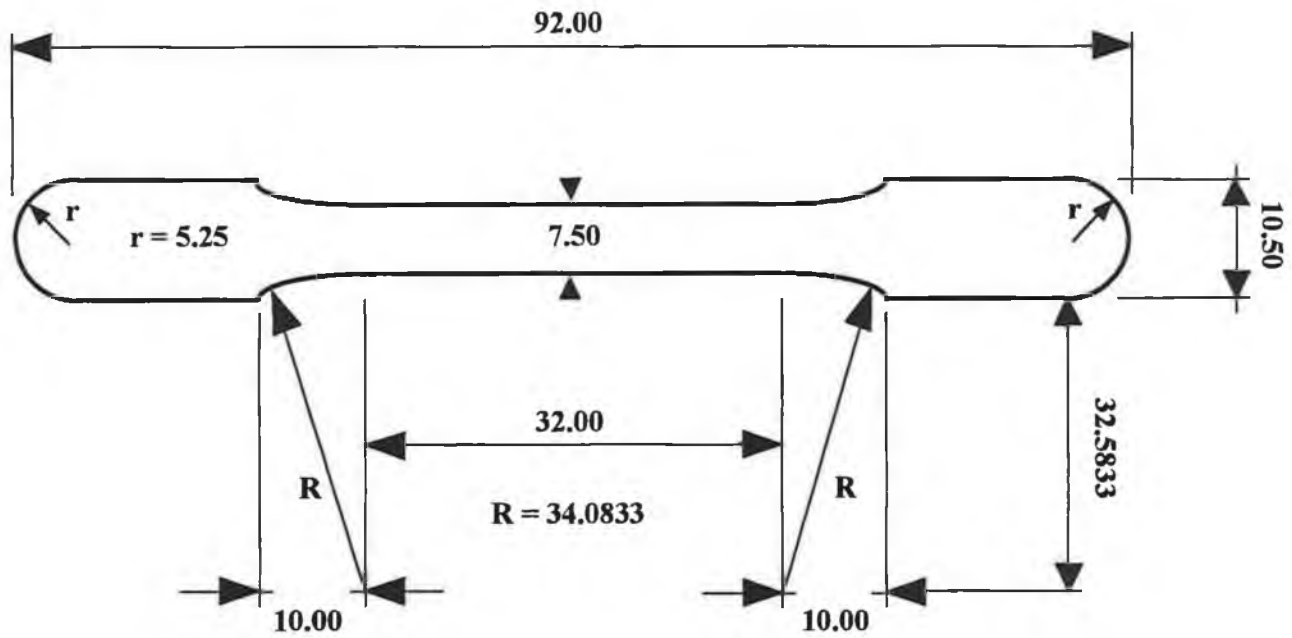
- [205] Brockenbrough J.R., Suresh S., Plastic Deformation of Continuous Fiber-Reinforced Metal-Matrix Composites: Effects of Fiber Shape and Distribution, *Scripta Metallurgica et Materialia*, Vol. 24, pp 325-330, 1990.
- [206] Brockenbrough J.R., Suresh S., Wienecke H.A., Deformation of Metal-Matrix Composites with Continuous Fibers: Geometrical Effects of Fiber Distribution and Shape, *Acta Metallurgica et Materialia*, Vol. 39, No. 5, pp 735-752, 1991.
- [207] Prangnell P.B., Barnes S.J., Roberts S.M., Withers P.J., The Effect of Clustering on Damage Formation in Particulate Reinforced MMCs Deformed in Compression, *Key Engineering Materials*, Vol. 127-131, pp 937-944, 1997.
- [208] Daymond M.R., Withers P.J., Examination of Tensile/Compressive Loading Asymmetries in Aluminium Based Metal Matrix Composites Using Finite Element Method, *Materials Science and Technology*, Vol. 11, pp 228-235, 1995.
- [209] Foo K.S., Banks W.M., Craven A.J., Hendry A., Interface Characterization of an SiC Particulate/6061 Aluminium Alloy Composite, *Composites*, Vol. 25, No. 7, pp 677-683, 1994.
- [210] Huda D., Optimization of the Sintering Process: Metal Matrix Composites and Zinc Oxide Varistors, Ph.D. Thesis, Dublin City University, Dublin, Ireland, 1994.
- [211] MPIF, Standard Test Methods for Metal Powders and Powder Metallurgy Products, ISBN No. 1-878954-55-5, 1995.
- [212] Braun R.D., Introduction To Chemical Analysis, McGraw-Hill Book Company, ISBN 0-07007280-9.
- [213] Bonollo F., Molinas B., Tangerini I., Zambon A., Diametral Compression Testing of Metal Matrix Composites, *Materials Science and Technology*, Vol. 10, pp 558-564, 1994.
- [214] Buehler, The Buehler Dialog Concept, 1995.
- [215] Begg A.R., Metal Matrix Composites by Powder Metallurgy, *Powder Metallurgy*, Vol. 36, No. 2, pp 107-110, 1993.
- [216] Evans A.G., Hutchinson J.W., McMeeking R.M., Stress-Strain Behavior of Metal Matrix Composites with Discontinuous Reinforcements, *Scripta Metallurgica et Materialia*, Vol. 25, pp 3-8, 1991.

- [217] Zienkiewicz O.C. The Finite Element Method in Engineering Science, McGraw-Hill, ISBN 07-094138-6, 1971.
- [218] ANSYS® 5.3 User's Manual I-IV, Swanson Analysis Systems, 1996.
- [219] A Million Random Digits with 100,000 Normal Deviates, The RAND Corporation, Macmillan Publishing Co., ISBN 0-02-925790-5, 1955.
- [220] Nutt S.R., Needleman A., Void Nucleation at Fiber Ends in Al-SiC Composites, *Scripta Metallurgica*, Vol. 21, pp 705-710, 1987.
- [221] Salvo L., Suery M., Legoux J.G., l'Esperance G., Influence of Particle Oxidation on Age-Hardening Behaviour of As-Fabricated and Remelted SiC Reinforced Al-1% Mg Alloys, *Materials Science Engineering*, Vol. A135, pp 129-133, 1991.
- [222] Arsenault R.J., Wu S.B., A Comparison of PM VS. Melted SiC/Al Composites, *Scripta Metallurgica*, Vol. 22, pp 767-772, 1988.
- [223] Stone I.C., Tsakiroopoulos P., The Effect of the Spatial Distribution of Reinforcement on the Fabrication and Heat Treatment of (Al-4wt.%Cu)-SiC Particle Metal Matrix Composites, *Materials Science and Engineering*, Vol. A189, pp 285-290, 1994.
- [224] Estrada J.L., Carreño V.M., Balmori H., Duszczek J., Relationship Between Sintering Atmospheres and Mechanical Properties of P/M Al-20Si-5Fe-2Ni Products, *Sintering Technology*, eds. German R.M., Messing G.L. and Cornwall R.G., Marcel Dekker Inc, New York, pp 277-284, ISBN 0-8247-9775-2, 1996.
- [225] Cohrt H., Vöhringer O., Braun G., Development of Near Net Shape Structural Parts of Metal Matrix Composites, *Advances in Powder Metallurgy & Particulate Materials-1992*, Vol. 9, pp 33-43, ISBN 1-878954-28-8, 1992.
- [226] Plumtree A., Mummery P., Accumulation of Damage in Aluminum MMCs, in *Proc. of ICCM-10*, Whistler, BC, Canada, Part 2, pp 257-262, August, 1995.
- [227] Kim Y-W., Griffith W.M., Froes F.H., Surface Oxides in P/M Aluminium Alloys, *Journal of Metals*, pp 27-33, August, 1985.
- [228] Bao G., Hutchinson J.W., McMeeking R.M., Particle Reinforcement of Ductile Matrices Against Plastic Flow and Creep, *Acta Metallurgica et Materialia*, Vol. 39, No. 8, pp 1871-1882, 1991.

- [229] Dong M., Schmauder S., Bidlingmaier T., Wanner A., Prediction of the Mechanical Behaviour of Short Fibre Reinforced MMCs by Combined Cell Models, *Computational Materials Science*, Vol. 9, pp 121-133, 1997.

APPENDIX A

Tensile Test Sample Dimensions



Pressure Area = 8.062 cm²

Note: General tolerance ± 0.010 mm.
Max. clearance between punch and die + 0.010 mm.

Note: Internal dimensions for die cavity.

DIE CAVITY

All Dims. mm

G. O'Donnell

Date: 6/12/98

APPENDIX B

Kiln PLC Programming and Module Run Procedure

In order for the kiln to follow a predetermined thermal cycle the PLC must be programmed to control the power input to the kiln heating elements. This is achieved by programming a **module**, which is an individual program capable of producing a thermal cycle consisting of four **stages**, each consisting of a ramp to a specified temperature in a specified time, followed by a dwell at this temperature. The PLC input/display panel is shown in figure B1. The procedures which must be followed in order to program a module and run a module are described below.

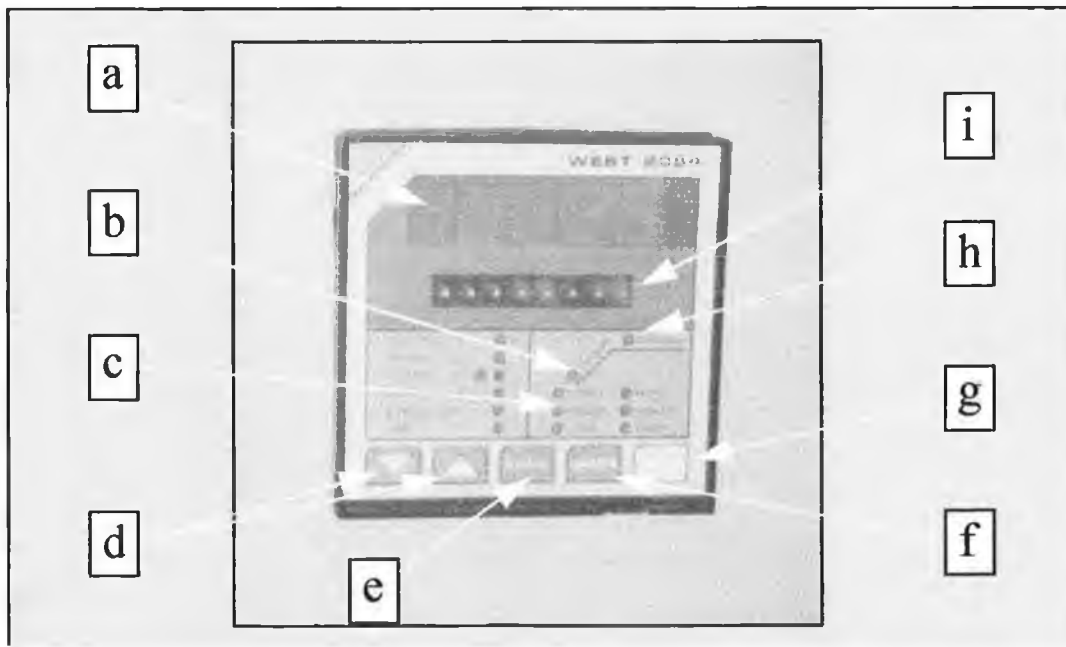


Figure B1. Kiln PLC (West 2054) input/display panel (a) top display, (b) RAMP light, (c) PROG light, (d) ▲ and ▼ buttons (increase value and decrease value respectively), (e) FUNC button, (f) MODE button, (g) RUN/HOLD button, (h) DWELL light and (i) bottom display.

Program a Module

1. Select programming mode.

Press MODE until PROG light illuminates.

2. Select a module (can be one of eight available, 1-8).

Press FUNC three times, MODULE is displayed (displayed in bottom display).

Use ▲ / ▼ to select the module to be programmed.

3. Start inputting program details (12 inputs, i.e. ramp temperature, ramp time and dwell time for each of the four available stages of the module).

- a. Press FUNC once, M1S1TEMP is displayed and the **RAMP** light illuminates (Module 1, Stage 1, **TEMP**erature at end of ramp).

Use ▲ / ▼ to select the temperature which is required to be reached at the end of this first ramp (displayed in top display ,units-°C).

- b. Press FUNC once, M1S1TIME is displayed and the RAMP light remains illuminated (Module 1, Stage 1, **TIME** for the temperature to increase or decrease from the set point temperature, *normally 15°C*, to the temperature defined in a). To adjust the set point temperature, refer to controller manual.

Use ▲ / ▼ to select the time for the temperature to increase or decrease from the set temperature to the temperature defined in a (units, hours . minutes).

Note: the combination of steps a and b defines the temperature to be reached and the rate of temperature rise or fall for Stage 1.

- c. Press FUNC once, M1S1TIME is displayed and the **DWELL** light illuminates (Module 1, Stage 1, TIME to remain at the temperature defined in a).

Use ▲ / ▼ to select the time to stay at the temperature reached at the end of ramp (units, hours . minutes).

Note: the combination of steps a, b and c defines Stage 1 of the module.

- d. Proceed as described in a, b and c above to define Stage 2 of the module.

- e. Proceed as described in a, b and c above to define Stage 3 of the module.

- f. Proceed as described in a, b and c above to define Stage 4 of the module.

Note: The combination of steps a to f defines the entire module. Press MODE to exit programming mode.

Run a module

Press RUN/HOLD once, MODULE is displayed.

Use ▲ / ▼ to select the required module.

Press RUN/HOLD once, the program begins, the display will show the set point temperature (and will subsequently increase or decrease at the defined ramp rate of the Stage 1 for the module) and both the run light and ramp light will illuminate.

Note: To abort from a program while it is running press RUN/HOLD for 10 seconds.

APPENDIX C

Results Data Information

Table No.	Samples Tested	Scatter of Result
4.1.	3 samples per powder type	$\pm 0.5\mu\text{m}$
4.2.	1 per powder batch	-

Figure No.	Samples Tested	Scatter of Results
4.1.	6 per powder batch	$\pm 0.3\%$ TD
4.2.	10 (Non-Annealed) per powder batch, 2 (Annealed) per powder batch	$\pm 0.4\%$ TD
4.3.	6 per powder batch	$\pm 0.3\%$ TD
4.4.	6 per powder batch	$\pm 0.3\%$ TD
4.5.	6 per powder batch	$\pm 0.3\%$ TD
4.6.	6 per powder batch	$\pm 0.3\%$ TD
4.7.	6 per powder batch	$\pm 0.3\%$ TD
4.8.	6 per powder batch	$\pm 0.3\%$ TD
4.9.	2 per powder batch	$\pm 0.1\%$ TD
4.10.	2 per powder batch	$\pm 0.1\%$ TD
4.11.	2 per powder batch	$\pm 0.11 \text{ N/mm}^2$, Zinc stearate $\pm 1.9 \text{ N/mm}^2$, Acrawax™
4.12.	2 (Non-Annealed) per powder batch, 1 (Annealed) per powder batch	$\pm 0.05 \text{ N/mm}^2$ (Non-Annealed)
4.15.	1-4 per powder batch	$\pm 0.31\%$ TD
4.16.	2-4 per powder batch	$\pm 0.18\%$ TD
4.17.	1 sample per powder batch, 4 readings per sample	± 2 HRB for the 4 readings per sample
4.18.	1 sample per powder batch, 4 readings per sample	± 1.5 HRB for the 4 readings per sample

Results Data Information Continued

Figure No.	Samples Tested	Scatter of Results
4.19.	1 sample per powder batch, 4 readings per sample	± 1.5 HRB for the 4 readings per sample
4.20.	1 per powder batch	-
4.25	3 per powder batch	shown on figure
4.26	3 samples tested per batch, flow curves displayed are the flow curves exhibiting the maximum flow stress for each batch	Scatter of UTS as in figure 4.25, scatter of true strain to failure ± 0.0015

In the interest of clarity it should be noted that,

1. The scatter of results stated in the above tables are based on the maximum scatter recorded in a single batch of powder unless otherwise stated.
2. In the case of the compressibility results (%TD) very little variation was recorded between samples from the same powder batch. The scatter for these results are based solely on the results of the maximum green density (green density after compaction at 220MPa) and can be taken as being representative of the scatter observed for the green densities recorded for lower compacting pressures.
3. Since very little variation in compressibility was observed for samples from the same powder batch, the results presented in figures 4.1 - 4.11, 4.15 and 4.16 are derived from individual samples from each batch and are representative of that batch.
4. The scatter stated for the hardness test results are based on the maximum scatter recorded for an individual sample based on the four readings taken on that sample.

APPENDIX D

Individual Sample Data

TEST MATRIX NO. 1

Sample Code:

Example; A1,1

"A"1,1 refers to the aluminium powder / SiC particle size combination.

A - 7 μ m AA6061 / 28.5 μ m SiC

B - 11 μ m AA6061 / 6 μ m SiC

C - 7 μ m AA6061 / 6 μ m SiC

D - 11 μ m AA6061 / 28.5 μ m SiC

E - 16 μ m AA6061 / 6 μ m SiC

F - 16 μ m AA6061 / 28.5 μ m SiC

A"1",1 refers to the volume fraction SiC.

1 - 10% SiC

2 - 20% SiC

3 - 30% SiC

A1,"1" refers to the sample number.

Compressibility Test Green Density (% TD) Results

As-supplied powder combinations compacted at 220 MPa.

Sample	% TD	Sample	% TD	Sample	% TD
A1,1	78.23	A2,1	78.91	A3,1	79.97
A1,2	78.02	A2,2	78.63	A3,2	80.03
A1,3	78.33	A2,3	78.95	A3,3	79.83
A1,4	77.97	A2,4	78.85	A3,4	79.92
A1,5	78.02	A2,5	78.95	A3,5	79.77
A1,6	77.55	A2,6	78.87	A3,6	79.57
B1,1	77.81	B2,1	76.19	B3,1	74.9
B1,2	78.07	B2,2	76.4	B3,2	74.97
B1,3	77.62	B2,3	76.38	B3,3	75.16
B1,4	77.81	B2,4	76.13	B3,4	75.03
B1,5	77.71	B2,5	76.19	B3,5	75.12
B1,6	77.81	B2,6	76.36	B3,6	75.24
C1,1	76.0	C2,1	75.07	C3,1	74.02
C1,2	75.88	C2,2	75.04	C3,2	74.12
C1,3	75.91	C2,3	75.03	C3,3	73.9
C1,4	76.27	C2,4	75.06	C3,4	75.27
C1,5	76.2	C2,5	74.52	C3,5	74.26
C1,6	76.16	C2,6	74.96	C3,6	74.03

Compressibility Test Green Density (% TD) Results Continued

Sample	% TD	Sample	% TD	Sample	% TD
D1,1	80.1	D2,1	80.4	D3,1	80.96
D1,2	80.33	D2,2	80.45	D3,2	80.77
D1,3	79.84	D2,3	80.33	D3,3	80.75
D1,4	79.91	D2,4	80.6	D3,4	80.78
D1,5	79.98	D2,5	80.42	D3,5	80.44
D1,6	79.83	D2,6	80.32	D3,6	80.82
E1,1	79.94	E2,1	78.11	E3,1	76.39
E1,2	79.64	E2,2	78.14	E3,2	76.44
E1,3	79.77	E2,3	78.33	E3,3	76.51
E1,4	79.81	E2,4	78.2	E3,4	76.46
E1,5	79.75	E2,5	78.22	E3,5	76.67
E1,6	79.74	E2,6	78.23	E3,6	76.57
		F2,1	81.81		
		F2,2	81.92		
		F2,3	81.93		
		F2,4	81.63		
		F2,5	81.72		
		F2,6	81.94		

TEST MATRIX NO. 2

Sample Code:

Example; B6A11

"B"6A11 refers to SiC volume fraction and powder heat treatment.

A - 0% SiC, Non-annealed.

B - 0% SiC, Annealed.

C - 10% SiC, Non-annealed.

D - 10% SiC, Annealed.

E - 20% SiC, Non-annealed.

F - 20% SiC, Annealed.

G - 30% SiC, Non-annealed.

H - 30% SiC, Annealed.

B"6"A11 refers to the matrix material AA6061.

Note: Test matrix no. 2 was designed to include AA2124 composites.

However, due to the very poor condition of the non-annealed AA2124 powders this section of the test matrix was terminated (section 4.2.7).

B6"A"11 refers to the powder heat treatment time applied.

A - 2 Hours.

B - 3 Hours.

B6A"1"1 refers to the powder heat treatment temperature applied.

1 - 350°C

2 - 415°C

3 - 470°C

B6A1"1" refers to the sample number.

Note: In the case of the non-annealed samples the third and fourth digits are not included, e.g. E63 is sample no. 3 for the AA6061/20% SiC non-annealed batch.

An example of the test data sheets used for the compressibility tests in the test matrix no. 2 is shown on page D6, followed by the calculated results for the individual samples.

COMPRESSIBILITY TEST READINGS AND RESULTS

SAMPLE DETAILS

Sample code: D61
Al. content (%v): 90
SiC content (%v): 10
Lub. content (%w): 0.5
Th. Len. (mm): 15
Th. Dia. (mm): 17
Th. volume (cm³): 3.405
Th. density (g/cm³): 2.764
Cal. mass (gms): 9.4097

TEST READING

Set load (kN)	Unloaded ext. (mm)	Unloaded len. (mm)
0	0	24.455
10	-3.74	20.715
20	-5.5	18.955
30	-6.59	17.865
40	-7.31	17.145
50	-7.82	16.635

Ejection force (kN)	3.9
---------------------	-----

Final length (mm)	16.635
-------------------	--------

Final diameter (mm)	17.035
---------------------	--------

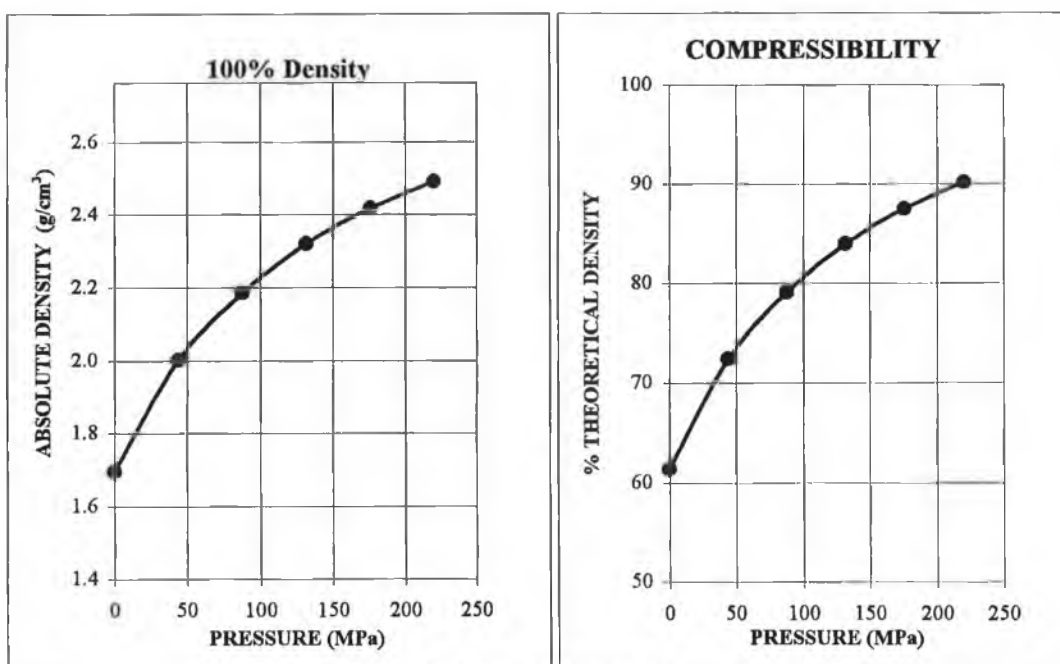
Final mass (gms)	9.406
------------------	-------

TEST RESULTS

Pressure (MPa)	Density (g/cm ³)	% Th. density
0	1.695	61.31
44.06	2.000	72.38
88.11	2.186	79.10
132.17	2.320	83.93
176.23	2.417	87.45
220.28	2.491	90.14

Max. density (g/cm³): 2.481

Final % th. density: 89.77



GRAPHIC RESULTS

NON-ANNEALED SAMPLES

Compressibility Test Green Density (% TD) Results

Code	% TD	Code	% TD	Code	% TD	Code	% TD
A61	DAM	C61	84.22	E61	81.64	G61	78.72
A62	DAM	C62	84.18	E62	81.63	G62	78.77
A63	DAM	C63	84.17	E63	81.64	G63	78.72
A64	85.61	C64	84.14	E64	81.7	G64	78.73
A65	DAM	C65	84.19	E65	81.69	G65	78.82
A66	85.86	C66	84.2	E66	81.75	G66	78.73
A67	85.32	C67	84.11	E67	81.68	G67	78.68
A68	86.18	C68	84.21	E68	81.72	G68	78.75
A69	85.78	C69	84.25	E69	81.75	G69	78.78
A610	86.18	C610	84.2	E610	81.64	G610	78.76

DAM refers to slightly damaged samples.

Green Strength Test Results

Code	Green Strength	Code	Green Strength	Code	Green Strength	Code	Green Strength
A61	1.1	C61	0.926	E61	0.67	G61	0.35
A62	1.213	C62	1.03	E62	0.65	G62	0.39

Green Strength in N/mm².

ANNEALED SAMPLES

Compressibility Test Green Density (% TD) Results

Code	% TD	Code	% TD	Code	% TD	Code	% TD
B6A11	90.44	D6A11	88.66	F6A11	86.14	H6A11	83.07
B6A12	91.16	D6A12	89.06	F6A12	86.25	H6A12	83.09
B6A21	91.50	D6A21	89.40	F6A21	86.84	H6A21	83.88
B6A22	91.38	D6A22	89.39	F6A22	86.86	H6A22	83.86
B6A31	91.66	D6A31	89.85	F6A31	86.89	H6A31	83.81
B6A32	91.65	D6A32	89.71	F6A32	86.84	H6A32	83.79
B6B11	90.79	D6B11	89.01	F6B11	86.21	H6B11	83.12
B6B12	90.88	D6B12	88.92	F6B12	86.10	H6B12	82.95
B6B21	91.54	D6B21	89.35	F6B21	86.62	H6B21	83.46
B6B22	91.53	D6B22	89.38	F6B22	86.54	H6B22	83.43
B6B31	90.94	D6B31	89.51	F6B31	86.83	H6B31	83.48
B6B32	90.68	D6B32	89.54	F6B32	86.80	H6B32	83.12

ANNEALED SAMPLES

Green Strength Test Results

Code	Green Strength	Code	Green Strength	Code	Green Strength	Code	Green Strength
B6A11	2.215	D6A11	2.13	F6A11	1.64	H6A11	0.95
B6A12		D6A12		F6A12		H6A12	
B6A21	2.40	D6A21	2.2145	F6A21		H6A21	
B6A22		D6A22		F6A22	1.70	H6A22	1.00
B6A31	3.51	D6A31	2.58	F6A31	1.85	H6A31	1.17
B6A32		D6A32		F6A32		H6A32	
B6B11	2.50	D6B11	2.22	F6B11	1.69	H6B11	0.99
B6B12		D6B12		F6B12		H6B12	
B6B21		D6B21		F6B21	1.74	H6B21	1.03
B6B22	2.56	D6B22	2.29	F6B22		H6B22	
B6B31	3.03	D6B31	2.94	F6B31	2.17	H6B31	
B6B32		D6B32		F6B32		H6B32	1.29

Green Strength in N/mm².

Sintered Density Readings

Code	Hardness HRB
A6	99.6
B6	96.9
C6	98.9
D6	97.1
E6	96.3
F6	95.7
G6	91.5
H6	88.4

These results are based on single samples per batch. Each sample was machined to remove the oxide layer from both flat faces before sintered density was recorded.

Hardness Readings

Code	Hardness HRB
A6	69.5
B6	64.6
C6	75.5
D6	70.5
E6	78.1
F6	71.8
G6	81.1
H6	68.1

Hardness calculated based on the average of four readings taken for each sample. The selection of the samples for hardness testing was based on sample quality after sintering.

Compressive Yield Strength Readings

Code	0.2% Yield Strength (N/mm ²)
A6	349
B6	290
C6	400
D6	343
E6	456
F6	396
G6	429
H6	356

Yield strength results attained from x-y recorded data for each sample. The selection of the samples for yield strength testing was based on sample quality after sintering.

TEST MATRIX NO. 3

Test matrix no. 3 was comprised of 3 sections.

Section 1 - To investigate the effects of various lubricant contents on powder compressibility, post-compaction ejection and green strength. All samples contained AA6061 combined with 10% SiC.

Sample Code:

Example; XA-0.5-1

"X"A-0.5-1 refers to the lubricant type used.

Z - Zinc stearate.

X - AcrawaxTM

X"A"-0.5-1 refers to the powder heat treatment atmosphere used.

A - Air

N - Nitrogen

XA-"0.5"-1 refers to the % lubricant (by weight) used.

0.5 - 0.5% lubricant

1 - 1% lubricant

2 - 2% lubricant

3 - 3% lubricant

XA-0.5-"1" refers to the sample number.

Compressibility Test Green Density Results (Section 1)

Code	% TD	Code	% TD
3XA-0.5-1	86.74	3ZA-0.5-1	87.74
3XA-0.5-2	86.34	3ZA-0.5-2	87.72
3XA-1-1	86.31	3ZA-1-1	87.46
3XA-1-2	86.32	3ZA-1-2	87.59
3XA-2-1	85.20	3ZA-2-1	86.66
3XA-2-2	85.23	3ZA-2-2	86.82
3XA-3-1	83.94	3ZA-3-1	85.99
3XA-3-2	83.86	3ZA-3-2	86.09

Code	% TD	Code	% TD
3XN-0.5-1	87.64	3ZN-0.5-1	88.50
3XN-0.5-2	87.10	3ZN-0.5-2	88.78
3XN-1-1	86.80	3ZN-1-1	88.60
3XN-1-2	86.96	3ZN-1-2	88.50
3XN-2-1	85.97	3ZN-2-1	87.80
3XN-2-2	85.97	3ZN-2-2	87.80
3XN-3-1	84.86	3ZN-3-1	86.87
3XN-3-2	84.80	3ZN-3-2	86.90

Ejection Stress Test Results (Section 1)

Code	Ejection Stress	Code	Ejection Stress
3XA-0.5-1	6.07	3ZA-0.5-1	5.37
3XA-0.5-2	8.72	3ZA-0.5-2	5.59
3XA-1-1	6.07	3ZA-1-1	5.04
3XA-1-2	6.12	3ZA-1-2	4.97
3XA-2-1	4.80	3ZA-2-1	4.63
3XA-2-2	4.87	3ZA-2-2	4.64
3XA-3-1	4.17	3ZA-3-1	4.17
3XA-3-2	4.2	3ZA-3-2	4.04

Code	Ejection Stress	Code	Ejection Stress
3XN-0.5-1	6.88	3ZN-0.5-1	4.78
3XN-0.5-2	10.75	3ZN-0.5-2	4.65
3XN-1-1	9.39	3ZN-1-1	4.26
3XN-1-2	7.72	3ZN-1-2	4.12
3XN-2-1	4.69	3ZN-2-1	3.86
3XN-2-2	4.57	3ZN-2-2	3.87
3XN-3-1	3.62	3ZN-3-1	3.35
3XN-3-2	3.59	3ZN-3-2	3.47

Ejection Stress in N/mm².

Green Strength Test Results (Section 1)

Code	Green Strength (N/mm ²)
3ZN-2-1	1.70
3XN-2-1	2.15
3XA-2-1	2.60
3ZA-2-1	2.91

Note: Tests carried out on samples containing 2% lubricant only.

Section 2 - To investigate the effects of compaction rate on the compressibility and ejection stress. All samples contained AA6061 combined with 10% SiC and 0.5% by weight zinc stearate.

Sample Code:

Example; N-1-1

"N"-1-1 refers to the powder heat treatment atmosphere used.

A - Air

N - Nitrogen

N-"1"-1 refers to the compaction rate used.

1 - 20mm/min, up to 50kN

2 - 100mm/min, up to 35kN followed by 20mm/min up to 50kN

3 - 500mm/min, up to 35kN followed by 20mm/min up to 50kN

N-1-"1" refers to the sample number.

Compressibility Test Green Density Results (Section 2)

Code	% TD	Code	% TD	Code	% TD
N-1-1	88.24	N-2-1	88.37	N-3-1	88.45
N-1-2	88.19	N-2-2	88.26	N-3-2	88.23
N-1-3	88.34	N-2-3	88.23	N-3-3	88.44
A-1-1	87.34	A-2-1	87.43	A-3-1	87.46
A-1-2	87.20	A-2-2	87.42	A-3-2	87.23
A-1-3	87.32	A-2-3	87.34	A-3-3	87.28

Ejection Stress Test Results (Section 2)

Code	Ejection Stress	Code	Ejection Stress	Code	Ejection Stress
N-1-1	5.87	N-2-1	5.88	N-3-1	5.79
N-1-2	5.70	N-2-2	5.63	N-3-2	6.72
N-1-3	7.55	N-2-3	5.98	N-3-3	5.47
A-1-1	4.89	A-2-1	5.34	A-3-1	5.33
A-1-2	4.92	A-2-2	4.99	A-3-2	5.80
A-1-3	5.07	A-2-3	5.03	A-3-3	5.17

Ejection Stress in N/mm².

Section 3 - To investigate the effects of sintering time and temperature on final sample density and macrohardness. All green samples tested contained 10% SiC and 0.5% by weight zinc stearate. All sintered samples were repressed to size after sintering. The ends of each sample were machined off to prepare the sample for density measurement. All samples were polished before hardness testing.

Sample Code:

Example; 2-1

"2"-1 refers to the matrix material.

2 - AA2124

6 - AA6061

2-"1" refers to the sample number.

Sintering Analysis Results (Section 3)

Code	Sintering Conditions	% TD	HRB (T4)
2-1	627°C-60 min.	95.28	75
2-2	633 °C -60 min.	93.86	75.5
2-3	633 °C -60 min.	93.24	-
2-4	617 °C -180 min.	97.85	-
2-5	617 °C -180 min.	98.18	82.5
2-6	617 °C -60 min.	96.71	-
2-7	617 °C -60 min.	97.07	78.5
2-8	617 °C -20 min.	93.23	70
2-9	Damaged	-	-
2-10	627 °C -20 min.	94.38	75.5
2-11	627 °C -20 min.	94.34	-
6-1	627 °C -60 min.	97.56	48.5 T4, 69 T6
6-2	627 °C -60 min.	97.38	-
6-3	627 °C -60 min.	97.83	-
6-4	627 °C -60 min.	97.46	-
6-5	633 °C -60 min.	97.52	51.0
6-6	633 °C -60 min.	97.45	-
6-7	617 °C -180 min.	97.34	-
6-8	617 °C -180 min.	97.33	50.5
6-9	617 °C -60 min.	97.11	-
6-10	617 °C -60 min.	97.21	50

TEST MATRIX NO. 4

Twelve batches of AA6061 aluminium powder combined with SiC particles were processed in test matrix no. 4, of which 8 batches contained 16 μ m aluminium powder, 2 contained 11 μ m aluminium powder and 2 contained 7 μ m aluminium powder. The batch details are listed in table appendix D. Four of the 16 μ m aluminium batches were combined with 24 μ m SiC particles in volume fractions of 5%, 10%, 15% and 20%. The remaining four 16 μ m aluminium batches were combined with either 6 μ m or 28.5 μ m SiC in volume fractions of 10% and 20%. All four batches containing the smaller aluminium powders were combined with 24 μ m SiC particles in volume fraction of 10% and 20%.

Three tensile test samples were produced for each batch listed in table D1. Also, twelve additional samples were produced from batch no. 1. These additional twelve samples were produced to investigate the effect of lubricant method on the composite material. Two of these twelve samples were produced using die wall lubrication only. The remaining ten samples were produced using mixed-in lubricant.

Table D1. Batch numbering and details for test matrix no. 4.

Average AA6061 Size (μm)	Average SiC Size (μm)	% Volume Fraction of SiC	Batch Reference No.
16	24	5	8
16	24	10	5
16	24	15	4
16	24	20	1 [†]
16	6	10	6
16	6	20	2
16	28.5	10	7
16	28.5	20	3
11	24	10	11
11	24	20	9
7	24	10	12
7	24	20	10

[†] 10 samples from batch No. 1 contained 0.75% by weight mixed-in zinc stearate solid.

APPENDIX E

Publications Arising From The Present Work

- Sternowsky S.B., O'Donnell G., Looney L., Effect of Particle Size on the Mechanical Properties of SiC Particulate Reinforced Aluminium Alloy AA6061, Key Engineering Materials, Vol. 127-131, Part 1, pp 455-462, 1997.
- O'Donnell G., Looney L., Effects of Pre-Compaction Annealing on Mechanical Properties of SiC_p/Al Composites, Key Engineering Materials, Vol. 127-131, Part 1, pp 479-486, 1997.
- O'Donnell G., Looney L., The Effect of Alloy Type and Processing Parameters on PM Aluminium Matrix Composites, in Proceedings of the 14th Conference of the Irish Manufacturing Committee, IMC 14, Trinity College Dublin, Ireland, September, 1997, eds. Monaghan J. and Lyons C.G., pp 291-299, 1997.
- O'Donnell G., Looney L., Modelling of Discontinuously Reinforced Metal Matrix Composites, Proceedings of the International Conference on Advances in Materials and Processing Technologies (AMPT 98), Kuala Lumpur, Malaysia, August, 1998, eds. Hamouda A.M.S., Sulaiman S. and Ahmadun M., pp 1028-1037, 1998.
- O'Donnell G., Looney L., Finite Element Modelling of Discontinuously Reinforced Metal Matrix Composites, in Proceedings of the 15th Conference of the Irish Manufacturing Committee, IMC 15, University of Ulster, Northern Ireland, September, 1998, eds. Hepburn C. and Harris D.M.J., pp 79-88, 1998.
- O'Donnell G., Looney L., Production of Aluminium Matrix Composite Components using Conventional PM Technology, submitted to Materials Science and Engineering, November, 1999.